Advanced Motion Control under Constraints in Application

September 2013

A thesis submitted in partial fulfilment of the requirements for the degree of
Doctor of Philosophy in Engineering

Keio University

Graduate School of Science and Technology
School of Integrated Design Engineering

Mizuochi, Mariko

（様式甲 3）

主　論　文　要　旨

報告番号	甲　　第　　号	氏　名	水落　麻里子

主論文題目：

Advanced Motion Control under Constraints in Application

（実システム制約下におけるモーションコントロールの高度化）

（内容の要旨）

近年，ロボット技術や計算機技術の発展に伴い，自動車等の一般社会に近い分野でもロボット技術の適用が進んでいる。人々を助けるための技術としてロボット技術をより広い分野で活用するためには，より複雑な動作を正確かつ信頼性高く実現することが重要である。本研究では，計測，制御の観点から加速度制御に基づくロバストモーションコントロールの高精度化，高度化に取り組んだ。本論文では特に，モーションコントロールの性能を妨げる様々な制約に着目し，モーションコントロールの性能を向上するための基礎技術とより高度なタスクを実現するための応用技術の両面から，制約下においてより高い性能を実現するための提案を行った。

第 1 章に，本研究の背景，目的および着眼点を概説した。

第 2 章では，本研究の基盤となる外乱オブザーバを用いた加速度制御に基づくロバストモーションコントロールについて説明し，これを実現する上での課題を明らかにした。

第 3 章および第 4 章では，外乱オブザーバの性能を制限する要因としてサンプリング周期および計測ノイズに着目し，ロバストモーションコントロールの性能向上のための基礎技術の研究に取り組んだ。第 3 章では，加速度制御のためのマルチレートサンプリング手法を，第 4 章では速度計測方法を提案した。マルチレートサンプリング手法は，入力，出力，制御の周期を独立に設計するものであるが，本研究では，加速度制御では，入力に対して短い周期で出力情報を取得することが重要であることを示し，その観点から従来手法とは異なる手法を提案した。また，速度計測では加速度制御に特に有効な同期計数法に着目し，この性能をさらに向上させる瞬時速度オブザーバを構築した。それぞれの手法による加速度制御の広帯域化のほか，提案手法を統合することにより，更なる性能向上が可能であることを確認した。

第 5 章および第 6 章では，ロバストモーションコントロールの応用技術の研究に取り組んだ。第 5 章では，ネットワークを介して制御されるシステムを対象とし，通信周期の制約を克服するために，サンプリング周期の設計手法および伝送信号の抽出，符号化手法を提案した。また，第 6 章では環境との接触を対象とし，動作中のリアルタイム接触検知を可能にするディザ信号を用いた接触検知法を提案した。各提案手法の有効性を解析および実験により検証した。

第 7 章に，結論として各章で得られた内容をまとめ，本研究の成果を要約した。また，提案技術の今後の発展について言及した。

SUMMARY OF Ph.D. DISSERTATION

School Integrated Design Engineering	Student Identification Number	SURNAME, First name MIZUOCHI, Mariko

Title

Advanced Motion Control under Constraints in Application

Abstract

With progress in robotic and computer technologies, application of robotic technology has been widened to the fields close to human life. It is important to achieve more sophisticated motion accurately and reliably for widening application of robotic technology to support human life. This research aims at improvement of accuracy and applicability of robust motion control based on acceleration control and focuses on the factors limiting its performance. The methods for achieving higher performance even under limitations are proposed both as the fundamental technology for improvement of motion control performance and as the applied technology for its application to more sophisticated tasks.

Chapter 1 describes the background, motivation, and viewpoints of this study.

Chapter 2 describes the basis of robust motion control based on acceleration control using disturbance observer (DOB) and clarifies the problems in application.

Chapters 3 and 4 develop the fundamental technologies by focusing on the sampling period and noise, respectively, as factors limiting the performance of DOB. Chapter 3 proposes a multirate sampling method for acceleration control by showing the significance of higher output sampling period than the input sampling period in acceleration control. Chapter 4 focuses on Synchronous measurement method as an effective velocity measurement method for acceleration control and proposes an instantaneous speed observer for the method to improve the measurement performance further. It is confirmed that the bandwidth of acceleration control is improved by each method and the performance is further improved by combined use of the methods.

Chapters 5 and 6 develop applied technologies by focusing on the networked control system and mechanical contact with environments, respectively. Chapter 5 proposes a design guideline of sampling periods and methods for processing transmitted signals to overcome the limitation on the packet transmission interval. Chapter 6 proposes a dither-based contact detection method for force sensor-less motion control. The validity of each method is verified by performance analysis and experiments.

Chapter 7 summarizes the results of this study and mentions future perspective.

Contents

List of Figures

List of Tables

Chapter 1

Introduction

1.1 Background: Development of Robots

With progress in robotic technologies, application of robotic technologies has accelerated and their application fields have been widened in this decade [1] [2] [3] [4]. There is an increased chance even for ordinary people to see the word "robot" not only in literatures, cartoons, or image of the future society but also in their daily lives. But then how many people can tell the definition of "robot" clearly? Should "robot" have human-like appearance and high intelligence? What is "robot" for? Actually, there is no single clear and standard definition of a robot. There are many kinds of definition and everyone, even ordinary people, seems to have their own definition. Prior to describing the author's definition of a robot and the motivation of this thesis, this chapter explains how the concept of a robot has been developed and what kind of discussion has been made.

The word "robot" was created and first used in the play "R.U.R. (Rossum's Universal Robots)" written by Karel Čapek in 1920 [5]. It comes from the word "robota", which means serf labor in Czech. The "robot" in the play is an artificial human for cheap labor developed as a product of the company named R.U.R. In this point, the origin of the idea of the robot dates back to ancient mythologies: mechanical servants were built by the Greek god, Hephaestus, in Greek mythology [6], an animated clay doll, Golem, appeared in Jewish legend [7], and many other automata or artificial human appeared in mythologies in many cultures. Meanwhile, a interesting point about the play "R.U.R." is that in addition to creating and using the word "robot" for the first time, it is the origin for many people of forming a feeling toward the robot and the basis of other science fictions about the robot, and contains a number of descriptions

as if the writer foresaw today's application of robotic technology. Here, most of robots appearing in literature including "R.U.R." are depicted as artificial humans. In terms of the feeling toward the robot, most people have a positive or amicable feeling in Japan and some Asian countries. In addition to religious background, literature, especially animated cartoons such as "Astro Boy", seems to impose the great influence. Since most of robots are depicted as friends of human beings or heroes that help human beings in the animated cartoons, many people believe that the robot is a good being. On the other hand, in Western countries, some people have a negative feeling to the robot and believe that the robot is an enemy of human beings. It is sometimes said that developing the robot is ethically wrong. The underlying thoughts, which are similar to "Frankenstein Complex" named by Isaac Asimov, are depicted in the play. The basic thought comes from religious background, blasphemy against the God by predominating over the God through creating life by science technology, and a fear of doing so. The "robot" in the play is basically developed as a machine that does not have soul or emotion, nevertheless ethical conflict continuing from Frankenstein [8] exists in the characters. Moreover, the "robot" in the play is intended to replace the work of human beings. Although it is intended to help human beings by releasing them from painful labor in a sense, the robot deprives the labor or employment of human beings in another sense. In addition, human beings are destroyed in the story by the revolt of the robot that has been modified to have a soul. These episodes seem to give the impression that the robot is an enemy and bring a fear to the robot. In terms of application of robotic technologies, the application of robotic soldiers and penitence for it are depicted as if argument in recent years against military use of robotic technology was foreseen.

Focusing on the technical elements and really existing robots, some kinds of automata had already been developed in the days before Christ especially in ancient Greek. From the age, many automata have been developed, and it is known that Leonardo da Vinci designed a humanoid in the 15th century [9]. In Japan, a number of complex automata called "karakuri" have been made since the 17th century [10]. These mainly relate to entertainment or art and are not for practical use, however. In the late 19th century, remote control technique was developed for vehicles for military use [11]. The first real humanoid robot, Elektro [12], was then developed by Westinghouse Electric Corporation in the 1930's, and the first master-slave manipulator was developed by Argonne National Laboratory in the 1950's [13]. As a great turning point of robotic technology, the first concept of the industrial robot was invented and patented by Devol as "programmable article transfer" in 1954 [14] and the robot was developed by Devol and Engelberger in 1956 as the product named "Unimate." After the invention of the industrial robot, many

kinds of robots or robotic technologies have been researched and developed, and these have been widely put into practical use especially in manufacturing. On the other hand, the robot in the practical use has long been something far away from those depicted in science fictions. In this decade, however, in addition to industrial robots, the application to various fields such as transportation, personal service, medical treatment, and military has been progressed greatly and the story in science fictions is becoming a reality [12] [15]. As the robot becomes more advanced and the application fields are widened, argument on robot ethics is revived [16] [17] [18] as follows: what is the basic rules that the robot should obey at the minimum, what is ethical use of the robot, whether it is ethically acceptable to apply the robot in battlefields, how human beings should react to the robot, and how to make the robot to make ethical decision. The best-known guidelines for the robot are "three laws of robotics" coined by a science fiction writer, Isaac Asimov, in 1942 in his book "I, Robot" [19]. Asimov created these laws to be free from "Frankenstein Complex." The three laws:

(1) a robot may not injure a human being or, through inaction, allow a human being to come to harm;

(2) a robot must obey the orders given it by human beings, except where such orders would conflict with the First Law; and

(3) a robot must protect its own existence as long as such protection does not conflict with the First or Second Laws;

are treated as basic rules that the robot should follow and introduced as a quotation from "Handbook of Robotics, 56th edition, 2058." These laws are often referred even in recent years when people discuss about ethics of the robot or machine. In reality, however, even fulfilling only the first law is still difficult besides the dilemmas in fulfilling it.

The author is not going to persist in the above-mentioned laws. The author wants to use the robot or robotic technology to assist human beings by supporting their lives. The first law, not harming human beings, must be important to fulfill the wish. Although the robot is required to be well adapted to the human society to that end, there still remain many technical problems on it. In this thesis, the author defines "robot" as what performs a certain task as a substitute of human beings based on instructions using electrical and mechanical mechanisms. Methods for supporting effective use of the robot as technology for assisting people from the technical standpoint are developed.

1.2 Motivation and Approach of Thesis

The primary objective of this research is to promote utilization of the robot for actually helping humans in a wider variety of fields. It is inevitable for achieving this objective to make the robot adaptive to the human environments and to give it techniques superior to those of humans. The word "environment" in this thesis stands for all the things around the robot including objects, walls, and grounds. Then "human environment" stands for the environment including human beings or the environment in which human beings live. The components of the robot are similar to those of a human and mainly consist of the followings:

- body structure (bone/skeleton)
- actuator (muscular system)
- sensory system (senses such as five senses)
- power source (nutrition and heart)
- controller (brain).

This thesis focuses mainly on the sensory system and the controller, in other words, sensing and control. The sensory system is a system acquiring information of the robot itself and surrounding environment in order to provide the basis of decision and the source of reference to the controller (brain). Although the controller as the brain includes something like artificial intelligence that makes upper level decision, this thesis only deals with a lower layer controller that generates commands for the actuator (muscle) to execute desired motions based on requests from an upper layer controller or a human and information from the sensory system.

Considering the above-mentioned goal from a viewpoint of sensing and control, improvements in accuracy and applicability of motion control are important. Improvement in accuracy means execution of required motions with higher accuracy. Improvement in applicability means widening of the range of application of robotic technology, including application to human environments and achievement of more complicated and sophisticated tasks. Improvement in accuracy can be regarded as improvement in basic performance of motion control and is fundamental for improvement in applicability. It is also important to attain desired motions in any situation. It is thus important to construct the system to be highly robust. "Robust" means strength against unexpected or exceptional inputs and situations, and parameter

variations of the controlled object. Acceleration control is a key technique for realization of robust motion control. Acceleration control is a type of control that gives an acceleration reference for achieving required motions to the system and controls the system to attain desired acceleration [20]. Motion control systems often require to deal with position and force at the same time. These variables can be dealt with in a unified manner by using acceleration. Moreover, acceleration control is known to be able to achieve higher robustness compared with control considering only position and velocity. Improvements in accuracy and applicability of robust motion control based on acceleration control are thus set as the technical goal of this research, and sensing and control technologies to achieve the goal are developed. There are various constraints, however, in implementation of acceleration control-based robust motion control to a real system. For example, there are limitations of performance of devices, which impose the adverse influence on the performance of the whole control system. In addition, usable devices and acquirable information are limited in some applications. Although a system works as modeled in theory, unexpected situations or discontinuous changes of states often occur in real application. A system should therefore be capable of dealing with these situations. This thesis focuses on the factors limiting the performance of robust motion control and provides methods for attaining higher performance even under the constrains. In order to promote application of motion control, both improvement in the basic performance and solutions for problems peculiar for each application are required. This thesis therefore deals with development of both fundamental technologies for improving basic performance of robust motion control and applied and advanced technologies for expanding application of robotic technology to more complicated and sophisticated tasks.

In the development of the fundamental technology, the author focuses on the disturbance observer, which is an effective tool to realize acceleration control. The disturbance observer regards all the elements disturbing the system to achieve desired motion as the disturbance [21]. The observer realizes acceleration control by estimating the disturbance in an acceleration dimension and compensating it. Acceleration control and robustness are attained not in all frequency ranges, however, when the disturbance observer is utilized. The bandwidth is determined by the cutoff frequency of a low-pass filter in the disturbance observer. Since there are various factors limiting the cutoff frequency, the disturbance observer may not work sufficiently in some systems or situations. This thesis focuses on limitations on the performance of the disturbance observer to improve the performance of the whole motion control system. The main factors limiting the performance of the observer are sampling periods and noise. Due to rapid development in computer technology, robotic systems are often controlled in discrete-time. The

sampling period imposes the great influence on the control performance when control is executed in discrete-time using a computer. Meanwhile, information of a robotic system such as position and force is usually obtained using sensors such as an encoder, a tachometer, and a force sensor. The accuracy and the noise of these sensors are also important elements determining the control performance. This thesis aims at realization of high performance robust motion control based on acceleration control by tackling the problems of performance limit from viewpoints of the sampling period and the noise. In terms of the sampling period, this thesis introduces the idea of the multirate sampling [22]. In terms of noise, velocity measurement is focused on to reduce noise in acceleration dimension. The performance is expected to be improved by each of the methods and improved further by combined use of the methods.

As the applied technologies, control of systems connected through a network and mechanical contact with environments are discussed. Due to a significantly rapid progress in communication technology, introduction of a network to the motion control system is increasing in many fields [23] [24]. Control over a network suffers from the problems of deterioration of stability and control performance, however, due to limitations on network performance [25]. This thesis mainly focuses on the limitation of a packet transmission interval. This thesis aims at achieving higher performance even under the limitation of the interval by tackling the issues from a viewpoint of the sampling period and transmission signals. At the same time, mechanical contact with environments is inevitable for the robot working in the human environments. The contact raises risks both for the environment and the robot: destroying the environment or the robot, destabilizing the robot, and so on. The difficulty in the contact limits application fields of robotic technology. In terms of stable operation with interaction with unknown objects, it is important to recognize and assess the state of the robot accurately in order to minimize the risks. This thesis thus deals with the research on contact detection.

1.3 Organization of Thesis

The outline of construction of this thesis is summarized in Fig. 1-1. This thesis consists of seven chapters including this chapter. The contents of the thesis are classified into the following three:

- introduction of existing motion control techniques that form the basis of the topics in this thesis (Chapter 2)
- development of fundamental technologies for improvement of motion control performance (Chapters 3 and 4); and

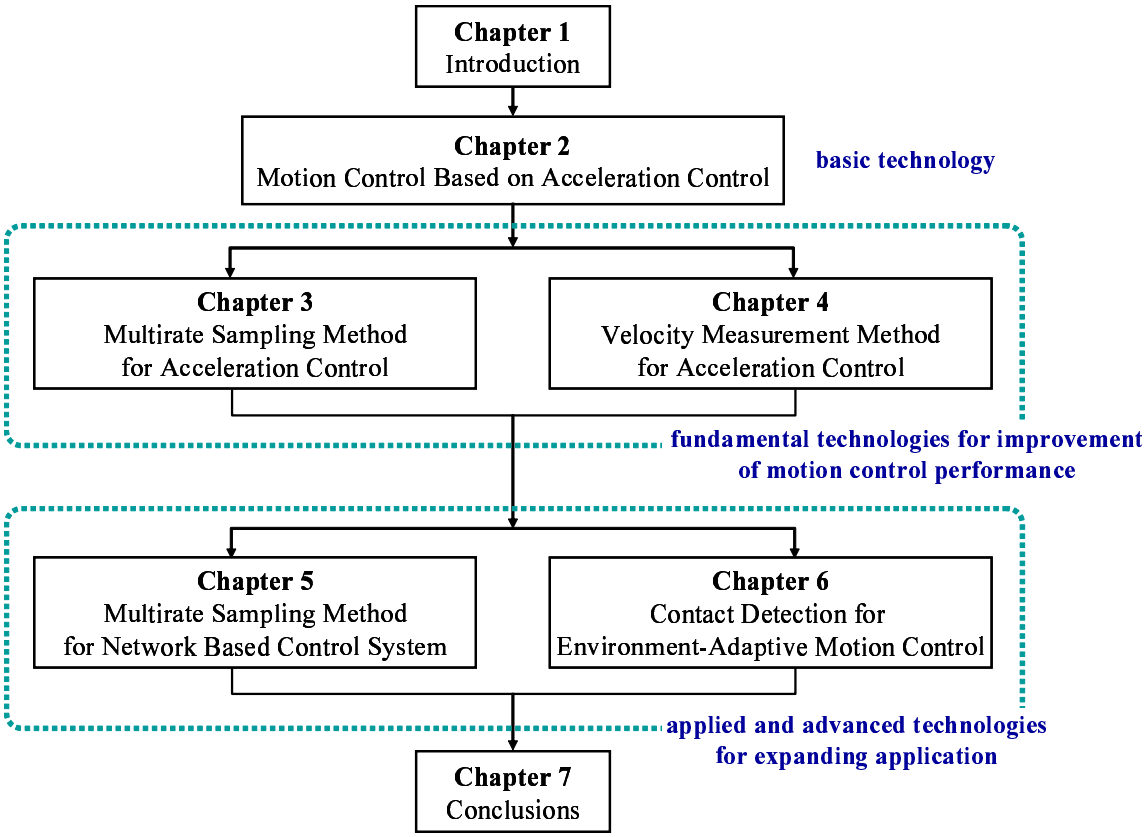

Fig. 1-1: Outline of construction of thesis

- development of applied and advanced technologies for expanding application of robotic technology to more complicated and sophisticated tasks (Chapters 5 and 6).

Firstly, Chapter 2 introduces a method for constructing the acceleration control system using the disturbance observer and examples of a robust motion control system based on acceleration control as the basis of the research in this thesis. This thesis uses one of the systems described here for verification of the proposed methods. The chapter also describes problems in implementation and application of acceleration control-based robust motion control and clarifies the matters to be tackled in this thesis.

Chapters 3 and 4 develop the fundamental technologies by focusing on the sampling period and noise, respectively, as factors limiting the performance of the disturbance observer. Chapter 3 tackles the performance limits of the disturbance observer from a viewpoint of the sampling period and proposes a multirate sampling method for acceleration control. The method is proposed based on the idea completely different from conventional methods. This chapter also redesigns the disturbance observer to fit

it to the multirate sampling system with a new definition of a disturbance torque. The validity of the proposed method is verified through stability analysis, simulations, and experiments on various motion control systems.

Chapter 4 tackles the performance limit of the disturbance observer by focusing mainly on the influence of noise. The velocity measurement method is focused on to reduce measurement noise in an acceleration dimension. This research focuses on synchronous measurement method (S method) [26] as a velocity measurement method effective especially in acceleration control. An instantaneous speed observer [27] is proposed for the method for improving the measurement performance further. Combined use of the measurement method and the multirate sampling method is also discussed. The validity is verified for the measurement method and the combined use of the measurement method and the multirate sampling method through simulations and experiments on velocity measurement and acceleration control-based position control.

Chapters 5 and 6 develop applied technologies by focusing on difficulties in the networked control system and mechanical contact with environments, respectively. Chapter 5 takes up the systems connected and controlled through a network as an advanced system applying motion control. This chapter aims at realization of high performance motion control even under the limitations on network performance. This thesis focuses especially on the limitation of the time interval of packet transmission. The limitation of the packet transmission interval is regarded as a problem relating to the sampling period and that relating to the transmission signal. The methods for overcoming the limitation are proposed both from viewpoints of the sampling period and the transmission signal. From a viewpoint of the sampling period, a design guideline of the sampling periods in the networked motion control system is proposed. Then from a viewpoint of the transmission signal, a signal transmission method and a coding scheme are proposed for minimizing the influence of the limitation of the packet transmission interval. The bilateral teleoperation system is taken up as an example of the system connected through a network and requiring high performance motion control. The validity of each method is verified by performance analysis, simulation, and experiments.

Chapter 6 deals with mechanical contact with environments, especially contact detection technique as an indispensable technique to overcome difficulty in stable contact operation and to expand application fields. The main focus is given on contact detection during force sensorless motion control in unstructured environments. The chapter aims at real-time detection of a contact event regardless of the magnitude of contact force and characteristics of a contact object, which is difficult in conventional meth-

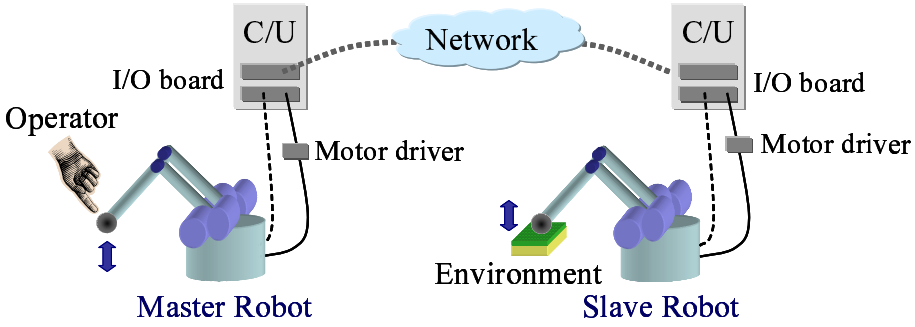

Fig. 1-2: Overview of bilateral teleoperation system

ods. Based on the idea of active sensing, a method using a dither signal is proposed. The effectiveness of the proposed method is verified through experiments on contact detection and bilateral teleoperation.

Finally, this thesis is summarized and concluded in Chapter 7. Contribution of this thesis and future perspective are also mentioned in the chapter.

The related studies are explained in the introduction sections in each chapter. The precise motivation of each topic is also described in the sections.

This thesis takes up bilateral teleoperation over a network as one of important applications. The role of each technology developed in this thesis is explained below by explaining the function of the technology in fulfilling requirements and overcoming difficulties in bilateral teleoperation. The bilateral control is a technique to execute precise teleoperation. An overview of a bilateral teleoperation system is shown in Fig. 1-2. The system is generally composed of a pair of master and slave devices. The master and slave devices are controlled to follow each other: the slave device is manipulated by an operator through the master device and the master device reproduces the situation in the slave side. In order to achieve high performance bilateral teleoperation, wide-band acceleration control is strongly required because of the following reasons: bilateral control requires to deal with position and force at the same time; high robustness is required since operations are not planned beforehand and the slave device often makes contact with objects; and reproduction of vivid tactile sensation requires control in wide bandwidth. Acceleration control introduced in Chapter 2 is thus the basic technology for bilateral teleoperation. Main difficulties in achieving high performance bilateral teleoperation based on acceleration control are performance limit of devices, control through a network, and contact with unknown objects. Each of the master and the slave device is mainly composed of motors, links, an end-effector, sensors, and a control unit. Each of the above-mentioned devices has limitations on its performance. Introduction of a net-

work in the system is required for operation from a remote area. A network raises difficulties in control and the performance of a network limits the performance of the whole system, however. In teleoperation, interaction with unknown objects is inevitable to execute tasks. As mentioned above, the contact increases a risk of destruction of an object and destabilization of the control system. Stable contact is difficult especially when a network exists, since contact operation requires quick reaction. Chapters 3 and 4 provide solutions for performance limits of devices. As mentioned above, the performance of acceleration control is limited by limitations on the sampling period and noise in measured signals. The technology dealt with in Chapter 3 plays a large role in solving the problem of limitations of the sampling period. The problem of noise is coped with the velocity measurement method developed in Chapter 4. These two approaches are expected to achieve wider-band acceleration control even under limitations of performance of devices. Chapter 5 deals with issues related to introduction of a network and provides solutions to overcome performance limit due to the network. With the technology developed in Chapter 5, high performance bilateral teleoperation based on wide-band acceleration control is expected be achieved even with introduction of a network. Then the contact detection method developed in Chapter 6 solves the difficulty in stable contact with unknown objects by providing additional information to a control system and an operator. Automatic adaptation in the slave side and notification of the contact state become possible even through a network, and stability and safety of bilateral teleoperation are expected to be improved. To cope with complex applications such as bilateral teleoperation composed of various components and various difficulties in achieving adequate performance for application in the real world, a variety of approaches are required in researches of both fundamental and applied technologies as described in this thesis. Since most of the technologies developed in this thesis are not specific for bilateral teleoperation, each technology can effectively be applied to many kinds of motion control systems other than the bilateral teleoperation system.

Chapter 2

Motion Control Based on Acceleration Control

2.1 Introduction

In this chapter, the basis of robust motion control schemes is described. Robust motion control is achieved by acceleration control [20]. The relationship between motion control and acceleration control and importance of acceleration control are described in Section 2.2. Then in Section 2.3, a disturbance observer [21] is introduced as an effective tool to achieve acceleration control. Section 2.4 shows examples of motion control systems based on acceleration control. The basic structure of each system, which is used in verification in this thesis, is also described. Finally, the issues to be solved in this thesis to improve performance and applicability of the motion control are noted in Section 2.5 by describing the problems and limitations on realization of wide-band acceleration control and application to various systems.

2.2 Robust Motion Control and Acceleration Control

This section is devoted to explain what robust motion control is and how to realize it. The relationship between robust motion control and acceleration control is then explained.

Motion control is a technology to realize various motions in electro-mechanical complex systems [20] [28]. The outputs of the system in a physical point of view are position, velocity, and force. The term “robust” means that the system is resistant to exceptional inputs, unknown disturbance, or parameter deviations of the controlled object. High robustness in motion control means that position, velocity, and force of the

system do not deviate from the command values even with a deviation of a load and system parameters or disturbance, and the desired outputs can be acquired in any situations. In other words, robustness shows the strictness of the system to the desired motion. Higher robustness is thus required when the desired motion becomes more complicated and the application situation is widened.

Motion control often requires not only robustness but also dealing with force and position at the same time [29]. The relation between position and force is expressed in the following equation.

$$F = g(\ddot{X}, \dot{X}, X) \tag{2.1}$$

Here, X denotes a position of a controlled object and F denotes a force imposed on the controlled object. The ideal position control inhibits deviation of position even with any force imposed on the system, while the ideal force control is to apply a desired force on an object wherever an end-effector exists. It means that force is indeterminate in the ideal position control, while position is indeterminate in the ideal force control. It means that position control and force control have controversial requirements. As an index that represents characteristics of motion, a stiffness defined in the following equation had been proposed [21].

$$\kappa = \frac{\partial F}{\partial X} \tag{2.2}$$

The position control and force control can be characterized using the stiffness. The stiffness is infinite in the above-mentioned ideal position control, while it should be zero in the ideal force control. A finite value of the stiffness means that compliance control with compliance $1/\kappa$ should be performed. Robust motion control requires achieving various levels of stiffness according to desired motions and surrounding environments. In realization of any stiffness, it is effective to use acceleration in order to deal with position and force in a unified manner. As shown in Fig. 2-1, acceleration is derived not only from a second order derivative of position or angle but also from dividing a force by a mass or dividing a torque by an inertia. It means that acceleration is a bridge to connect position and force. It is thus necessary in motion control to focus on acceleration as a unified state variable and to control a system to attain desired acceleration. This type of control is called acceleration control.

There is another advantage in controlling acceleration that robustness and the stiffness or tracking performance can be designed independently. When a general control system is considered, the stiffness corresponds to a position gain. Since the influence of parameter variation and disturbance can be suppressed by increasing the gain, higher robustness in position control can be achieved by heightening the stiffness. On the other hand, the ideal force control requires the stiffness to be zero. It seems to

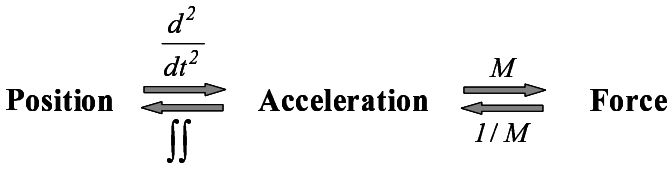

Fig. 2-1: Relationship between force and position

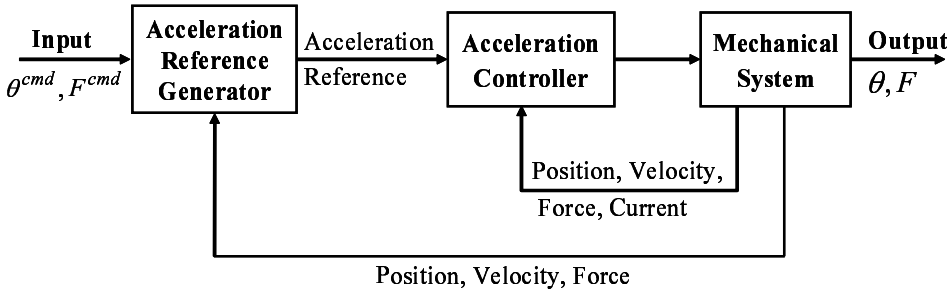

Fig. 2-2: Basic structure of robust motion control based on acceleration control

be difficult to attain high robustness in force control. The high robustness is attained regardless of the stiffness, however, by using acceleration as a unified state variable and attaining robustness in an acceleration dimension using acceleration control. The basic structure of acceleration control-based robust motion control is shown in Fig. 2-2. An acceleration reference to achieve desired motion or the stiffness is calculated in a reference generator in the outer loop. Then the system is controlled to attain the desired acceleration by an acceleration controller in the inner loop. Since the stiffness is determined in the outer loop and the robustness is determined in the inner loop, these can be designed independently by using the above-mentioned structure.

The key points of robust motion control are summarized as follows:

- stiffness is an effective index to represent characteristics of desired motion;
- acceleration is used to deal with position and force in a unified manner;
- stiffness and robustness can be designed independently by applying robust acceleration control; and
- robust motion control consists of an acceleration reference generator in the outer loop and an acceleration controller in the inner loop.

This thesis focuses especially on the performance of the inner loop acceleration control.

2.3 Basic Technique for Acceleration Control

2.3.1 Disturbance Observer

As an effective tool to realize robust acceleration control, the disturbance observer (DOB) has been proposed [21]. The robust acceleration control is realized by estimating a disturbance force or torque and compensating it using acceleration information.

The equation of the motion of a rotary motor is expressed in the following equation:

$$J\frac{d^2\theta}{dt^2} = K_t I_a - \tau_l, \tag{2.3}$$

where J denotes an inertia, θ denotes angle, K_t denotes a torque constant of a motor, I_a denotes armature current, and τ_l denotes a mechanical load. A similar equation can be obtained for a linear motor by substituting position for angle, force for torque, and a mass for an inertia. Since motor drivers used for robot control generally have a current inner loop with a large gain, wide-band current control is attained. A real current can therefore be considered to be always equal to the current reference. Examples of the components of the mechanical load τ_l are listed below.

- external torque (τ_{ext}): a load attributed to reaction force from an object in the contact motion
- interference torque (τ_{int}): Coriolis and centrifugal forces
- gravitational torque (τ_g): a load generated by gravity
- friction torque ($D(\dot{\theta})$): a load due to Coulomb or viscous friction

With consideration of the above elements, the mechanical load is expressed as follows:

$$\tau_l = \tau_{ext} + \tau_{int} + \tau_g + D(\dot{\theta}). \tag{2.4}$$

Here, τ_{ext} is a force occurring only in the contact state and others are those occurring even in the non-contact state. The block diagram of a motor is then expressed as shown in Fig. 2-3. Here, τ_m is a torque generated by a motor when a current is inputted and s denotes the Laplace operator.

The disturbance observer estimates a disturbance torque including all elements not considered in a nominal model. The total disturbance torque τ_{dis} mainly consists of the mechanical torque, a varied self-inertia torque $\Delta J\ddot{\theta}$, and a torque ripple of the motor $\Delta K_t I_a^{ref}$.

$$\tau_{dis} = \tau_l + \Delta J\ddot{\theta} - \Delta K_t I_a^{ref} \tag{2.5}$$

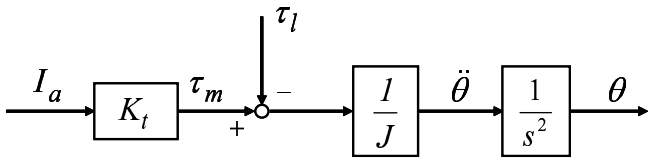

Fig. 2-3: Block diagram of motor

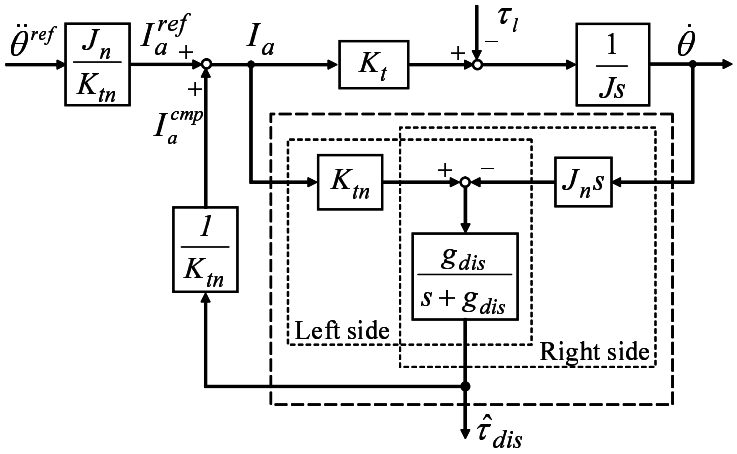

Fig. 2-4: First order disturbance observer

Here, $\Delta J = J - J_n$, $\Delta K_t = K_t - K_{tn}$, and subscript n denotes a nominal value. The disturbance torque is calculated by the equation below.

$$\tau_{dis} = K_{tn} I_a - J_n \ddot{\theta} \tag{2.6}$$

Since derivative calculation amplifies noise, an estimated disturbance torque is obtained through a low-pass filter (LPF) in the disturbance observer.

Fig. 2-4 shows the disturbance observer with a first order LPF. Here, g_{dis} denotes a cutoff frequency of the disturbance observer, $\hat{\tau}_{dis}$ denotes an estimated disturbance torque, $\ddot{\theta}^{ref}$ denotes an acceleration reference generated by the outer loop controllers, I_a^{ref} denotes a current reference calculated from $\ddot{\theta}^{ref}$, I_a^{cmp} denotes a compensation current calculated in the disturbance observer, and I_a denotes a total current reference given to a motor driver. The estimated disturbance torque is derived with the equation below.

$$\hat{\tau}_{dis} = \frac{g_{dis}}{s + g_{dis}} (K_{tn} I_a - J_n s^2 \theta) \tag{2.7}$$

The first term $K_{tn} I_a$ in (2.7) is based on an input signal, while the second $J_n s^2 \theta$ is based on the output signal. In other words, the first corresponds to the left side of the disturbance observer in Fig. 2-4, while

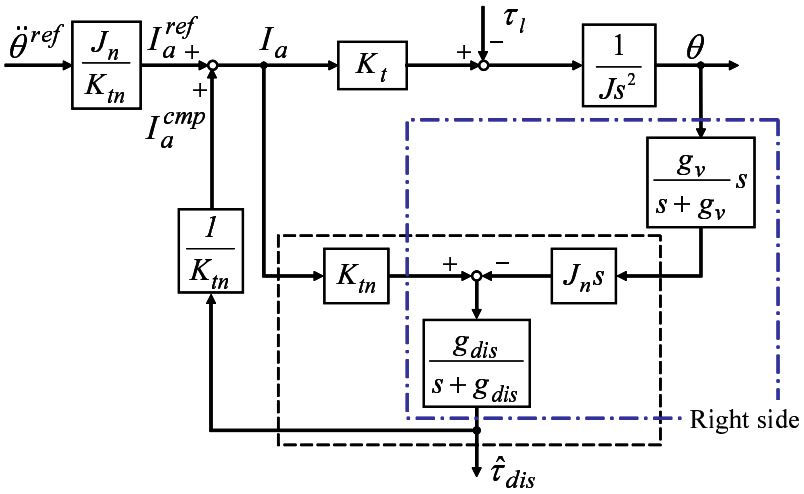

Fig. 2-5: First order disturbance observer in practical use

the second corresponds to the right side.

Here, the signal acquired in experimental systems is mainly an angular or position signal from an optical encoder. On the other hand, disturbance estimation in the disturbance observer is based on the acceleration. Thus, twice of derivative calculation are performed in the right side of the observer. Since it is usually difficult in experiments to use a derivative value directly because of noise mainly derived from a quantization error of the encoder, pseudo-derivative calculation with an LPF is often introduced. The velocity is calculated as follow with pseudo-derivative calculation:

$$\hat{\dot{\theta}} = s\frac{g_v}{s+g_v}\theta, \tag{2.8}$$

where g_v denotes a cutoff frequency of an LPF for velocity calculation. With consideration of pseudo-derivative calculation, the block diagram of the disturbance observer is rewritten as Fig. 2-5 and estimation is performed with the following equation.

$$\hat{\tau}_{dis} = \frac{g_{dis}}{s+g_{dis}}(K_{tn}I_a - J_n\frac{g_v}{s+g_v}s^2\theta) \tag{2.9}$$

This equation shows that two LPFs are introduced into the right side, the output side, of the disturbance observer to realize acceleration control, considering pseudo-derivative and disturbance calculation.

Equations (2.7) and (2.9) show that disturbance estimation is performed in an acceleration dimension. Thus, compensating disturbance in an acceleration dimension with introduction of the disturbance observer realizes acceleration control and improves robustness of the system. In fact, the robustness is not

assured in the frequency range higher than the cutoff frequency of the disturbance observer. In addition, the cutoff frequency determines disturbance suppression performance. It is thus important to set the cutoff frequency high. There are limitations on the cutoff frequency, however. The upper limit of the cutoff frequency in the discrete-time system depends on the sampling period [30][31]. The sampling period is required to be shortened in order to set the cutoff frequency higher. Noise in a measured signal also limits the cutoff frequency. Since a higher cutoff frequency improves disturbance suppression ability but it also increases noise in the estimated disturbance torque, there is thus the trade-off relation between the cutoff frequency and noise effect.

2.3.2 Reaction Force Observer

The basic structure of the disturbance observer is also utilized for estimating an external force. As a means to measure an external force, force sensors have been widely utilized. A force sensor such as a strain gage or a load cell provides a force value by electrically amplifying the strain generated by an applied force. Although implementing force sensors is the simplest and general way to measure the force value, various problems have been reported about the implementation [32] [33] [34]. Examples of the problems are listed below.

- bandwidth of measurement is limited due to structure and noise of the sensor
- force sensors should be implemented to all the places where force is supposed to be applied
- cost of sensor is high

As an alternative method of force sensors, the reaction force observer (RFOB) shown in Fig. 2-6 has been proposed [35]. The reaction force observer has a structure similar to that of the disturbance observer. The estimated disturbance torque in the disturbance observer contains many elements other than the external torque. The external torque τ_{ext} is calculated by extracting those elements from the estimated disturbance torque as follows:

$$\hat{\tau}_{ext} = \frac{g_e}{s+g_e}(K_t I_a - Js^2\theta - (\tau_{int} + \tau_g + F + D(\dot{\theta}))), \tag{2.10}$$

where g_e denotes a cutoff frequency of an LPF in the RFOB. It is necessary to use real values K_t and J instead of nominal values K_{tn} and J_n in the calculation to acquire a real value of the external force. It is also indispensable to detect amounts of τ_{int}, τ_g, F, and $D(\dot{\theta})$. In order to reduce an estimation error, a

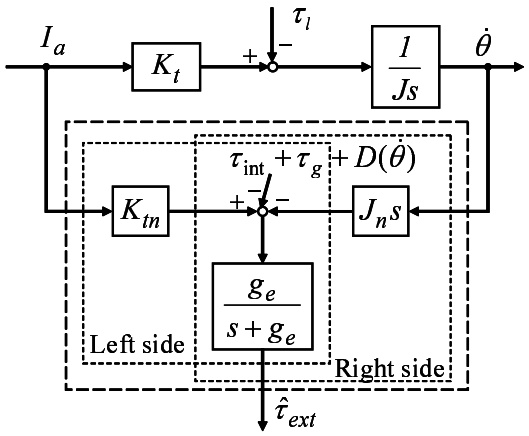

Fig. 2-6: Reaction force observer

constant velocity test and a step velocity test are often executed to identify a friction model and a mass or an inertia [35] [36]. In a practical use, pseudo derivative calculation explained for the disturbance observer in the previous subsection is also applied to the reaction force observer for the calculation of velocity.

The bandwidth of force sensing depends on the cutoff frequency g_e. Since wide-band force measurement is necessary to attain stable contact with various environments [37], it is important to heighten g_e in order to cope with unknown environments. As in the case of the cutoff frequency of the disturbance observer, g_e is limited, however, due to the sampling period and the noise of the signal.

2.4 Motion Control Based on Acceleration Control

This section introduces several examples of motion control systems based on acceleration control. Verifications in this thesis are performed using one of the systems described here.

2.4.1 Position Control

The ideal position control is to make a system track a position command even under disturbance or parameter variation. The block diagram of a basic position control system is shown in Fig. 2-7(a). Here, K_p denotes a position gain, K_v denotes a velocity gain, and superscripts res and cmd denote response and command, respectively. An acceleration reference is given as the following equation.

$$\ddot{\theta}^{ref} = K_p(\theta^{cmd} - \theta^{res}) + K_v(\dot{\theta}^{cmd} - \dot{\theta}^{res}) \tag{2.11}$$

The characteristics of position control, the stiffness and robustness, are decided by K_p and K_v.

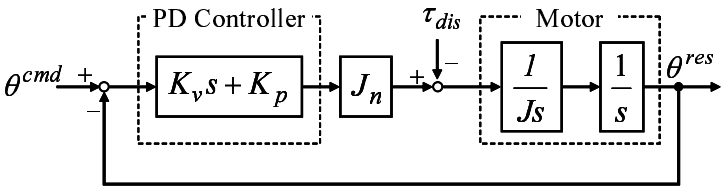

(a) basic position control

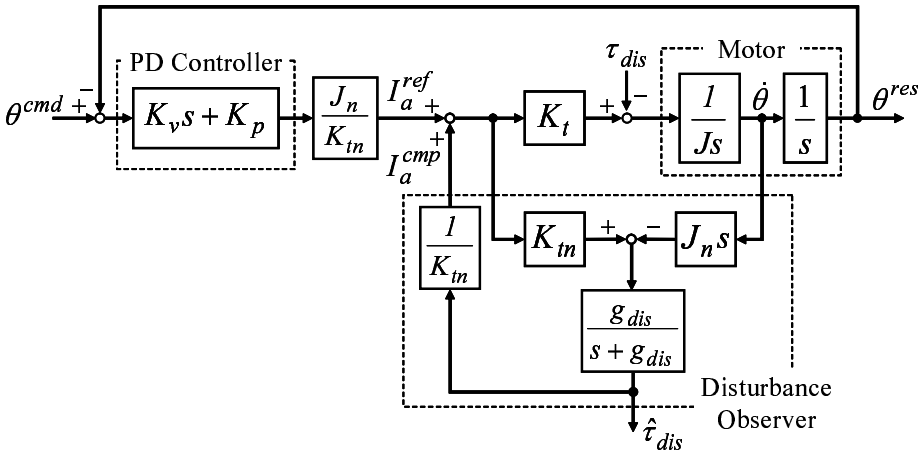

(b) position control based on acceleration control

Fig. 2-7: Position control system

In order to improve robustness of position control, the control system is modified to be an acceleration control system by applying the disturbance observer. The block diagram of a position control system based on acceleration control is expressed as shown in Fig. 2-7(b).

2.4.2 Force Control

Many researches have been conducted on force control since it is one of the fundamental techniques of motion control [38] [39]. The ideal force control is to make a system into contact with an object with a commanded force or torque without vibration no matter where the end-effector exists. The block diagram of a basic force control system is shown in Fig. 2-8(a). Here, τ^{cmd} denotes a desired contact torque and K_f denotes a force gain. An acceleration reference is derived as follows:

$$\ddot{\theta}^{ref} = K_f(\tau^{cmd} - \hat{\tau}_{ext}). \tag{2.12}$$

The force control system requires a mechanism to measure an external force imposed on an object. Force sensors have been utilized in many conventional researches as a means to measure the force. Although

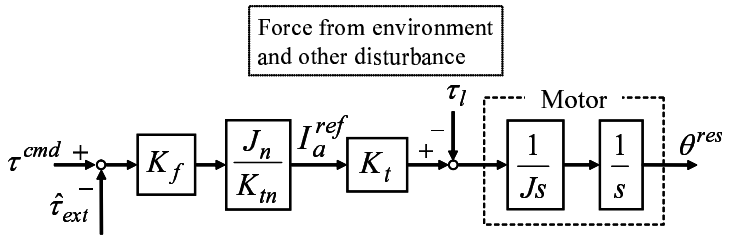

(a) basic force control

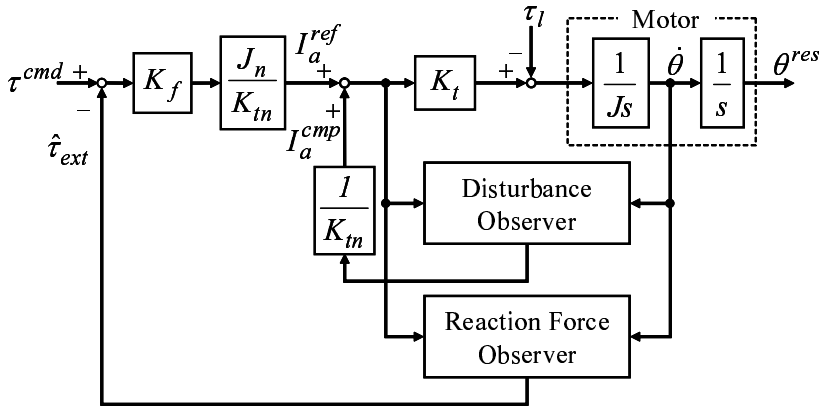

(b) force control based on acceleration

Fig. 2-8: Force control system

implementing force sensors is the simplest and general way to measure the force value, various problems have been reported about the implementation [34]. With consideration of those points, this thesis uses the reaction force observer introduced in Section 2.3.2 instead of force sensors.

In order to attain higher robustness in force control without position feedback, the idea of acceleration control is introduced. Fig. 2-8(b) shows the block diagram of a robust force control based on acceleration control using the disturbance observer and the reaction force observer.

The following requirements are pointed out for force control to impose a desired force on an object.

- attain stable contact with any environment
- impose exact desired force in rapid response

The first requirement is prerequisite for the second the force cannot be imposed constantly when contact is unstable. It is known that wide-band force measurement is necessary to attain stable contact with various environments [37]. Moreover, the amount of delay in the force signal is also an important factor to determine the performance of force control although the only important thing is the accuracy of an

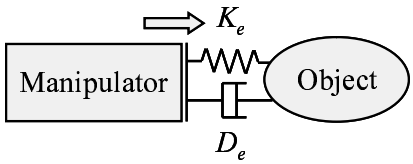

Fig. 2-9: Model of environment

acquired force signal when a focus is given just on force measurement. It means that wide-band and small-delay force measurement is necessary to satisfy the former requirement. Then in order to satisfy the latter requirement, the force gain should be set high. In this thesis, a main focus is given to the former point. The wide-band force measurement with the reaction force observer and precise force control using the reaction force observer are set as one of the objectives of this thesis.

In simulation or analysis, environments are modeled as a spring and damper model shown in Fig. 2-9. Here, K denotes a spring coefficient, D denotes a damper coefficient, and subscripts e denotes environment. The reaction force from the environment is given in the following equation.

$$F_e = \begin{cases} K_e(-X_e + X) + D_e\dot{X} & (X > X_e) \\ 0 & (X \leq X_e), \end{cases} \tag{2.13}$$

where X denotes position.

2.4.3 Bilateral Control

This thesis deals with a bilateral teleoperation system as a system requiring high performance motion control based on acceleration control. The bilateral control is a technique to execute precise teleoperation and it has been studied for a long time from various viewpoints [40] [41] [42] [43] [44] [45]. Teleoperation has been utilized widely for years to execute tasks in places where a man cannot enter, such as space, under water, and nuclear plants [13] [46] [47]. The system for teleoperation is generally composed of a pair of master and slave devices. A master device is usually a human interface in the operator side and a slave device is a device executing tasks in the remote side. Unlike in unilateral control, which transmits an operational command from an operator (master) unilaterally to a remote device (slave), master and slave devices are controlled to follow each other in the bilateral control. A slave device is manipulated by an operator through a master device and a master device reproduces the situation in the slave side. Since an operator can recognize the situation in the remote side during operation, application fields of teleoperation are expanded with bilateral control [48] [49] [50]. It is also possible in the bilateral

teleoperation to transmit force occurring in the remote side to an operator. It is important to enable an operator to feel an accurate reaction force from a contact object especially in tasks that require accurate and careful operation, such as surgery and handling of hazardous material. Coupled with the growth of minimal invasive surgery in recent years, application of robotic technology to the medical field has been accelerated [51] [52]. Technologies such as computer-aided diagnosis, surgical navigation, and robot-assisted surgery are becoming common. In the field of surgical robots, it is important to provide sufficient information including vivid tactile sensation to a surgeon in terms of safety. Because of the above situation, many researches have been performed to transmit vivid tactile sensation [53] [54] [55] [56] [57]. Since bilateral control requires control of position and force at the same time and wide-band acceleration control is inevitable for accurate reproduction of tactile sensation, bilateral control is a good example to evaluate the performance of motion control based on acceleration control.

Researches on bilateral control have been performed since the 1980's, and many types of controllers such as position-position, position-force, force-position, force-force, impedance-base, and four-channel architectures have been investigated [40] [44] [58]. Despite those controllers, researches for new controllers are still ongoing. Concurrently with the development of controllers, the definitions of the ideal condition of the bilateral teleoperation system or evaluation indices for bilateral teleoperation performance have been discussed [43] [55] [59]. Yokokohji and Yoshikawa defined the ideal responses of the bilateral teleoperation system with the idea of kinesthetic coupling [55]. Hannaford proposed a two-port circuit representation of the bilateral teleoperation system and defined the ideal responses using a hybrid matrix [43]. Lawrence proposed the idea of "transparency" as the ideal condition based on the hybrid matrix [44]. Those definitions are also utilized for performance evaluation of the bilateral teleoperation system. Aliaga *et al.* proposed an experimental evaluation method based on six types of matrices of the two-port model [60]. The concept of "transparency" was extended to "operationality" and "'reproducibility" by Iida *et al.* [56]. Those indices have been used also for designing new control architectures. Stability evaluation of the bilateral teleoperation system has also been discussed [44] [61].

The followings are devoted to explain representation and evaluation of the bilateral teleoperation system using a hybrid matrix as the basic technique for performance evaluation and introduce controllers used in this thesis.

Hybrid Matrix

The hybrid matrix is one of the matrices representing the relation between voltage and current in a two-port circuit. It is widely used also to express a bilateral teleoperation system. Considering that a teleoperation system consists of an operator, an environment, and a mechanical and electronic system, a bilateral teleoperation system can be modeled as Fig. 2-10(a). Here, Z_h and Z_e denote impedances of an operator and an environment. The relationship between the master system and the slave system can be modeled as a two-port model as shown in Fig. 2-10(b) and represented using the hybrid matrix as shown in the following equation [43]:

$$\begin{bmatrix} F_m \\ X_s \end{bmatrix} = \begin{bmatrix} H_{11} & H_{12} \\ H_{21} & H_{22} \end{bmatrix} \begin{bmatrix} X_m \\ F_s \end{bmatrix}, \tag{2.14}$$

where F denotes force, X denotes position, subscripts m and s denote a master device and a slave device, respectively. The meanings of elements of the hybrid matrix are described as follows:

- H_{11}: impedance in the master;
- H_{12}: scaling gain of force;
- H_{21}: scaling gain of position; and
- H_{22}: inverse number of the slave impedance.

The control goal of the bilateral control is complete agreement between the master device and the slave device in terms of position and force, which is called transparency [44]. If the hybrid matrix satisfies the following equation, the ideal teleoperation and perfect transparency are achieved.

$$\begin{bmatrix} F_m \\ X_s \end{bmatrix} = \begin{bmatrix} 0 & -1 \\ 1 & 0 \end{bmatrix} \begin{bmatrix} X_m \\ F_s \end{bmatrix} \tag{2.15}$$

The performance of bilateral teleoperation can be evaluated by deriving the elements of the hybrid matrix and comparing them with the ideal condition shown in (2.15).

Performance Indices

This thesis also introduces the following five indices to evaluate the performance of bilateral teleoperation: reproducibility, operationality, tracking, drift, and stability. Reproducibility P_r and operationality P_o [56] mainly focus on a force generated on the master side and is defined as follows:

$$F_m = (P_o + P_r Z_e) X_m. \tag{2.16}$$

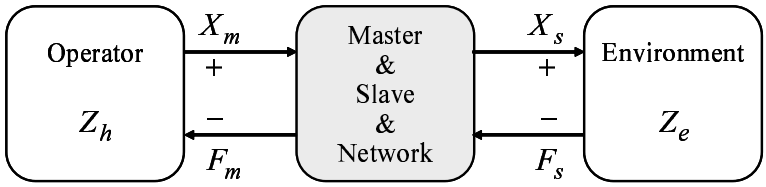

(a) structure of bilateral teleoperation system

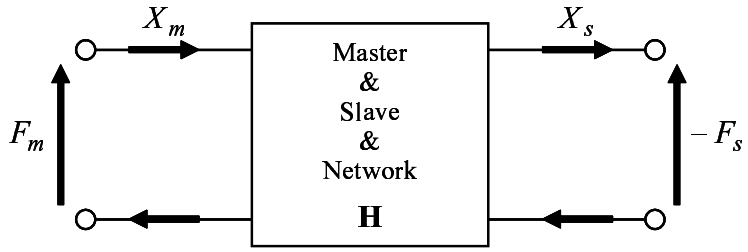

(b) two-port expression

Fig. 2-10: Bilateral teleoperation system

Those are derived from the following equations.

$$P_r(s) = \frac{F_m}{Z_e X_m}\Big|_{F_s=Z_e X_s} \tag{2.17}$$

$$P_o(s) = \frac{F_m}{X_m}\Big|_{F_s=0} \tag{2.18}$$

The reproducibility is an index of reproduction of the environmental impedance on the master side and should satisfy $|P_r| = 1$. The operationality evaluates the magnitude of the force an operator feels other than the real reaction force from the environment and should satisfy $|P_o| = 0$.

A position difference between a master device and a slave device was evaluated by the tracking and the drift [62]. The tracking P_t evaluates the difference during the movement without interaction with environments and the drift evaluates the difference when the slave comes into contact with environments. These indices are defined as follows:

$$P_t(s) = \frac{X_m - X_s}{F_m}\Big|_{F_s=0} \tag{2.19}$$

$$P_d(s) = \frac{X_m - X_s}{F_m}\Big|_{F_s=Z_e X_s}. \tag{2.20}$$

P_t and P_d should satisfy $|P_t| = 0$ and $|P_d| = 0$ for perfect coincidence of position both in non-contact and contact motions.

Stability can be evaluated by analyzing the open loop transfer function of a bilateral teleoperation system [63]. Considering the structure shown in Fig. 2-10, the system forms a loop structure connected by an operator and an environment. The open transfer function is derived from the hybrid parameters as follows:

$$P_s(s) = \frac{H_{21}H_{12}Z_e}{(1 - Z_eH_{22})(Z_h - H_{11})}. \tag{2.21}$$

Bilateral Controllers

As mentioned above, the ideal state of the bilateral teleoperation is complete agreement on the position and the force between a master device and a slave device. The control goal can thus be represented by the equations below.

$$X_m - X_s = 0 \tag{2.22}$$

$$F_m + F_s = 0 \tag{2.23}$$

The former equation means perfect position tracking between master and slave devices, while the latter equation means realization of the law of action and reaction between the master and the slave. As a controller design strict to the above goal, coordinate transformation is widely used [64]. Equations (2.22) and (2.23) can be considered as two independent goal: control difference of position to be zero and control sum of force to be zero. Two types of controllers are utilized in this thesis. Both of them are based on the above-mentioned goal and the coordinate transformation. The first controller is a controller proposed based on the idea of functionality [57]. It divides the master-slave system into two independent virtual systems using coordinate transformation and designs a controller for each virtual system. As an advantage of the idea of functionality, controller design becomes simple and clear. The second controller [56] is a controller proposed based on a four-channel architecture [44]. The four-channel-based controller was modified to satisfy the control goal shown in (2.22) and (2.23), and was designed to be acceleration control.

The controller based on functionality is shown in Fig. 2-11. It defines two categories of functions for bilateral teleoperation: a function of coupling and a function of the entire motion. The coupling function is accomplished by controlling a position gap between two devices, while the entire motion function relates to the sum of the state the devices. The master-slave system is thus transformed into two perfectly independent function coordinate systems, which are a common coordinate and a differential coordinate,

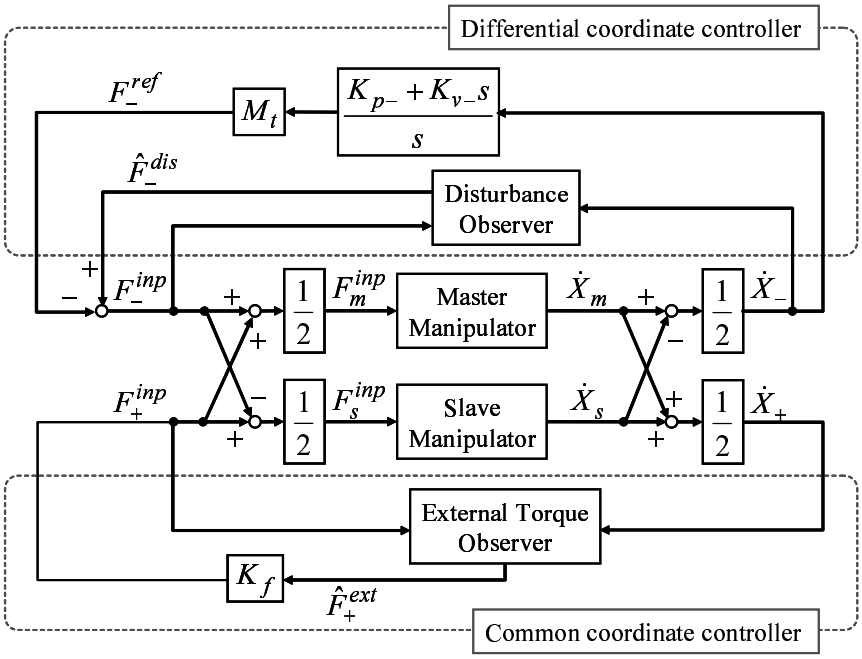

Fig. 2-11: Bilateral controller based on functionality

by using the Hadamard matrix.

$$\begin{bmatrix} X_+ \\ X_- \end{bmatrix} = \frac{1}{2}\begin{bmatrix} 1 & 1 \\ 1 & -1 \end{bmatrix}\begin{bmatrix} X_m \\ X_s \end{bmatrix} = \frac{1}{2}\mathbf{H}_2\begin{bmatrix} X_m \\ X_s \end{bmatrix} \tag{2.24}$$

$$\begin{bmatrix} F_+^{ext} \\ F_-^{ext} \end{bmatrix} = \begin{bmatrix} 1 & 1 \\ 1 & -1 \end{bmatrix}\begin{bmatrix} F_m^{ext} \\ F_s^{ext} \end{bmatrix} = \mathbf{H}_2\begin{bmatrix} F_m^{ext} \\ F_s^{ext} \end{bmatrix}, \tag{2.25}$$

where subscripts $+$ and $-$ denote common and differential coordinates, F^{ext} denotes an external force, F^{inp} denotes a control input, and $\mathbf{H}_2$ denotes the quadratic Hadamard matrix. The velocity $\dot{X}$ is transformed in parallel to position, and the control input F^{inp} is transformed in parallel to the external force. Since master and slave devices are transformed into independent coordinates without any interference element, it is possible to treat the entire system as two independent virtual objects. The dynamics of the virtual objects are expressed in the following equations:

$$M_t\ddot{X}_+ + c_t\dot{X}_+ = F_+^{inp} + F_+^{ext} \tag{2.26}$$

$$M_t\ddot{X}_- + c_t\dot{X}_- = F_-^{inp} + F_-^{ext}, \tag{2.27}$$

where

$$M_t = M_m + M_s$$

$$c_t = c_m + c_s.$$

Here, c denotes a friction coefficient. Position control and the disturbance observer are applied to the differential coordinate to realize the rigid coupling function and the reaction force observer and force control are applied to the common coordinate to realize the inertia manipulation function. The control input of each coordinate is given as the equations below.

$$F_+^{inp} = K_f \hat{F}_+^{ext} \tag{2.28}$$

$$F_-^{inp} = -M_t(K_{p-}X_- + K_{v-}\dot{X}_-) + \hat{F}_-^{dis}, \tag{2.29}$$

where $\hat{F}_+^{ext}$ denotes an estimated external force in the common coordinate acquired through the reaction force observer and $\hat{F}_-^{dis}$ denotes an estimated disturbance force in the differential coordinate acquired through the disturbance observer. The inputs to the master and slave devices are derived as follows:

$$\begin{bmatrix} F_m^{inp} \\ F_s^{inp} \end{bmatrix} = \frac{1}{2}\begin{bmatrix} 1 & 1 \\ 1 & -1 \end{bmatrix}\begin{bmatrix} F_+^{inp} \\ F_-^{inp} \end{bmatrix} = \frac{1}{2}\mathbf{H}_2^{-1}\begin{bmatrix} F_+^{inp} \\ F_-^{inp} \end{bmatrix}. \tag{2.30}$$

The controller proposed in [56] is explained next. The whole structure of the controller is shown in Fig. 2-12. It is based on the four-channel-based controller that describes the general structure of the bilateral teleoperation system [44][65]. In order to satisfy the ideal condition shown in (2.15), controllers C_1, C_4, C_m, and C_s are designed as position controllers, and C_2, C_3, C_5, and C_6 are designed as force controllers.

$$C_1 = C_4 = C_m = C_s = C_p(s) = K_p + K_v s \tag{2.31}$$

$$C_2 = C_3 = C_5 = C_6 = C_f(s) = K_f \tag{2.32}$$

The acceleration references for the master and slave devices are derived as follows:

$$\ddot{X}_m^{ref} = -C_p(s)X_D - C_f(s)F_C \tag{2.33}$$

$$\ddot{X}_s^{ref} = C_p(s)X_D - C_f(s)F_C, \tag{2.34}$$

where

$$X_D = X_m - X_s \tag{2.35}$$

$$F_C = F_m + F_s. \tag{2.36}$$

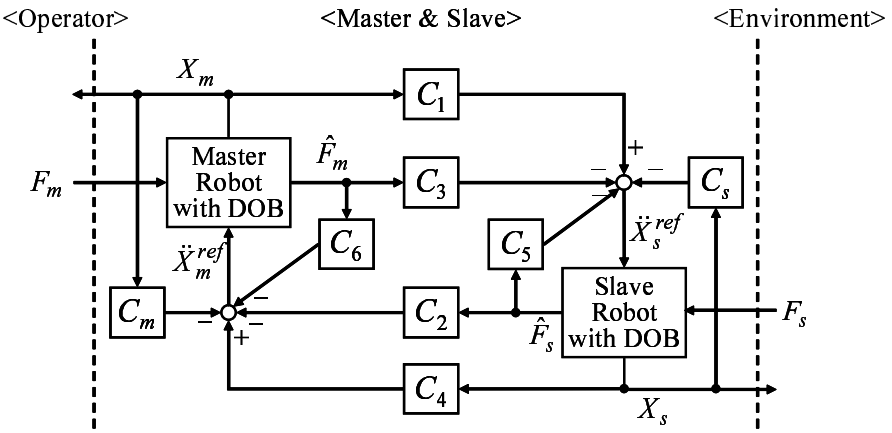

Fig. 2-12: Bilateral controller based on four-channel structure

The disturbance observer is applied to each manipulator in order to achieve the acceleration equal to the reference.

The two types of controllers explained above were designed from a different standpoints. However, they have many common points: they have the same control goal; position control and force control are designed separately; and both are based on acceleration control. The main difference is that the controller shown in Fig. 2-11 achieves acceleration control in the function (mode) coordinate, while the controller shown in Fig. 2-12 achieves it with a focus on each robot. Since the idea of functionality is intuitive and easily understandable, the design of the controller shown in Fig 2-11 is simple and clear. The controller shown in Fig. 2-12 is preferable in some cases, however, since it assures the robustness in each manipulator. The controller is easier to be implemented in the cases where the systems are largely different between the master and the slave, the system parameters are unknown, or the master device and the slave device need to be controlled separately due to a network between them. This thesis therefore uses the controller shown in Fig. 2-11 for a system without a network and uses the controller shown in Fig. 2-12 for a system connected through a network.

In the simulation or analysis, the input of an operator and an environment are modeled as a spring and damper model as shown in Fig. 2-13 and the following equations.

$$F_h = K_h(-X_h + X_m) + D_h(-\dot{X}_h + \dot{X}_m) \tag{2.37}$$

$$F_e = \begin{cases} K_e(-X_e + X_s) + D_e\dot{X}_s & (X_s > X_e) \\ 0 & (X_s \leq X_e) \end{cases} \tag{2.38}$$

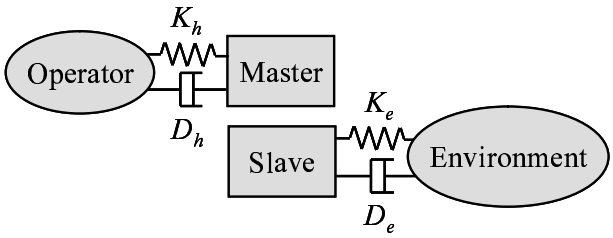

Fig. 2-13: Model of operator and environment

2.5 Problems in Application of Robust Motion Control Based on Acceleration Control

In application of motion control to real systems, there are various factors limiting the performance. This section explains examples of the limiting factors and their influences. Through the discussion, this section also clarifies issues to be tackled in order to improve performance of motion control based on acceleration control and to expand its application to a variety of systems.

As mentioned in Section 2.2, acceleration control is a key technique for robust motion control since position and force can be dealt with in a unified manner by using acceleration and higher robustness can be attained regardless of desired motions by acceleration control. In acceleration control-based systems, the performance of the disturbance observer imposes the great influence on the performance of the whole control system. Since disturbance suppression performance is determined by the cutoff frequency and acceleration control is achieved only in the frequency range lower than the cutoff frequency of the disturbance observer, it is important to heighten the cutoff frequency. The followings are listed as main factors that limit the cutoff frequency.

- sampling period
- noise

Both factors relate to derivative calculation. The sampling period has the profound influence on the performance of motion control because control of a robot is executed in discrete-time using a device such as a computer in recent years. Higher performance is usually achieved with a shorter sampling period. The relationship between the sampling period and the limitation of the cutoff frequency of the disturbance observer has also been discussed [30] [31] [66]. The upper limit of the cutoff frequency for stable operation is increased theoretically by shortening the sampling period. The sampling period cannot be

shortened, however, due to various limitations. It is therefore important to deal with the limitations on the sampling period. A calculation time of a computer, a processing time of a counter, an analog-to-digital (A/D) converter, or a digital-to-analog (D/A) converter, a frequency of pulse width modulation (PWM), and processing rates of sensors are examples of factors limiting the sampling period. Meanwhile, the main cause of noise in the motor control is quantization errors of an encoder for position measurement. Derivative calculation amplifies the errors and generates high frequency noise. High frequency noise imposes a negative effect and even destabilizes the system. Since calculation in the disturbance observer is performed in an acceleration dimension, twice of derivative calculation is required when a position signal from an encoder is used for control. Two low pass filters are then introduced in the observer calculation to suppress the high frequency noise. It is usually impossible to distinguish noise from other signals. The magnitude of noise and the cutoff frequency are thus in the trade-off relation. Although the noise can be suppressed greatly by setting the cutoff frequency low, a negative effects are easily conceived that delay becomes long, disturbance suppression performance deteriorates, and the bandwidth of measurement and acceleration control become narrow. On the other hand, the performance is improved by heightening the cutoff frequency but the system is easily affected by the noise. A method for suppressing the noise due to derivative calculation is therefore required for improvement of motion control performance.

Toward expansion of application, there are various problems and limitations peculiar for each application in addition to the limitations on performance of the disturbance observer. For example, network constraints such as communication delay, packet losses, a limitation of throughput or that of a packet transmission interval the performance of a system connected through a network. Difficulties in adaptation to human environments and handling of unknown objects prevent robotic technologies to be used in human environments. Moreover, acquirable information is often limited in complex systems. These issues should be solved upon application. Since introduction of a network to the system and heightening complexity and sophistication of feasible operations are important issues to accelerate future applications, this thesis focuses especially on the difficulties in networked control systems and those in contact motion. Although acquisition of wide-band and accurate signals and an extremely short sampling period are essential for achieving robust motion control, these are limited in the networked control system. The performance of the whole system is thus affected by these limitations [25] [67]. The control system easily becomes unstable when large communication delay exists. Other factors such as packet losses, a throughput limitation, and a limitation of the packet transmission interval can be regarded as limitations on the sampling period and that on quality of transmission signals. Moreover, when a data size

is enlarged without consideration of throughput or a packet transmission interval is set too short, communication delay surges and frequent packet losses occur due to network congestion [68]. In addition to improvement in the network technology itself, acquiring an output signal accurately and adequately and utilizing it appropriately even under the limitations is the key for improving control performance. Thus, delay compensation, appropriate design of sampling periods, data compression, and abstraction and processing of transmission signals are required in correspondence with the above-mentioned limitations. In application to more complicated tasks, contact to and manipulation of unknown objects are inevitable. Difficulties in the contact motion limit the performance of the whole operation. The contact motion increases a risk of destruction of objects and the robot itself and that of destabilization of the control system. The difficulty in the contact motion mainly comes from limitations on acquirable information about the contact and sudden and discontinuous changes in situation: it is difficult to know when the contact event occurs exactly and the characteristics of the objects before making into contact with them. Moreover, it is difficult to grasp the state of the robot accurately when the contact operation is made gently due to noise and error in force measurement. Acquisition of adequate and accurate information, especially recognition of the contact state of the robot, in real-time is a key for a stable contact motion.

The following chapters are devoted to tackle the problems relating to the limitations mentioned above in order to improve performance of robust motion control and to expand application fields of the motion control.

2.6 Summary

This chapter explained robust motion control based on acceleration control as a cornerstone of the topics dealt with in this thesis. Acceleration is a key element in a physical system and wide-band acceleration control is thus necessary to achieve high performance motion control. The disturbance observer was introduced as an effective tool to realize acceleration control. The reaction force observer, which has a structure similar to that of the disturbance observer, was also introduced as a tool to estimate force or torque without a force sensor. The structures of the position control system, force control system, and bilateral control system were shown as examples of motion control systems based on acceleration control. This thesis treats the systems as evaluation targets. The problems and limitations on realization of wide-band acceleration control were described. The issues to be dealt with in this thesis to improve motion control performance and to widen the application fields of motion control were clarified.

Chapter 3

Multirate Sampling Method for Acceleration Control

3.1 Introduction

Robotic systems are generally controlled in discrete-time in recent years, and a controller designed for continuous-time systems (analog) is often converted into that for discrete-time systems (digital) by using zero-order-hold technique. The discretization of a controller raises various control problems, however [69] [70] [71]. Higher performance is usually achieved with the short sampling period. In terms of acceleration control, it is shown that shortening the sampling period is effective to widen the bandwidth in which acceleration control is realized [30]. On the other hand, sampling periods have limitations relating to hardware performances even with recent development of hardware. A calculation time of a computer, a processing time of a counter, an A/D converter or a D/A converter, a frequency of PWM, and processing rates of sensors can be mentioned as examples of limiting factors. In general, one constant sampling period is selected for input ($u(t)$), output ($y(t)$), and controller ($r(t)$). In this thesis, "input" is defined as an input torque or current to a controlled object. "Output" is then defined as information of a controlled object such as position or force acquired with sensors. Considering limitations of sampling periods, the sampling period for a system is usually selected so as to be equal to the longest of those three. In order to achieve better performance under limitations on sampling periods, multirate sampling control has been proposed [22]. In multirate sampling control, sampling periods of input, output, and controller are designed individually. As a result, better performance can be acquired despite hardware limitations. Many studies on multirate sampling control have been performed on systems in

which output information cannot be acquired fast enough for control or input, such as hard-disk drives or visual servo systems [72] [73] [74]. The methods interpolate the output information with a focus on the state between sampling points and update the actuation input with the shorter sampling period. Although tracking of a target trajectory is important in many applications, perfect tracking is usually impossible in general discrete-time control systems because of unstable zeros generated by zero-order holds [69] [70]. Fujimoto *et al.* had proposed the perfect tracking controller (PTC), which realizes zero tracking error by applying multirate feed-forward control, to solve the problem [74]. Multirate sampling methods are also utilized to save computation and to change sampling periods among controllers [75] [76]. In addition, the multirate sampling technique has been widely used in the field of signal processing [77] [78]. Although these researches focus on the limitations on the output or control sampling period, these sampling periods in systems without vision sensors become able to be set shorter these days thanks to improvement in computation performance. Many motor control systems therefore have more severe limitations on the input sampling period than on the output or the control sampling periods.

Output information in motor control is mainly acquired from an optical encoder. Many studies have been performed to increase the rate of acquisition of an encoder signal [79]. It can be acquired in proportion to the clock time of FPGA or DSP. On the other hand, a frequency of a current input is limited by performance of an amplifier or a frequency of PWM and it is difficult to heighten the frequency even with new devices. The output sampling period can therefore be set shorter than the input in many cases. There are only a few researches that set the output sampling period shorter than the input. An example is for utility interactive inverter focusing on behavior during the sampling period which is not compensated in deadbeat control [80].

The aim of this chapter is realization of wide-band acceleration control. This thesis focuses on the relationship between the performance and the sampling frequency of acceleration control. The needs for a higher sampling frequency for an output than for an input are described. From this point of view, this chapter proposes a novel multirate sampling method with a shorter output sampling period. The disturbance observer is redesigned to fit to the multirate sampling system with a new definition of a disturbance torque. The output information acquired in the short sampling period is used only to correct the input value in [80]. In the proposed method, however, the information is utilized not only for correction but for overall controller. As a result, the performance is expected to become close to that of the system which has the short sampling period for both an output and an input. Stability analyses and experiments are performed to make a comparison with single-rate control and to verify the validity of the proposal.

Although the method can be applied to various systems, analyses and experiments are carried out with a single-input single-output (SISO) system to simplify the discussion. Sampling periods focused on in this chapter are as follows:

- input sampling period T_u: sampling period for renewal of current input reference;
- output sampling period T_y: sampling period for acquisition of sensor signal; and
- control sampling period T_r: sampling period for calculation of control input.

3.2 Multirate Sampling Method for Acceleration Control

This section proposes a novel multirate sampling method for precise and wide-band acceleration control. When the disturbance observer shown in Fig. 2-4 is utilized to realize acceleration control, the cutoff frequency of the disturbance observer determines the bandwidth of acceleration control. Robustness is not assured and acceleration control is not realized in the frequency range higher than the cutoff frequency. The maximum value of the cutoff frequency depends on the sampling period of the observer [30]. It is thus important to shorten the sampling period. As mentioned in Section 2.3.1, disturbance calculation in the disturbance observer is performed in an acceleration dimension. Twice of derivative calculation and two LPFs are therefore introduced into the right side (output side) of the disturbance observer. Since the signal acquired through an LPF is delayed, acceleration information in the second term of (2.7) calculated from an encoder signal is delayed compared with the current reference in the first term. It is thus important to reduce the delay by acquiring an output signal in the shorter sampling period rather than inputting delayed values in a high rate. In other words, it is preferable to acquire an output signal in a higher rate than the renewal of an actuation input in order to minimize the influence of the delay.

The author therefore proposes the method shown in Fig. 3-1, in which an output signal is acquired and control calculation is performed several times during one input sampling period. The sampling periods are selected to satisfy Fig. 3-2 and the following equations.

$$T_u = nT_y \tag{3.1}$$

$$T_r = T_y, \tag{3.2}$$

where n is an integer number. The equations show that an input sampling period is set as an integer multiple of the output sampling period and the sampling period of control is set to the same value as the

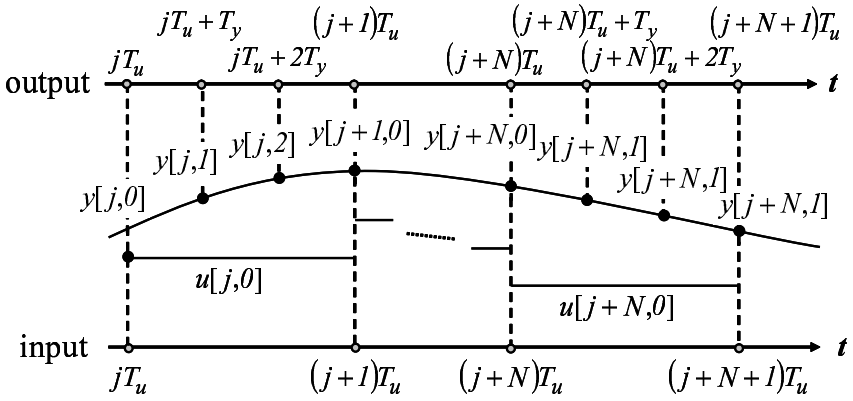

Fig. 3-1: Multirate sampling method for acceleration control

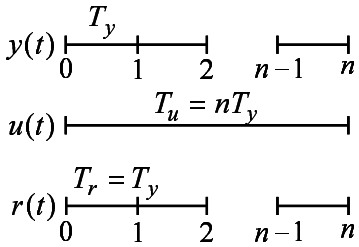

Fig. 3-2: Sampling periods in proposed multirate sampling method

output sampling period. It means that control calculation is performed at every output sampling point and n times in one input sampling period.

The limitations of the sampling periods due to hardware performance also support the adequacy of the proposal. In motor control systems, the main output signal is angular or position information acquired through an optical encoder when vision sensors are not implemented on the system. The limitations of the input sampling period are generally more severe than those on the output in those system. The output sampling period can be selected in proportion to the clock signal of DSP or FPGA. The control sampling period is limited only by the calculation time. Those sampling periods become able to be set shorter and shorter, considering the development of devices such as FPGA or improvement in performance of computers [81] [82]. On the other hand, the frequency of the current input is limited strictly by performance of an amplifier or the frequency of PWM. The output sampling period can therefore be set shorter than the input in many cases and the proposed method is effective also in the practical aspect.

The details of the proposed method are explained below by using state-space equations with consid-

eration of a continuous-time plant represented as follows:

$$\dot{\boldsymbol{x}}(t) = \mathbf{A}\boldsymbol{x}(t) + \boldsymbol{b}u(t) \tag{3.3}$$

$$y(t) = \boldsymbol{c}\boldsymbol{x}(t). \tag{3.4}$$

Assuming that the sampling periods of the input, the output, and control are T_s and the input $u(t)$ remains constant from $t = t_0$ to $t = t_0 + T_s$, the discrete-time plant is represented as follows:

$$\boldsymbol{x}[i+1] = \mathbf{A}_d\boldsymbol{x}[i] + \boldsymbol{b}_d u[i] \tag{3.5}$$

$$y[i] = \boldsymbol{c}_d\boldsymbol{x}[i], \tag{3.6}$$

where $\boldsymbol{x}[i] = \boldsymbol{x}(iT_s)$. Matrix $\mathbf{A}_d$, vectors $\boldsymbol{b}_d$ and $\boldsymbol{c}_d$ are given by

$$\mathbf{A}_d = e^{\mathbf{A}T_s}, \quad \boldsymbol{b}_d = \int_0^{T_s} e^{\mathbf{A}\tau}d\tau\boldsymbol{b}, \quad \boldsymbol{c}_d = \boldsymbol{c}.$$

When a feedback control law is given as $u(t) = f(\boldsymbol{x}(t))$, it is rewritten into the equation below in discrete-time.

$$u[i] = f(\boldsymbol{x}[i]) \tag{3.7}$$

The state-space equations in a multirate sampling system are represented as follows:

$$\boldsymbol{x}[i,k+1] = \mathbf{A}_m\boldsymbol{x}[i,k] + \boldsymbol{b}_m u[i,k] \tag{3.8}$$

$$y[i,k] = \boldsymbol{c}_m\boldsymbol{x}[i,k], \tag{3.9}$$

where

$$\boldsymbol{x}[i,k] = \boldsymbol{x}((i+\frac{k}{n})T_u) = \boldsymbol{x}(iT_u + kT_y)\ (k=0,\cdots,n-1)$$

$$\mathbf{A}_m = e^{\mathbf{A}T_y}, \quad \boldsymbol{b}_m = \int_0^{T_y} e^{\mathbf{A}\tau}d\tau\boldsymbol{b}, \quad \boldsymbol{c}_m = \boldsymbol{c}.$$

Here, i and k are positive integers. The feedback control law in the proposed multirate sampling system is given by the following equation since an actuation input is updated only when $t = iT_u$.

$$u[i,k] = u[i,0] = f(\boldsymbol{x}[i,0]) \tag{3.10}$$

This equation shows that the actuation input remains constant from $t = iT_u$ to $t = (i+1)T_u$. In the proposed multirate sampling method, the state-space equations (3.5) and (3.6) are therefore rewritten into the equations below, with consideration of the relation between the input and output sampling periods.

$$\boldsymbol{x}[i,k+1] = \mathbf{A}_m\boldsymbol{x}[i,k] + \boldsymbol{b}_m u[i,0] : k \neq n-1 \tag{3.11}$$

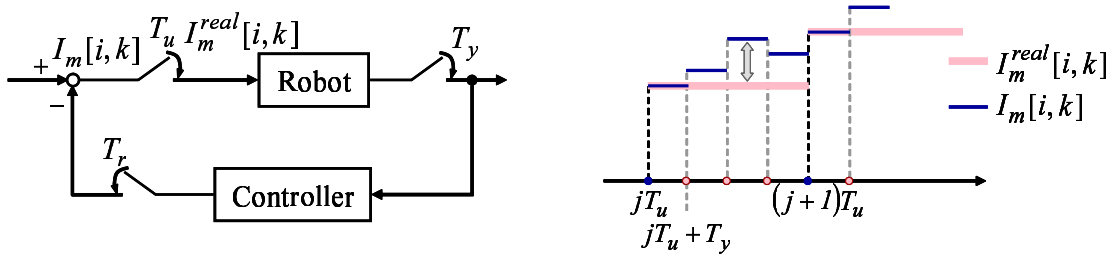

(a) structure of system

(b) renewal of desired and real inputs

Fig. 3-3: Relation between two input values in the proposed multirate sampling method

$$\boldsymbol{x}[i+1,0] = \mathbf{A}_m\boldsymbol{x}[i,n-1] + \boldsymbol{b}_m u[i,0] : k{=}n-1 \tag{3.12}$$

$$y[i,k] = \boldsymbol{c}_m\boldsymbol{x}[i,k] \tag{3.13}$$

3.3 Observers for Multirate Sampling System

This section proposes a disturbance observer and a reaction force observer for the proposed multirate sampling system. Application of observers to multirate sampling systems was discussed in [83]. However, it shows just an extension of observers to multirate sampling systems and does not focus especially on the characteristics of a system with the short control sampling period. The author therefore presents design of the observers with a focus on the characteristics of the system and the role of each observer. As the characteristics of the proposed multirate sampling system, there are two values of an input: a desired input value $I_m[i,k]$ and a real input value $I_m^{real}[i,k]$. The desired input value is the output of the controller calculated at the output sampling rate and the real input value is the real input reference value renewed at the input sampling rate. Considering (3.10), the relation between those two values can be expressed as in Fig. 3-3 and the following equation.

$$I_m^{real}[i,k] = I_m[i,0] \tag{3.14}$$

This equation shows that a difference exists between those two values when $k \neq 0$, i.e., $t \neq iT_u$. The following subsections propose observers for the multirate sampling system with a focus on the difference between those two input values.

The role of each observer is discussed before explaining the proposals of observers. Although the disturbance observer and the reaction force observer have almost the same structure, their roles differ largely. The disturbance observer is to estimate and compensate the entire disturbance, which is an aspect

not expected to exist, to realize robust acceleration control. A designer can determine the definition of the disturbance estimated in the disturbance observer with consideration of a desired state in the control. On the other hand, the reaction force observer is expected to estimate a real external force. It means that the aspect to be estimated by the reaction force observer is always the real external force, regardless of the idea of a designer. The disturbance observer and the reaction force observer for the multirate sampling system are proposed considering the above-mentioned points.

Observers are designed by using the Gopinath's method [84] in discrete-time because the multirate sampling system is a discrete-time system. In this thesis, however, the author dares to use the Laplace variable in figures and equations to make the correspondence of each figure or equation with those shown in Chapter 2.

3.3.1 Disturbance Observer for Multirate Sampling System

Application of Conventional Disturbance Observer

The conventional disturbance observer is expanded to the multirate sampling system in Fig. 3-4(a). The disturbance torque defined in the conventional disturbance observer shown in (2.5) is represented by the following equation in the multirate sampling system.

$$\tau_{dis}[i,k] = \tau_l[i,k] + \Delta J\ddot{\theta}[i,k] - \Delta K_t I_m^{real}[i,k] \tag{3.15}$$

The disturbance torque is estimated from a real input reference value $I_m^{real}[i,k]$ and the velocity using the equation below.

$$\hat{\tau}_{dis} = \frac{g_{dis}}{s+g_{dis}}(K_{tn} I_m^{real}[i,k] - J_n s^2\theta[i,k]) \tag{3.16}$$

Disturbance Observer for Proposed Multirate Sampling System

Equation (3.14) shows that there is a deviation between a desired input value and a real input reference value when $t \neq iT_u$. It means that a control input is calculated but the value is not applied to the real input in some sampling points. Although the influence of the deviation is not considered in the conventional disturbance observer, it may affect the system. With a focus on that, a total disturbance torque of the multirate sampling system is redefined as the equation below to include the influence of the deviation of the input values.

$$\tau_{mdis}[i,k] = \tau_l[i,k] + \Delta J\ddot{\theta}[i,k] - \Delta K_t I_m[i,k] + (K_{tn} + \Delta K_t)\Delta I_m[i,k], \tag{3.17}$$

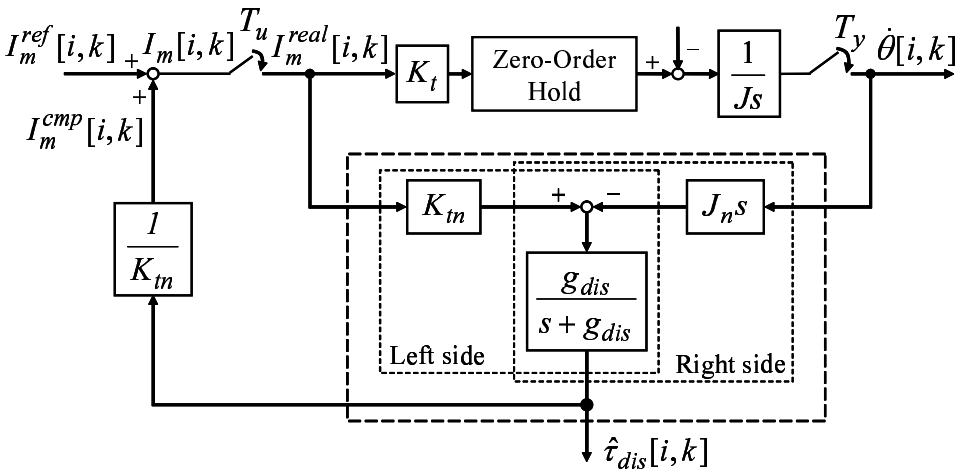

(a) conventional disturbance observer in multirate sampling system

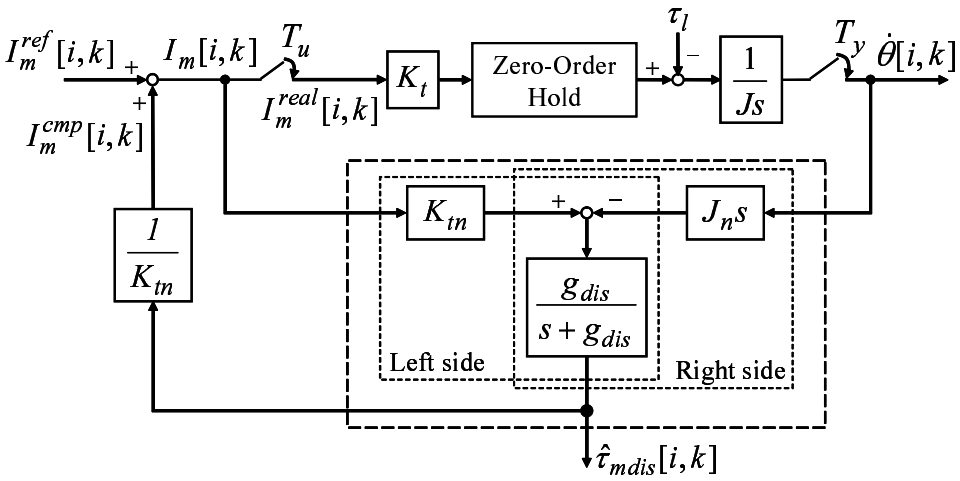

(b) proposed disturbance observer for multirate sampling system

Fig. 3-4: Disturbance observer for multirate sampling system

where

$$\Delta I_m[i,k] = I_m[i,k] - I_m^{real}[i,k].$$

The absence of updating the input value, in other words, the influence of the input sampler, is considered as a sort of disturbance in this definition. It is expressed in the last term of (3.17): $(K_{tn}+\Delta K_t)\Delta I_m[i,k]$. It is necessary to use $I_m[i,k]$ instead of $I_m^{real}[i,k]$ to include the influence of the sampler existing between a desired value and a real value. The disturbance observer in the multirate sampling system is therefore proposed as shown in Fig. 3-4(b). The total disturbance torque of the multirate sampling system is

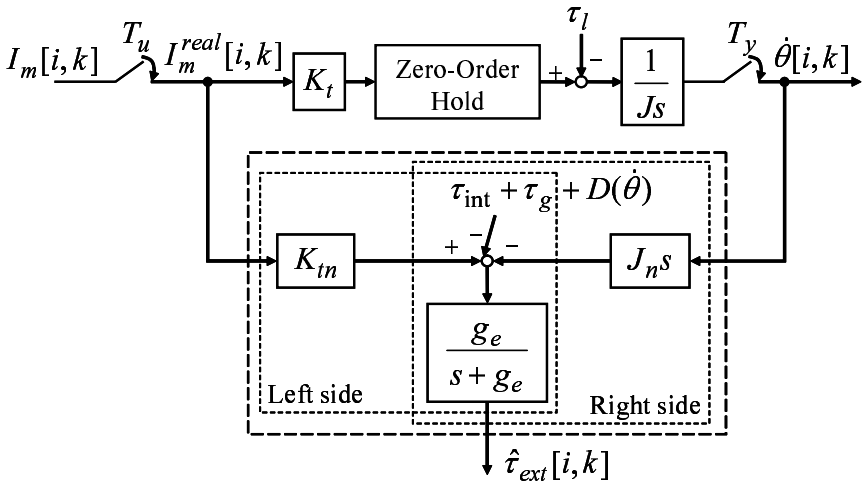

Fig. 3-5: Reaction force observer for multirate sampling system

estimated by the following equation.

$$\hat{\tau}_{mdis} = \frac{g_{dis}}{s + g_{dis}}(K_{tn} I_m[i,k] - J_n s^2 \theta[i,k]) \tag{3.18}$$

By compensating the estimated disturbance torque $\hat{\tau}_{mdis}[i,k]$, it is possible to compensate the influence of a difference between desired and real input values, which occurs due to renewal of the input value with the longer sampling period than the output. The system is expected to become similar to that with the short sampling period for both input and output by using the proposed disturbance observer.

3.3.2 Reaction Force Observer for Multirate Sampling System

The reaction force observer explained in Section 2.3.2 is expanded to the multirate sampling system in this subsection. Although the reaction force observer and the disturbance observer have almost the same mechanism, their roles differ largely. Since the disturbance observer is to estimate and compensate the entire disturbance on the system, a desired input value $I_m[i,k]$ is utilized. On the other hand, the reaction force observer is expected to estimate the real external force. It is therefore required in the reaction force observer to use a real current input to a motor. Assuming that current feedback loop is fast enough, the real input current is considered to be equal to $I_m^{real}[i,k]$. The reaction force observer is thus expanded as shown in Fig. 3-5 in the proposed multirate sampling method. The reaction torque is estimated through an LPF as shown in the equation below.

$$\hat{\tau}_{ext}[i,k] = \frac{g_e}{s + g_e}(K_{tn} I_m^{real}[i,k] - J s^2 \theta[i,k] - (\tau_{int} + \tau_g + F + D(\dot{\theta}))) \tag{3.19}$$

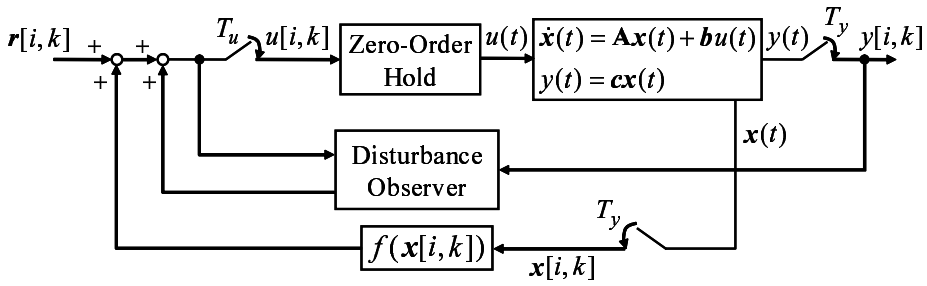

Fig. 3-6: Multirate acceleration control system

Note that a real input reference value $I_m^{real}[i,k]$ is utilized instead of $I_m[i,k]$ in the reaction torque estimation.

3.4 Expected Advantage of Application of Multirate Sampling Method

The overall structure of the proposed method is shown in Fig. 3-6. The following advantages are expected for the proposed multirate sampling method:

- cutoff frequencies of the observers can be set higher; and
- information of disturbance can be detected in an early timing.

The first advantage is derived from its higher sampling frequency and larger number of sampled data for observer calculation. The influence of discretization is decreased by shortening the sampling period of the observer. The limitation of the cutoff frequency relates to the sampling period and noise. The short sampling period reduces noise by repeated calculation. The cutoff frequency can therefore be set higher with the shorter sampling period, as described in [30]. The limitation of the cutoff frequency becomes high with the multirate sampling method since both noise and the influence of discretization are reduced. The second advantage is explained referring to Fig. 3-7. In the single-rate system, the influence of the disturbance τ_{dis1} exerted at $t = t_1$ and τ_{dis2} at $t = t_2$ are both recognized at $t = t_0 + T_u$. On the other hand, in the multirate sampling system, the influence of τ_{dis1} and τ_{dis2} are recognized at $t_0 + T_y$ and $t_0 + T_u$, respectively. Detection of the disturbance influence is generally delayed half the output sampling period in average. When the sampling periods in the multirate control satisfy $T_u = nT_y = T_s$ and those in the single-rate control satisfy $T_u = T_y = T_s$, the average length of delay is $T_s/2n$ in the multirate and $T_s/2$ in the single-rate. It shows that the average length of delay becomes n times shorter with the

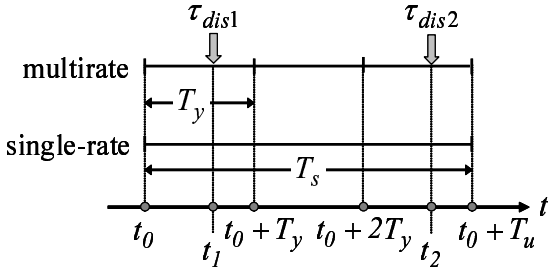

Fig. 3-7: Delay in disturbance detection

multirate sampling method. In other words, detection becomes early for $(n-1)T_s/2n$ in average.

The proposed multirate sampling method has a similarity to the upsampling technique in the point that output sampling points are inserted between input sampling points. These are completely different, however, in how output values between input sampling points are acquired. The upsampling technique is one of signal processing techniques, which is used to increase a sampling rate of a signal. An output signal is actually measured in the proposed method, while the values are not measured but produced by interpolation in the upsampling. The upsampling technique increases the sampling rate by inserting zero at sampling points between the original sampling points and filtering it using an anti-aliasing filter. Since the sampling period for observer calculation is shortened also in the upsampling, decrease in the influence of discretization of the observer is also expected in the upsampling. Heightening of the cutoff frequency of the disturbance observer can thus be expected. On the other hand, a bandwidth of a measured signal is not widened in the upsampling since measurement is not performed with a high sampling rate. Moreover, the second advantage of the proposed method, which is the early detection of the disturbance, cannot be achieved with the upsampling. The advantage is achieved only when an output signal is measured with the short sampling period. The proposed method is thus superior to the upsampling method.

Next, expected effects of the above-mentioned points are explained. The effect of the former point is that control performance improves owing to decrease in the delay in information in an acceleration dimension. Robustness also improves since the bandwidth of acceleration control is widened. The latter point is achieved only by acquiring a real signal with the short sampling period without using any interpolation schemes. Owing to the latter point, the response to disturbances becomes faster and robustness against disturbance improves.

On the other hand, the absence of updating the compensation input that occurs in the proposed method may limit or even deteriorate the performance. The proposed disturbance observer enables the system to

estimate the disturbance including the influence of the absence of updating. Higher performance can be obtained by compensating the value. The performance is expected to become close to that achieved with the short sampling period for both input and output.

With consideration of the above-mentioned points, it is preferable to set the output sampling period as short as possible. The problems caused by shortening the output sampling period are easily imagined, however. One is increase in calculation cost. Since a control sampling period is set to be equal to the output sampling period, calculation cost increases by shortening the output sampling period. Another is increase of noise in velocity. When M method, which calculates the velocity by counting the number of pulses generated in the constant sampling period, is used to derive the velocity from a position signal, the velocity and acceleration resolutions deteriorate by shortening the sampling period. The problem due to encoder resolution is discussed in later chapters.

The following sections are devoted to verify the effectiveness of the proposed multirate sampling method in various applications in terms of stability, performance and applicability.

3.5 Application to Position Control

This section applies the multirate sampling method proposed in Section 3.2 and the disturbance observer proposed in Section 3.3 to the acceleration control-based position control system shown in Fig. 2-7(b). The influence of the proposed method on stability and robustness of the system are verified through stability analysis, simulations, and experiments.

3.5.1 Stability Analysis

Stability analyses of both the single-rate control and the proposed multirate control were performed to verify the validity of the proposed method. The block diagram of the whole system utilized for the analysis is shown in Fig. 3-8.

Modeling

A dynamic equation of a single-link manipulator in discrete-time is shown in the following equation:

$$\begin{bmatrix} \theta[i+1] \\ \dot{\theta}[i+1] \\ \tau_{dis}[i+1] \end{bmatrix} = \begin{bmatrix} 1 & T_s & -\frac{T_s^2}{2J} \\ 0 & 1 & -\frac{T_s}{J} \\ 0 & 0 & 1 \end{bmatrix} \begin{bmatrix} \theta[i] \\ \dot{\theta}[i] \\ \tau_{dis}[i] \end{bmatrix} + \begin{bmatrix} \frac{T_s^2}{2J} \\ \frac{T_s}{J} \\ 0 \end{bmatrix} \tau_m[i], \tag{3.20}$$

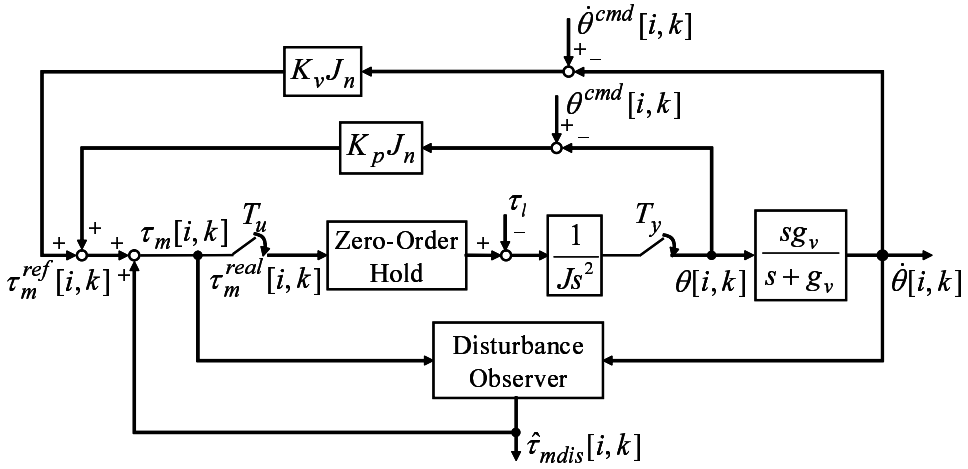

Fig. 3-8: Analysis model of multirate position control

where τ_m denotes an input torque. The input torque and the disturbance torque are assumed to be constant between two consecutive sampling points. A PD controller and the disturbance observer are applied to the system. The sampling periods T_u and T_y are set to be equal in the single-rate control and set to satisfy $T_u = nT_y$ in the multirate control. The control sampling period T_r is set to be equal to T_y in both cases.

Firstly, modeling in the single-rate control is described below. The state-space equation (3.20) is expanded so as to include state variables in the disturbance observer $w_1[i]$ and in pseudo-derivative $w_2[i]$. The disturbance observer is designed based on the Gopinath's method, and pseudo-derivative calculation is utilized to derive velocity from the position signal. The state-space equations are represented as follows:

$$\boldsymbol{x}[i+1] = \mathbf{A}_d \boldsymbol{x}[i] + \boldsymbol{b}_d u[i] \tag{3.21}$$

$$y[i] = \boldsymbol{c}_d \boldsymbol{x}[i], \tag{3.22}$$

where

$$\boldsymbol{x}[i] = \begin{bmatrix} \theta[i] & \dot{\theta}[i] & \tau_{dis}[i] & w_1[i] & w_2[i] \end{bmatrix}^T,\ u[i] = \tau_m[i]$$

$$\mathbf{A}_d = \begin{bmatrix} 1 & T_s & -\frac{T_s^2}{2J} & 0 & 0 \\ 0 & 1 & -\frac{T_s}{J} & 0 & 0 \\ 0 & 0 & 1 & 0 & 0 \\ \hat{b}g_v & 0 & 0 & \hat{a} & \hat{b}g_v(\beta-1) \\ 1 & 0 & 0 & 0 & \beta \end{bmatrix},\ \boldsymbol{b}_d = \begin{bmatrix} \frac{T_s^2}{2J} \\ \frac{T_s}{J} \\ 0 \\ \hat{j} \\ 0 \end{bmatrix}$$

$$\boldsymbol{c}_d = \begin{bmatrix} 1 & 0 & 0 & 0 & 0 \end{bmatrix}^T$$

$$\begin{aligned}\hat{a} &= \alpha,\ \hat{j} = 1-\alpha,\ \hat{b} = \frac{J}{T_s}(1-\alpha)^2,\\ \alpha &= e^{-g_{dis}T_s},\ \beta = e^{-g_v T_s}.\end{aligned}$$

The velocity calculated with pseudo-derivative technique and the estimated disturbance torque are given by the following equations:

$$\hat{\dot{\theta}}[i] = g_v(\beta-1)w_2[i] + g_v\theta[i] \tag{3.23}$$

$$\hat{\tau}_{dis}[i] = w_1[i] - l_1\hat{\dot{\theta}}, \tag{3.24}$$

where

$$l_1 = \frac{J}{T_s}(1-\alpha). \tag{3.25}$$

The control law is expressed by the following equations:

$$\boldsymbol{w}[i+1] = \hat{\mathbf{A}}\boldsymbol{w}[i] + \hat{\boldsymbol{b}}\theta[i] + \hat{\boldsymbol{j}}\tau_m[i] \tag{3.26}$$

$$\hat{\boldsymbol{x}}[i] = \hat{\mathbf{C}}\boldsymbol{w}[i] + \hat{\boldsymbol{d}}\theta[i] \tag{3.27}$$

$$\tau_m[i] = \boldsymbol{k}_d^T(\boldsymbol{r}[i] - \hat{\boldsymbol{x}}[i]), \tag{3.28}$$

where

$$\begin{aligned}\boldsymbol{w}[i] &= \begin{bmatrix} w_1[i] & w_2[i] \end{bmatrix}^T,\ \hat{\boldsymbol{x}} = \begin{bmatrix} \theta[i] & \hat{\dot{\theta}}[i] & \hat{\tau}_{dis}[i] \end{bmatrix}^T\\ \hat{\mathbf{A}} &= \begin{bmatrix} \hat{a} & \hat{b}g_v(\beta-1) \\ 0 & \beta \end{bmatrix},\ \hat{\boldsymbol{b}} = \begin{bmatrix} \hat{b}g_v \\ 1 \end{bmatrix},\ \hat{\boldsymbol{j}} = \begin{bmatrix} \hat{j} \\ 0 \end{bmatrix}\\ \hat{\mathbf{C}} &= \begin{bmatrix} 0 & 0 \\ 0 & g_v(\beta-1) \\ 1 & -l_1 g_v(\beta-1) \end{bmatrix},\ \hat{\boldsymbol{d}} = \begin{bmatrix} 1 \\ g_v \\ -l_1 g_v \end{bmatrix}\\ \boldsymbol{k}_d &= \begin{bmatrix} K_p J_n & K_v J_n & -1 \end{bmatrix}^T,\end{aligned}$$

and $\boldsymbol{r}[i]$ denotes a control reference, i.e., a command. Equations (3.26) and (3.27) can be rewritten in the following equation.

$$\hat{\boldsymbol{x}}[i] = \boldsymbol{k}_y(z)\theta[i] + \boldsymbol{k}_u(z)\tau_m[i] \tag{3.29}$$

Here, $\boldsymbol{k}_y(z)$ and $\boldsymbol{k}_u(z)$ are 1×3 vectors derived from (3.26) and (3.27) by transforming them into transfer function expression. The transfer function of the system $L(z)$ and that of the controller $G_1(z)$ in Fig. 3-9

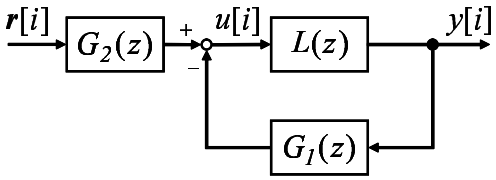

Fig. 3-9: Structure of general control system

are obtained as follows:

$$L(z) = \boldsymbol{c}_d(z\mathbf{I} - \mathbf{A}_d)^{-1}\boldsymbol{b}_d \tag{3.30}$$

$$G_1(z) = (1 + \boldsymbol{k}_d^T \cdot \boldsymbol{k}_u)^{-1}\boldsymbol{k}_d^T \cdot \boldsymbol{k}_y. \tag{3.31}$$

Next, the modeling of the system with the multirate sampling method and the disturbance observer proposed in the previous sections is described. Considering that there are two types of the input torque, the state-space equations are represented as follows:

$$\boldsymbol{x}[i, k+1] = \mathbf{A}_m\boldsymbol{x}[i, k] + \mathbf{B}_m \begin{bmatrix} \tau_m^{real}[i, k] \\ \tau_m[i, k] \end{bmatrix} \tag{3.32}$$

$$y[i, k] = \boldsymbol{c}_m\boldsymbol{x}[i, k], \tag{3.33}$$

where

$$\begin{aligned} \mathbf{A}_m &= \mathbf{A}_d \\ \mathbf{B}_m &= \begin{bmatrix} \frac{T_s^2}{2J} & \frac{T_s}{J} & 0 & 0 & 0 \\ 0 & 0 & 0 & \hat{j} & 0 \end{bmatrix}^T \\ \boldsymbol{c}_m &= \boldsymbol{c}_d,\ T_s = T_y. \end{aligned}$$

Here, τ_m denotes a desired input torque and τ_m^{real} denotes a real input torque. The input torques are given by the following equations when the reference is assumed as $\boldsymbol{r}[i] = \mathbf{0}$.

$$\tau_m[i, k] = J_n(-K_p\theta[i, k] - K_v\hat{\dot{\theta}}[i, k]) + \hat{\tau}_{mdis}[i, k] \tag{3.34}$$

$$\tau_m^{real}[i, k] = \tau_m[i, 0] \tag{3.35}$$

Equations (3.32) and (3.33) are state-space equations described for the shorter sampling period, that is, the output sampling period. It is necessary for analysis, however, to describe the system for the longer sampling period. In order to rewrite the system for the longer sampling period, there are two types of alternatives. One is to choose a high-dimensional state-space and obtain a set of equations with simple

coefficients. The other is to choose a low dimensional state-space and obtain a set of equations with more complicated coefficients. The former method [85] proposed by Araki *et al.* is used in this thesis. The state vectors are expanded as follows:

$$\boldsymbol{x}_M[i] = \begin{bmatrix} \boldsymbol{x}[i-1,1] \\ \vdots \\ \boldsymbol{x}[i-1,n-1] \\ \boldsymbol{x}[i,0] \end{bmatrix}, \boldsymbol{y}_M[i] = \begin{bmatrix} y[i,0] \\ \vdots \\ y[i,n-1] \end{bmatrix}. \tag{3.36}$$

The expanded reference $\boldsymbol{r}_M[i]$ and the expanded control signal $\boldsymbol{\tau}_{mM}[i]$ are defined in parallel to $\boldsymbol{y}_M[i]$. The state-space equations of the expanded system are represented in the equations below.

$$\boldsymbol{x}_M[i+1] = \mathbf{A}_M\boldsymbol{x}[i] + \mathbf{B}_M\boldsymbol{\tau}_{mM}[i] \tag{3.37}$$

$$\boldsymbol{y}_M[i] = \mathbf{C}_M(\mathbf{U}_1\boldsymbol{x}_M[i+1] + \mathbf{U}_2\boldsymbol{x}_M[i]), \tag{3.38}$$

where

$$\mathbf{A}_M = \begin{bmatrix} 0 & \cdots & 0 & \mathbf{A}_m \\ \vdots & \ddots & \vdots & \vdots \\ 0 & \cdots & 0 & \mathbf{A}_m^n \end{bmatrix}$$

$$\mathbf{B}_M = \begin{bmatrix} \mathbf{B}_0 \\ \mathbf{A}_m\mathbf{B}_0 + \mathbf{B}_1 \\ \vdots \\ \mathbf{A}_m^{n-1}\mathbf{B}_0 + \mathbf{A}_m^{n-2}\mathbf{B}_1 + \cdots + \mathbf{A}_m\mathbf{B}_{n-2} + \mathbf{B}_{n-1} \end{bmatrix}$$

$$\mathbf{B}_p = \begin{bmatrix} \boldsymbol{b}_1 & \cdots & \boldsymbol{b}_{p+1} & \cdots & \boldsymbol{b}_n \end{bmatrix}$$

$$\boldsymbol{b}_1 = \begin{bmatrix} \frac{T_s^2}{2J} & \frac{T_s}{J} & 0 & 0 & 0 \end{bmatrix}^T$$

$$\boldsymbol{b}_{p+1} = \begin{bmatrix} 0 & 0 & 0 & \hat{j} & 0 \end{bmatrix}^T$$

$$\boldsymbol{b}_q = \begin{bmatrix} 0 & 0 & 0 & 0 & 0 \end{bmatrix}^T \ (q \neq 1, p+1)$$

$$\mathbf{C}_M = \begin{bmatrix} \mathbf{0} & \cdots & \cdots & \mathbf{0} & \boldsymbol{c}_m \\ \boldsymbol{c}_m & \mathbf{0} & \cdots & \cdots & \mathbf{0} \\ \mathbf{0} & \boldsymbol{c}_m & \mathbf{0} & \cdots & \mathbf{0} \\ \vdots & & \ddots & & \vdots \\ \mathbf{0} & \cdots & \cdots & \boldsymbol{c}_m & \mathbf{0} \end{bmatrix}$$

$$\mathbf{U}_1 = \text{block diag}\,(\mathbf{I}_n, \cdots, \mathbf{I}_n, \mathbf{0})$$

$$\mathbf{U}_2 = \text{block diag}\,(\mathbf{0}, \cdots, \mathbf{0}, \mathbf{I}_n),$$

and a subscript M denotes the expanded matrices. The control law must also be rewritten for the longer sampling period. The expanded variable $\boldsymbol{w}_M[i]$ is defined in parallel to $\boldsymbol{x}_M[i]$, while $\hat{\boldsymbol{x}}_M[i]$ is in parallel to $\boldsymbol{y}_M[i]$. The control law expressed in (3.26) to (3.28) is expanded for the expanded system as the following equations.

$$\begin{aligned}
\boldsymbol{w}_M[i+1] &= \hat{\mathbf{A}}_M \boldsymbol{w}_M[i] + \hat{\mathbf{B}}_M \boldsymbol{y}_M[i] + \hat{\mathbf{J}}_M \boldsymbol{\tau}_{mM}[i] && (3.39)\\
\hat{\boldsymbol{x}}_M[i] &= \hat{\mathbf{C}}_M(z\bar{\mathbf{U}}_1 + \bar{\mathbf{U}}_2)\boldsymbol{w}_M[i] + \hat{\mathbf{D}}_M \boldsymbol{y}_M[i] && (3.40)\\
\boldsymbol{\tau}_{mM}[i] &= \mathbf{K}_{dM}(\boldsymbol{r}_M[i] - \hat{\boldsymbol{x}}_M[i]), && (3.41)
\end{aligned}$$

where

$$\begin{aligned}
\hat{\mathbf{B}}_M &= \begin{bmatrix} \hat{\mathbf{B}} & \mathbf{0} & \cdots & \mathbf{0} \\ \hat{\mathbf{A}}\hat{\mathbf{B}} & \hat{\mathbf{B}} & \mathbf{0} & \mathbf{0} \\ \vdots & & \ddots & \\ \hat{\mathbf{A}}^{n-1}\hat{\mathbf{B}} & \hat{\mathbf{A}}^{n-2}\hat{\mathbf{B}} & \vdots & \hat{\mathbf{B}} \end{bmatrix} \\
\hat{\mathbf{J}}_M &= \begin{bmatrix} \hat{\boldsymbol{j}} & \mathbf{0} & \cdots & \mathbf{0} \\ \hat{\mathbf{A}}\hat{\boldsymbol{j}} & \hat{\boldsymbol{j}} & \mathbf{0} & \mathbf{0} \\ \vdots & & \ddots & \\ \hat{\mathbf{A}}^{n-1}\hat{\boldsymbol{j}} & \hat{\mathbf{A}}^{n-2}\hat{\boldsymbol{j}} & \vdots & \hat{\boldsymbol{j}} \end{bmatrix} \\
\bar{\mathbf{U}}_1 &= \text{block diag}\,(\mathbf{I}_2, \cdots, \mathbf{I}_2, \mathbf{0}) \\
\bar{\mathbf{U}}_2 &= \text{block diag}\,(\mathbf{0}, \cdots, \mathbf{0}, \mathbf{I}_2) \\
\hat{\mathbf{D}}_M &= \text{block diag}\,(\hat{\boldsymbol{d}}, \cdots, \hat{\boldsymbol{d}}).
\end{aligned}$$

The expanded matrices $\hat{\mathbf{A}}_M$, $\hat{\mathbf{C}}_M$, and $\mathbf{K}_{dM}$ are expanded expression of $\hat{\mathbf{A}}$, $\hat{\mathbf{C}}$, and $\boldsymbol{k}_d$ defined in parallel to $\mathbf{A}_M$, $\mathbf{C}_M$, and $\hat{\mathbf{D}}_M$, respectively. Equations (3.39) and (3.40) can be rewritten in the following equation.

$$\hat{\boldsymbol{x}}_M[i] = \mathbf{K}_{yM}\boldsymbol{y}_M[i] + \mathbf{K}_{uM}\boldsymbol{\tau}_{mM}[i] \qquad (3.42)$$

Here, $\mathbf{K}_{yM}$ and $\mathbf{K}_{uM}$ are matrices derived from (3.39) and (3.40) by transforming them to transfer function expression. The transfer function of the expanded system $\mathbf{L}(z)$ and that of the controller $\mathbf{G}_1(z)$ are obtained as follows:

$$\begin{aligned}
\mathbf{L}(z) &= \mathbf{C}_M(z\mathbf{U}_1 + \mathbf{U}_2)(z\mathbf{I} - \mathbf{A}_M)^{-1}\mathbf{B}_M && (3.43)\\
\mathbf{G}_1(z) &= (\mathbf{I} + \mathbf{K}_{dM}\mathbf{K}_{uM})^{-1}\mathbf{K}_{dM}\mathbf{K}_{yM}. && (3.44)
\end{aligned}$$

Table 3-1: Control parameters in stability analysis of multirate position control

Position gain	K_p	900	$1/\mathrm{s}^2$
Velocity gain	K_v	60	1/s
Cutoff frequency of velocity calculation	g_v	13000	rad/s
Cutoff frequency of disturbance observer	g_{dis}	7000	rad/s

Stability Analysis Results

Nyquist criterion in continuous-time is obtained by transforming $\det[\mathbf{I}+\mathbf{L}(z)\mathbf{G}_1(z)]-1$ using bilinear transform and drawing Nyquist diagram of it. Analyses were performed with the assumption that the limitation of the input sampling period was 0.1 ms. The following three cases were considered.

- single-rate control with long sampling period ($T_s(=T_u=T_y)=0.1$ ms)
- single-rate control with short sampling period ($T_s(=T_u=T_y)=0.05$ ms)
- multirate control with the proposed disturbance observer ($T_u=0.1$ ms, $T_y=0.05$ ms)

The control gains used in the analysis are shown in Table 3-1.

Nyquist diagram of the position control system is shown in Fig. 3-10. The result for the proposed method shows improvement of stability compared with the single-rate control with $T_s = 0.1$ ms, although it did not come up with the result with $T_s = 0.05$ ms. Here, note that the single-rate control with $T_s = 0.05$ ms does not satisfy the assumption on the minimum input sampling period. The result indicates that shortening the output sampling period is effective to improve stability, especially when there is a limitation of the input sampling period. As mentioned before, the limitation of the input sampling period is usually more severe than that on the output. The proposed method is therefore effective for improving stability in majority of motion control systems.

3.5.2 Experiments

The results of the stability analysis indicate that the shorter the sampling periods are, the higher the stability becomes. The problems involved in shortening the output sampling period are easily conceived, however. One problem is that a shorter output sampling requires more computations. Another is the problem with a quantization error of an encoder. Although the error is not considered in the stability analysis, it is necessary to consider the error for practical application. Experiments on the proposed

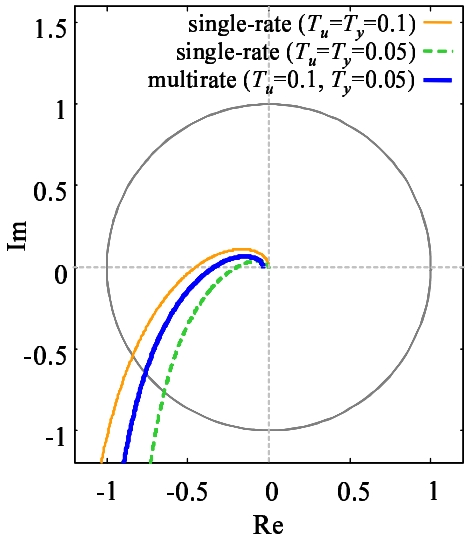

Fig. 3-10: Nyquist diagram of multirate position control system

multirate control were executed and the results are compared with those of the single-rate control in this subsection to show the feasibility and effectiveness.

Experimental Setup

Experiments were executed with the single-link manipulator shown in Fig. 3-11. The manipulator is composed of a rotary motor, an optical encoder, and an arm. Specifications of the motor and the encoders are presented in Table 3-2. The friction effect is extremely small since the manipulator has a direct drive mechanism and the arm is very light. The gravity term is also negligible since the rotational plane of the manipulator is horizontal. The output of the system is only an angular signal from the encoder. Two types of encoders were used to verify the influence of the quantization error. The pulses of the encoders were used as quadrature encoder to improve resolution. The program of the controller is written in C language and implemented on RT-Linux.

Experimental Results

First, the manipulator with the high resolution encoder was used to verify the influence of application of the proposed method. In this experiment, 0.05 Nm torque disturbance was added as a step input from $t = 7.0$ s to $t = 7.5$ s and from $t = 10.5$ s to $t = 11.0$ s while the manipulator was moved as a sine wave

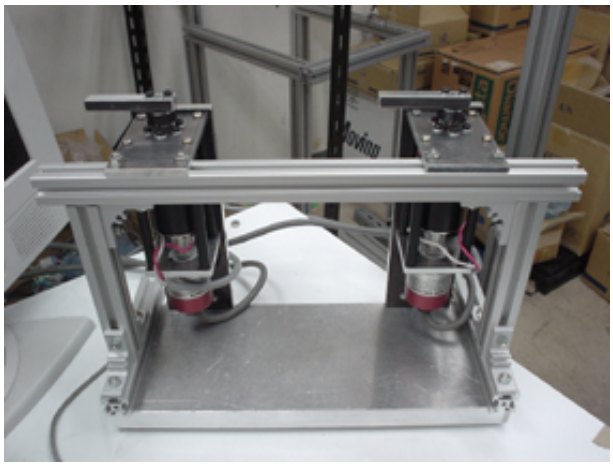

Fig. 3-11: Experimental equipment: single-link manipulator

Table 3-2: Specification of single-link manipulator

Type of encoder	Canon R-1O	
Number of pulses	81,000	pulse/rev
Max. response rotation speed	360	rpm
Type of encoder	Maxon HEDS 5540	
Number of pulses	500	pulse/rev
Max. response rotation speed	30000	rpm
Type of motor	Maxon RE-40	
Stall torque	2500	mNm
Max. continuous torque	201	mNm
Torque constant	60.3	mNm/A
Arm length	0.06	m

with the following position command.

$$\theta^{cmd} = \begin{cases} 0 & (t < 5.0) \\ 0.5\sin(0.5(t-5.0)) & (t \geq 5.0) \end{cases} \tag{3.45}$$

The position and velocity gains were $K_p = 1500\ 1/\mathrm{s}^2$ and $K_v = 100$ 1/s in all cases. The cutoff frequency of velocity calculation g_v was set higher than that of the disturbance observer g_{dis}. Then g_{dis} was heightened to the maximum value with which the system did not oscillate significantly or diverge. Fig. 3-12 shows the position command and the response. The shaded areas show the response with the disturbance. The experiments were performed under the assumption that the limitation of the input sampling period was 0.3 ms. In order to verify the effects of shortening the output sampling period and

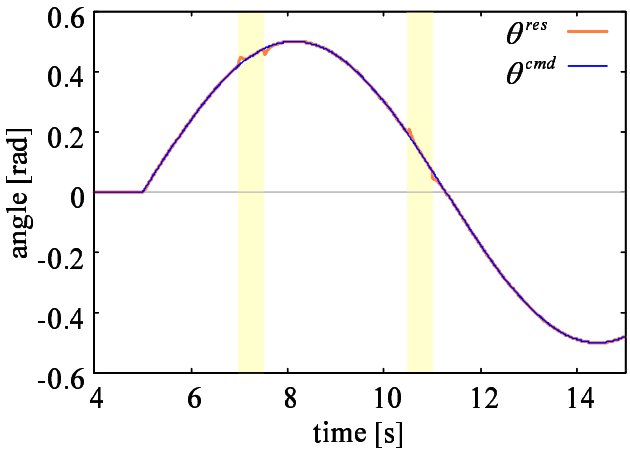

Fig. 3-12: Experimental results: position command and response in multirate position control

Table 3-3: Settings in experiments on multirate position control with high resolution encoder

	T_u [ms]	T_y [ms]	g_v [rad/s]	g_{dis} [rad/s]
Case 1: Single-rate (long)	0.3	0.3	1900	650
Case 2: Single-rate (short)	0.15	0.15	2500	1800
Case 3: Multirate (τ_{dis})	0.3	0.1	2500	1800
Case 4: Multirate (τ_{mdis})	0.3	0.1	2500	1800

of the proposed disturbance observer, experiments were executed for four cases listed below.

- Case 1: single-rate control with long sampling period ($T_s(= T_u = T_y) = 0.3$ ms)
- Case 2: single-rate control with short sampling period ($T_s(= T_u = T_y) = 0.15$ ms)
- Case 3: multirate control with conventional disturbance observer ($T_u = 0.3$ ms, $T_y = 0.1$ ms)
- Case 4: multirate control with proposed disturbance observer ($T_u = 0.3$ ms, $T_y = 0.1$ ms)

The sampling periods and the cutoff frequencies in each experiment are shown in Table 3-3. The input sampling period was set to the same value in Cases 1, 3, and 4.

Figs. 3-13, 3-14, and 3-15 show the position error when the disturbance was added. Fig. 3-13 compares Case 1 and Case 4, which are the single-rate and the multirate controls with the same input sampling period. In the single-rate control, the manipulator oscillated and became unstable with g_{dis} higher than 700 rad/s. On the other hand, in the multirate control, g_{dis} could be set much higher. As a result, the

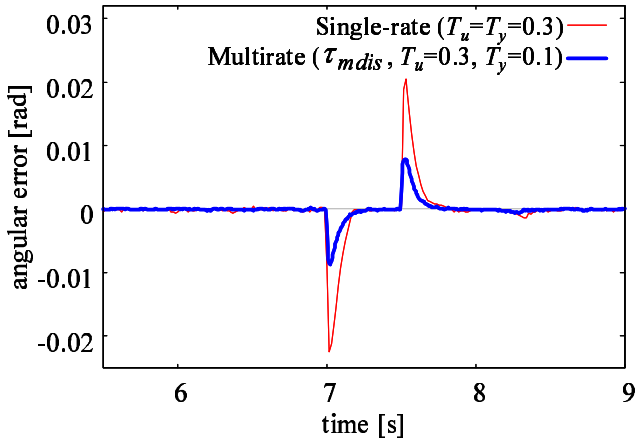

Fig. 3-13: Experimental results: position control error in single-rate (long) and multirate

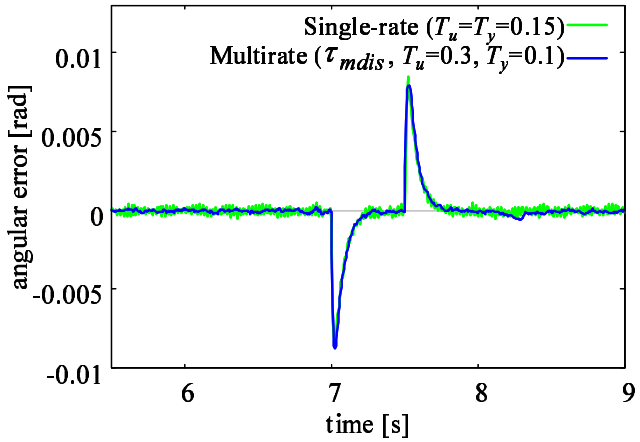

Fig. 3-14: Experimental results: position control error in single-rate (short) and multirate

influence of the disturbance was greatly reduced and convergence was also improved. In order to verify the advantage of shortening the output sampling period more clearly, the result of the multirate control (Case 4) was compared with that of the single-rate control with the shorter sampling period (Case 2) in Fig. 3-14. Note that the sampling period of the single-rate control (Case 2) was shorter than the assumed limitation. Although g_{dis} could be set as in the case of the multirate control, oscillation was confirmed in Case 2, which was not confirmed in the multirate control. The result indicates that better performance can be acquired even with the longer input sampling period by shortening the output sampling period.

Fig. 3-15 compares the proposed disturbance observer with the conventional disturbance observer in the multirate control. Although both of them showed almost the same response to the disturbance, they

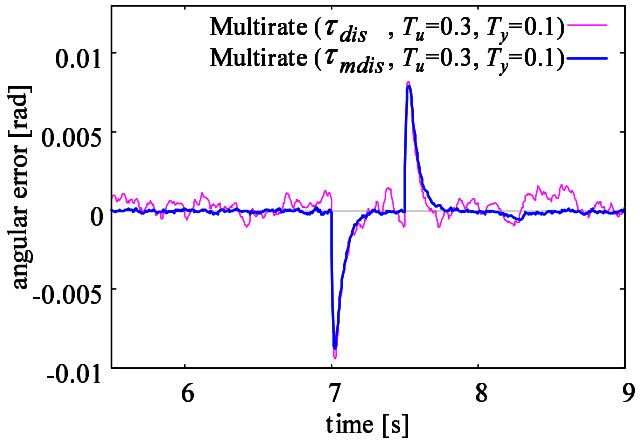

Fig. 3-15: Experimental results: comparison of disturbance observers in multirate position control

differed in the response without the disturbance. In the case of the conventional disturbance observer, there was an error in a steady state. The amount was almost the same as that in the single-rate with the long sampling period (Case 1). The fact indicates that the multirate control with the conventional disturbance observer can improve only the maximum value of g_{dis} and does not improve the behavior in a steady state. This may occur since a real input value differs from a desired input value at $t \neq iT_u$. The proposed disturbance observer considers the difference in input values as a sort of disturbance and compensates it. It led to improvement in the whole behavior: not only the maximum value of the cutoff frequency but also the performance in a steady state. The system therefore became close to the system with the short sampling period for both input and output. The result shows superiority of the proposed disturbance observer.

Experimental Results with Low Resolution Encoder

This subsection applies the proposed method for a system with a low resolution encoder to verify its applicability on the system with a large quantization error. This research used M method, i.e., fixed-time method, for velocity calculation among several measurement methods. M method is the most common velocity measurement method. It counts the number of pulses generated in a fixed time interval and calculates velocity by finite-different derivative. The details of velocity measurement methods are explained in Chapter 4. The acceleration resolution R_a in this method is in inverse proportion to the

Table 3-4: Settings in experiments on multirate position control with low resolution encoder

	T_u [ms]	T_y [ms]	g_v [rad/s]	g_{dis} [rad/s]
Case 5: Single-rate ($T_s = 0.3$)	0.3	0.3	700	2300
Case 6: Single-rate ($T_s = 0.2$)	0.2	0.2	700	3500
Case 7: Multirate	0.4	0.2	700	3500

square of the sampling period as shown in the equation below.

$$R_a = \frac{2\pi}{PT_s^2} \tag{3.46}$$

Here, P denotes the number of pulses per revolution in an encoder. Since the resolution becomes large by shortening the output sampling period, the multirate sampling method has a risk to increase the influence of the quantization error. In order to verify applicability of the method for a system with a low resolution encoder, experiments were executed with an encoder of 500 pulses/rev for the following three cases.

- Case 5: single-rate control with long sampling period ($T_s (= T_u = T_y) = 0.3$ ms)
- Case 6: single-rate control with short sampling period ($T_s (= T_u = T_y) = 0.2$ ms)
- Case 7: multirate control with long input sampling period ($T_u = 0.4$ ms, $T_y = 0.2$ ms)

The proposed disturbance observer was applied in the multirate control in Case 7. In this experiment, 0.1 Nm torque disturbance was added as a step input from $t = 5.0$ s to $t = 5.5$ s while the manipulator was moved as a sine wave with the following position command.

$$\theta_{cmd} = \begin{cases} 0.0 & (t < 3.0) \\ \cos(t - 3.0) - 1.0 & (t \geq 3.0) \end{cases} \tag{3.47}$$

The cutoff frequency for velocity calculation was set to $g_v = 700$ rad/s in all cases so as to keep the influence of the quantization error small. The position and velocity gains were $K_p = 900$ and $K_v = 60$. The sampling periods and cutoff frequencies in each experiment are presented in Table 3-4. Fig. 3-16 shows the position command and response. The shaded area in Fig. 3-16 shows the response with the disturbance and Fig. 3-17 shows the position error when the disturbance torque was imposed. In the single-rate control with $T_s = 0.3$ ms (Case 5), the system became unstable and diverged with g_{dis} higher than 3000 rad/s. The maximum value of g_{dis} was the same, $g_{dis} = 4500$ rad/s, in the single-rate control with $T_s = 0.2$ ms (Case 6) and the multirate control (Case 7). As a result, the position error with the

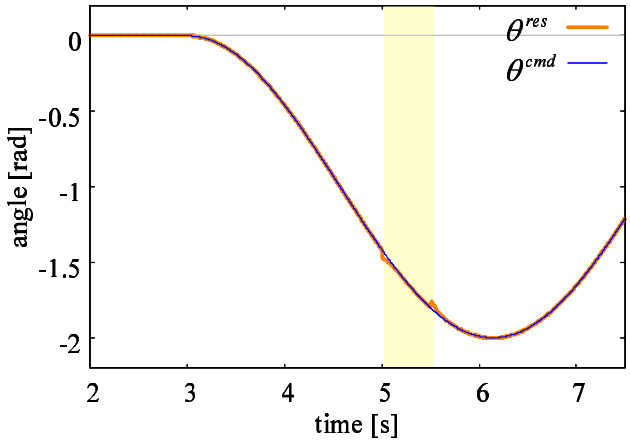

Fig. 3-16: Experimental results: multirate position control with low resolution encoder

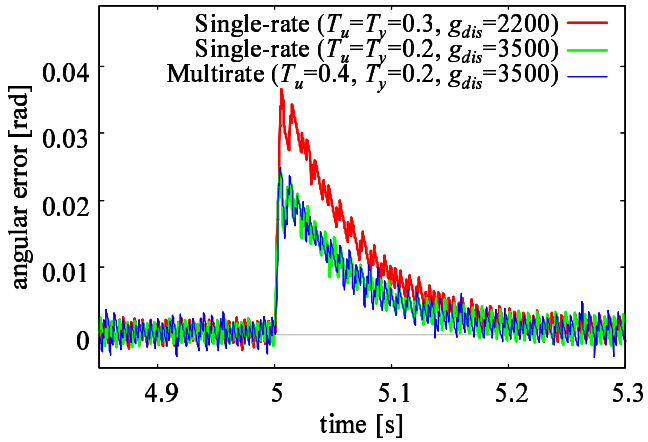

Fig. 3-17: Experimental results: position control error with low resolution encoder

disturbance torque was smaller in Case 7 than in Case 5 as shown in Fig. 3-17. The noise confirmed in Fig. 3-17 is due to the low resolution of the encoder and does not mean oscillation of the equipment. Even though the input sampling period was longer in the multirate control, the result of Case 7 was almost the same as that of the single-rate control with the short sampling period in Case 6. These results show applicability and effectiveness of the proposed method even to the system with a low resolution encoder. It is also useful to use the proposed method with other measurement methods in the case when the resolution is extremely low or the output sampling period is further shortened. Application of different measurement methods are discussed in Chapter 4.

Influence of Input and Output Sampling Periods

Simulations were conducted to verify the influence of the input and output sampling periods precisely and quantitatively. The input sampling period was set as 0.6 ms, while the output sampling period was decided by varying the ratio n between the input and output sampling periods from 1 to 5. The resolution of an encoder was assumed to be the same as that of a high resolution encoder in the experimental system. The manipulator was moved as a sine wave and 0.1 Nm torque disturbance was added as a step input from $t = 1.5$ s to $t = 2.3$ s. The cutoff frequency of the disturbance observer was heightened to the maximum value without large oscillation or divergence, and that of velocity calculation was set as $g_v = 1.2g_{dis}$. A root mean square (RMS) of the position error from $t = 1.5$ s to $t = 1.9$ s was calculated. The same simulations were conducted for the single-rate control. The sampling period was varied from 0.12 ms to 0.6 ms in the single-rate.

Table 3-5 presents sampling periods, cutoff frequencies, and the RMS values. Fig. 3-18 shows the change in RMS values both in the multirate and single-rate controls. A line in the figure is an approximate curve in the multirate control. It shows that the RMS value decreased in proportion to the output sampling period even though the input sampling period was the same in all cases. Comparing the RMS values concretely, the value decreased from the single-rate ($n = 1$) by 42.5% in the multirate with $n = 2$ and 66.5% in that with $n = 5$ when the input sampling period was the same. These results indicate that control performance improves by enlarging the ratio n, i.e., by shortening the output sampling period. Comparing the single-rate (short) and the multirate with the same output sampling period in Fig. 3-18, better results were obtained for the single-rate control since the input sampling periods were also set short the same as the output sampling periods in the single-rate control. Although the performance of the multirate control could not catch up with that of the single-rate control with a short sampling period, the multirate followed the single-rate very well. This result shows the ability of the proposed method of making the performance to be close to that with a short sampling period both for input and output. Focusing on the influence of changing sampling periods, the RMS value decreased by 63.3% in the case where the input sampling period was 0.6 ms and the output sampling period was shortened to one-fourth, from 0.6 ms to 0.15 ms. On the other hand, the decrease was only 28.1% when the output sampling period was 0.15 ms and the input sampling period was shortened to one-fourth, from 0.6 ms to 0.15 ms. The result shows that the influence of changing the output sampling period is much greater than that of the input. In other words, a higher priority should be given to the sampling period of the output

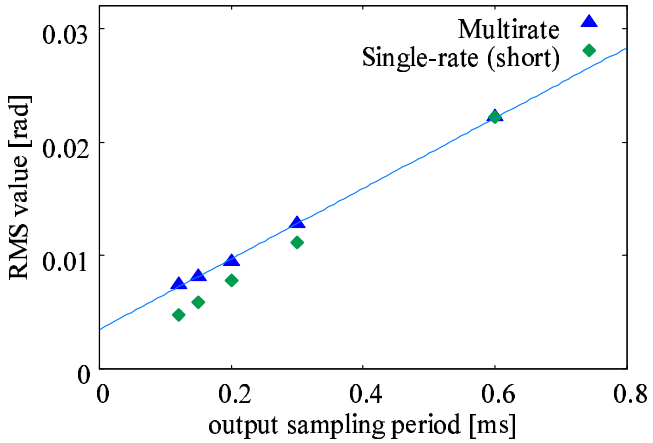

Fig. 3-18: Simulation results: relation of RMS values and output sampling period in position control

Table 3-5: Settings and RMS values in simulations on multirate position control

	T_u [ms]	T_y [ms]	g_{dis} [rad/s]	RMS Value [rad]	Rate of RMS
Multirate					
n=1	0.6	0.6	800	2.21×10^{-2}	1.0
n=2	0.6	0.3	1400	1.27×10^{-2}	0.575
n=3	0.6	0.2	1900	9.39×10^{-3}	0.424
n=4	0.6	0.15	2200	8.14×10^{-3}	0.368
n=5	0.6	0.12	2500	7.42×10^{-3}	0.335
Single-rate					
	0.6	0.6	800	2.21×10^{-2}	1.0
	0.3	0.3	1600	1.12×10^{-2}	0.505
	0.2	0.2	2300	7.83×10^{-3}	0.353
	0.15	0.15	3100	5.85×10^{-3}	0.264
	0.12	0.12	3800	4.80×10^{-3}	0.217

compared to that of the input in acceleration control.

3.6 Application to Force Control

This section applies the multirate sampling method proposed in Section 3.2 and the observers proposed in Section 3.3 to the acceleration control-based force control system shown in Fig. 2-8(b). Firstly, expected effects of implementation of the proposed multirate sampling method on force measurement and force control are discussed. Secondly, the influence on stability is analyzed. And finally, the effects

on the real system are verified by experiments.

3.6.1 Advantage in Application to Force Control

This subsection discusses expected advantages of application of the proposed multirate sampling method to an acceleration control-based force control system. The effects mentioned in Section 3.4 can also be achieved in force control. In addition to those effects, there are effects particular for force control. In the point of force measurement, implementation of the multirate sampling method for acceleration control is clearly effective since the reaction force observer is based on acceleration information as in the disturbance observer. Some of the effects on force control are similar to the effects mentioned in Section 3.4 because of similarity of the structures between the disturbance observer and the reaction force observer. As the effect of the proposed multirate sampling method, the cutoff frequency of the reaction force observer can be set higher and wide-band and high-precision force measurement thus becomes possible. As mentioned before, the maximum value of g_e depends on characteristics of the right side loop of the reaction force observer shown in Fig. 3-5, which is derived from $\dot{\theta}[i,k]$. As in the case of the cutoff frequency of the disturbance observer, g_e can be set higher by shortening the sampling period of observer calculation according to shortening of the sampling period of the right side loop, which is the output sampling period. Another advantage is reduction in delay in measured force information. When only acquisition of force information is considered, not the delay but only accuracy is important. In the case of force control, however, the delay in force information may deteriorate the performance since the measured force value is fed back. The multirate sampling method decreases the delay of force information owing to the following two reasons:

- decrease of delay generated in calculation process due to LPF by heightening g_e; and
- detection of external force at early timing.

The signal acquired through an LPF has a sort of delay and the magnitude of the delay depends on the cutoff frequency of the LPF. The cutoff frequencies of two LPFs, g_v for velocity calculation and g_e for the reaction force observer, thus affect force measurement. The calculation delay can be reduced with implementation of the multirate sampling method since the method enables the cutoff frequencies to be set higher. The principle of the second point is the same as that mentioned in Section 3.4 about disturbance detection. Detection becomes early for $((n-1)/2n)T_s$ and the delay is reduced to one nth by implementing the multirate sampling method and shortening the output sampling period to satisfy

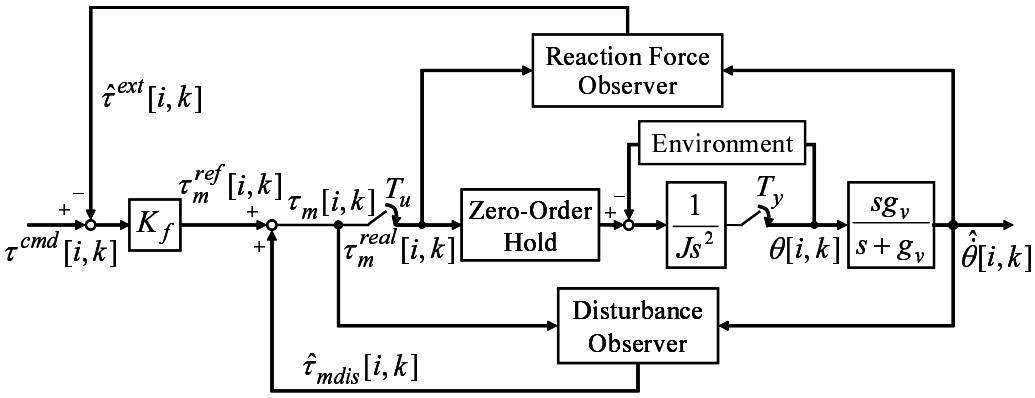

Fig. 3-19: Multirate force control system

$T_u = nT_y = T_s$. The whole structure of multirate force control with the proposed multirate sampling method is shown in Fig. 3-19.

3.6.2 Verification of Influence on Accuracy of Force Sensing

This subsection verifies how accuracy of force sensing changes with the multirate sampling method. Simulations were executed instead of experiments since the real force value can be acquired only in the simulation. Application of the multirate sampling method shortens both the sampling period for acquisition of the output information and that for the reaction force observer. Force control was performed with $T_u = T_y = 0.1$ ms in all cases and several reaction force observers were implemented to compare the accuracy of estimated forces. Simulations were performed based on parameters of the experimental equipment shown in Fig. 3-11 and a quantization model of the encoder was introduced. The pulse number of an encoder was assumed as 81000 pulses/rev. The environment was modeled as a spring and damper model as shown in Fig. 2-9.

Fig. 3-20 shows the influence of changing the cutoff frequency g_e. Here, τ_e is not a value estimated with the observer but the real value given in the simulation by (2.13). A certain value of the external force was detected around $t = 1.0$ s although the manipulator did not touch the environment. It is caused by the fact that the force value calculated with the observer contains an inertia torque. The result showed that the estimated value became closer to the real value by heightening the cutoff frequency. The value oscillated and diverged, however, when g_e was further heightened. The ability of force sensing therefore improves if the maximum value of g_e can be increased.

The influences of the sampling period on the maximum value of the cutoff frequency were verified

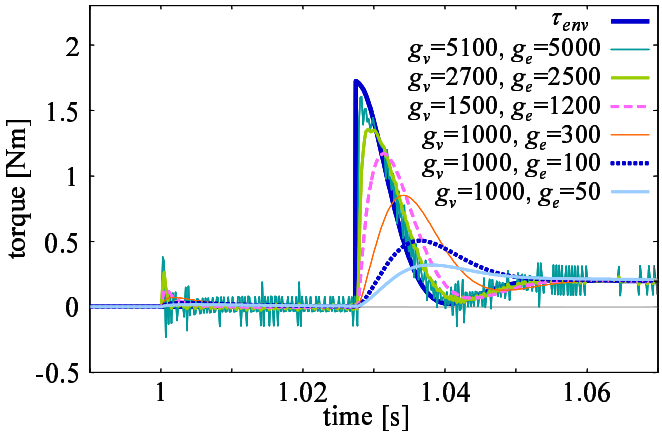

Fig. 3-20: Simulation results: change in accuracy of force sensing with g_e

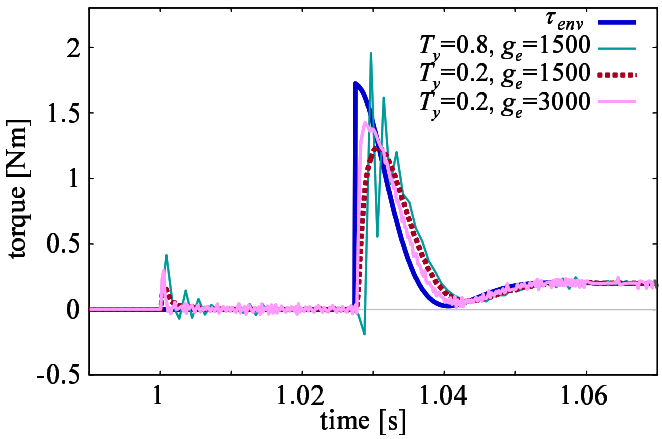

Fig. 3-21: Simulation results: change in limitation of g_e with sampling periods

next. Fig. 3-21 compares the estimated torque between long and short sampling periods: 0.8 ms and 0.2 ms. In the case with the long sampling period, the oscillation was confirmed with g_e higher than 1500 rad/s. On the other hand, the cutoff frequency g_e could be set much higher without oscillation when the sampling period was short. It shows the advantage of the multirate sampling method with a shorter sampling period for the observer calculation.

Another advantage is early recognition of the external force. Fig. 3-22 compares the estimated torque among various sampling periods to verify the effect of the early recognition on force sensing. The cutoff frequency was set to be the same in all cases. The force estimated as negative was an estimation error caused by the inertia torque. The rise time became earlier and convergence to the real value became faster by shortening the output sampling period. The result therefore indicates that the shorter the sampling

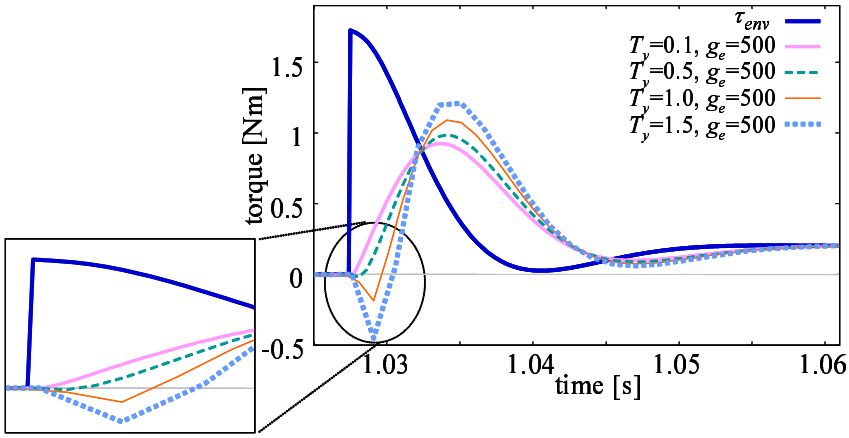

Fig. 3-22: Simulation results: change in accuracy of force sensing with sampling periods

period for observer calculation became, the earlier estimation became.

The advantages of applying the multirate sampling method to force estimation confirmed in the simulations are summarized as follows:

- the maximum value of the cutoff frequency became higher with the shortened sampling period of the observer, and thus accuracy improved and delay decreased; and
- recognition and estimation became early with the shortened sampling period for acquiring output information.

3.6.3 Stability Analysis

The effects of application of the multirate sampling method to force control were verified in terms of stability in this subsection. The main focus in the analysis is not the disturbance observer but the reaction force observer and the whole force control system.

Modeling

Analyses are executed for the single-link manipulator expressed by (3.20). In the force control system, the state variable of the reaction force observer $w_3[i]$ is included as a state variable in addition to the state variable of the disturbance observer $w_1[i]$ and that of pseudo derivative calculation $w_2[i]$. The state-space equations of the single-rate control are represented as follows:

$$\boldsymbol{x}[i+1] \quad = \quad \mathbf{A}_d\boldsymbol{x}[i] + \boldsymbol{b}_d u[i] \tag{3.48}$$

$$y[i] = \boldsymbol{c}_d \boldsymbol{x}[i], \tag{3.49}$$

where

$$\begin{aligned}
\boldsymbol{x}[i] &= \left[\begin{array}{cccccc} \theta[i] & \dot{\theta}[i] & \tau_{dis}[i] & w_1[i] & w_2[i] & w_3[i] \end{array}\right]^T,\ u[i] = \tau_m[i], \\
\mathbf{A}_d &= \left[\begin{array}{cccccc} 1-\frac{T_s^2}{2J}K_e & T_s-\frac{T_s^2}{2J}D_e & -\frac{T_s^2}{2J} & 0 & 0 & 0 \\ -\frac{T_s}{J}K_e & 1-\frac{T_s}{J}D_e & -\frac{T_s}{J} & 0 & 0 & 0 \\ 0 & 0 & 1 & 0 & 0 & 0 \\ \hat{b}_1 g_v & 0 & 0 & \hat{a}_1 & \hat{b}_1 g_v(\beta-1) & 0 \\ 1 & 0 & 0 & 0 & \beta & 0 \\ \hat{b}_2 g_v & 0 & 0 & 0 & \hat{b}_2 g_v(\beta-1) & \hat{a}_2 \end{array}\right],\ \boldsymbol{b}_d = \left[\begin{array}{c} \frac{T_s^2}{2J} \\ \frac{T_s}{J} \\ 0 \\ \hat{j}_1 \\ 0 \\ \hat{j}_2 \end{array}\right], \\
\boldsymbol{c}_d &= \left[\begin{array}{cccccc} 1 & 0 & 0 & 0 & 0 & 0 \end{array}\right]^T, \\
\hat{a}_1 &= \alpha,\ \hat{j}_1 = 1-\alpha,\ \hat{b}_1 = \frac{J}{T_s}(1-\alpha)^2,\ \hat{a}_2 = \gamma,\ \hat{j}_2 = 1-\gamma,\ \hat{b}_2 = \frac{J}{T_s}(1-\gamma)^2, \\
\alpha &= e^{-g_{dis}T_s},\ \beta = e^{-g_v T_s},\ \gamma = e^{-g_e T_s}.
\end{aligned}$$

Estimation of the external force and disturbance is performed with the equations below.

$$\boldsymbol{w}[i+1] = \hat{\mathbf{A}}\boldsymbol{w}[i] + \hat{\boldsymbol{b}}\theta[i] + \hat{\boldsymbol{j}}\tau_m[i] \tag{3.50}$$

$$\hat{\boldsymbol{x}}[i] = \hat{\mathbf{C}}\boldsymbol{w}[i] + \hat{\boldsymbol{d}}\theta[i] \tag{3.51}$$

$$\tau_m[i] = \boldsymbol{k}_d(\boldsymbol{r}[i] - \hat{\boldsymbol{x}}[i]), \tag{3.52}$$

where

$$\begin{aligned}
\boldsymbol{w}[i] &= \left[\begin{array}{ccc} w_1[i] & w_2[i] & w_3[i] \end{array}\right]^T,\ \hat{\boldsymbol{x}} = \left[\begin{array}{cc} \hat{\tau}_{dis}[i] & \hat{\tau}_{ext}[i] \end{array}\right]^T, \\
\hat{\mathbf{A}} &= \left[\begin{array}{ccc} \hat{a}_1 & \hat{b}_1 g_v(\beta-1) & 0 \\ 0 & \beta & 0 \\ 0 & \hat{b}_2 g_v(\beta-1) & \hat{a}_2 \end{array}\right],\ \hat{\boldsymbol{b}} = \left[\begin{array}{c} \hat{b}_1 g_v \\ 1 \\ \hat{b}_2 g_v \end{array}\right],\ \hat{\boldsymbol{j}} = \left[\begin{array}{c} \hat{j}_1 \\ 0 \\ \hat{j}_2 \end{array}\right], \\
\hat{\mathbf{C}} &= \left[\begin{array}{ccc} 1 & -l_1 g_v(\beta-1) & 0 \\ 0 & -l_2 g_v(\beta-1) & 1 \end{array}\right],\ \hat{\boldsymbol{d}} = \left[\begin{array}{c} -l_1 g_v \\ -l_2 g_v \end{array}\right], \\
l_1 &= \frac{J}{T_s}(1-\alpha),\ l_2 = \frac{J}{T_s}(1-\gamma).
\end{aligned}$$

The state-space equations of the multirate sampling system described for the shorter sampling period, which is the output sampling period, are represented as follows:

$$\boldsymbol{x}[i,k+1] = \mathbf{A}_m \boldsymbol{x}[i,k] + \mathbf{B}_m \left[\begin{array}{c} \tau_m^{real}[i,k] \\ \tau_m[i,k] \end{array}\right] \tag{3.53}$$

$$y[i,k] = \boldsymbol{c}_m \boldsymbol{x}[i,k], \tag{3.54}$$

where

$$\mathbf{A}_m = \mathbf{A}_d,\ \boldsymbol{c}_m = \boldsymbol{c}_d,\ T_s = T_y$$
$$\mathbf{B}_m = \begin{bmatrix} \frac{T_s^2}{2J} & \frac{T_s}{J} & 0 & 0 & 0 & \hat{j}_2 \\ 0 & 0 & 0 & \hat{j}_1 & 0 & 0 \end{bmatrix}^T.$$

Although Fig. 3-19 uses both the proposed disturbance observer and the reaction force observer, this subsection verifies the influence not of the proposed disturbance observer but of the multirate sampling method on the stability of the whole force control system including the reaction force observer. Analysis was therefore executed for the system excluding the disturbance observer. With consideration of the above point, the control input is derived as follows:

$$\tau_m[i] = K_f(\tau_{cmd}[i] - \hat{\tau}_{ext}[i]). \tag{3.55}$$

Equation (3.53) is rewritten to the form with the longer sampling period in order for analysis by using the method used in the case of multirate position control described in Section 3.5.1.

Stability Analysis Results

The following three patterns of sampling periods were selected for the analyses.

- single-rate control with long sampling period ($T_s(= T_u = T_y) = 0.3$ ms)
- single-rate control with short sampling period ($T_s(= T_u = T_y) = 0.15$ ms)
- multirate control with short output sampling period ($T_u = 0.3$ ms, $T_y = 0.15$ ms)

The following two types of environment were assumed.

- soft (Fig. 3-23): $K_e = 1000$ Nm/rad, $D_e = 10.0$ Nm·s/rad
- hard (Fig. 3-24): $K_e = 3000$ Nm/rad, $D_e = 10.0$ Nm·s/rad

Nyquist diagram in the continuous domain was derived as shown in Figs. 3-23 and 3-24. Fig. 3-23 shows the result with the soft object and Fig. 3-24 shows that with the hard object. Fig. 3-23 shows that the point crossing the real axis moved to right and then moved back to left when g_e was changed from low to high. The result clearly showed that stability was improved by heightening g_e. It is owing to

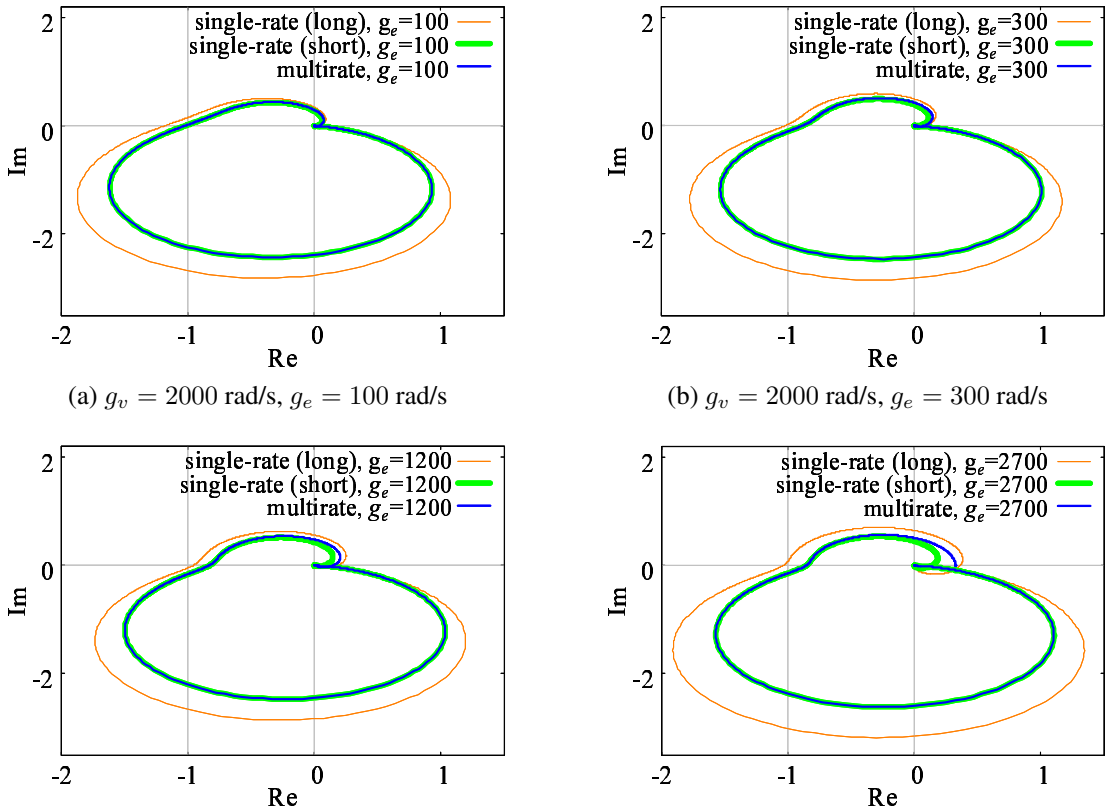

(a) $g_v = 2000$ rad/s, $g_e = 100$ rad/s

(b) $g_v = 2000$ rad/s, $g_e = 300$ rad/s

(c) $g_v = 2000$ rad/s, $g_e = 1200$ rad/s

(d) $g_v = 2800$ rad/s, $g_e = 2700$ rad/s

Fig. 3-23: Nyquist diagram of multirate force control with soft environment

improvement of accuracy and decrease of the delay. The stability was adversely affected when g_e was further heightened because of the influence of discretization. Comparison between the multirate control and the single-rate control with the long sampling period showed that stability was always much better in the multirate control than in the single-rate control (single-rate (long)) even though the input sampling period was the same. When $g_e = 100$ rad/s, both the single-rate (long) and the multirate controls were unstable. Not the single-rate (long) but the multirate control became stable with $g_e = 300$ rad/s. Then, $g_e = 1200$ rad/s stabilized all cases. The single-rate control (long) became unstable with $g_e = 2700$ rad/s, while the multirate control kept stable. It shows that even though the single-rate (long) and the multirate had the same input sampling period, the single-rate control was easily destabilized by heightening g_e. The noteworthy is that the results of the multirate control were almost the same as those of the single-rate with the short sampling period, although the input sampling period was longer in the multirate control.

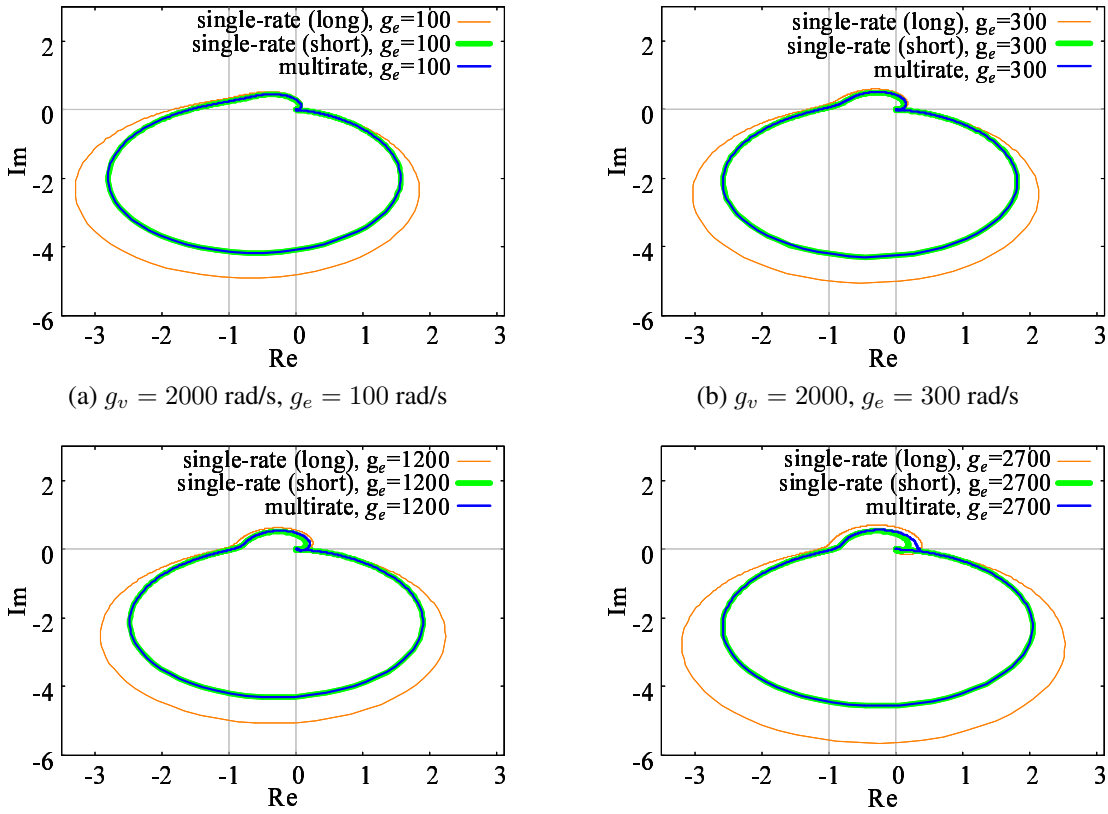

(a) $g_v = 2000$ rad/s, $g_e = 100$ rad/s

(b) $g_v = 2000$, $g_e = 300$ rad/s

(c) $g_v = 2000$ rad/s, $g_e = 1200$ rad/s

(d) $g_v = 2800$ rad/s, $g_e = 2700$ rad/s

Fig. 3-24: Nyquist diagram of multirate force control with hard environment

When the environment was harder, the system was unstable with $g_e = 300$ rad/s in all cases as shown in Fig. 3-24(a). It means that a higher g_e was required for stabilization when the environment was hard. The system became stable in the multirate control and the single-rate control with the short sampling period when $g_e = 1200$ rad/s or $g_e = 2700$ rad/s. As a result, the system could not be stabilized in the single-rate control with the long sampling period while stable control was possible in the multirate control.

The results of stability analysis are summarized as follows:

- multirate control improved stability of force control;
- the system was stable with higher g_e in multirate control; and
- multirate control enables adaptation to harder environments with higher g_e.

Table 3-6: Settings in experiments on multirate force control

	T_u [ms]	T_y [ms]	g_v [rad/s]	g_{dis} [rad/s]	g_e [rad/s]
Case 1: single-rate	3.0	3.0	200	150	150
Case 2: multirate	3.0	1.0	200	150	150
Case 3: multirate (long)	4.0	2.0	200	150	150
Case 4: multirate (high)	3.0	1.0	300	250	250

The most remarkable was that stability in the multirate control was almost the same as that in the single-rate control with the short sampling period even though the input sampling period was longer in the multirate. These results clearly show and strongly support the advantages of applying the proposed multirate sampling method to force control. Moreover, comparison of the analysis result of position control (Fig. 3-10) with that of force control (Figs. 3-23 and 3-24) clarifies that the influence of the proposed multirate sampling method is much greater in force control. This is considered as the result of the positive influence of the proposed method on both accuracy of measurement and control. Requirement for faster reaction in the contact motion compared with position control can also be considered as another reason.

3.6.4 Experiments

Experiments were conducted using the single-link manipulator shown in Fig. 3-11. The manipulator was controlled to make contact with an aluminum block with a force command. The force command was given as a step input changing from 0.0 to 0.04 Nm. Experiments were conducted under the following four conditions.

- Case 1: single-rate control ($T_s (= T_u = T_y) = 3.0$ ms)
- Case 2: multirate control ($T_u = 3.0$ ms, $T_y = 1.0$ ms)
- Case 3: multirate control with longer sampling periods ($T_u = 4.0$ ms, $T_y = 2.0$ ms)
- Case 4: multirate control with higher cutoff frequencies ($T_u = 3.0$ ms, $T_y = 1.0$ ms)

The sampling periods and cutoff frequencies of each experiment are presented in Table 3-6. The force gain was set to $K_f = 2.0$. Fig. 3-25 compares the position and force responses between the single-rate control (Case 1) and the multirate control (Case 2). In the single-rate control, the manipulator

was repeatedly shifted between contact and non-contact states several times and finally the response diverged at around $t = 5.1$ s. On the other hand, stable contact was attained in the multirate control even though the input sampling period was not changed. Fig. 3-26 shows the results of the multirate control with longer sampling periods (Case 3). Although hunting was confirmed in Fig. 3-26, stable contact was attained finally even with longer sampling periods. The result strongly supports the validity of the proposed method. Noteworthy is that the difference between Case 1 and Case 2 was only the output sampling period, and the cutoff frequencies were not changed. Furthermore, better performance could be acquired even with a longer input sampling period by shortening the output sampling period. The first factor is explained in Section 3.4. Noise and the bandwidth of force sensing have the trade-off relationship. Both the narrow bandwidth and the noise of force information due to discretization might affect the performance in the single-rate control. The noise might be reduced and its influence might thus also be reduced to attain stable contact in the multirate control. Reduction in the influence of discretization was confirmed in Fig. 3-27. The cutoff frequency could be set higher in the multirate control, while the system became unstable and could not be operated in the single-rate control. The result shows that the bandwidth of force control could be widened by shortening the output sampling period. Accordingly, the multirate sampling method enabled the manipulator to cope with various environments.

The experimental results shown above well correspond to the stability analysis results shown in Section 3.6.3. The advantages of application of the proposed multirate sampling method to force control are summarized as follows:

- stable contact becomes possible even with the same cutoff frequencies; and
- the cutoff frequencies can be set higher and adaptability to unknown environment improves.

3.7 Application to Bilateral Teleoperation

This section focuses on a bilateral teleoperation system as a system that requires high performance acceleration control. It is required in bilateral control to deal with position and force at the same time. High robustness and adaptability are also required since operations are not planned beforehand and the slave device often makes contact with unknown objects during operation. Moreover, reproduction of vivid tactile sensation requires control in wide bandwidth. Wide-band acceleration control is thus required in the system. The objective of implementation of the proposed multirate sampling method is transmission

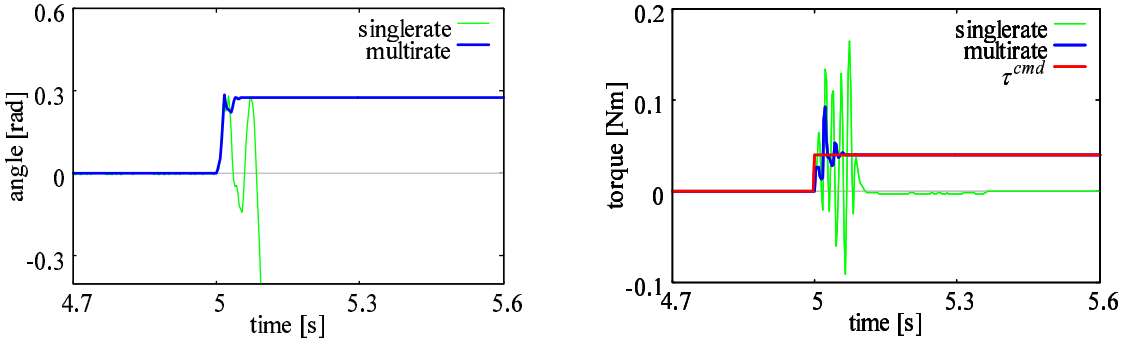

(a) position response (b) force response

Fig. 3-25: Experimental results: multirate force control (Case 1: single-rate and Case 2: multirate)

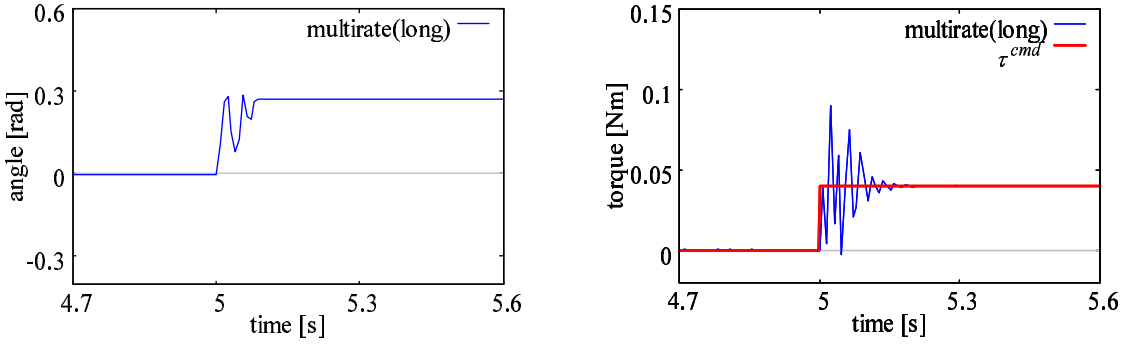

(a) position response (b) force response

Fig. 3-26: Experimental results: multirate force control (Case 3: multirate (long))

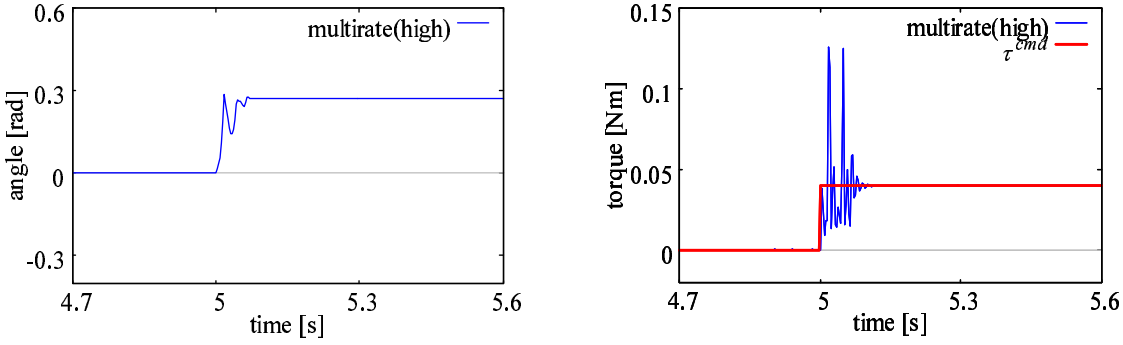

(a) position response (b) force response

Fig. 3-27: Experimental results: multirate force control (Case 4: multirate (high))

Table 3-7: Control parameters in simulations on multirate bilateral teleoperation

Spring coefficient of operator	K_h	400.0	N/m
Damper coefficient of operator	D_h	40.0	N·s/m
Spring coefficient of environment	K_e	10000.0	N/m
Damper coefficient of environment	D_e	10.0	N·s/m
Position of operator	θ_h	$\pi/10.0$	rad
Position of environment	θ_e	$\pi/20.0$	rad
Inertia	J	0.000223	Kgm^2
Arm length	l	0.06	m
Number of pulses	P	81000	pulse/rev

of more accurate and precise tactile sensation. For the simplicity reason, existence of a network is not considered in this section. Each of the master or the slave device was the single-link manipulator shown in Fig. 3-11 and used for experiments of position control and force control. The high resolution encoder was used for bilateral teleoperation. This section applied the controller shown in Fig. 2-11 as a bilateral controller.

3.7.1 Simulations

In this simulation, the environment was assumed to be fixed at $\theta_e = \pi/20.0$ rad. The operator input was given as a step input with $\theta_h = \pi/10.0$ rad from $t = 1.0$ s to $t = 3.0$ s, and the slave manipulator was made into contact with the environment during this period. The positions of the environment and the operator are derived from $x_e = l\theta_e$ and $x_h = l\theta_h$ by using the link length l. The parameters used in the simulation are shown in Table 3-7. In order to simulate the real system, a quantization error model of an encoder was introduced.

Effects of multirate sampling method

First, simulations were conducted under the following two conditions to verify the influences of application of the proposed multirate sampling method.

- single-rate control ($T_s (= T_u = T_y) = 2.0$ ms)
- multirate control with long input sampling period ($T_u = 3.0$ ms, $T_y = 1.0$ ms)

Table 3-8: Settings in simulations and experiments on multirate bilateral teleoperation

	T_u [ms]	T_y [ms]	g_v [rad/s]	g_{dis} [rad/s]
Simulation 1				
single-rate	2.0	2.0	500	50
multirate (long)	3.0	1.0	1700	280
Simulation 2				
single-rate ($T_s = 0.5$ ms)	0.5	0.5	3500	1500
single-rate ($T_s = 1.0$ ms)	1.0	1.0	1900	650
multirate (τ_{dis})	1.5	0.5	1500	850
multirate (τ_{mdis})	1.5	0.5	3800	900
Experiments				
single-rate	0.2	0.2	2000	480
multirate (long)	0.3	0.1	3300	800

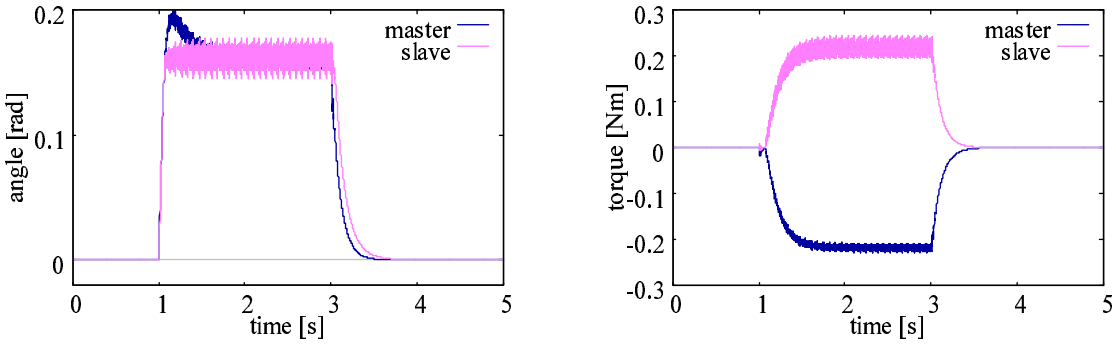

(a) position response

(b) force response

Fig. 3-28: Simulation results: bilateral control (single-rate)

The sampling periods and cutoff frequencies used in the simulation are shown in Table 3-8. As shown in Fig. 3-28, vibration occurred in the single-rate control when the slave manipulator was made into contact with the environment. When the multirate sampling method was applied, however, the vibration was completely suppressed and stable contact was achieved as shown in Fig. 3-29 even though the input sampling period was set longer than that in the single-rate control. This result shows that high control performance can be achieved by shortening the output sampling period even if the input sampling period is set long. The influence of changing the output sampling period was thus confirmed to be greater than that of the input. The above results confirm the validity of the idea of the proposed method, which sets the output sampling period shorter than the input sampling period.

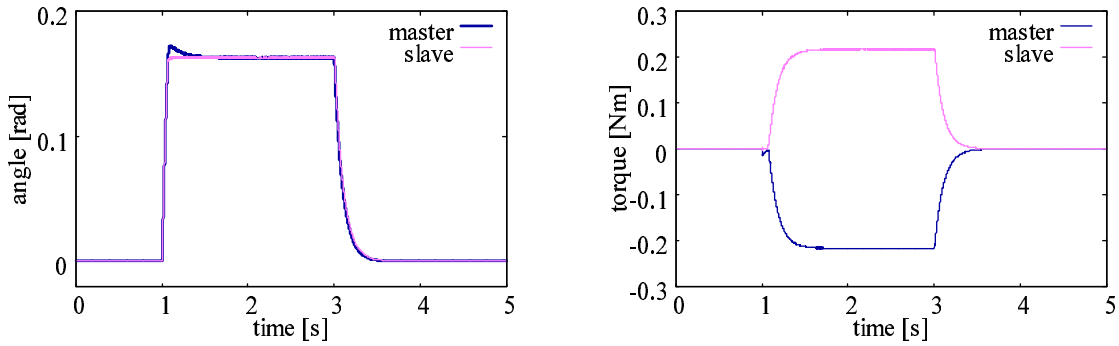

(a) position response

(b) force response

Fig. 3-29: Simulation results: bilateral control (multirate)

Effects of Proposed Disturbance Observer

In order to verify the influence of the input sampling period on the performance and that of the proposed disturbance observer shown in Fig. 3-4, simulations were next executed under the following four conditions.

- single-rate control with short sampling period ($T_s (= T_u = T_y) = 0.5$ms and 1.0 ms)
- multirate control with the conventional disturbance observer ($T_u = 1.5$ ms, $T_y = 0.5$ ms (τ_{dis}))
- multirate control with the proposed disturbance observer ($T_u = 1.5$ ms, $T_y = 0.5$ ms (τ_{mdis}))

The sampling periods and cutoff frequencies used in the simulation are shown in Table 3-8. Since the disturbance observer was implemented for the differential coordinate in the controller shown in Fig 2-11, the following verification focuses on the responses of the differential coordinate.

Fig. 3-30 is an enlarged view of the response of the differential coordinate at the moment of contact. Since the differential coordinate represents a difference between the master and the slave, a small absolute value in the position response of the coordinate indicates that the system has high tracking performance. Comparing the result of the single-rate with $T_s = 0.5$ ms and that with $T_s = 1.0$ ms, it is obvious that better performance can be achieved by setting both the input and output sampling periods shorter. In other words, control performance deteriorates by lengthening both the input and output sampling periods. Actually, the value of the response in the differential coordinate was larger and tracking performance deteriorated when the input sampling period was set longer in the multirate control with the conventional disturbance observer. On the other hand, performance better than that obtained with the single-rate control with $T_s = 1.0$ ms was achieved with the input sampling period $T_u = 1.5$ ms when the proposed

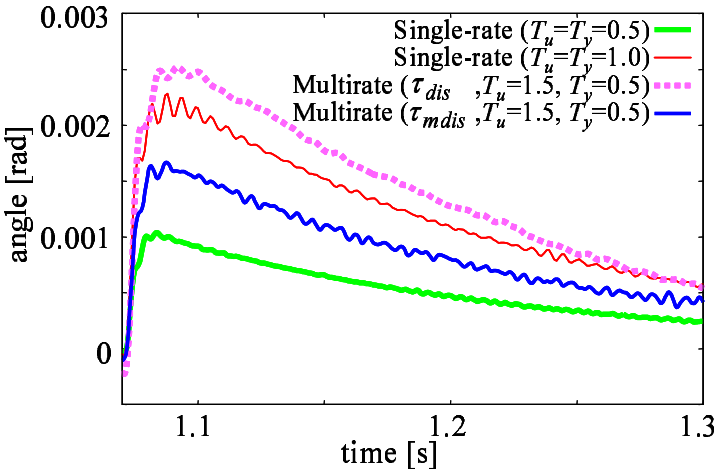

Fig. 3-30: Simulation results: position response of differential coordinate in multirate bilateral control

disturbance observer was used for the multirate control. The result shows that the performance became close to that obtained with the short sampling period also for the input, even though the input sampling period was set to be triple of the output sampling period. The above results confirm that application of the proposed disturbance observer enables the system to achieve performance similar to the case with a short sampling period both for input and output by shortening only the output sampling period; which is achieved by defining the disturbance torque as τ_{mdis} and compensating the influence of a difference between a desired input value and a real input command.

Influence of Input and Output Sampling Periods

Finally, the influence of changing the output sampling period on control performance was verified quantitatively and compared with that of changing the input sampling period. The input sampling period was set to 1.2 ms in all cases and the output sampling period was determined to satisfy $T_u = nT_y$ $(1 \leq n \leq 5)$ in the multirate control. The cutoff frequency was heightened to the maximum value in each case, with which large oscillation or divergence did not occur. The position response in the differential coordinate and the RMS value of it at the start-up and the moment of contact were then compared.

Table 3-9(a) shows the sampling periods, the cutoff frequencies, and the RMS value from $t = 1.0$ s to $t = 2.0$ s in each case. Fig. 3-31 shows the comparison of the position response in the differential coordinate. The results show that the cutoff frequencies could be set higher and the absolute value of the response of the differential coordinate decreased by setting n larger, in other words, setting the output sampling period shorter.

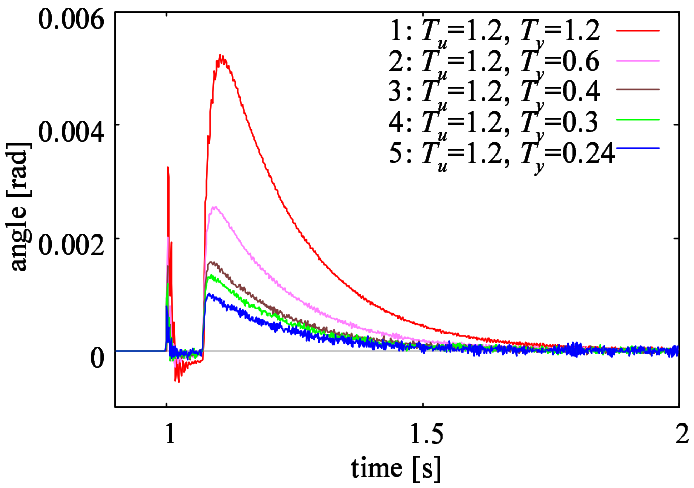

Fig. 3-31: Simulation results: influence of output sampling period on differential coordinate position

Similar simulations were executed for the single-rate control with the sampling period satisfying $nT_s = 1.2$ ms ($1 \leq n \leq 5$). Here, the input sampling period was also shortened in the single-rate, while it was kept long in the multirate. Table 3-9(b) shows the sampling periods, the cutoff frequencies, and the RMS value from $t = 1.0$ s to $t = 2.0$ s in each case. Variation of the RMS value is compared between the single-rate (short) and the multirate control in Fig. 3-32. The line in the figure is the approximate curve in the multirate control. It shows that the RMS value decreased in proportion to the output sampling period although the input sampling period was not changed in the multirate control. Comparing the RMS value concretely, the RMS value in the multirate control decreased by 54.2 % with $n = 2$ and by 83.1 % with $n = 5$ compared with that in the single-rate control ($n = 1$). The results show that control performance improves by enlarging n, in other word, by shortening the output sampling period.

The comparison of the influence of changing the sampling period between the input and the output is discussed below. The RMS value decreased by 83.1 % when the input sampling period was 1.2 ms and the output sampling period was changed to one-fifth, from 1.2 ms to 0.24 ms, while the decrease was only 27.5 % when the output sampling period was 0.24 ms and the input sampling period was changed to one-fifth, from 1.2 ms to 0.24 ms. This result indicates that the influence of changing the output sampling period is much greater than that of the input. Although the results of the multirate control did not reach those of the single-rate control with short sampling periods both for input and output, similar performance and similar tendency were achieved. The above results show that the performance close to that with the short sampling period for both input and output could be expected by shortening only the

Table 3-9: Settings and RMS values in simulations on multirate bilateral teleoperation

	T_u [ms]	T_y [ms]	g_v [rad/s]	g_{dis} [rad/s]	RMS Value	Rate of RMS
Multirate						
n=1	1.2	1.2	1600	240	1.76×10^{-2}	1.000
n=2	1.2	0.6	2800	540	8.06×10^{-4}	0.458
n=3	1.2	0.4	4300	920	4.76×10^{-4}	0.273
n=4	1.2	0.3	4600	1100	4.02×10^{-4}	0.229
n=5	1.2	0.24	5000	1500	2.97×10^{-4}	0.169
Single-rate						
	1.2	1.2	1600	240	1.76×10^{-2}	1.000
	0.6	0.6	2800	700	6.25×10^{-4}	0.355
	0.4	0.4	4300	1200	3.67×10^{-4}	0.209
	0.3	0.3	4600	1600	2.76×10^{-4}	0.157
	0.24	0.24	5000	2050	2.16×10^{-4}	0.123

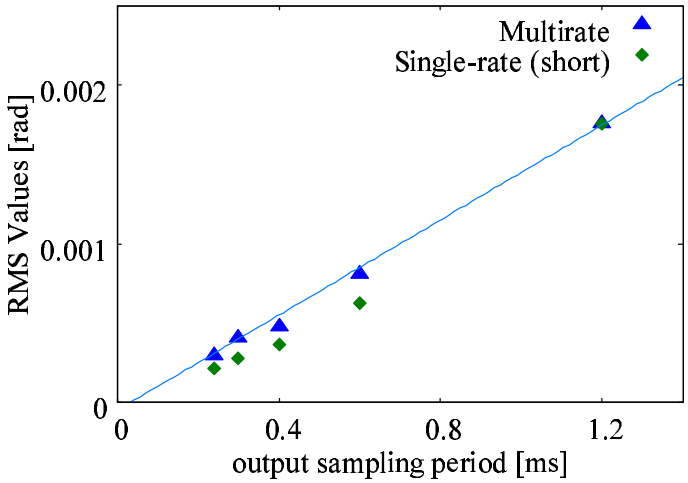

Fig. 3-32: Simulation results: relation of RMS value and output sampling period in bilateral control

output sampling period in the proposed method.

3.7.2 Experiments

The experiments were conducted under the following two conditions to verify the validity of application of the proposed multirate sampling method to bilateral teleoperation in the real system.

- single-rate control ($T_s(= T_u = T_y) = 0.2$ ms)

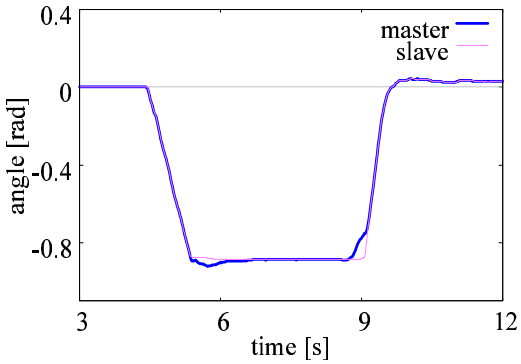

(a) position response

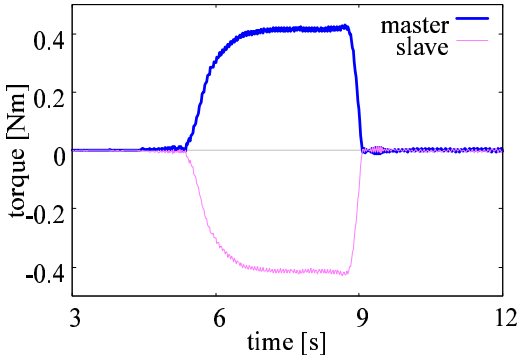

(b) force response

Fig. 3-33: Experimental results: bilateral control (single-rate)

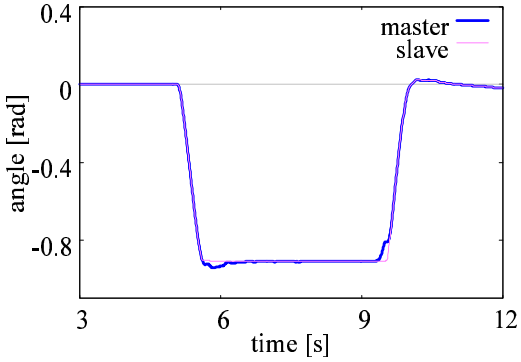

(a) position response

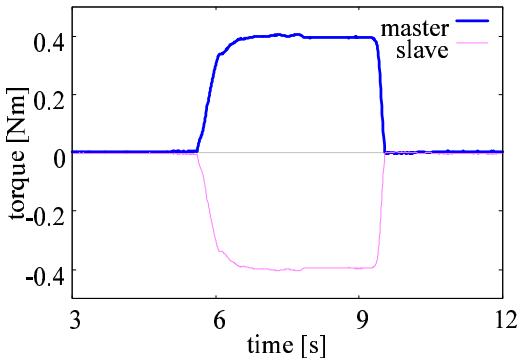

(b) force response

Fig. 3-34: Experimental results: bilateral control (multirate)

- multirate control with long input sampling period ($T_u = 0.3$ ms, $T_y = 0.1$ ms)

In the experiments, an operator manipulated the master manipulator to make the slave manipulator into contact with an aluminum object for several seconds. The sampling periods and cutoff frequencies used in the experiments are shown in Table 3-8.

Fig. 3-33 shows the position and force responses of the master manipulator and the slave manipulator in the single-rate control and Fig. 3-34 shows those in the multirate control. The position and force corresponded well between the master and the slave in both cases. The same as in the simulations shown in the previous subsection, small oscillation occurred in the single-rate control, however, when the slave was made into contact with the object. Moreover, the system became unstable when g_{dis} was set higher than 500 rad/s. On the other hand, in the case with the proposed method, an operator could manipulate stably even when g_{dis} was set higher than 500 rad/s and oscillation in the contact state was not confirmed. It is confirmed from the results that the bandwidth in which acceleration control is realized can be widen

by application of the proposed method even if the input sampling period is kept long. The above results imply that more accurate and precise tactile sensation can be transmitted by using the proposed method since the bandwidth of acceleration control greatly affects force transmission performance.

3.8 Summary

This chapter shows higher significance of shortening the sampling period of the output than that of the input in acceleration control with a focus on the relationship between sampling periods and the performance of acceleration control. A novel multirate sampling method with the shorter output sampling period was proposed for an acceleration control system from a viewpoint different from conventional methods. A disturbance torque in the proposed multirate sampling system was newly defined and the disturbance observer and reaction force observer were redesigned for the system. The proposed method is expected to improve robustness against disturbance by promoting faster response against disturbance and widening the bandwidth of acceleration control. The performance equivalent to that with short input and output sampling periods is also expected by applying the proposed method with the proposed disturbance observer. The validity of the proposed method was verified by applying the method to position control, force control, and bilateral teleoperation systems. The results of stability analysis for position control and force control systems are summarized as follows:

- position control: stability in the proposed method was almost middle between that in the single-rate control with the long sampling period and that with the short sampling period; and
- force control: stability in the proposed method was equivalent to that in the single-rate control with the short sampling period.

The followings were confirmed from the experiments.

- the cutoff frequency of the disturbance observer could be set higher and better performance was achieved by using the proposed method even with the longer input sampling period.
- the performance became close to that with the short sampling period for both input and output by applying the proposed observer.
- the proposed method was effective even in the system with a low resolution encoder.

Although the proposed method worked effectively even with a low resolution encoder, it is also effective to use a velocity measurement method other than M method in order to take the maximum advantage of the shortened sampling period when the resolution of an encoder is extremely low or the output sampling period can be set extremely short. The proposed method can be applied to any kind of motion control system and is effective especially for systems that require wide-band acceleration control. In application to various systems, time-variants characteristics achieved by the proposed multirate sampling method may also impose a positive effect, although the discussion and verification in this chapter mainly focused on the importance of shortening the output sampling period. Moreover, the sampling period for control can be designed differently among controllers, especially between inner loop and outer loop controllers, although this chapter set the control sampling period to the same value as the output sampling period. What is important is shortening the sampling period of the inner loop, which is an acceleration controller, and the sampling period for outer loop controllers can be designed independently considering the characteristics and requirements of controllers and a controlled object.

Chapter 4

Velocity Measurement Method for Acceleration Control

4.1 Introduction

A short sampling period and accurate acceleration information are vital for high-performance motion control. On the other hand, the sampling periods have limitations relating to hardware performance. In order to acquire better performance despite such limitations, the author proposed the multirate sampling method for acceleration control in Chapter 3. The output sampling period is set shorter than the input in the method. The control performance and stability of motion control were confirmed to be improved by the method. There is a problem, however, that a quantization error of an encoder affects the performance when the output sampling period is shortened. Although no negative effect was confirmed in the previous chapter, velocity resolution is deteriorated by shortening the sampling period when the fixed-time method (M method) [86]is used.

Meanwhile, many researches have been conducted over a long period of time on velocity measurement or estimation using pulses of an encoder. Among them, the fixed-time method (M method) and the fixed-position method (T method) [87] are most commonly used. M method counts the number of pulses from an encoder generated during a fixed time interval and calculates velocity by finite-different derivative. On the other hand, T method calculates velocity by measuring a time interval between two consecutive pulses and dividing an inter-pulse angle by the interval. Accuracy deteriorates in a low-speed range or with the short sampling period in M method, while T method achieves high accuracy. T method is applicable only to the low-speed range, however, since the time interval cannot be measured in a high-speed range.

M/T method was then proposed as a combination of the above-mentioned two methods [79]. M/T method has high accuracy in a low-speed range and works in all speed ranges. The method has been applied in many studies since it is effective for a practical use [88] [89]. The method is extended to a constant sample-time digital tachometer (CSDT) [90]. It can be incorporated more easily into a controller operated with a constant sampling time. The above-mentioned methods derive the velocity without using a model of a system. Researches on the topic had mainly been conducted by the 1980's and only a few effective methods have been proposed after M/T method. Under the situation, the synchronous measurement method (S method) was proposed to achieve high accuracy in all speed ranges [26]. S method calculates velocity in synchronization with alteration of the number of pulses generated in a fixed time interval and expands high accuracy of T method to a high-speed range. Accuracy is high only in a low-speed range in M/T method, while high accuracy is achieved in all speed ranges in S method. There are problems also in S method, however, such as existence of sampling points at which velocity is not calculated.

As model-based velocity estimation methods, the methods using Kalman filter [91] or an instantaneous speed observer are well known [27] [92]. Utilization of Kalman filter improves standard deviations in velocity measurement. The instantaneous speed observer is an effective tool to acquire the velocity between encoder pulses or sampling points. The observer is unique in the point that the observer regards an estimation error as a result of an error in an initial velocity value or uncertainty of the estimated disturbance and divides the error into these two factors using weighting coefficients. It is also interesting that the convergence of the observer can be designed using the weighting coefficients.

The aim of this chapter is to improve the performance of motion control based on acceleration control by improving the performance of velocity measurement. Firstly, M method, T method, M/T method, and S method are introduced as velocity measurement methods without models and relationship between the sampling period and measurement accuracy in each method is described. This chapter focuses on S method and aims at decreasing the influence of the quantization error of an encoder by improving performance of S method. The idea of the instantaneous speed observer is explained as a method for supporting velocity measurement methods. The instantaneous speed observer for S method is then proposed to solve the problems in S method. Utilization and the effect of the proposed measurement method based on S method and the instantaneous speed observer are described. This chapter also proposes combined use of the proposed velocity measurement method with the multirate sampling method proposed in Chapter 3. The proposed measurement method is applied to the position control system and experiments are conducted to verify the validity of the proposal in acceleration control-based motion control.

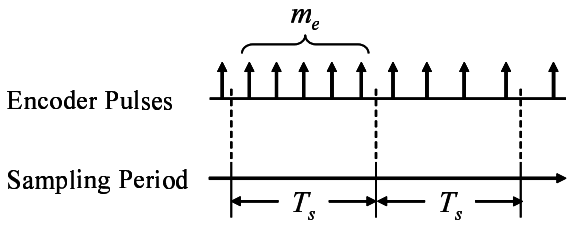

Fig. 4-1: Principal of M method

4.2 Velocity Measurement Methods

This section introduces M method [86] and T method [87] as most generally used velocity measurement methods. M/T method [79], which combines above two methods, is also explained. S method is described as the method effective especially for acceleration control [26]. Then the relationship between the sampling period and measurement accuracy in each method is described.

In the description below, a unit angle R_p and a unit velocity R_v are used as performance indices. The unit angle is the amount of angle per a pulse of an encoder. The unit velocity is the velocity when one pulse is generated in one sampling period. Those are defined as follows:

$$R_p = \frac{2\pi}{P} \tag{4.1}$$

$$R_v = \frac{2\pi}{PT_s}, \tag{4.2}$$

where P denotes pulses per revolution of an encoder and T_s denotes the sampling period for velocity measurement.

4.2.1 M method

M method, or a fixed-time method, is the most commonly used for measuring velocity from encoder pulses. The idea of the method is to count the number of pulses generated in a fixed time interval T_s. The principle is shown in Fig. 4-1. Here, m_e is the number of pulses generated in a fixed time interval (pulse number). The velocity is calculated by finite-difference derivative. The measured velocity $\bar{\omega}$ is obtained by the following equation.

$$\bar{\omega} = \frac{2\pi m_e}{PT_s} \tag{4.3}$$

The velocity resolution Q_v and the measurement time T_m are represented as follows:

$$Q_v = \frac{2\pi}{PT_s} = R_v \tag{4.4}$$

$$T_m = T_s. \tag{4.5}$$

The advantages of this method are as follows: the method can deal with all velocity ranges and the measurement time is constant and can be set arbitrarily. However, (4.4) shows that velocity resolution becomes larger as the sampling period becomes shorter. It is therefore difficult to acquire accurate velocity with a combination of a low resolution encoder and the short sampling period. An adverse effect of a quantization error may be imposed on the system when the output sampling period is shortened as in the multirate sampling method.

The easiest way to improve the accuracy is to average velocity values. The average velocity of n sampling periods is acquired as follows:

$$\bar{\omega}(i) = \frac{2\pi \sum_{j=0}^{n} m_e(i-j)}{nPT_s}. \tag{4.6}$$

The velocity resolution and measurement time are represented as follows:

$$Q_v = \frac{2\pi}{nPT_s} = \frac{R_v}{n} \tag{4.7}$$

$$T_m = nT_s. \tag{4.8}$$

The above equations show that averaging improves the velocity resolution by $1/n$ times and lengthens the measurement time by n times.

4.2.2 T method

T method measures an interval time between two consecutive pulses to calculate velocity. Fig. 4-2 shows the idea of the method. Here, T_e denotes an interval time between two consecutive pulses (pulse interval) and m_{sp} denotes the number of sampling points during the pulse interval (sampling number). Since T_e is measured as an integer multiple of the sampling period for pulse detection T_s, i.e., $T_e = m_{sp}T_s$, it contains an error smaller than T_s. The velocity is obtained by dividing the interpulse angle R_p by the pulse interval time as shown in the equation below.

$$\bar{\omega} = \frac{R_p}{M_{sp}T_s} = \frac{2\pi}{m_{sp}PT_s} \tag{4.9}$$

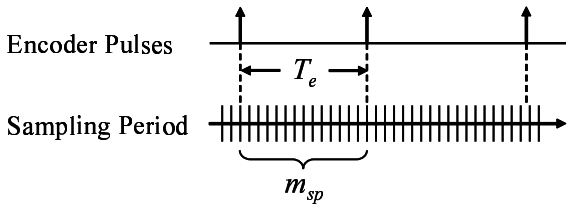

Fig. 4-2: Principal of T method

The velocity resolution and the measurement time are represented as in the following equations when the interpulse angle of the encoder is completely accurate.

$$Q_v = \frac{2\pi}{m_{sp}(m_{sp}-1)PT_s} = \frac{R_v}{m_{sp}(m_{sp}-1)} \tag{4.10}$$

$$T_m = m_{sp}T_s \tag{4.11}$$

It is shown from the equations that T method reduces the maximum error inversely proportional to $m_{sp}(m_{sp}-1)$ while the measurement time becomes m_{sp} times longer compared with M method. There are several problems, however, in this method. The largest problem is that the pulse interval cannot be measured when the interval is shorter than the sampling period. This method is therefore applicable only to a low-speed range. The maximum measurable speed in T method is the unit velocity of an encoder. In order to attain a wide measurable velocity range, this method is generally used for an ultra low resolution encoder or with a device that can implement a hardware counter and set the sampling period extremely short. Another problem of this method is that the measurement time T_m fluctuates depending on the velocity. In particular in velocity around zero, an interval time between two consecutive pulses becomes extremely long and thus the measurement delay becomes large. It may impose a great impact on the control performance. This method should therefore be used with a method for modification of the measurement time to prevent the system to be unstable. As the time modification method, Periomatic™ [93], CET [94], and the method focusing on the relation between the measurement time and quantization error [95] [96] can be applied.

When considering the application to the multirate sampling method, T method is preferable in the point that measurement accuracy depends on the sampling period and improves when the sampling period is short. The sampling period should be set extremely short. Although an applicable system is limited, T method is effective when it is used in combination with the multirate sampling method in the system that realizes a high sampling rate.

4.2.3 M/T method

M/T method [79] is a combination of M method and T method. Its performance is similar to that of T method in a low-speed range and to that of M method with averaging in a high-speed range. This method is therefore applicable to all speed ranges and improves measurement accuracy in the low-speed range.

4.2.4 S method

Synchronous-measurement method (S method) has been proposed as an effective method for acceleration control [26]. Acceleration control requires high accuracy in velocity information. The objective of S method is acquisition of high accuracy in all speed ranges. The method was proposed focusing on the mechanism that gives high accuracy to T method. High accuracy of T method is derived from synchronization of velocity calculation with the timing of pulse generation. In this point, T method can be regarded as a method that calculates the average velocity during two consecutive pulses. It is impossible in a high-speed range to synchronize calculation with the pulse generation because multiple pulses are generated during one sampling period. S method therefore focuses on patterns of the number of pulses generated in the sampling period. As shown in Fig. 4-3, the patterns in the high-speed range are confirmed to be quite similar to those in the low-speed range although several pulses always occur in the high-speed range. Then the patterns are presumed as occasional pulses with a certain amount of offset. S method monitors the alteration of the pulse numbers, which is called "pulse alteration", and calculates velocity in synchronization with occurrence of pulse alteration. The outline of velocity calculation in S method is shown in Fig. 4-4. Here, T_a denotes a time interval between two consecutive pulse alterations. T_a is measured as $T_a = m_{sa}T_s$ using the constant sampling period T_s and includes a measurement error smaller than T_s. m_{sa} is the sampling number between two consecutive pulse alterations. S method can be regarded as a method calculating an average velocity during two consecutive pulse alterations in synchronous with pulse alteration. The procedures of the velocity measurement are as follows:

(1) count the pulse number $m_e(i)$ in each sampling period;

(2) do not update the velocity value when the pulse number is the same as that in the previous sampling point; and

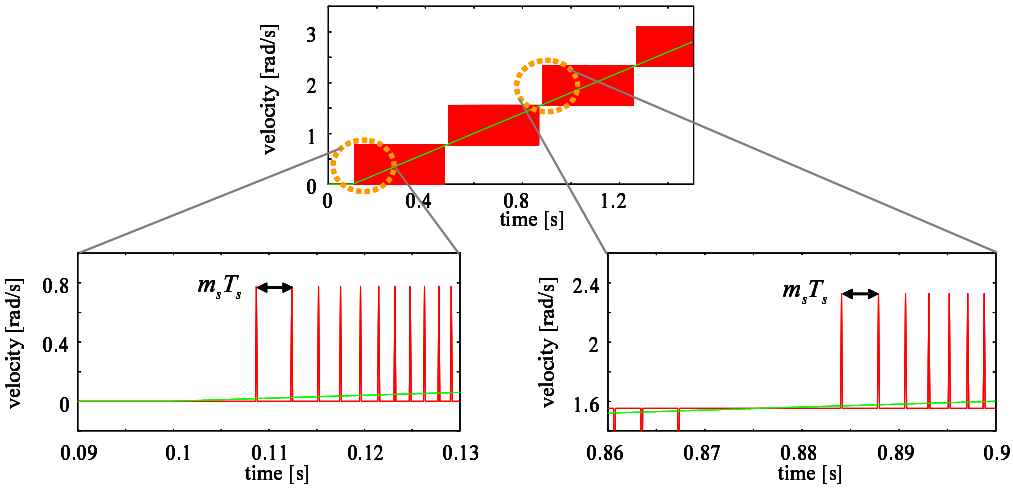

Fig. 4-3: Pulse pattern in low and high-speed ranges

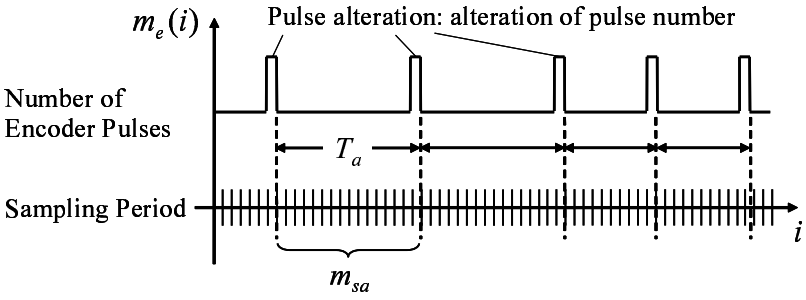

Fig. 4-4: Principle of S method

(3) calculate and update the velocity value if the pulse number alters (i.e., if pulse alteration occurs).

The measured velocity $\bar{\omega}$ at a sampling point i is derived by the equation below.

$$\bar{\omega}(i) = \frac{2\pi \sum_{j=0}^{m_{sa}} m_e(i-j)}{m_{sa} P T_s} \tag{4.12}$$

The equation (4.12) is quite similar to that for M method with averaging shown in (4.6). The difference is that averaging calculation of the S method is performed in synchronous with pulse alteration. The velocity resolution Q_v and the measurement time T_m are represented by the following equations.

$$Q_v = \frac{2\pi}{m_{sa}(m_{sa}-1)PT_s} \tag{4.13}$$

$$T_m = m_{sa} T_s \tag{4.14}$$

Equation (4.13) shows that velocity resolution equal to that in T method is acquired in S method. Moreover, an applicable speed range is not limited in S method. Since calculation is synchronized not with

pulse but with pulse alteration in this method, high accuracy of T method, which synchronizes velocity calculation with pulse occurrence, is expanded to a high-speed range.

The advantage of this method is applicability to a system with the relatively long sampling period since it works in all speed ranges regardless of the sampling period. Note that T method often requires an additional processor for the quite short sampling period to extend its measurable speed range. Furthermore, S method is also applicable to a system with an auxiliary processor to acquire the shorter sampling period. Accuracy of velocity measurement improves with the shorter sampling period. The problem in this method is that the measurement time becomes extremely long when the velocity is around a multiple of the unit velocity. Measurement time modification methods [93] [94] [95] can be applied to overcome this problem. In terms of combination with the multirate sampling method, S method is considered to be highly effective since the method is applicable to any system and improves measurement accuracy by shortening the sampling period.

4.2.5 Comparison of Velocity Measurement Methods

The performance of the velocity measurement method was compared in terms of accuracy by simulation. The pulse number of an encoder P was set as 2000 pulses/rev and the sampling period T_s was set as $T_s = 0.5$ ms. As shown in Fig. 4-5(a), the resolution did not change depending on the velocity in M method. In T method, resolution in a low-speed range was much higher than that of M method but the measurable speed range was limited. Fig. 4-5(b) shows that M/T method had resolution the same as that of T method in the low-speed range and the measurable speed range was expanded to all speeds. On the other hand, the resolution in the high-speed range was the same as that of M method with averaging of three samples. The resolution was much lower in the high-speed range compared with that in the low-speed range. In S method, however, high resolution was achieved in all speed ranges as shown in Fig. 4-5(c). The results indicate that S method is superior to other methods in terms of velocity resolution.

This research thus focuses on S method as an effective velocity measurement method for acceleration control. There are problems also in S method, however, such as existence of sampling points without velocity measurement. It occurs since velocity calculation in S method is performed only when pulse alteration occurs. This problem should be solved for further improvement in control performance using S method.

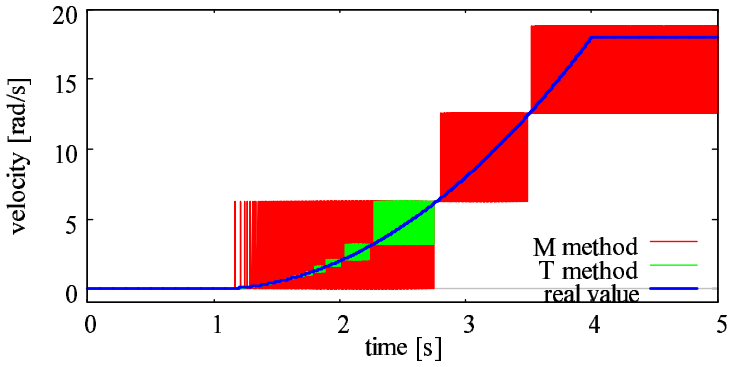

(a) measured velocity in M method and T method

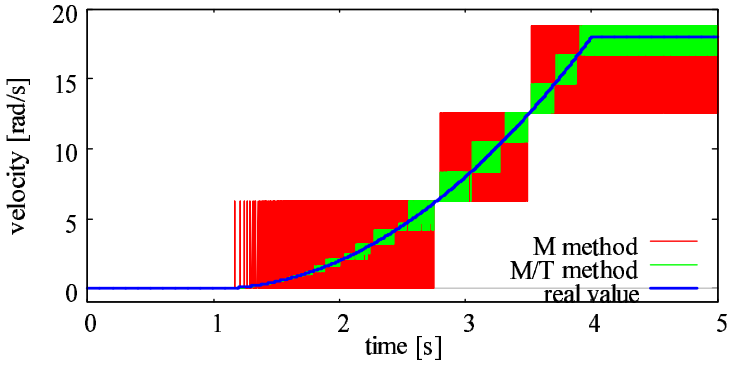

(b) measured velocity in M method and M/T method

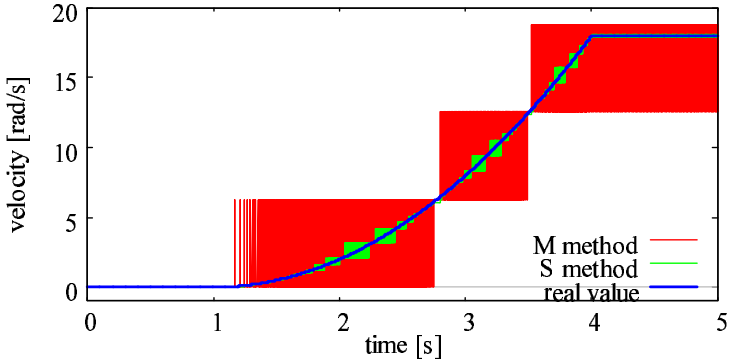

(c) measured velocity in M method and S method

Fig. 4-5: Comparison of measured velocity in velocity measurement methods

4.3 Instantaneous Speed Observer for S method

This research applies the instantaneous speed observer to solve the problem of existence of sampling points without velocity measurement in S method. After explaining the basis of the instantaneous speed observer, the observer for S method is proposed.

4.3.1 Instantaneous Speed Observer

The instantaneous speed observer [92] is a method for supplementing velocity measurement using encoder pulses. The instantaneous speed observer has been proposed to estimate the instantaneous speed of a motor between two consecutive sampling points or that between two consecutive encoder pulses. The observer is composed of the following two parts.

(1) velocity estimation when information from an encoder cannot be acquired

(2) modification of the estimated value at the timing when information from an encoder is acquired

In the case of T method, the observer considers the interval time between two consecutive pulses T_e as the modification sampling period T_1 and the sampling period for measurement and control T_s as the estimation sampling period T_2. Estimation is therefore executed at every T_2 while modification is executed for T_1. Here, T_1 is assumed to be longer than T_2. For simplicity, $t = \sum_{j=0}^{m} T_1(j) + nT_2$ $(n = 0, \cdots, N)$ is expressed as $|m, n|$. Here, $T_1(j)$ denotes an interval time between jth and $(j+1)$th pulses and m is a positive integer number.

The total acceleration torque τ_{mech} calculated at every T_2 is given by the sum of a motor torque $K_{tn}I_m|m, n|$ and an estimated disturbance torque $\hat{\tau}_{dis}$ as follows:

$$\tau_{mech}|m, n| = K_{tn}I_m|m, n| - \hat{\tau}_{dis}|m|. \tag{4.15}$$

$K_{tn}I_m|m, n|$ is renewed at every T_2 and $\hat{\tau}_{dis}$ is assumed to be constant during T_1. By integrating (4.15), the estimated instantaneous velocity and position are acquired as follows:

$$\hat{\omega}|m, n| = \hat{\omega}|m, n-1| + \frac{T_2}{2}\left(\frac{\tau_{mech}|m, n| + \tau_{mech}|m, n-1|}{J_n}\right) \tag{4.16}$$

$$\hat{\theta}|m, n| = \hat{\theta}|m, n-1| + \frac{T_2}{2}(\hat{\omega}|m, n| + \hat{\omega}|m, n-1|). \tag{4.17}$$

At the sampling point where an encoder signal is acquired, the position estimation error $\Delta\theta = \hat{\theta}|m, N| - \theta|m+1, 0|$ is calculated from the encoder pulse at $T_1(m+1)$. Then it is utilized for modification. There are two main factors that cause the error: an error of an initial velocity value used for estimation $\Delta\omega$ and uncertainty of the estimated disturbance torque $\Delta\tau_{dis}$. The position estimation error is divided into those two factors using weighting coefficients γ_1 and γ_2 as follows:

$$\gamma_1\Delta\theta = T_1\Delta\omega,\ \gamma_2\Delta\theta = \frac{T_1^2}{2J_n}\Delta\tau_{dis}. \tag{4.18}$$

The values used in the next interval are modified in the following equations.

$$\hat{\tau}_{dis}|m+1| = \hat{\tau}_{dis}|m| - \Delta\tau_{dis} \tag{4.19}$$

$$\hat{\omega}|m+1, 0| = \hat{\omega}|m, N| - \frac{T_1}{J_n}\Delta\tau_{dis} - \Delta\omega \tag{4.20}$$

The convergence of the observer can be designed by weighting coefficients γ_1 and γ_2. The relationship between poles of the observer and the weighting coefficients is represented in the equation below.

$$z^2 + (\gamma_1 + 3\gamma_2 - 2)z - \gamma_1 - \gamma_2 + 1 = 0, \tag{4.21}$$

where roots of the equation are the poles of the observer.

4.3.2 Instantaneous Speed Observer for S method

The method for implementing of the instantaneous speed observer to M method and T method had already been proposed [27] [92]. In the case of S method, however, implementation of the observer has not yet been proposed. This subsection proposes the instantaneous speed observer for S method.

The important issue in the instantaneous speed observer is designing the estimation period T_2 and the modification period T_1 appropriately. The estimation period is generally set equal to the control sampling period. Since measurement and control calculation are generally performed with the same sampling period in S method, the estimation period T_2 should be set as the sampling period for output and control T_s. On the other hand, the modification period is set differently in M method and T method since information from an encoder is required for modification of the estimated value. The modification period is set as follows in each method:

- T method: period in which pulse occurs; and
- M method: predetermined constant period for acquisition of an encoder signal.

The period fluctuates depending on the velocity in T method, while it is constant but usually set long enough to avoid deterioration of the velocity resolution in M method. The number of pulses generated in one modification period is always one in T method, while it is generally a plural number in M method. In S method, no pulse occurs in the measurement sampling period when velocity is low and multiple pulses occur when velocity is high. If the modification is performed with a predetermined constant period as in M method, there is a risk that no pulse occurs in the modification period and the estimation error cannot be calculated accurately. This problem can be solved by performing modification at the sampling point when pulse occurs the same as in T method. But there is another problem in this case that modification is performed at every sampling point when the velocity is high. Considering the convergence of the observer, it is obvious that executing modification at every sampling point imposes a negative effect on the performance since convergence of the observer cannot be assured. A novel design of the modification period is necessary for application of the instantaneous speed observer to S method.

The author focuses on the event on which the modification of the estimated values is performed in synchronization with in T method and M method. The modification is performed synchronized with a pulse in T method, while it is performed with a constant measurement period in M method. It means that modification is performed in synchronization with velocity measurement. The modification in S method should thus be performed also in synchronization with velocity measurement, i.e., pulse alteration. Since the pulse alteration occurs in a similar interval both in low and high-speed ranges, both the problem that modification is performed without pulse information in the low-speed range and the problem that modification in the high-speed range is performed at every sampling point can be avoided.

In addition to the above point, the following two points should be considered in modification in S method. Firstly, a pulse does not occur at every sampling point at which pulse alteration occurs. As shown in Fig. 4-6, no pulse occurs but pulse alteration occurs when the pulse number changes from 1 to 0 or from -1 to 0. Here, a negative number of pulse means that the actuator moves to the negative direction. The modification should not be performed at those sampling points because pulse information cannot be acquired. The second point is treatment in the case when pulse alteration dose not occur for a long period. The interval of pulse alteration is extremely long when velocity is around a multiple of the unit velocity. The system may become unstable when the estimated value is not modified for a long period. Since a similar problem occurs in T method, the method for dealing with the variant modification period has been proposed [97]. This method can also be used in S method. In this research, however, an alternative method is proposed with a focus on the characteristics of S method. In S method, there is a

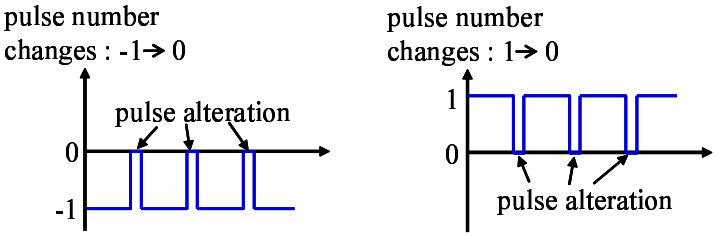

Fig. 4-6: Pulse alteration without pulse occurrence

possibility of occurrence of the pulse even when no pulse alteration occurs. The modification is therefore performed in synchronization with the pulse when no pulse alteration occurs for a certain period.

Fig. 4-7 shows the flow charts of the modification in T method and that in S method proposed in this subsection. The flow chart of the whole procedure of the proposed velocity measurement, which is a combination of S method and the instantaneous speed observer, is shown in Fig. 4-8. The situations are classified into the following four cases and position and velocity values to be outputted are determined depending on the situation:

(a) neither pulse nor pulse alteration occurs;

(b) pulse occurs but no pulse alteration occurs;

(c) pulse alteration occurs but no pulse occurs; and

(d) both pulse and pulse alteration occur.

Velocity calculation based on S method is executed in Case (c) and Case (d) while observer modification is basically executed in Case (d). Case (b) and Case (c) show a difference between S method and T method. Selection of values to be used for control in each case is explained next. In Case (a), the estimated values of the instantaneous speed observer are used both for position and velocity since neither position nor velocity information can be obtained from the encoder. In Case (b), position information from the encoder is used instead of the estimated value while the estimated value is used for velocity. The estimated position of the observer and the measured velocity value with S method are used in Case (c). In Case (d), both position and velocity are based on the measured values: encoder information and the calculated value in S method.

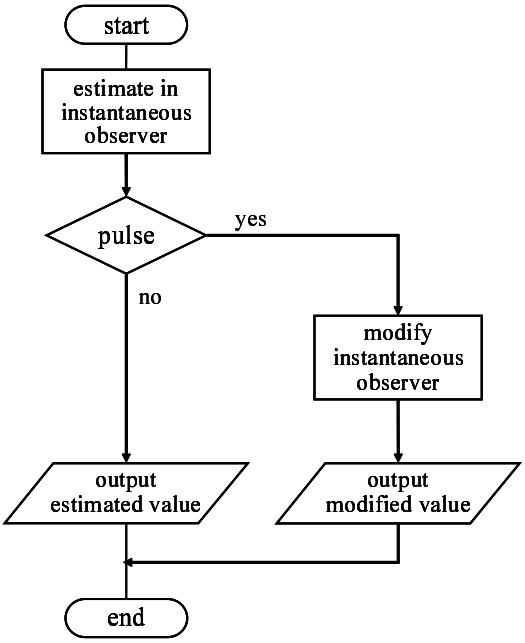

(a) T method

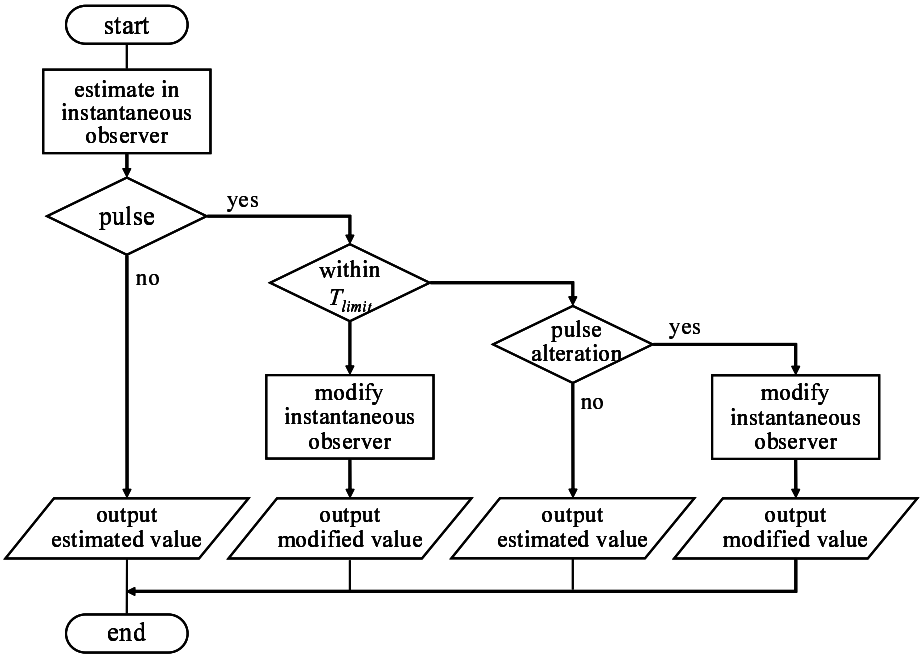

(b) S method

Fig. 4-7: Flow charts of modification process of instantaneous speed observer

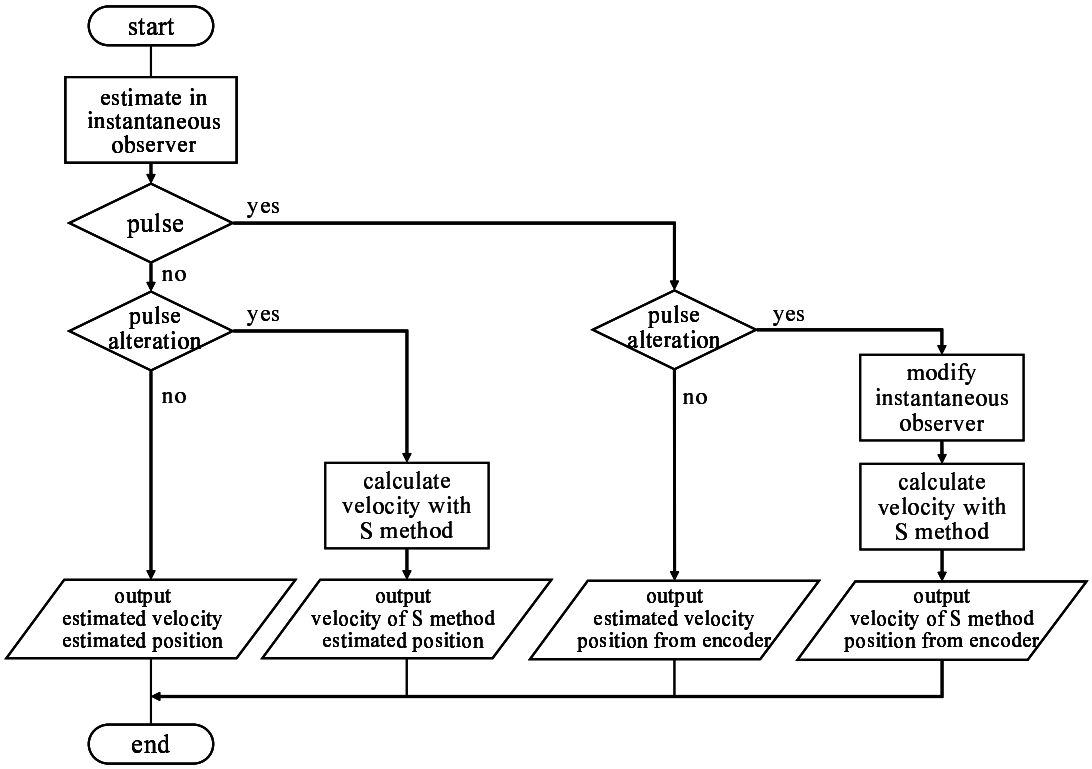

Fig. 4-8: Flow chart of velocity measurement in S method with instantaneous speed observer

4.3.3 Technical Issues in Application of Observer

There are some technical issues in application of the instantaneous speed observer to real systems. This subsection discusses the issues and provides solutions to them.

The problems of the instantaneous speed observer confirmed in the preliminary experiments are listed below.

- excess of the estimated value because of a long interval time of modification
- gap of the estimated value due to modeling errors such as friction and sudden and large disturbance
- jump in the estimated value

These are mainly due to the model-based structure of the observer. It is indispensable to deal with those issues to improve performance.

In this subsection, the author proposes to provide limiting values to the estimated position and velocity. Since the estimated values are modified when a pulse occurs, no modification means that no pulse occurs.

In this case, position should be within a unit angle from the previously acquired position. It indicates that the real position at the sampling point must be in the range of $R_p(p_n(i)-1) < \theta < R_p(p_n(i)+1)$. Here, $p_n(i)$ denotes a total number of pulses occurring by the sampling point iT_s and $R_p p_n(i)$ denotes previously acquired position from the encoder. The upper and lower limits for the estimated position can therefore be given as follows:

- upper limit : $R_p(p_n(i)+1)$; and
- lower limit : $R_p(p_n(i)-1)$.

The limiting value is used for control instead of the estimated value when the estimated position value exceeds the limits. The limiting value is renewed only when a new pulse is detected.

A method for preventing a large error in the estimated velocity is described next. In S method or T method, the maximum and minimum velocities at a sampling point can be derived in the velocity calculation process. Although the following discussion focuses on S method, a similar scheme can be applied to T method. In S method, no velocity calculation at a sampling point means that the number of pulses generated in the present sampling period is equal to that in the previous sampling period. The minimum or maximum velocity is determined based on an assumption that pulse alteration occurs in the next sampling period. If the pulse number in the next sampling period is larger than that in the present sampling period by one, the calculated velocity becomes the maximum value. On the other hand, if the pulse number is lower by one, the calculated velocity becomes the minimum value. The limiting values for the estimated velocity can therefore be derived as follows:

$$V_{max} = \frac{R_v(p_{sum}(i) + (m_e(i)+1))}{(m_{sa}(i)+1)} \tag{4.22}$$

$$V_{min} = \frac{R_v(p_{sum}(i) + (m_e(i)-1))}{(m_{sa}(i)+1)}. \tag{4.23}$$

Here, $p_{sum}(i)$ denotes a sum of the pulse numbers from the previous velocity calculation, $m_e(i)$ denotes the pulse number in the present sampling period, and $m_{sa}(i)$ denotes the sampling number from the previous velocity calculation. The limiting value is used for control instead of the estimated value when the estimated velocity value exceeds the limits. The limiting value is renewed at every sampling point concurrently with checking occurrence of pulse alteration.

Fig. 4-9 shows the flow charts of the proposed limiting processes. Note that limiting values are used only for control and the original estimation processes are continued even if the estimated values exceed

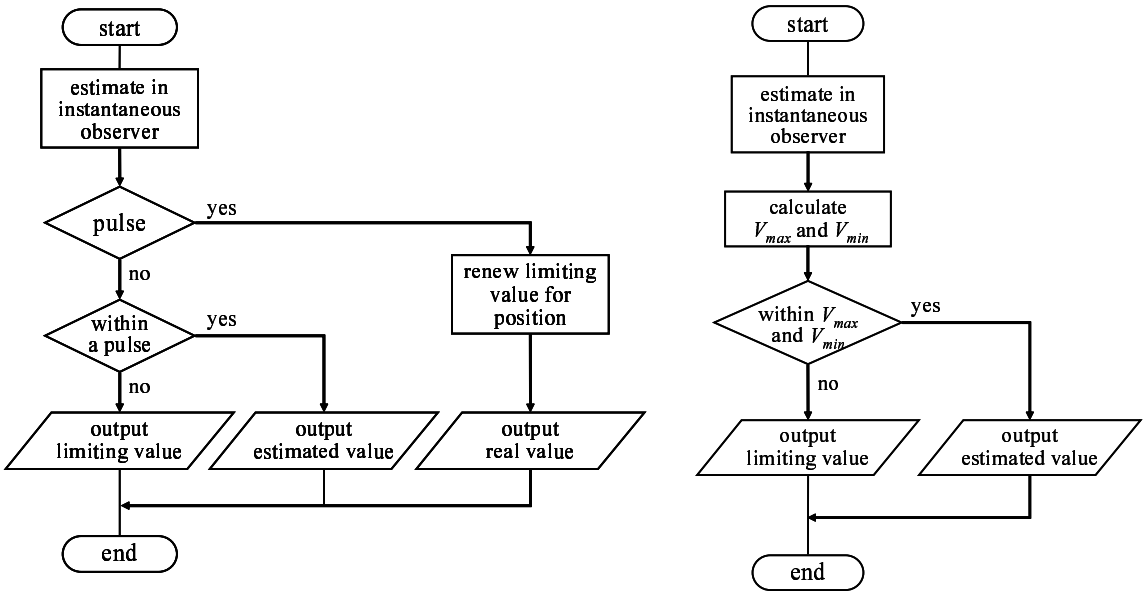

(a) position (b) velocity

Fig. 4-9: Flow charts of limiting process for estimated values

the limiting values. The modification of the observer is executed based on the value of the original estimation.

4.4 Application of S Method with Instantaneous Speed Observer to Multirate Sampling System

This subsection discusses combined use of the multirate sampling method proposed in Chapter 3, S method, and the instantaneous speed observer. The advantages of the combination and the role of each scheme in the combination are discussed.

The advantages of the multirate sampling method based on M method confirmed in Chapter 3 are summarized as follows:

- information of disturbance is detected at early timing; and
- influence of discretization is suppressed.

As a result, higher performance is achieved with wider bandwidth acceleration control. The expected advantages of the combination of the multirate sampling method, S method, and the instantaneous speed observer are described with a focus on the relationship among the time interval of pulse alterations T_a,

the time interval of pulses T_e, and the input sampling period T_u. The output and control sampling periods are set shorter than the input sampling period in the multirate sampling period.

(a) $T_a < T_u$: pulse alteration occurs during one input sampling period

(b) $T_a > T_u,\ T_e < T_u$: no pulse alteration but pulse occurs during one input sampling period

(c) $T_a < T_u,\ T_e < T_u$: neither pulse nor pulse alteration occurs during one input sampling period

The role of the instantaneous speed observer in the multirate sampling system based on S method is to provide interpolation values when the velocity is not calculated in S method. The instantaneous speed observer can also provide an interpolating position value when a pulse is not generated at the sampling point. Velocity calculation based on S method is executed only when a pulse alteration occurs, and the instantaneous speed observer is modified when both a pulse and a pulse alteration occur.

In Case (a), both of the advantages mentioned above for the multirate sampling method with M method are expected while the effect of the instantaneous speed observer is small. The instantaneous speed observer hardly affects the system especially when a pulse alteration occurs several times in one input sampling period. In Cases (b) and (c), S method does not provide velocity at any output sampling point. The instantaneous speed observer plays a large role in those cases. In Case (b), position information from an encoder can be acquired and the instantaneous speed observer is modified in the shorter sampling period when the multirate sampling method is applied. The performance may be improved and destabilization of the system is prevented. It is therefore described as an advantage of the multirate sampling method. The advantage of application of the instantaneous speed observer in this case is that the estimated velocity can be used for control. It may solve the problem of a long holding time in S method that degrades the control performance and even destabilizes the system. Even in Case (c), the instantaneous speed observer provides the estimated position and velocity for control with a shorter sampling period. Application of the instantaneous speed observer enables the system to be controlled in the shorter sampling period and to prevent an adverse effect of the long holding time in S method.

In summary, the multirate sampling method enables the system to be controlled with the shorter sampling period, S method supports the method by improving velocity resolution, and the instantaneous speed observer supports the method and plays a large role in providing positive effects of the short control sampling period especially when the velocity or position value cannot be acquired from the encoder.

The interesting point in the combination of the multirate sampling method, S method, and the instantaneous speed observer is that the combination imposes positive effects on each method. From a

viewpoint of the multirate sampling method, S method solves the problem of deterioration of velocity resolution with the short sampling period. Implementation of the instantaneous speed observer enables the method to execute control calculation using the estimated values even at sampling points at which the position or velocity information cannot be acquired from an encoder. The effectiveness of the short sampling period in the multirate sampling method can therefore be expected in any situations. From a viewpoint of S method, the multirate sampling method decreases the measurement error in S method by shortening the sampling period T_s. The instantaneous speed observer solves the problem of the long holding time in S method by providing the estimated values at sampling points at which S method cannot renew the velocity value. From a viewpoint of the instantaneous speed observer, the multirate sampling method shortens the modification period and makes the modified value more accurate. The stability of the observer thus improves. Application of S method enables the system to set the limiting values to the estimated values of the instantaneous speed observer. It decreases the error of the estimated value and thus prevents the negative influence of application of the observer.

A unique point of the combination from the standpoint of the instantaneous speed observer is that the sampling period for the instantaneous speed observer is shorter than that for renewal of the input. The instantaneous speed observer is usually utilized to fit an output sampling period to the input sampling period. In the proposed combination, however, the observer is used to support other methods and the estimated values are used only when the values from an encoder or S method cannot be acquired.

4.5 Verification

Experiments were conducted to verify the effects of S method with the proposed instantaneous speed observer and the combination of the measurement method and the multirate sampling method on velocity measurement accuracy and motion control performance. There are several issues to be considered in implementation of S method: coping with irregular pulse alteration, calculation of an LPF, and so on. This section applied the schemes explained in [96] to solve those issues.

4.5.1 Experimental Setup

The single-link manipulator shown in Fig. 3-11 was used in the experiments. The pulses of the encoder were used as quadrature encoder to acquire data for verification and the pulses were reduced in software to simulate the system with a low resolution encoder. In experiments on S method with the instantaneous

Table 4-1: Control parameters in experiments on velocity measurement method

position gain	K_p	3600	$1/\mathrm{s}^2$
velocity gain	K_v	120	1/s
weighting coef. (initial velocity)	γ_1	0.909	
weighting coef. (disturbance)	γ_2	0.091	
S method with instantaneous speed observer			
assumed pulse number	P	4000	pulse/rev
input sampling period	T_u	0.2	ms
output sampling period	T_y	0.2	ms
measurable velocity in T method	V_{maxT}	7.85	rad/s
Combination with multirate sampling method			
assumed pulse number	P	8100	pulse/rev
input sampling period	T_u	0.5	ms
output sampling period	T_y	0.1 or 0.5	ms
measurable velocity in T method	V_{maxT}	7.75 or 1.55	rad/s

speed observer, the pulse number was assumed as 4000 pulses/rev and the sampling periods were set as $T_u = T_y = 0.2$ ms. The measurable maximum velocity in T method was about 7.85 rad/s in this case. In experiments on the combined use of the measurement method and the multirate sampling method, the pulse number was assumed as 8100 pulses/rev and the sampling periods were set as $T_u = T_y = 0.5$ ms in the single-rate and $T_u = 0.5$ ms, $T_y = 0.1$ ms in the multirate. The measurable maximum velocity in T method was about 7.75 rad/s with $T_y = 0.1$ ms and about 1.55 rad/s with $T_y = 0.5$ ms. The manipulator was controlled with a position command given in the equation below by applying a PD controller with the disturbance observer shown in Fig. 2-7(b).

$$\theta^{cmd} = 4.3\cos(2t - 5.0) - 4.3 \tag{4.24}$$

A pseudo disturbance torque of 0.1 Nm was applied as a current input during the operation from $t = 7.0$ s to $t = 7.5$ s. The parameters used in the experiments are shown in Table 4-1. Since the considerable maximum velocity in (4.24) exceeds the measurable maximum velocity in T method in all cases, T method was not applicable.

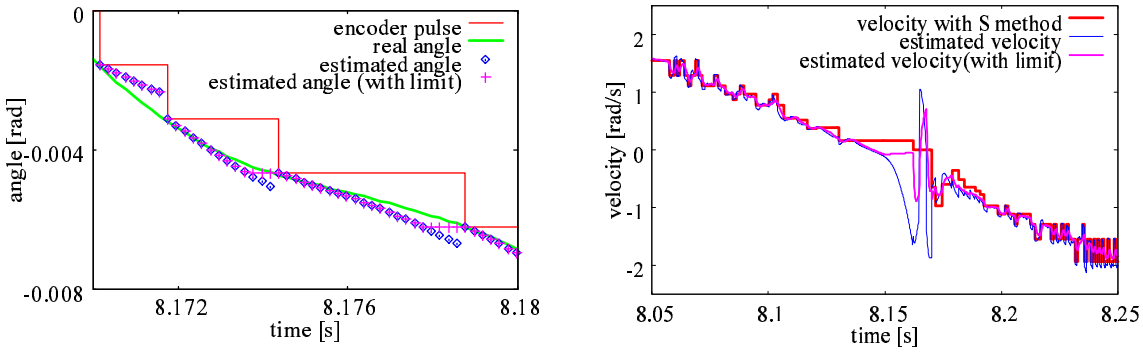

(a) position

(b) velocity

Fig. 4-10: Experimental results: limiting process for estimated values

4.5.2 Experimental Results on Instantaneous Speed Observer for S Method

First, effectiveness of the proposed solution to the technical issues of excess in estimated values, which sets the limiting values to the estimated values, was verified. In Fig. 4-10(a), the estimated position value exceeded the value of the next pulse and a large gap between the estimated value and the real value existed in some sampling points. Here, the real angle was derived from the output of a high resolution encoder. The modification of the estimated value was executed only when the value exceeded the limiting value. The excess in the estimated position was properly suppressed by introducing the limiting value. Fig 4-10(b) shows the results of velocity. A large deviation was confirmed in the estimated value around zero velocity. It was due to the long modification period of the observer. The deviation could be prevented perfectly by introducing the limiting value. Utilization of the limiting value is more effective when the influence of friction is larger since nonlinearity due to the friction is one of the causes of the estimation error.

Secondly, the effectiveness of design of the modification timing was verified. In the proposed design, the modification was performed in synchronization with a pulse alteration. The performance with the proposed design was compared with that in the case of performing the modification in synchronization with a pulse. Each of the estimated values was used for control and control performance was compared. Fig. 4-11 shows the estimated velocity in each case. The results show that deviation in the estimated value existed especially in the high speed range when modification was performed in synchronization with a pulse. It can be considered as a result of deterioration of convergence of the observer due to performing modification at every sampling point. The deviation was not confirmed in the case of performing the modification in synchronization with a pulse alteration. Moreover, noise in the estimated velocity was

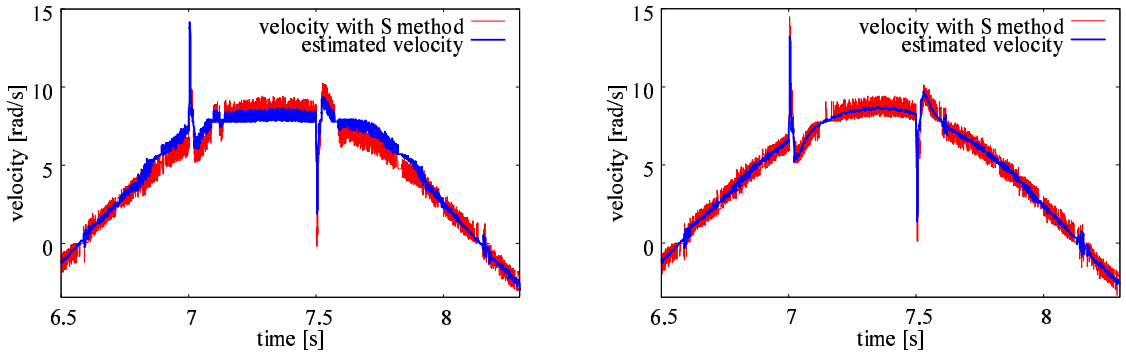

(a) synchronized with pulse

(b) synchronized with pulse alteration

Fig. 4-11: Experimental results: comparison of modification methods on estimated velocity

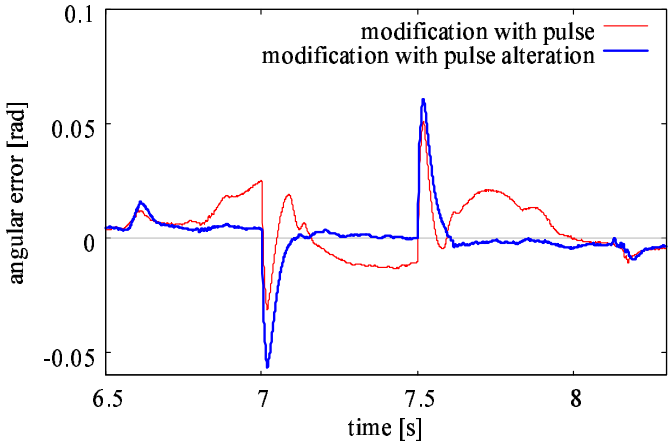

Fig. 4-12: Experimental results: comparison of modification methods on position control error

much smaller than that in the measured velocity. The influence on the control performance is verified in Fig. 4-12. As a result of the deviation in the estimated velocity, an angular error existed steadily when the modification was performed in synchronization with a pulse. In the case of performing the modification in synchronization with a pulse alteration, on the other hand, the steady state error disappeared. It is therefore effective in S method to perform the modification synchronous with pulse alteration.

The influence of the application of the instantaneous speed observer to S method on control performance and the response to disturbance was verified next. Fig. 4-13 compares the following three cases of the single-rate control:

- S method only (S);
- S method with the instantaneous speed observer (S+i); and

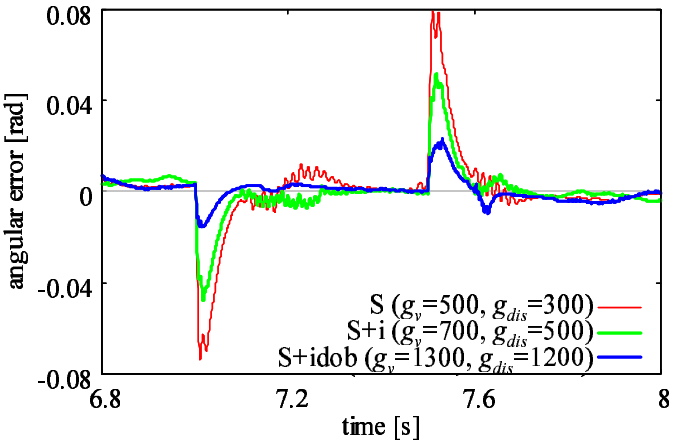

Fig. 4-13: Experimental results: conventional S method and proposed S method

- S method with the instantaneous speed observer and using the estimated values in the disturbance observer (S+idob).

In the experiments, the modification of the instantaneous speed observer was performed in synchronization with a pulse alteration and the limiting process was applied. When only S method was applied, large oscillation occurred and the system could not be operated stably when the cutoff frequency of the disturbance observer was higher than 300 rad/s. The cutoff frequency could be set much higher and oscillation in a steady state disappeared when the instantaneous speed observer was applied. Utilization of the estimated value of the instantaneous speed observer for disturbance calculation increased the maximum value of the cutoff frequency further and solved the problem of oscillation occurring around zero velocity. The cutoff frequency could be set about four times higher in this case compared with the case of using only S method. The influence of disturbance was therefore greatly suppressed by applying the instantaneous speed observer and using estimation values for disturbance calculation.

Finally, the proposed S method with the instantaneous speed observer was compared with M method in Fig. 4-14. Although the velocity value calculated with M method or S method was used for control, Fig. 4-14(b) shows the velocity value of each case calculated by S method in order for fair comparison. The difference was small but the noise was larger in M method from $t = 7.1$ s to $t = 7.5$ s. Moreover, a large sound noise occurred in the experiment with M method and it was unbearable in the practical use. The sound was not confirmed in S method with the instantaneous speed observer. Although the difference confirmed in the measured data was small, the proposed method was superior in terms of

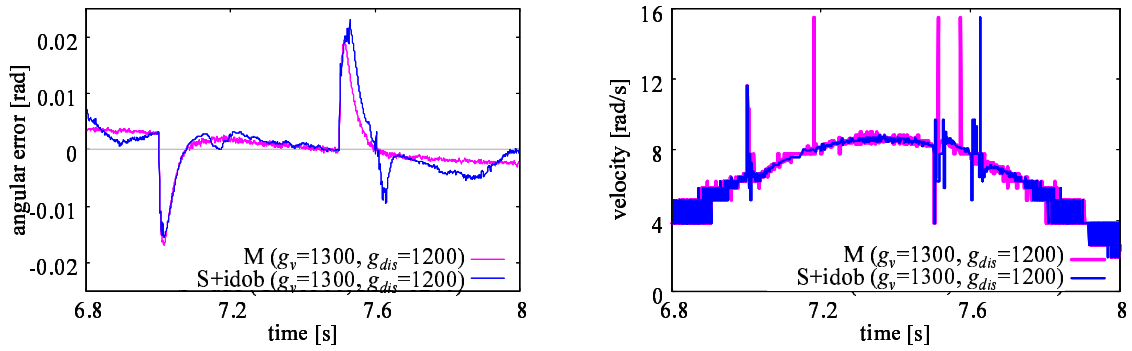

(a) position error (b) velocity response

Fig. 4-14: Experimental results: M method and proposed S method

practicability.

The above results show that the proposed method improves the performance by solving the problem of existence of sampling points without measurement. Noise, which was the problem in M method, was also greatly reduced. When the sampling period is short, the resolution deteriorates in M method, while it improves in the proposed method. The difference may therefore be more obvious when the sampling period is shorter.

4.5.3 Experimental Results on Combination of S Method and Multirate Sampling Method

This subsection verifies the effectiveness of combined use of the multirate sampling method, S method, and the instantaneous speed observer. Fig. 4-15 shows a comparison of the single-rate control and the multirate control with S method. The maximum value for the cutoff frequency of the disturbance observer was 300 rad/s in the single-rate control. On the other hand, the system was stably operated even with 600 rad/s in the multirate control. Fig. 4-16 compares the single-rate and the multirate when S method with the instantaneous speed observer was used for velocity measurement and the estimated value was used for disturbance calculation in the disturbance observer. The cutoff frequency of the disturbance observer could be set higher by applying the multirate sampling method the same as in the cases in Fig. 4-15. Since the cutoff frequency could be set higher, the influence of the disturbance was smaller in the multirate. No adverse influence of shortening the output sampling period with the multirate sampling method was confirmed.

Fig. 4-17 compares the following three cases of the multirate control: only S method (S); S method with the instantaneous speed observer (S+i); and S method with the instantaneous speed observer and

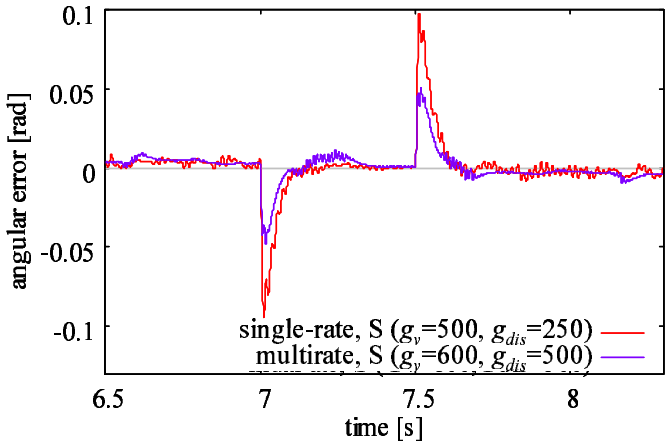

Fig. 4-15: Experimental results: S method in single-rate and multirate

the disturbance observer based on the estimated values (S+idob). Application of the instantaneous speed observer heightened the maximum cutoff frequency. Utilization of the estimated values in the disturbance observer not only heightened the cutoff frequency further but also reduced oscillation around zero velocity. As a result, the influence of disturbance was the smallest in "S+idob". This tendency of performance in comparison was similar to that in the single-rate control shown in Fig. 4-13. Then in Fig. 4-18, the proposed combination was compared with the conventional S method using the single-rate control. The maximum cutoff frequency could be heightened more than five times in the proposed combination compared with the conventional S method with the single-rate control. As a result, the influence of the disturbance was suppressed to extremely small by using the proposed combination. Furthermore, the oscillation occurring steadily during the operation was greatly suppressed. These results show validity of both application of the multirate control and that of the instantaneous speed observer to the multirate sampling system based on S method.

Finally, the proposed combination is compared with M method in Fig. 4-19. An amplitude of noise was smaller in the proposed method than in M method although the cutoff frequency was a bit higher. Fig. 4-19(b) shows the velocity value of each case. In order for fair comparison, measured values using S method are shown in all cases. When M method was used for control, a large noise occurred in the velocity value from $t = 7.1$ s to $t = 7.6$ s. On the other hand, the noise was kept small when S method was used. Furthermore, a large sound noise occurred in the experiment with M method. It is not acceptable in the practical use. This result is similar to that in the comparison in the single-rate control but the influence of using the S method was greater in the multirate control. These results show that the

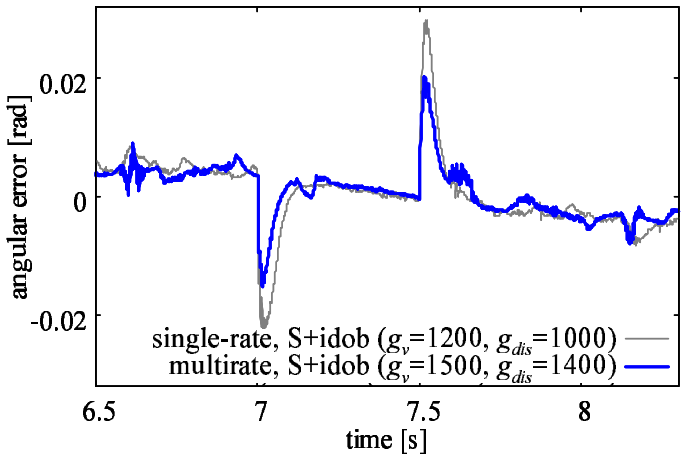

Fig. 4-16: Experimental results: proposed S method in single-rate and multirate

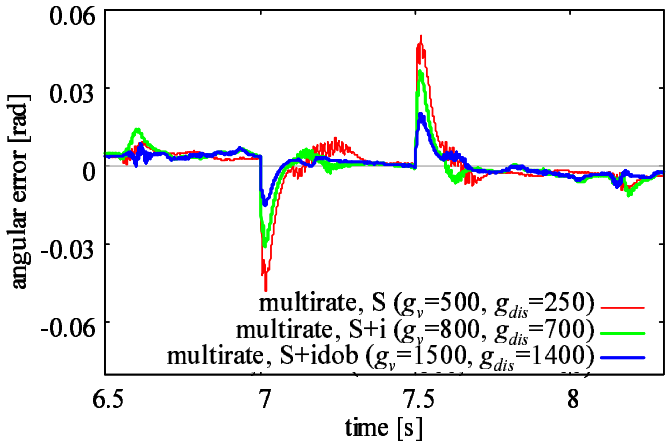

Fig. 4-17: Experimental results: conventional S method and proposed S method in multirate control

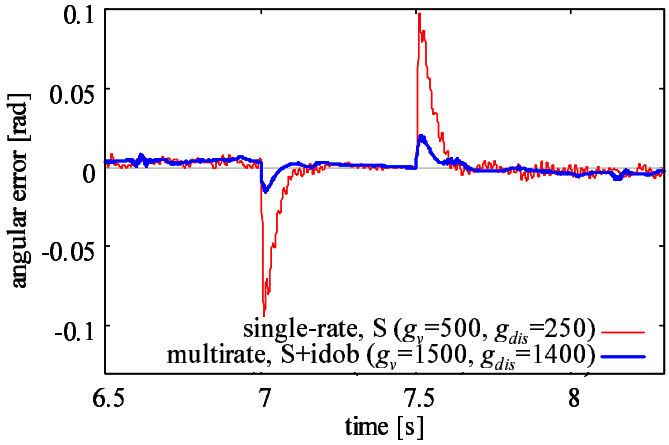

Fig. 4-18: Experimental results: S method (single-rate) and proposed combination

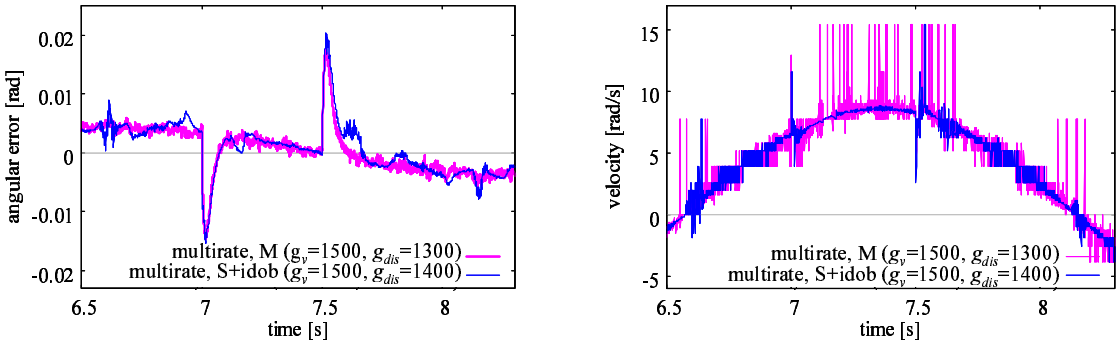

(a) position error (b) velocity response

Fig. 4-19: Experimental results: M method and proposed S method in multirate

proposed method is superior to M method both in noise reduction and performance improvement. Wider bandwidth acceleration control can thus be achieved by combined use of the multirate sampling method, S method, and the instantaneous speed observer even in the case where a resolution of an encoder is relatively low.

4.6 Summary

This chapter focused on the synchronous-measurement method (S method) as an effective velocity measurement method for acceleration control and proposed the instantaneous speed observer for the method. The proposed observer solves the problems of destabilization and performance limitation relating to the existence of sampling points without measurement. The method of giving the limit to the estimated value in the observer was also proposed in order to prevent large estimation errors due to the model-base structure of the observer. Since the velocity resolution is high even with the short sampling period in S method, the control performance is improved further by using the measurement method together with the multirate sampling method proposed in Chapter 3. Based on the experimental results, the validity of the proposed method was confirmed as follows:

- utilization of the proposed observer greatly widened the bandwidth of acceleration control and improved the performance dramatically compared with the result with only S method; and
- deterioration of the velocity resolution due to the short sampling period was solved and thus the noise during operation was suppressed compared with M method.

Chapter 5

Multirate Sampling Method for Network Based Control System

5.1 Introduction

Due to recent rapid progress in communication technology, introduction of a network to motion control systems is increasing in many fields [23] [24] [98] [99]. Control over a network suffers from problems of deterioration of stability and control performance, however, due to limitations of the network performances such as throughput and communication delay [25] [67] [100]. Researchers have attempted to clarify the trade-offs in networked control systems with communication constraints to improve performance [101] [102] [103]. In order to realize stable operation under communication delay, time delay compensation such as Smith predictor [104], communication disturbance observer [105], or H∞ based control [106], has been introduced to the control systems. In order to transmit high-quality signals under the limitation of a data rate, various quantization methods such as optimal dynamic quantizer have been proposed [107]. Data compression is also effective to reduce a data volume. Discrete cosine transform (DCT) based methods have been used widely in the fields of sound and image processing and they are also applied to compression of control signals [108] [109].

In addition to the above-mentioned issues, limitations on the interval of packet transmission impose the significant influence on the performance of the networked motion control system [110]. The packet transmission interval is limited due to the performance of communication lines and devices. The risk of network congestion is increased by shortening the interval even if a total data volume is small enough when a congestion avoidance mechanism is not implemented [68]. Since network congestion causes a

large communication delay and significant packet loss and seriously deteriorates the performance of the control system, the packet transmission interval should be set long enough. The limitation of the packet transmission interval raises problems relating to the sampling period and those relating to the quality of a transmission signal. If one constant sampling period is selected for a system, it should be set long enough to avoid network congestion. The bandwidth of the signal is limited since frequency components higher than Nyquist frequency cannot be reproduced due to aliasing. The performance of motion control is likely to be deteriorated when the sampling period is long and the bandwidth of the transmission signals used for the control is narrow.

This chapter focuses especially on sampling periods and the transmission signal in networked motion control systems in order to overcome limitations on the system and to improve the performance. This chapter tackles the problems in precise networked motion control based on acceleration control through the following three approaches:

- design of sampling periods;
- selection of data to be transmitted; and
- coding and decoding of transmission signal.

A bilateral teleoperation over a network is selected as a main target system in this chapter since control over a network and high-precision control are strongly required at the same time. Introduction of a network enables operators to execute tasks from safe and convenient areas. There are increasing demands for precise bilateral teleoperation with wide-band haptic sensation for application of a system to surgical or other complicated tasks [98]. As mentioned in Section 2.4.3, many researches on bilateral teleoperation have been conducted to achieve safe and efficient operations in various environments. A variety of control and performance evaluation methods have been proposed also for the system with communication delay [65] [111] [112]. Even with a number of researches, large or time-variant time delay makes stable operation difficult. When the bandwidth of a transmission signal is limited, reproduction of haptic sensation is greatly limited and the operator thus cannot feel real characteristics of remote objects. In this sense, bilateral teleoperation systems are greatly affected by network constrains.

The first approach focuses on the limitations on the sampling periods in networked motion control systems. In the point of sampling periods, a system connected through a network suffers from the limitation of the packet transmission interval. Although the previous chapter proposes the method focusing on

the input, output, and control sampling periods, the influence of the limitation of the packet transmission interval is needed to be considered in the networked control systems. As mentioned above, the limitation of the packet transmission interval is generally much severer than that on other sampling periods in motor control. Since the packet transmission interval should be set long enough to avoid network congestion, it is often set longer than other sampling periods [113]. A long packet transmission interval means that a time interval of data renewal of the signal acquired through a network is long. The multirate sampling method for acceleration control proposed in Chapter 3 mainly focuses on the cases in which the output sampling period can be set shorter than the input sampling period, in other words, the cases in which the signal can be acquired with an interval shorter than the interval for changing the real input to the motor. In a system with a network, however, some or all of the signals cannot be acquired in a short interval but only with a long interval. No clear guideline has been provided for design of each sampling period in that kind of system. The basic idea in this thesis is that the best performance under limitations on the system can be acquired by designing sampling periods independently for each sampling period with consideration only of limitations on the corresponding sampling period. A question here is whether or not and how meaningful it is to shorten the input, output, and control sampling periods when some information or signal is not renewed. In [113], attention was given to avoidance of network congestion to avoid large communication delay and the influence of changing sampling periods itself has not been verified. In Section 5.2, the influence of each sampling period on the performance is verified concretely and a design guideline for sampling periods, which is a multirate sampling method for a networked control system, is established as basic knowledge or technique for motion control over a network.

The second approach is consideration of what signals or values to be transmitted to attain better performance under the limitations. The time interval of data renewal of the signals acquired through a network is generally longer than that of other signals due to the limitation on the packet transmission interval as mentioned above. It causes discontinuity of the transmission signal and limits the bandwidth of the signal. It may deteriorate the stability and performance of the system. In order to transmit a higher quality signal even under limitations due to a network, it is important to improve a communication protocol and to process and transmit appropriate signals properly. A high quality signal here means a signal with preferable characteristics for utilization in control such as: small delay, small deviation from the real value, wide bandwidth, and a short data renewal interval. In order to solve the problem of a long data renewal interval due to the limitation of the packet transmission interval, a method of transmitting data at multiple sampling points as a packet has been proposed [114]. Although the adverse influence of

discontinuity of the transmission signal can be reduced with the method, there still remains a problem that the method causes delay since transmitted data is used from the oldest. It may differ depending on types of signals and control that which of continuity and bandwidth or delay should be prioritized. It may thus be possible to minimize the influence of a network by deciding the kind of data or signal to transmit, with consideration of the influence of time interval of data renewal or bandwidth and delay on control performance. This thesis mainly focuses on the bilateral teleoperation system and investigates the influence of quality of each of three signals, position, velocity, and force. A signal transmission method for bilateral teleoperation is then proposed in Section 5.3 based on the investigation. The basic idea is that performance under limitations can be improved by selecting transmitted data appropriately considering the influence of each signal on the performance.

This thesis also deals with processing of transmission signals as the third approach. The above-mentioned signal transmission method is also one of processing schemes. The third approach provides a scheme more generally applicable. The second approach requires investigation of the influence of the interval of data renewal and that of the delay on control performance every time when signals or control are changed. Although the method can improve the performance, it needs time and effort. Then the motivation for the third approach is whether or not it is really impossible to transmit wide-band signals with small delay when the packet transmission interval is limited. This thesis focuses on the trade-off between the data renewal interval and the delay in the transmission signal. A delay due to the transmission process is small when a long data renewal interval, in other words, low bandwidth, is accepted. A higher frequency signal is also required in control, however. Based on the above discussion, a coding and decoding scheme realizing wide-band small-delay signal transmission by dealing with the low frequency component and the high frequency component in different manners is proposed in Section 5.4. The scheme is applicable not only to bilateral teleoperation but also to any other signal transmission. Furthermore, a method for reducing calculation cost and the transmission packet size while maintaining high performance is proposed for signal transmission in bilateral teleoperation. The basic idea of the method is similar to the second approach mentioned above.

The validity of the hypothesis and the proposed methods derived from above-mentioned three approaches was verified by analysis and experiments.

5.2 Multirate Sampling Method for Systems with Network Constraints

This section focuses on the limitations on the sampling periods in acceleration control-based motion control systems connected through a network and proposes a design guideline for the sampling periods. The sampling periods focused on in this section are as follows: the input sampling period T_u; the output sampling period T_y; the control sampling period T_r; and the packet transmission interval T_c. The packet transmission interval is a time interval between consecutive packet transmissions. In order to acquire better performance even under limitations, it is important to design each sampling period independently. The design guideline is proposed by concrete verification of the influences of the sampling periods on the performance with reference to the existing method [113] and the multirate sampling method proposed in Chapter 3.

5.2.1 Multirate Sampling Method Focused on Packet Transmission Sampling Period

This subsection introduces the multirate sampling method proposed in [113]. This method was proposed for a networked control system to reduce an adverse impact of a network on the control performance. When systems are connected through a network, the performance is limited due to communication constraints such as communication delay, packet loss, throughput, and the packet transmission rate. The throughput and the packet transmission rate are limited by the performance of the communication lines and the communication devices. The increase in communication delay by shortening the packet transmission interval was shown in [113]. Especially when the packet transmission interval is set shorter than a certain value, communication delay surges and significant packet losses occur due to network congestion. It was also confirmed from the performance analysis that the adverse influence of the packet transmission interval on transparency was smaller than that of communication delay [115]. It was then proposed to design the packet transmission interval independently of the control sampling period. The packet transmission interval is set longer than the control sampling period in this method.

$$T_c > T_r \tag{5.1}$$

The packet transmission interval is set to the value long enough to avoid network congestion by identifying the characteristics of a network before implementation.

5.2.2 Design of Sampling Periods in Motion Control over Network

This subsection provides a design guideline for sampling periods in acceleration control-based motion control systems connected through a network and discusses the matters to be verified. The basic idea is that the best performance under limitations on the system can be acquired by setting the period to the shortest value that does not impose the adverse influences, with consideration of the limitations on each sampling period. The precise design procedure is described below.

In terms of stability and performance of the system connected through a network, it is important to keep communication delay short. The packet transmission interval should therefore be set to the value long enough to avoid network congestion as explained in the previous subsection. Since better performance is generally acquired with a shorter packet transmission interval if the communication delay is the same, the interval T_c should be set to the shortest value that can avoid network congestion. As explained in Chapter 3, it is important to set the output and control sampling periods short in acceleration control. Although the output sampling period is strictly limited in a system with a vision sensor, it can be set to the same as the control sampling period when an encoder or a potentiometer is used. The output and control sampling periods, T_y and T_r, are then set to the shortest values with consideration of the processing time for control calculation. It is also effective to set T_y and T_r shorter than the input sampling period. The input sampling period T_u is determined with consideration of the processing time of D/A converter and the frequency of PWM. The relationship among the sampling periods determined based on the above-mentioned design guideline is expressed as shown in Fig. 5-1 and the following equations.

$$T_y = T_r \tag{5.2}$$

$$T_u = nT_r \tag{5.3}$$

$$T_c = mT_r, \tag{5.4}$$

where n and m denote positive integer numbers.

The advantages expected with the design guideline and the matters to be verified are described below. The following points are listed as main expected advantages of utilization of the guideline.

- convergence of feedback control improves
- cutoff frequency of the disturbance observer can be set higher and the bandwidth of acceleration control is thus widened

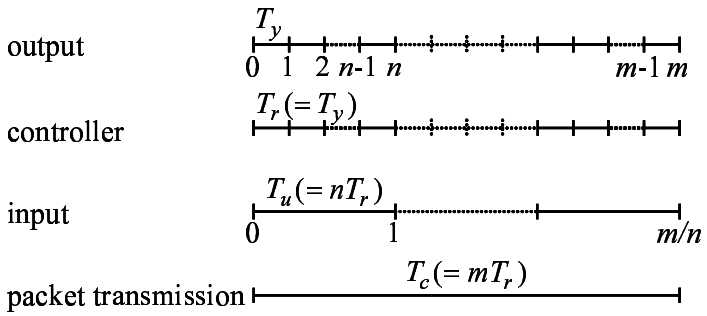

Fig. 5-1: Design of sampling periods in networked motion control system

The first point is owing to execution of control in the short sampling period. The renewal interval of the signal acquired through a network is generally limited to T_c. When information in both local and remote sides is utilized for control, however, some of signals, such as the information in the local side, which is usually the reference or the response for the control, can be acquired with the output sampling period, the short sampling period in the guideline. This is a key for the first advantage. For example, in the case of the bilateral teleoperation system, the response signals for the controller, which are the output of the local side robot, can be obtained in a short sampling period even if the packet transmission interval is long. T_c longer than T_y and T_r in bilateral teleoperation therefore means that the reference values for control calculation, the outputs of the remote side robot, are not renewed at some control sampling points. The convergence to the reference is expected to be improved even in this case by obtaining output information and executing feedback control repeatedly with the short sampling period.

The second point is an advantage associated with shortening output and control sampling periods according to the guideline. The maximum value of the cutoff frequency depends on the sampling period for the disturbance observer. Since the sampling period of observer calculation is shortened in the guideline, the cutoff frequency can be set higher than that in the case where all sampling periods are set equal to the packet transmission interval. As a result, the bandwidth of acceleration control is expected to be widened. In terms of bilateral teleoperation, performance such as reproducibility and drift is expected to be improved.

There is another advantage expected when there is a jitter in a communication delay. When a remote signal does not arrive at a scheduled sampling point due to the jitter, a system has to wait renewal of a value of the remote signal until the next scheduled sampling point of packet transmission or change the control sampling period according to change in the communication delay. The former increases the delay

and the influence of discretization and the latter is not preferable in many systems in terms of stability and convergence. The increase in the delay and the influence of discretization can be minimized by using the proposed design guideline, since the received value is reflected earlier at a control sampling point just after the remote signal arrives even between packet transmission intervals.

When the proposed design guideline is used, several sampling periods exist in a system. As a method of manipulating sampling periods, upsampling and downsampling are generally used. The relation and difference between those methods and the proposed design guideline are described below. A packet transmission interval is longer than the output sampling period, which is the same as in downsampling. When considering a packet transmission interval as a reference, output, control, and input sampling periods are shortened in the proposed design guideline. It is different from upsampling, however. The major difference is that the output signal is actually measured and control calculation is performed in the sampling points between packet transmission sampling points in the proposed design guideline while the output value is generated by interpolation in upsampling. Acquisition of a wide-band signal and detection of the influence of the disturbance in an early timing are therefore possible by using the proposed design guideline but not by upsampling. Meanwhile, application of upsampling seems to be effective for heightening a sampling rate of a transmission signal in the received side. Although the transmission signal is assumed to be held for a packet transmission interval in this section, introduction of upsampling enables a system to renew a value of a remote signal in a sampling period the same as a local signal. Although the bandwidth of the signal does not improve, the influence of discretization may decrease.

The matters to be verified in this section are then discussed below. As an advantage of shorting T_y and T_r, it was confirmed in Chapter 3 that better performance can be acquired even with a longer T_u. On the other hand, the effectiveness of shortening T_y and T_r in the case with limitations on T_c and existence of communication delay has not yet been confirmed. The multirate sampling method in which T_r is set longer than T_c described in [113] focuses just on avoidance of performance deterioration due to network congestion. Thus a focus was given only on design of the packet transmission interval and the influence of changing T_y and T_r has not been verified. Whether or not shortening T_y and T_r is effective in the case where T_c is limited and how the proposed guideline influences on the control performance are needed to be verified. The following subsections conduct concrete verification with a focus on the influence of the shortened sampling periods itself and that of changing the cutoff frequency of the disturbance observer according to the sampling periods. In the verifications in the following subsections, a bilateral teleoperation system connected through a network is taken up as an example of the system that requires

acceleration control-based motion control over a network.

5.2.3 Performance Analysis

In this subsection, frequency analyses were conducted to clarify the influences of the design guideline, especially the influences of setting the input, output, and control sampling periods shorter than the packet transmission interval on the motion control performance. A bilateral teleoperation system was taken up as an example of motion control systems connected through a network. The analyses were conducted for the system with a four-channel-based controller shown in Fig. 5-2. The controller is expansion of the controller shown in Fig. 2-12 to the system connected through a network. Here, N denotes a communication path and subscripts ms and sm denote transmission from the master side to the slave side and that from the slave side to the master side, respectively. $\tilde{X}$ and $\tilde{F}$ represent received and decoded signals of X and F. The same as in the controller shown in Fig. 2-12, C_1, C_2, C_m, and C_s represent position controllers, and C_2, C_3, C_5, and C_6 represent force controllers. A Smith predictor [104] based delay compensation is assumed to be applied to the controller. The disturbance observer and the reaction force observer are implemented on each robot. The estimated force $\hat{F}_m$ and $\hat{F}_s$ were assumed to be obtained through an LPF as shown in the equation below.

$$\hat{F}_m = \frac{s}{s+g_e}F_m \tag{5.5}$$

$$\hat{F}_s = \frac{s}{s+g_e}F_s \tag{5.6}$$

An operator and an environment were modeled as a spring and damper model expressed in (2.37) and (2.38). The communication line was modeled as shown in Fig. 5-3. Here, $S(s)$ denotes a sampler, $H(s)$ denotes a zero-order-holder, the subscripts of $S(s)$ and $H(s)$ denote the sampling period and the holding period, and L_c denotes communication delay. Although the method with high-dimensional state-space equation [85] should be used for precise analysis on the multirate system as described in Section 3.5.1, the equations become too complicated for calculation when the number of sampling periods is large. This chapter therefore uses models of a sampler and a zero-order holder instead for simplified analysis. The sampler and holder were assumed to be an ideal sampler and zero-order holder. Laplace domain transfer functions of the sampler and the holder are represented as follows [116]:

$$S_{T_c}(s) = 1/T_c \tag{5.7}$$

$$H_{T_c}(s) = \frac{1-e^{-T_c s}}{s}. \tag{5.8}$$

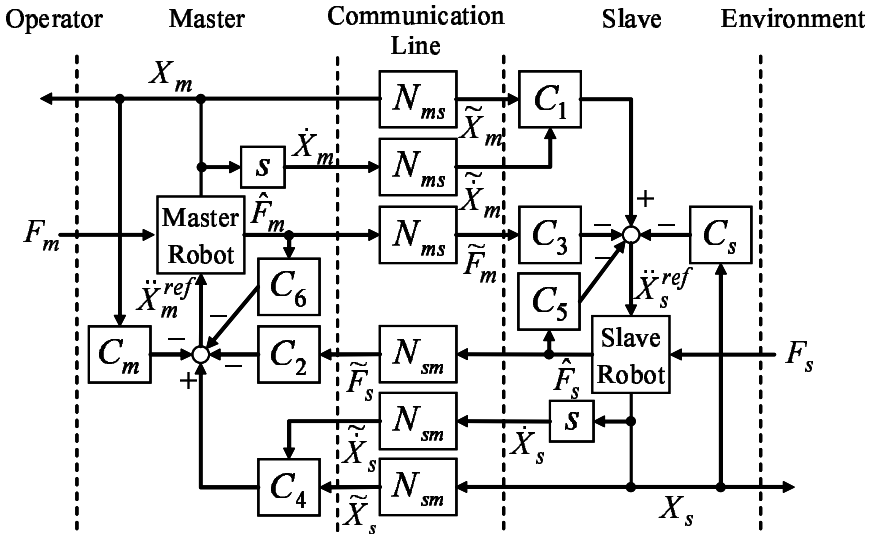

Fig. 5-2: Four-channel-based controller for bilateral teleoperation over network

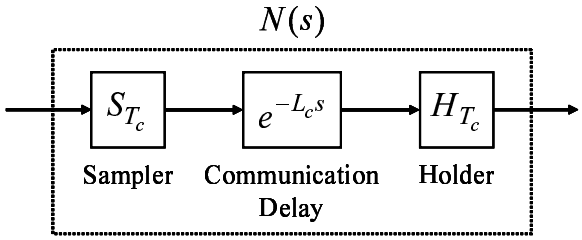

Fig. 5-3: Communication path: $N(s)$

This study introduces the following four indices explained in Section 2.4.3 to evaluate the performance of bilateral teleoperation: reproducibility, operationality, tracking, and drift. Reproducibility P_r should satisfy $|P_r| = 1$ for reproduction of the environmental impedance perfectly. The operationality evaluates the magnitude of the force an operator feels other than the real reaction force from the environment and should satisfy $|P_o| = 0$. Tracking P_t and drift P_d evaluate the position difference between the master device and the slave device in a non-contact motion and a contact motion, respectively. The ideal conditions for perfect coincidence of position are $|P_t| = 0$ and $|P_d| = 0$.

Analyses were conducted for the following three cases:

- Case A: single-rate ($T_c = T_r = T_y = T_u$);
- Case B: multirate with same g_{dis} ($T_c = mT_r = mT_y = mT_u$); and

Table 5-1: Control parameters in analysis on design guideline of sampling periods

Position feedback gain	K_p	3600.0	$1/\mathrm{s}^2$
Velocity feedback gain	K_v	120.0	1/s
Force feedback gain	K_f	1.0	m/Ns^2
Communication delay	L_c	1.0	ms
Nominal mass	M_n	0.5	kg
Spring coefficient of operator	K_h	400.0	N/m
Damping coefficient of operator	D_h	40.0	Ns/m
Spring coefficient of environment	K_e	10000.0	N/m
Damping coefficient of environment	D_e	10.0	Ns/m

Table 5-2: Settings in analysis on design guideline of sampling periods

	T_r [ms]	T_c [ms]	g_{dis} [rad/s]
Case A	5.0	5.0	500.0
Case B	1.0	5.0	500.0
Case C	1.0	5.0	2000.0

- Case C: multirate with higher g_{dis} ($T_c = mT_r = mT_y = mT_u$).

Here, Case B and Case C are the cases with the design guideline. Since the sampling periods of output, control, and input were set equal in all cases, these sampling periods are expressed as the control sampling period T_r in the following explanation for simplicity. The cutoff frequencies of the reaction force observer g_e were set to be equal to those of the disturbance observer g_{dis} in all cases. The cutoff frequencies were set to the same value in Case A and Case B. The cutoff frequency can be set higher in the multirate sampling system than in Case A, however, since the sampling period for observer calculation is shortened. The cutoff frequency was thus set higher in Case C. Comparison between Case A and Case B shows the influence of shortening the control sampling period itself, not including the influence on the maximum value of g_{dis}. Then comparison between Case B and Case C shows the influence of heightening the cutoff frequency by shortening the control sampling period. The parameters used in the analyses are represented in Tables 5-1 and 5-2.

Fig. 5-4 shows the bode diagram of each index. Fig. 5-4(a) shows the bode diagram of reproducibility. Although the packet transmission period and the cutoff frequency of the disturbance observer were the same in Case A and Case B, the gain peak at around 200 rad/s confirmed in Case A decreased and the bandwidth improved in Case B. When g_{dis} was set higher in Case C, the bandwidth was further improved. Fig. 5-4(b) shows the bode diagram of operationality. Fluctuations of the gain and the phase

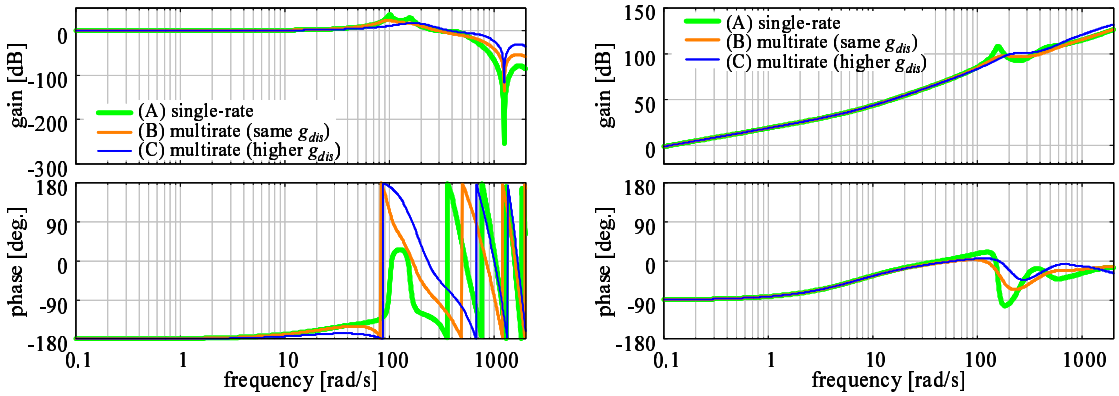

(a) reproducibility P_r

(b) operationality P_o

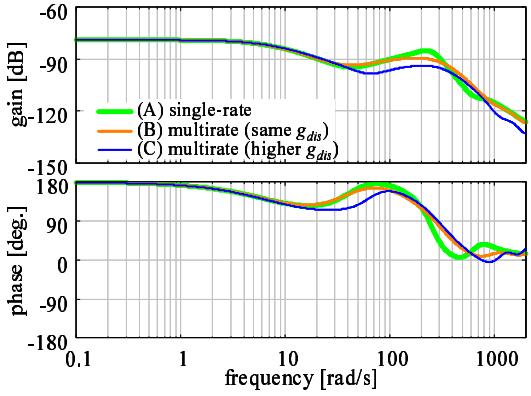

(c) tracking P_t

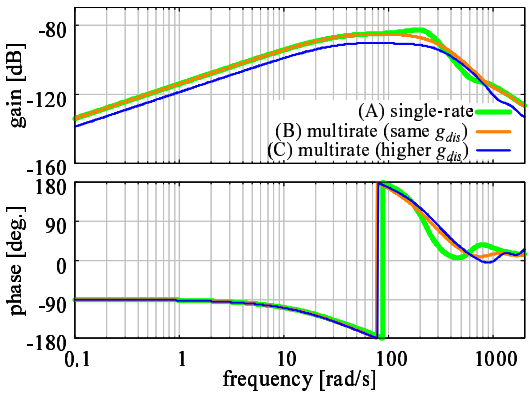

(d) drift P_d

Fig. 5-4: Analysis on influence of sampling periods on performance indices

were confirmed at around 200 rad/s in Case A. They were greatly alleviated and almost disappeared when the control sampling period was set shorter in Cases B and C. Although the gain in the high frequency range was larger in Case C, it may not impose the great influence on the operation since the frequency of motions of a human operator is usually not very high. Figs. 5-4(c) and (d) show the bode diagrams of tracking and drift, respectively. The gains were small enough in all cases to consider the ideal condition was satisfied. Both in tracking and drift, fluctuations of the gain and the phase were confirmed at around 200 rad/s in Case A. They were suppressed in Case B and Case C. The performance of tracking in the high frequency range improved in Case C. In terms of drift, the gain was the smallest in Case C in almost all frequencies.

The above results show that performance was better in Case B than in Case A, and better in Case C than in Case B, although the difference among the methods appeared mainly in reproducibility and the

difference was small in other indices. It means that performance improves by shortening the control sampling period even if the packet transmission period is kept long and the cutoff frequencies of the observers are kept low. The performance improvement with the guideline is thus expected even in the cases where the cutoff frequency of the disturbance observer is limited due to noise of a sensor or a mechanical structure of a robot. The results also show that the performance was further improved by setting the cutoff frequency higher according to the shortening the control sampling period. Improvement was significant especially in reproducibility.

5.2.4 Simulations and Experiments

Simulations and experiments were conducted to verify the influence of the design guideline on motion control performance when limitations on the packet transmission interval and communication delay existed. An example of a target system is shown in Fig. 5-5(a). In this verification, the limitations on the sampling periods were set to the values in the target experimental system. The limitation of the control sampling period was 0.05 ms and that on the input sampling period was 0.1 ms. The basic values for the packet transmission sampling period and the communication delay were determined referring to the results shown in [113]: $T_c = 1.2$ ms and $L_c = 1.0$ ms. A Smith predictor [104] based delay compensation was used for compensation of the communication delay. The length of communication delay was acquired from the time stamp of the packet. In order to verify the influence of the output and control sampling periods, sampling periods were set as follows:

- multirate: $T_c = mT_r = 1.2$ ms; and
- single-rate (short): $mT_c = mT_r = 1.2$ ms.

Here, m is $m = 1,\ 2,\ 3,\ 4,\ 6,\ 12,\ 24$. The output sampling period was set to be equal to T_r. The input sampling period was set to be the longer of T_r and the limitation of the input sampling period, 0.1 ms. The multirate with m higher than 1 follows the design guideline. Note that not only the control sampling period but also the packet transmission interval was set shorter in the single-rate (short). The communication delay may thus greatly increase in single-rate (short) when it is applied to the real system. Since the sampling periods of output, control, and input were set equal in almost all the cases, these sampling periods are expressed as the control sampling period T_r in the following explanation for simplicity.

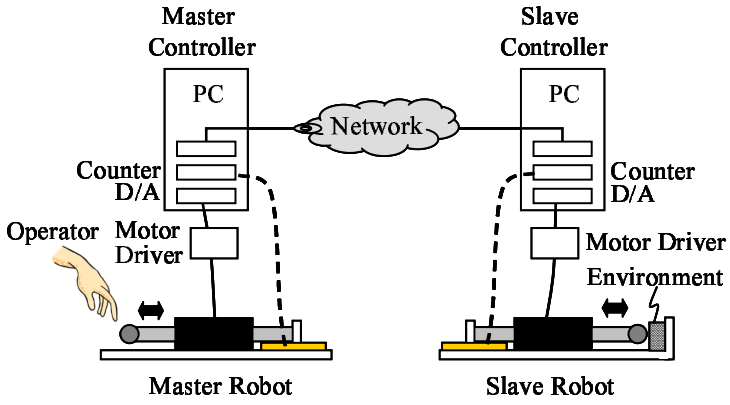

(a) target system

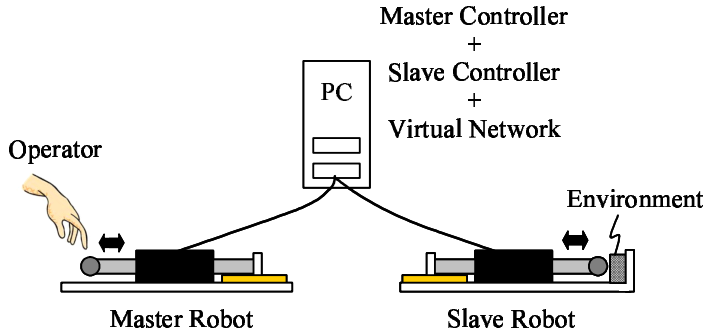

(b) experimental system

Fig. 5-5: Experimental bilateral teleoperation system

Simulation

Simulations were conducted to verify both the influences of the shortened control sampling period itself and those of changing the cutoff frequency of the disturbance observer according to the sampling period. First, the cutoff frequency of pseudo-derivative for velocity calculation g_v, that of the disturbance observer g_{dis}, and that of the reaction torque observer g_e were set to the same values in all cases in order to verify the direct influences of shortening the sampling periods with the design guideline. Then, the cutoff frequencies were heightened gradually and set to the best value for the respective cases. The cutoff frequency of the reaction force observer was always set to the same value as that of the disturbance observer. Simulations were conducted for the cases without communication delay and with a constant communication delay. An operator and an environment were modeled as a spring and damper model represented in (2.37) and (2.38). Parameters used in the simulation are shown in Table 5-3.

Table 5-3: Control parameters in simulation on design guideline of sampling periods

Sampling period	T_s	0.05 - 1.2	ms
Communication delay	L_c	0.0 and 1.0	ms
Position feedback gain	K_p	1600.0	$1/s^2$
Velocity feedback gain	K_v	80.0	1/s
Force feedback gain	K_f	2.0	m/Ns^2
Spring coefficient of operator	K_h	400.0	N/m
Damping coefficient of operator	D_h	40.0	Ns/m
Spring coefficient of environment	K_e	10000.0	N/m
Damping coefficient of environment	D_e	10.0	Ns/m

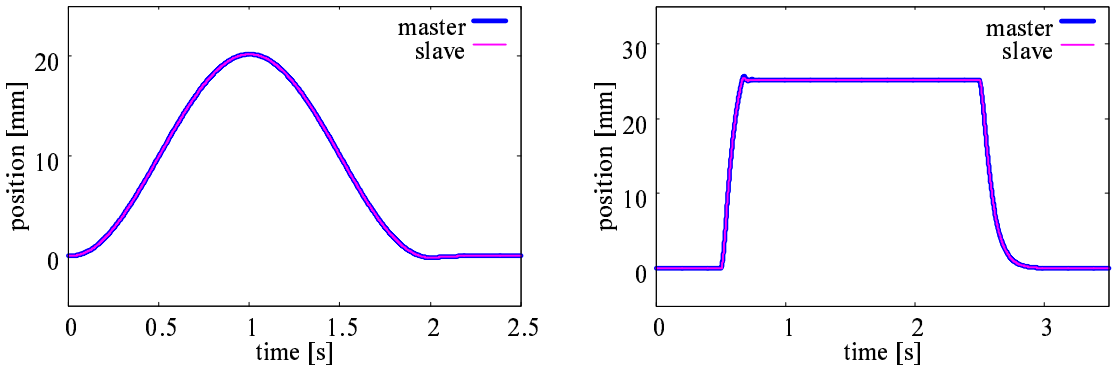

(a) free motion (b) contact motion

Fig. 5-6: Simulation results: position response in bilateral teleoperation

The result in $m = 1$ with communication delay is shown in Fig. 5-6 to show the outline of the motion in the simulation. The error between positions of the master and slave devices at a contact moment was compared in Figs. 5-7 and 5-8. Fig. 5-7 compares the results with the same cutoff frequencies for all cases. The error decreased by shortening T_r even though T_c or g_{dis} was not changed. This results show the validity of the design guideline even in the cases when g_{dis} is limited. Fig. 5-8 shows the results with heightened cutoff frequencies. The cutoff frequencies for each case are shown in Table 5-4. The cutoff frequencies could be heightened by shortening T_r as listed in Table 5-4 even if the packet transmission interval was kept long. Comparing the values in Fig. 5-7 and Fig. 5-8, the error decreased further by increasing the cutoff frequencies according to shortening the control sampling period. These results show the positive influences of both shortening of the control sampling period itself and heightening of the cutoff frequencies by the shortened sampling period.

The relationship between T_r and the position error is verified concretely in Figs. 5-9 to 5-11 for

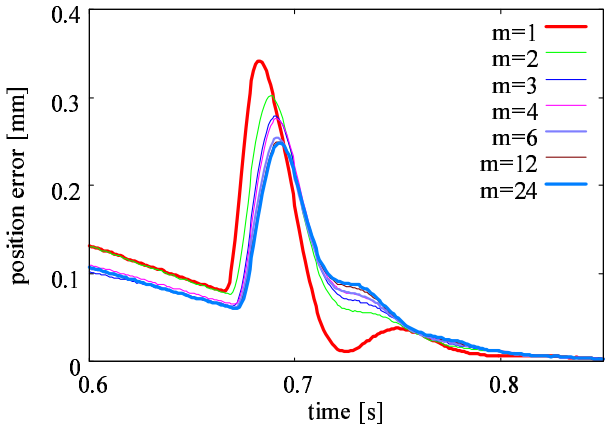

Fig. 5-7: Simulation results: position error at contact moment (same g_{dis}, $T_c = mT_r = 1.2$ ms)

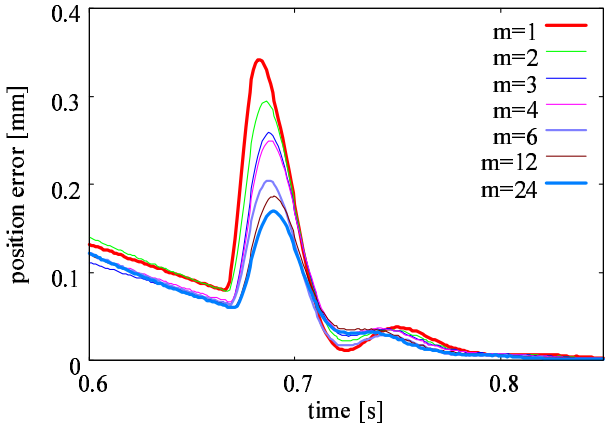

Fig. 5-8: Simulation results: position error at contact moment (heightened g_{dis}, $T_c = mT_r = 1.2$ ms)

the cases with the same cutoff frequencies and in Figs. 5-12 to 5-14 for the cases with the heightened cutoff frequencies. The maximum and average values of the position error in the contact motion and the average value of the position error in the free motion were selected as performance evaluation indices. The maximum position error in the free motion was almost the same in all cases when the communication delay was the same. As shown in Fig. 5-9, the maximum error in the contact motion decreased when T_r was shortened even though T_c was kept long and not changed in the multirate. The decrease was significant especially when $L_c = 1.0$ ms, which is similar to the condition in the real system. Although the performance improvement in the multirate was much smaller than that in the single-rate (short), which shortened T_c according to T_r, when $L_c = 0.0$ ms, the performance improved greatly even with long T_c and difference between the multirate and single-rate (short) was small when $L_c = 1.0$ ms. The

Table 5-4: Settings in simulations on design guideline of sampling periods

(a) multirate

				$L_c = 0.0$ ms		$L_c = 1.0$ ms	
m	T_c [ms]	$T_r(= T_y)$ [ms]	T_u [ms]	g_v [rad/s]	g_{dis} [rad/s]	g_v [rad/s]	g_{dis} [rad/s]
1	1.2	1.2	1.2	800	500	800	500
2	1.2	0.6	0.6	1500	1200	1000	800
3	1.2	0.4	0.4	1800	1600	1200	1000
4	1.2	0.3	0.3	2200	2000	1500	1300
6	1.2	0.2	0.2	2500	2300	2200	2000
12	1.2	0.1	0.1	4000	3500	2200	2000
24	1.2	0.05	0.1	5500	5000	4000	3800

(b) single-rate with short T_c

				$L_c = 0.0$ ms		$L_c = 1.0$ ms	
m	T_c [ms]	$T_r(= T_y)$ [ms]	T_u [ms]	g_v [rad/s]	g_{dis} [rad/s]	g_v [rad/s]	g_{dis} [rad/s]
1	1.2	1.2	1.2	800	500	800	500
2	0.6	0.6	0.6	1500	1300	1000	800
3	0.4	0.4	0.4	2300	2100	1300	1200
4	0.3	0.3	0.3	3100	2900	1500	1400
6	0.2	0.2	0.2	4500	4300	2200	2000
12	0.1	0.1	0.1	5700	5500	2500	2300
24	0.05	0.05	0.1	6200	6000	4000	3800

difference shows the influence of T_c. Fig. 5-10 shows the average position error in the contact motion. The error slightly heightened by shortening T_r when T_c was kept long with $L_c = 0.0$ ms. Since decrease in the error was slight even in the cases where both T_c and T_r were shortened in single-rate (short), the influence of the sampling periods on magnitude of the error is considered to be small when $L_c = 0.0$ ms. On the other hand in $L_c = 1.0$ ms, the error decreased by shortening T_r even with long T_c. A tendency similar to the cases with short sampling periods also for packet transmission (single-rate (short)) was attained in the multirate. Fig. 5-11 shows the average position error in the free motion. The error decreased by shortening T_r regardless of T_c. Although the amount of decrease in the multirate was less than that of the single-rate with short T_c when $L_c = 0.0$ ms, the error was almost the same in both cases when $L_c = 1.0$ ms. This result shows that the control sampling period is the key element to decrease the average position error in the free motion. The above-mentioned results show the effectiveness of

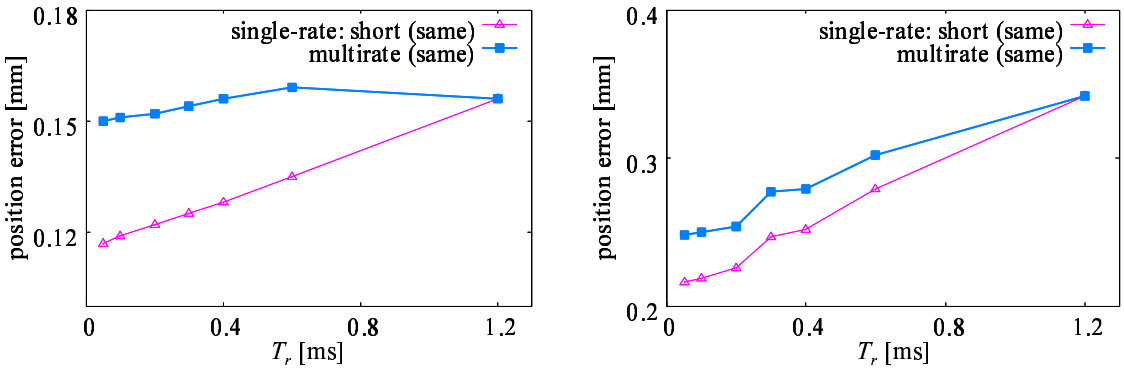

(a) $L_c = 0.0$ ms (b) $L_c = 1.0$ ms

Fig. 5-9: Simulation results: maximum position error in contact motion with same g_{dis}

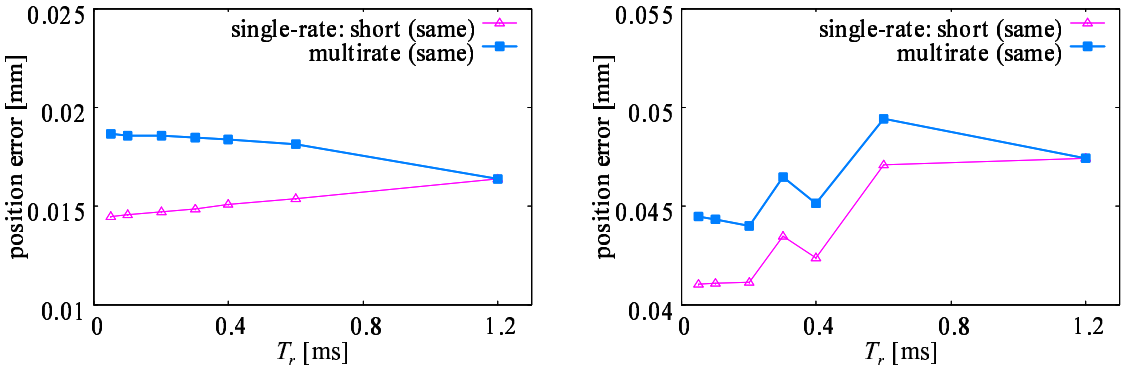

(a) $L_c = 0.0$ ms (b) $L_c = 1.0$ ms

Fig. 5-10: Simulation results: average position error in contact motion with same g_{dis}

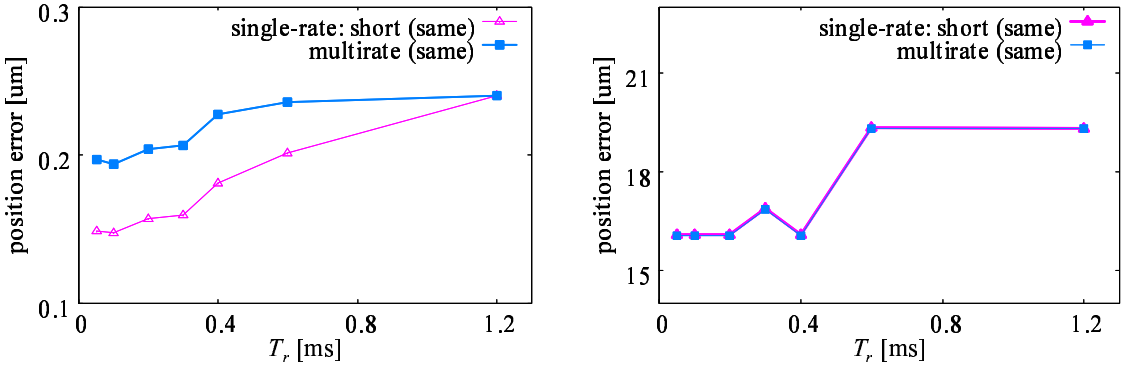

(a) $L_c = 0.0$ ms (b) $L_c = 1.0$ ms

Fig. 5-11: Simulation results: average position error in free motion with same g_{dis}

shortening T_r even when T_c and g_{dis} are limited.

The tendency of the relationship between T_r and the position error was almost the same in the cases with the heightened cutoff frequencies as shown in Figs. 5-12 to 5-14. The performance change by shortening T_r with the same g_{dis} was compared with the change when g_{dis} was heightened to the best value in each case in Figs. 5-15 to 5-17. The packet transmission interval was set to the same value, $T_c = 1.2$ ms, in all cases. Except for the average error in the free motion with the communication delay, the errors decreased further by heightening g_{dis}. Difference between the result of $T_r = 1.2$ ms and that of a shorter T_r with the same T_c and g_{dis} shows the influence of the shortened control sampling period itself. On the other hand, difference between the results in the cases when g_{dis} was not changed (multirate (same)) and those in the cases when g_{dis} was heightened (multirate (dif)) with T_r shorter than 1.2 ms shows the influence of the heightened cutoff frequency of the disturbance observer by shortening the control sampling period.

Finally, the influence of changing T_r was compared with that of changing T_c concretely with a focus on the maximum error in the contact motion. This verification focused on the cases with heightened cutoff frequencies. The results are summarized in Table 5-5. In the cases with $L_c = 0.0$ ms, the error decreased by 34.6% when $T_c = 1.2$ ms and T_r was shortened from 1.2 ms to 0.4 ms, while the decrease was 55.9% when $T_r = 0.4$ ms and T_c was shortened from 1.2 ms to 0.4 ms. In the cases with $L_c = 1.0$ ms, the decrease achieved by changing T_r was 24.3% and that by changing T_c was 14.3%. These results show that although the influence of changing T_c is larger than that of changing T_r when communication delay is negligibly small, the influence of changing T_r is larger than that of changing T_c when communication delay is $L_c = 1.0$ ms, which is similar to the condition in the real system.

The validity of implementation of the multirate sampling method described in Chapter 3 to a system with a limitation of the packet transmission interval can be clarified by comparing the results with $T_r = 0.1$ ms and those with $T_r = 0.05$ ms. Although T_c and T_u were kept long, the errors decreased by shortening T_r and T_y. In terms of the maximum error in the contact motion, the decrease achieved by shortening T_r and T_y from 0.1 ms to 0.05 ms was 15.8% in $L_c = 0.0$ ms and 9.1% in $L_c = 1.0$ ms.

The above results support the validity of the design guideline described in Section 5.2.2. It was confirmed from the results that the performance improved by shortening the control sampling period even if the packet transmission period was kept long and the cutoff frequencies of the observers were kept low. It implies the effectiveness of the design guideline even in the system with constraints on the cutoff frequency due to noise or mechanical structure. Moreover, the cutoff frequency can usually be set

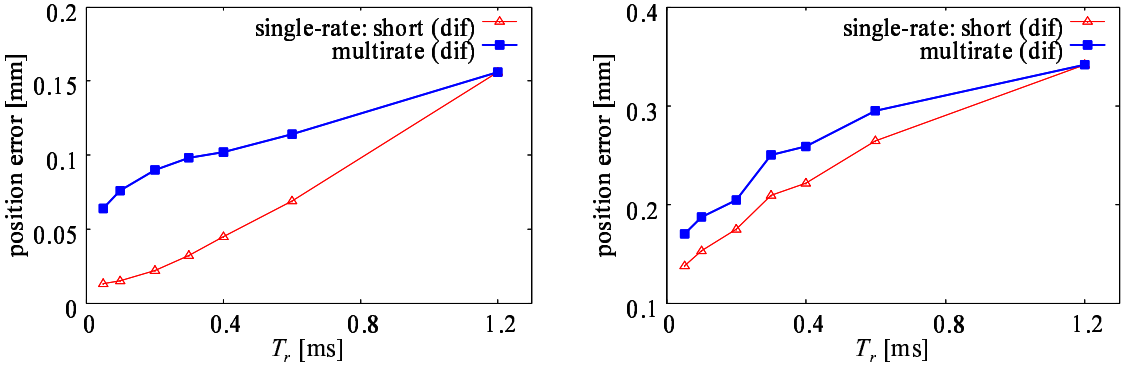

(a) $L_c = 0.0$ ms (b) $L_c = 1.0$ ms

Fig. 5-12: Simulation results: maximum position error in contact motion with heightened g_{dis}

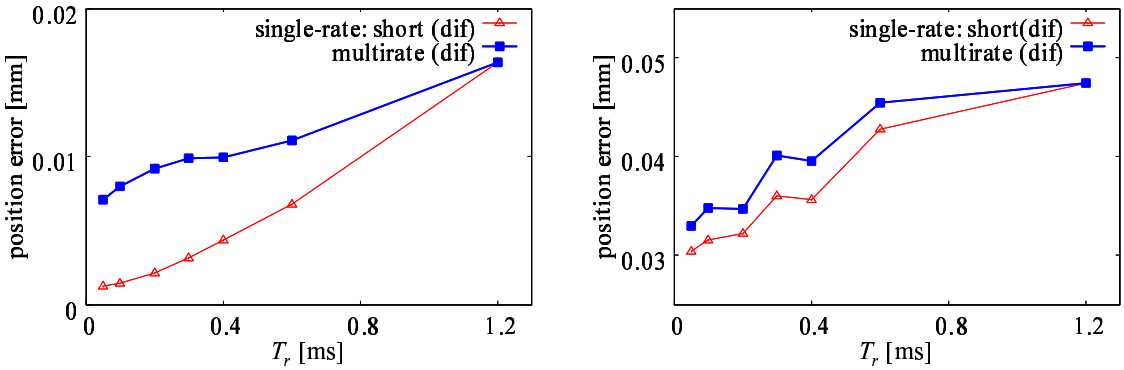

(a) $L_c = 0.0$ ms (b) $L_c = 1.0$ ms

Fig. 5-13: Simulation results: average position error in contact motion with heightened g_{dis}

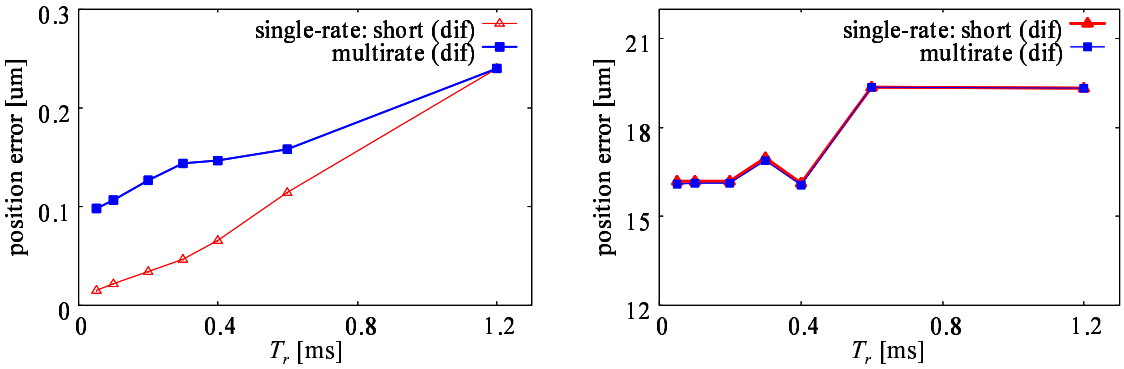

(a) $L_c = 0.0$ ms (b) $L_c = 1.0$ ms

Fig. 5-14: Simulation results: average position error in free motion with heightened g_{dis}

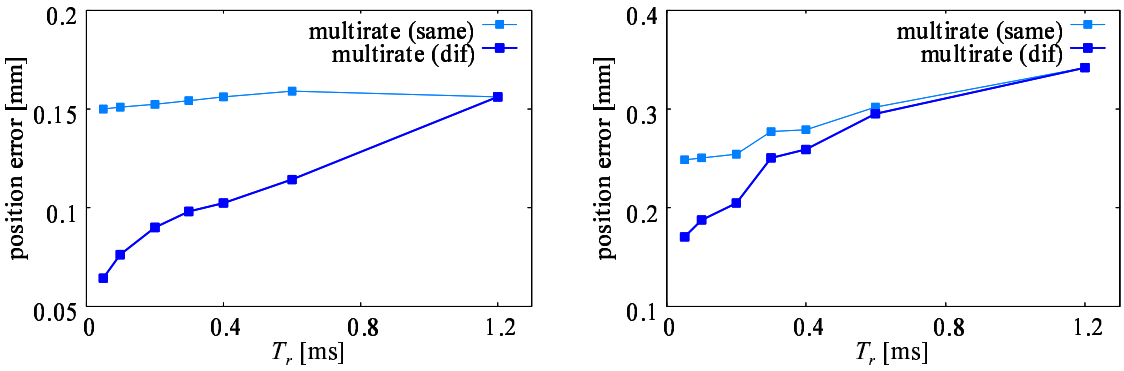

(a) $L_c = 0.0$ ms (b) $L_c = 1.0$ ms

Fig. 5-15: Simulation results: maximum position error in contact motion in multirate

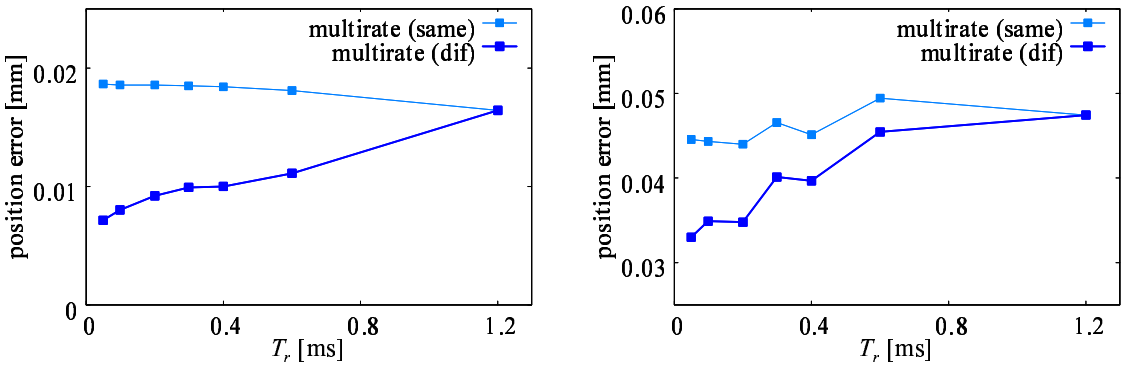

(a) $L_c = 0.0$ ms (b) $L_c = 1.0$ ms

Fig. 5-16: Simulation results: average position error in contact motion in multirate

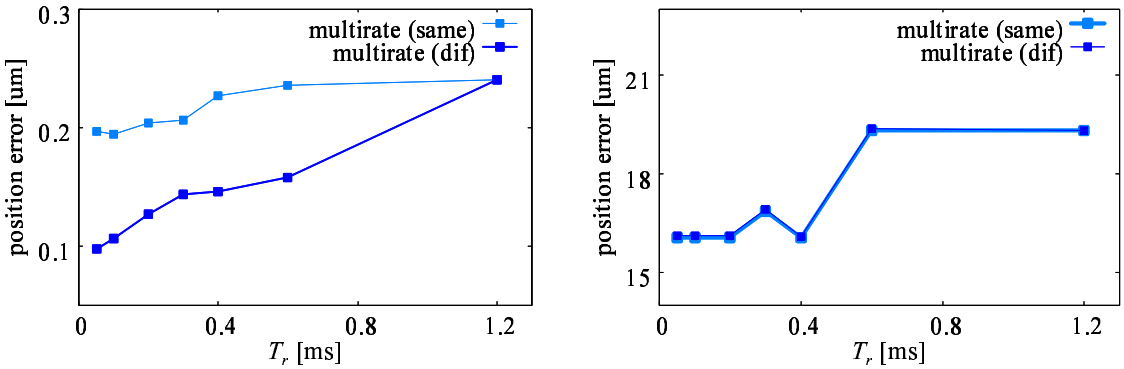

(a) $L_c = 0.0$ ms (b) $L_c = 1.0$ ms

Fig. 5-17: Simulation results: average position error in free motion in multirate

Table 5-5: Position error in simulations on design guideline of sampling periods

(a) $L_c = 0.0$ ms

		multirate ($T_c = 1.2$ ms)			single-rate (short: $T_c = T_r$)		
		contact motion		free motion	contact motion		free motion
m	$T_r(= T_y)$ [ms]	Max.	Ave.	Ave.	Max.	Ave.	Ave.
1	1.2	0.156	$1.64e^{-2}$	$2.40e^{-4}$	0.156	$1.64e^{-2}$	$2.40e^{-4}$
2	0.6	0.114	$1.11e^{-2}$	$1.58e^{-4}$	0.069	$6.70e^{-3}$	$1.14e^{-4}$
3	0.4	0.102	$9.95e^{-3}$	$1.46e^{-4}$	0.045	$4.33e^{-3}$	$6.52e^{-5}$
4	0.3	0.098	$9.90e^{-3}$	$1.44e^{-4}$	0.032	$3.17e^{-3}$	$4.64e^{-5}$
6	0.2	0.090	$9.18e^{-3}$	$1.27e^{-4}$	0.022	$2.14e^{-3}$	$3.36e^{-5}$
12	0.1	0.076	$7.99e^{-3}$	$1.06e^{-4}$	0.015	$1.46e^{-3}$	$2.20e^{-5}$
24	0.05	0.064	$7.10e^{-3}$	$9.76e^{-5}$	0.013	$1.27e^{-3}$	$1.44e^{-5}$

(b) $L_c = 1.0$ ms

		multirate ($T_c = 1.2$ ms)			single-rate (short: $T_c = T_r$)		
		contact motion		free motion	contact motion		free motion
m	$T_r(= T_y)$ [ms]	Max.	Ave.	Ave.	Max.	Ave.	Ave.
1	1.2	0.342	$4.74e^{-2}$	$1.93e^{-2}$	0.342	$4.74e^{-2}$	$1.93e^{-2}$
2	0.6	0.295	$4.54e^{-2}$	$1.94e^{-2}$	0.264	$4.28e^{-2}$	$1.94e^{-2}$
3	0.4	0.259	$3.96e^{-2}$	$1.61e^{-2}$	0.222	$3.57e^{-2}$	$1.61e^{-2}$
4	0.3	0.250	$4.01e^{-2}$	$1.69e^{-2}$	0.209	$3.60e^{-2}$	$1.70e^{-2}$
6	0.2	0.204	$3.47e^{-2}$	$1.61e^{-2}$	0.175	$3.22e^{-2}$	$1.62e^{-2}$
12	0.1	0.187	$3.48e^{-2}$	$1.61e^{-2}$	0.153	$3.15e^{-2}$	$1.62e^{-2}$
24	0.05	0.170	$3.29e^{-2}$	$1.61e^{-2}$	0.138	$3.04e^{-2}$	$1.62e^{-2}$

higher by shortening the control sampling period and the performance improves further by setting g_{dis} higher according to shortening T_r. Although details of results are not shown here, the same tendency was confirmed in the cases under time-varying communication delay with $L_c = 1.0 - 2.0$ ms. The performance is thus expected to be improved even under time-varying communication delay by using the proposed design guideline.

Experiments

Experiments were conducted to verify the influence of sampling periods and the validity of the design guideline on sampling periods in the real system using the equipment shown in Fig. 5-18. Each of the

Fig. 5-18: Experimental equipment: master-slave system with linear motor

Table 5-6: Specification of master-slave system using linear motor

Type of encoder	RENISHAW RGH24Y
Resolution	0.1 μm
Max. response speed	250 mm/s
Type of motor	GMC Hillstone S160Q
Continuous force	20 N
Max. force	78 N
Force constant	33.0 N/A
Forcer weight	0.3 Kg
Total mass	0.5 Kg

master and slave robots is composed of a 1DOF linear motor and a linear encoder. Specifications of the system are shown in Table 5-6. In this experiment, the master and slave robots were controlled using the same computer and a network was constructed virtually in the computer to conduct experiments under various situations. The controller gains were set as follow: $K_p = 3600.0$, $K_v = 120.0$, and $K_f = 2.0$. The communication delay was set as $L_c = 1.0$ ms. Settings of the sampling periods were the same as those in the simulation. The input sampling period was set to satisfy its limitation, 0.1 ms. The cutoff frequencies in the experiments are shown in Table 5-7. Although T_c could be set shorter than 1.2 ms with the same delay in the experiments shown in this section since the network was just constructed in the computer virtually, significant delay and packet losses due to network congestion may occur with short T_c if the real communication is implemented.

Only the contact motion was conducted in the experiments. The error between positions of the master and slave devices at contact moment with $T_c = 1.2$ ms is compared in Fig. 5-19. The maximum and average errors from $t = 0.5$ s to $t = 1.0$ s are shown in Fig. 5-20 and Table 5-8. As in the simulation,

Table 5-7: Settings in experiments on design guideline of sampling periods

		multirate ($T_c = 1.2$ ms)		single-rate (short: $T_c = T_r$)	
m	$T_r (= T_y)$ [ms]	g_v [rad/s]	g_{dis} [rad/s]	g_v [rad/s]	g_{dis} [rad/s]
1	1.2	500	250	500	250
2	0.6	500	350	600	500
3	0.4	700	600	1100	1000
4	0.3	1100	1000	1700	1500
6	0.2	2000	1800	2000	1800
12	0.1	2200	2000	2200	2000
24	0.05	2200	2000	2200	2000

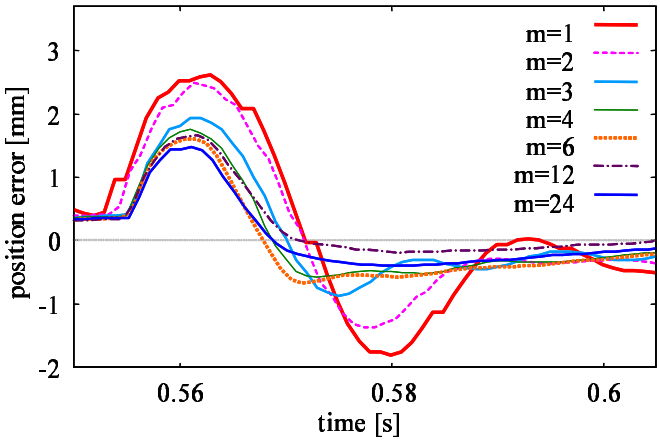

Fig. 5-19: Experimental results: position error at contact moment (heightened g_{dis}, $T_c = mT_r = 1.2$ ms)

the error was decreased by shortening T_r even if T_c was kept long. The difference between the single-rate with short T_c and the multirate was small in the experiments. It means that shortening T_r improves performance even when T_c is limited. These results show that the best performance under limitations on the system can be acquired by designing sampling periods independently, considering only limitations on the corresponding sampling period.

5.3 Signal Transmission Method for Bilateral Teleoperation

This section proposes a signal transmission method for achieving higher performance even under the limitation of the packet transmission interval. Although the previous section shows that the performance can be improved by setting input, output, and control sampling periods short even if the packet transmission interval is long, the performance cannot catch up with that with the shorter packet transmission

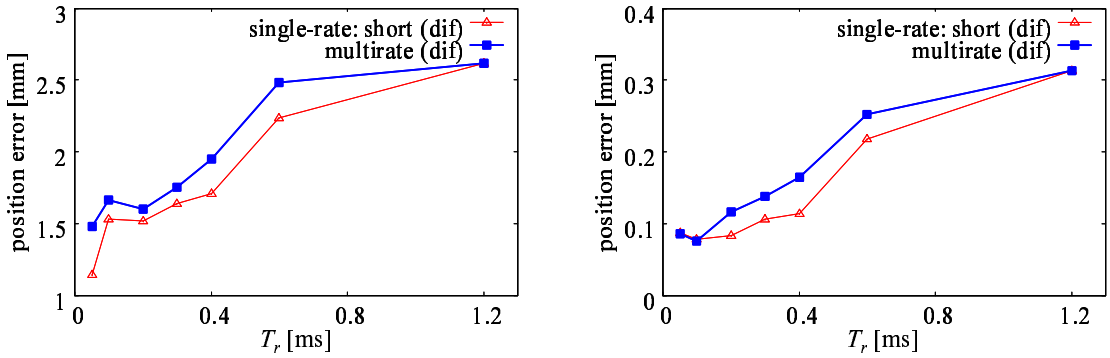

(a) maximum position error

(b) average position error

Fig. 5-20: Experimental results: position error in contact motion with heightened g_{dis}

Table 5-8: Position error in experiments on design guideline of sampling periods

		multirate ($T_c = 1.2$ ms)		single-rate (short: $T_c = T_r$)	
m	$T_r (= T_y)$ [ms]	Max.	Ave.	Max.	Ave
1	1.2	2.618	0.314	2.618	0.314
2	0.6	2.485	0.252	2.233	0.217
3	0.4	1.952	0.164	1.710	0.113
4	0.3	1.754	0.138	1.636	0.106
6	0.2	1.601	0.116	1.519	0.084
12	0.1	1.667	0.076	1.531	0.078
24	0.05	1.482	0.085	1.141	0.087

interval. It is due to the bandwidth limitation and discontinuity of the transmission signal owing to the long interval. It is important for further improvement of the performance to transmit appropriate signals properly. A signal transmission method that transmits a packet filled with selected signals is proposed with a focus on the influence of quality of each signal used for control on the performance. Here, high quality of the signal means preferable characteristics for utilization in control, such as small delay, small deviation from the real value, wide bandwidth, and a short time interval of data renewal.

5.3.1 Related Researches on Signal Transmission Method

This subsection introduces the signal transmission methods proposed in the previous researches. The advantages and disadvantages of the conventional methods are also described in terms of signal data quality.

Fig. 5-21 shows conventional signal transmission methods. Transmitting data at every control sam-

pling point described as Method A is the simplest method. The time interval of signal transmission T_c, the time interval of data renewal T_d, and a transmitting packet $\boldsymbol{p}[i]$ at $t = iT_c$ in this method are represented as follows:

$$T_c = T_r \tag{5.9}$$

$$T_d = T_r \tag{5.10}$$

$$\boldsymbol{p}[i] = \boldsymbol{y}[i], \tag{5.11}$$

where $\boldsymbol{y}$ is an output signal. In this method, network congestion may occur when the control sampling period is short. In order to avoid the network congestion while keeping the control sampling period short, a method in which the sampling period of signal transmission is set longer than the control sampling period has been proposed [113] as described in Section 5.2.1. In this method, data of the latest sampling point is transmitted once every n control sampling periods as shown in Fig. 5-21(b) as Method B. The time interval of signal transmission T_c, the time interval of data renewal T_d, and transmitted packet $\boldsymbol{p}[i]$ in this method are described in the equations below.

$$T_c = nT_r \tag{5.12}$$

$$T_d = T_c \tag{5.13}$$

$$\boldsymbol{p}[i] = \boldsymbol{y}[i] \tag{5.14}$$

Although Method B solves the problem of occurrence of network congestion even with the short control sampling period, the time interval of data renewal is sacrificed. A method for solving the problem of discretization of data in Method B has also been proposed [114]. This method transmits a package of data at multiple sampling points once every n control sampling periods as shown in Fig. 5-21(c) as Method C. The time interval of signal transmission T_c, the time interval of data renewal T_d, and the transmitting packet $\boldsymbol{p}[i]$ in this method are described as follows:

$$T_c = nT_r \tag{5.15}$$

$$T_d = T_c/m \tag{5.16}$$

$$\boldsymbol{p}[i] = \left[\ \boldsymbol{y}[i-1,1], \cdots, \boldsymbol{y}[i-1,m-1], \boldsymbol{y}[i,0] \ \right], \tag{5.17}$$

where

$$\boldsymbol{y}[i,k] = \boldsymbol{y}(iT_c + kT_d) \ (k = 0, \cdots, m-1).$$

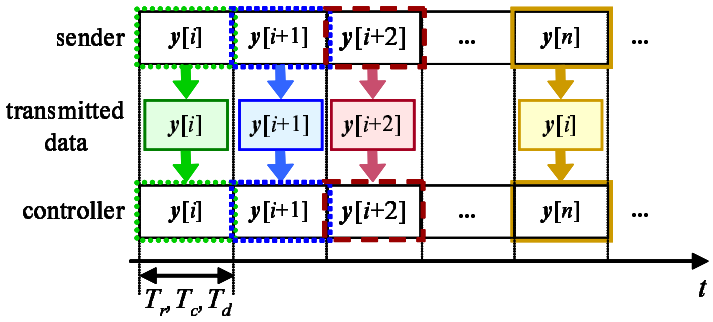

(a) Method A: send data at every sampling periods

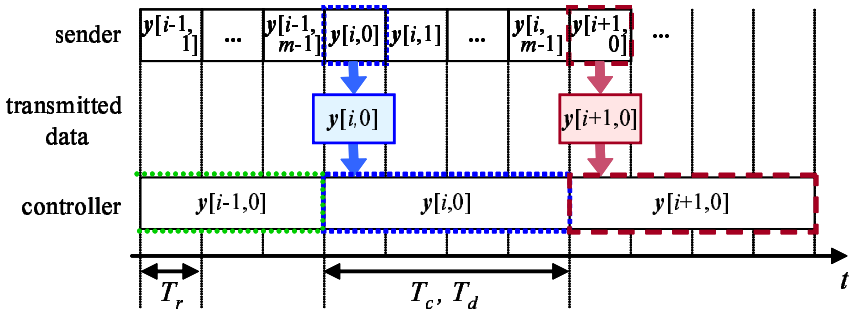

(b) Method B: send the latest data at every n sampling periods

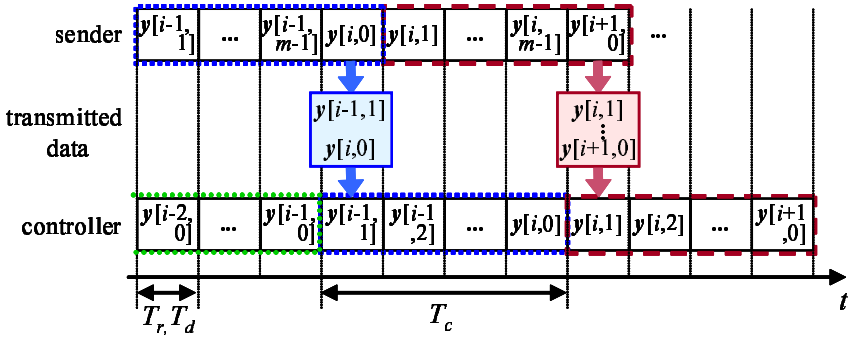

(c) Method C: send set of data at every n sampling periods

Fig. 5-21: Conventional signal transmission methods

The advantages and disadvantages of the signal transmission methods introduced above are discussed below in terms of signal data quality. In Method A, which transmits signals at every control sampling point, data can be acquired in a short time interval when capacity and performance of a network is enough. However, congestion of a network may occur when the control sampling period is too short, and it leads large communication delay and significant packet losses. The congestion can be avoided in Method B and Method C owing to a long time interval for signal transmission. The communication

delay may therefore become relatively short in those methods. This is a great advantage in terms of stability of a control system. In Method B, the sampling period of data renewal is then scarified instead of communication delay. The same data is used at several control sampling points since the time interval of signal transmission is set longer than the control sampling period. The discontinuity of data may deteriorate the stability and performance of the system. As an advantage of Method C, a time interval of data renewal can be kept short by transmitting values at multiple sampling points as one package. A delay of data increases, however, in Method C. As shown in Fig. 5-21(c), data in the transmission packet is used from the oldest in control in Method C. The delay therefore increases by $(m-1)T_p/m$ as compared with Method B. Although the Smith predictor [104] based delay compensation can be effectively applied since the delay is known and constant, the influence of delay cannot be eliminated perfectly. In addition, the size of the transmission packet in Method C is larger than that in Method B.

5.3.2 Signal Transmission Method for Bilateral Teleoperation

This subsection proposes a signal transmission method that transmits a packet filled with data selected with consideration of characteristics and the influence of the respective signals on motion control performance in order to achieve higher performance even under the limitation of the packet transmission interval.

Signal Transmission Method Considering Influence of Signal Data Quality

This subsection focuses especially on packet transmission in bilateral teleoperation. As mentioned in the previous subsection, Method B, which transmits only one data at the latest sampling point, is superior to Method C, which transmits a package of data at multiple sampling points, in terms of delay and the size of the transmission packet. On the other hand, Method C is superior to Method B in terms of the time interval of data renewal. In conventional researches, one signal transmission method is selected for a system. In other words, the same method is applied to all signals in the system. On the other hand, the influence of signal data quality, such as accuracy, a data renewal interval, and delay, differ depending on a command trajectory and types of signals in position control [117]. The influence of the time interval of data renewal and delay may differ depending on the types of signals also in other motion control systems. Better performance is expected to be achieved by determining data to be filled in a transmission packet independently for each signal used for control with consideration of the influence of the quality of the respective signals. This subsection focuses especially on bilateral teleoperation system. The bilateral

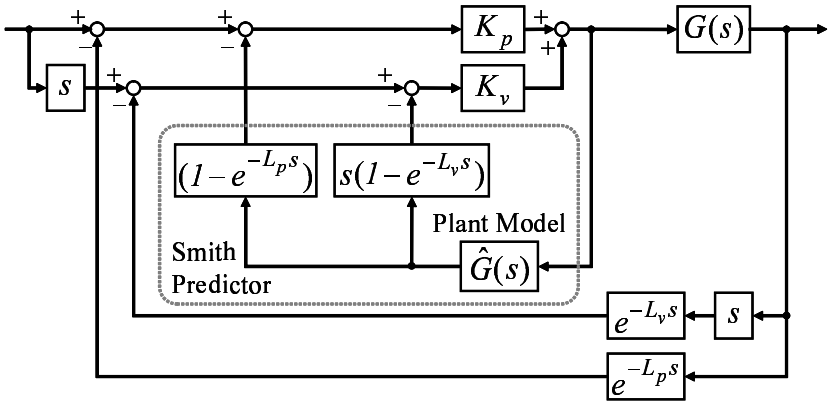

Fig. 5-22: Smith predictor for the proposed system

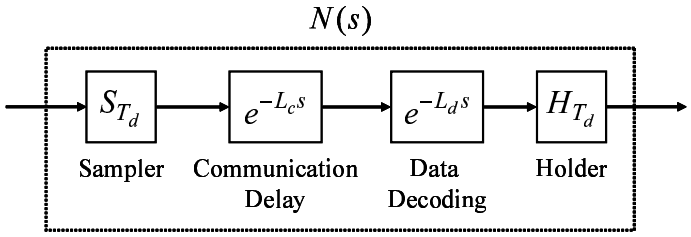

Fig. 5-23: Communication path including data decoding: $N(s)$

controller shown in Fig. 5-2 is composed of position and force controls. Since a PD controller is generally applied to the position control, signals used in the controller are position, velocity, and force of the master and slave devices. This section proposes to determine data filled in a transmission packet independently for position, velocity, and force signals. Either data only at the latest sampling point or data at multiple sampling points is selected for each signal to be in a transmission packet.

The communication line $N(s)$ between the master and slave devices is assumed to contain the delay due to the process of utilization of transmission signals in this section as shown in Fig. 5-23. A Smith predictor [104] based delay compensation is applied to reduce the influence of the delay due to utilization of data in a transmission packet from the oldest and that of communication delay. The Smith predictor is modified in this research as shown in Fig. 5-22 to cope with the difference in the delay among signals. Here, L_p denotes sum of the communication delay L_c and the delay due to utilization of data L_d in the position signal and L_v denotes that in the velocity signal. The smith predictor is designed to compensate both the communication delay and the delay due to utilization of the transmitted data. Fig. 5-24 shows the whole bilateral teleoperation system to which the proposed method is applied.

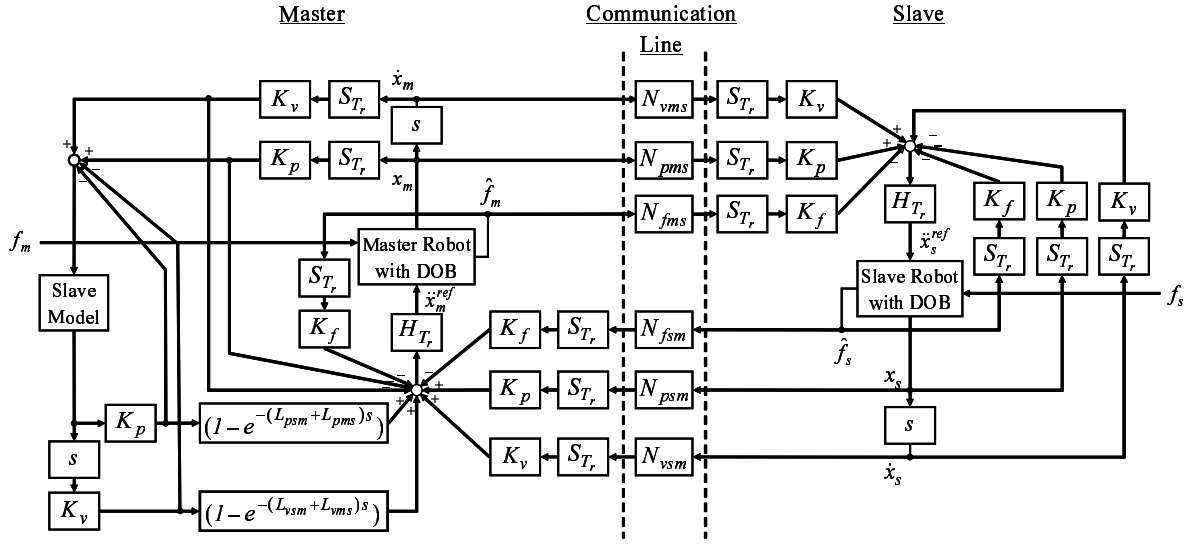

Fig. 5-24: Bilateral teleoperation system with the proposed method

It is determined which is to be filled in a transmission packet, only the latest data or data at multiple sampling points, for each of position, velocity, and force signals based on analysis on the influence of the data renewal interval and data delay of each signal on bilateral teleoperation performance.

Analysis using Hybrid Matrix

The influence of the interval and the delay were analyzed using the hybrid matrix for each of the position, velocity, and force signals. Analyses were conducted for the following combinations of T_d and L_d to evaluate the influence.

- Case 1: $T_d = 0.2$ ms, $L_d = 0.0$ ms
- Case 2: $T_d = 0.2$ ms, $L_d = 4.0$ ms
- Case 3: $T_d = 4.0$ ms, $L_d = 0.0$ ms
- Case 4: $T_d = 4.0$ ms, $L_d = 4.0$ ms
- Case 5: $T_d = 2.0$ ms, $L_d = 2.0$ ms

In order to evaluate the influence of signal data quality of position, velocity, and force signals independently, the parameters of the velocity and force signals were set as in Case 1 and only the parameters of the position signal were changed from Case 1 to Case 5 in analyses on the position signal. The same as

Table 5-9: Control parameters in analysis and experiments on signal transmission methods

Control sampling period	T_r	0.2	ms
Communication delay	L_c	0.0 or 2.0	ms
Position feedback gain	K_p	3600.0	$1/s^2$
Velocity feedback gain	K_v	120.0	1/s
Force feedback gain	K_f	1.0	m/Ns^2
Analysis			
Spring coefficient of environment	K_e	10000.0	N/m
Damping coefficient of environment	D_e	10.0	N/m
Spring coefficient of operator	K_h	400.0	N/m
Damping coefficient of operator	D_h	40.0	N/m
Signal transmission sampling period	T_c	2.0	ms
Experiments			
Cutoff frequency of DOB	g_{dis}	2500	rad/s
Signal transmission sampling period	T_c	5.0	ms

above, only the parameters of the velocity were changed in analyses on the velocity signal, and only the parameters of the force were changed in analyses on the force signal. The samplers S_* and the holders H_* were assumed to be ideal samplers and zero-order holders. The parameters used for analyses are shown in Table 5-9.

The ideal conditions of the hybrid parameters represented in (2.15) can be understood as follows:

- gains of H_{11} and H_{22} are small enough; and
- gains of H_{12} and H_{21} are 0 dB.

In terms of the frequency range, the response in the low frequency range is important in H_{12} and H_{21} since these are parameters relating to an operator's position and the frequency of human operator's motions is generally low. On the other hand, all frequency ranges from low to high should be considered in H_{12} and H_{22} since these parameters relate to the force of the slave and high frequency elements exist when the slave is made into contact with a hard object.

The analysis results on the position signal are shown in Fig. 5-25. The influence of L_d and T_d were confirmed in H_{11} and H_{12}. The gain of H_{11} in the low frequency range increased when T_d was long. Gain drop of H_{21} in the middle frequency range was greater when L_d was longer. No difference was confirmed in H_{12} or H_{22}.

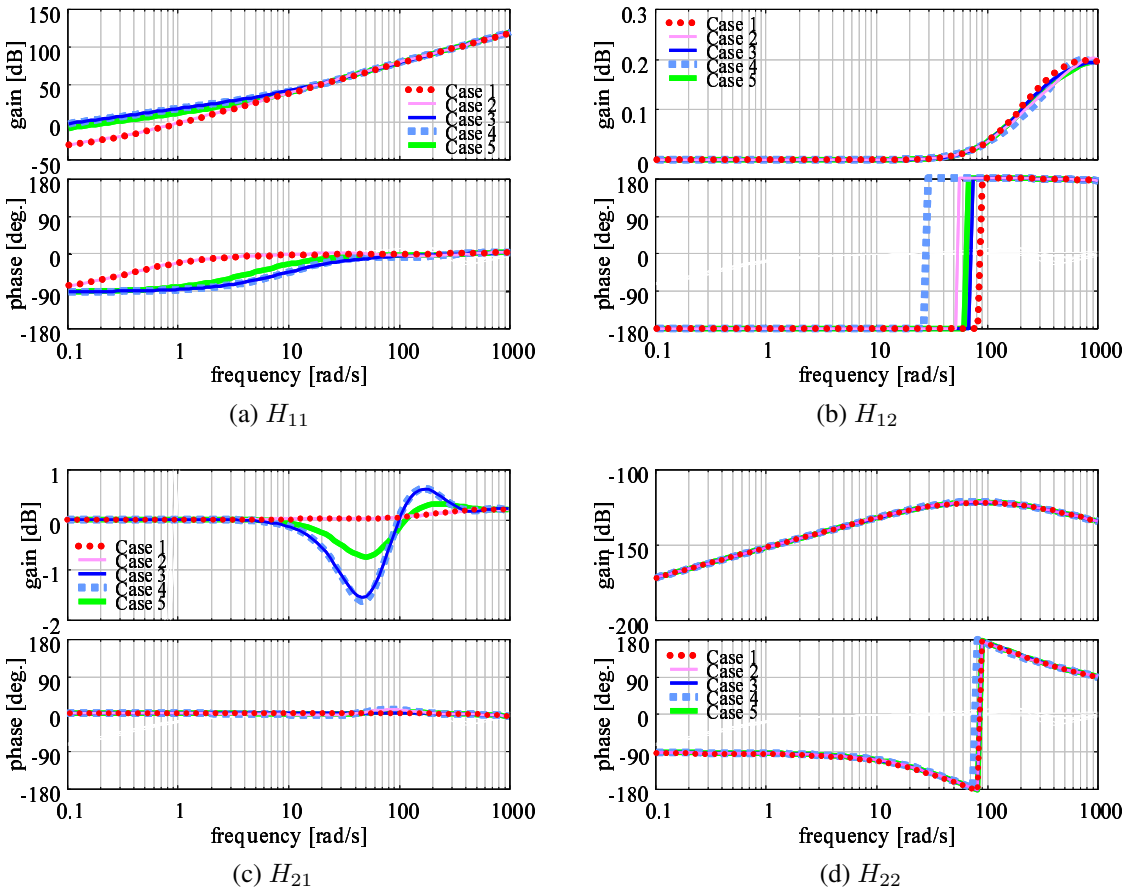

(a) H_{11} (b) H_{12}

(c) H_{21} (d) H_{22}

Fig. 5-25: Analysis on influence of position signal on bilateral teleoperation performance

Fig. 5-26 shows the results of analyses on the velocity signal. The influence of L_d and T_d were confirmed in the middle and high frequency ranges of H_{12} and the middle frequency range of H_{21}. Except for Case 1, H_{12} had a peak value in a frequency depending on the parameters of the velocity signal although the value was small. The gain dropped to minus at frequencies higher than the peak. The zero-crossing frequency in each case was in the following order: Case 4<Case 2<Case 5<Case 3(<Case 1). It implies that the influence of delay is larger than that of the time interval in H_{12}. Focusing on H_{21}, it had a peak value and dropped to minus when delay existed. The peak value and the level of the drop depended only on the length of delay. No difference was confirmed in H_{11} or H_{22}.

The results of analysis on the force signal are shown in Fig. 5-27. H_{12} and H_{21} show similar characteristics. They had peak values in the middle frequency range, and the delay rather than the time interval imposed the influence on the magnitude of the peak value. The magnitude was in the following order: Case 4>Case 2>Case 5>Case 3>Case 1. On the other hand, the influence of the time interval was larger

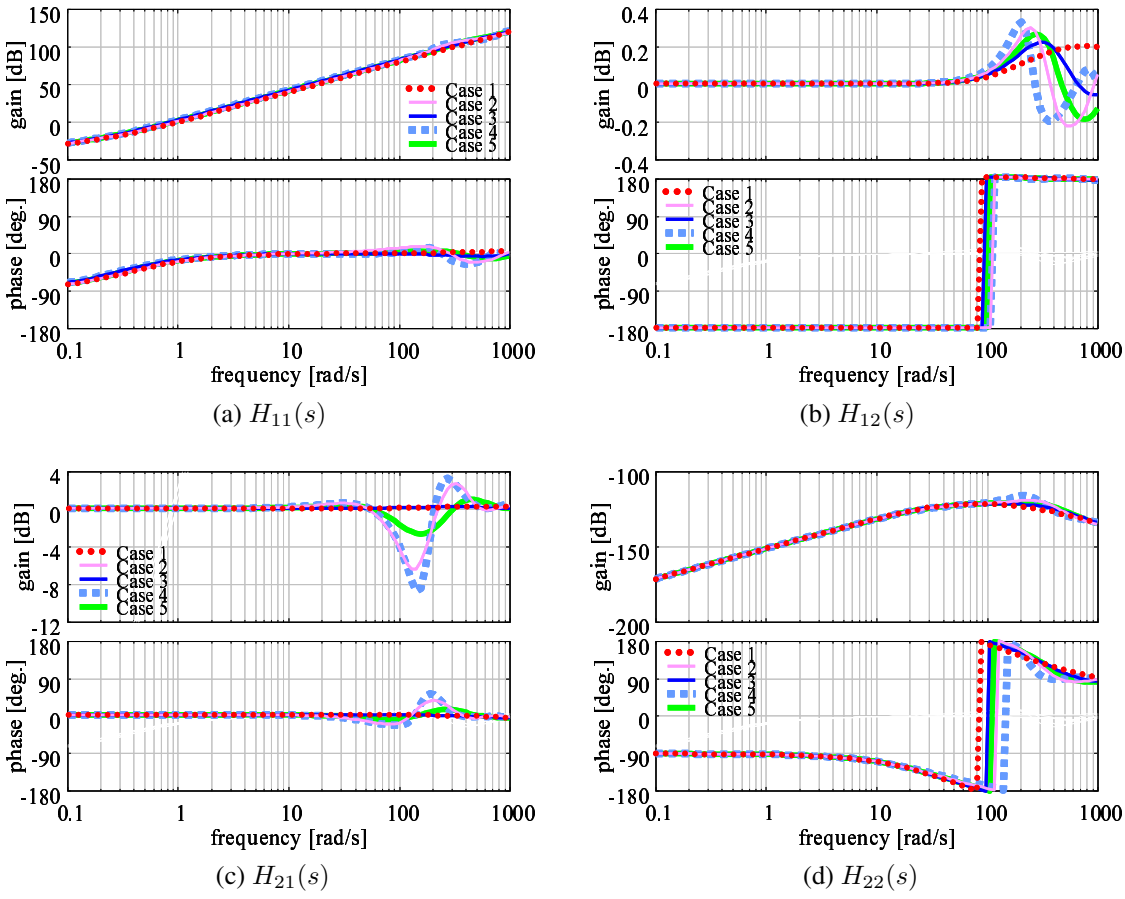

(a) $H_{11}(s)$ (b) $H_{12}(s)$

(c) $H_{21}(s)$ (d) $H_{22}(s)$

Fig. 5-26: Analysis on influence of velocity signal on bilateral teleoperation performance

than that of delay in terms of frequency at which gain became minus. The frequency was in the following order: Case 4<Case 3<Case 5<Case 2<Case 1. There was no difference confirmed in H_{11}. In terms of H_{22}, the gain was small enough and the ideal condition expressed in (2.15) was satisfied in all cases, although the response differed depending on the parameters.

In a standpoint of hybrid parameters, the results are summarized as follows:

- gain of H_{11} in the low frequency range depended on the time interval of the position signal;
- gain of H_{12} in the middle and high frequency ranges depended on the delay and the time interval of the force signal;
- gain of H_{21} in the middle and high frequency ranges depended on the delay of the velocity signal and the delay and the time interval of the force signal; and

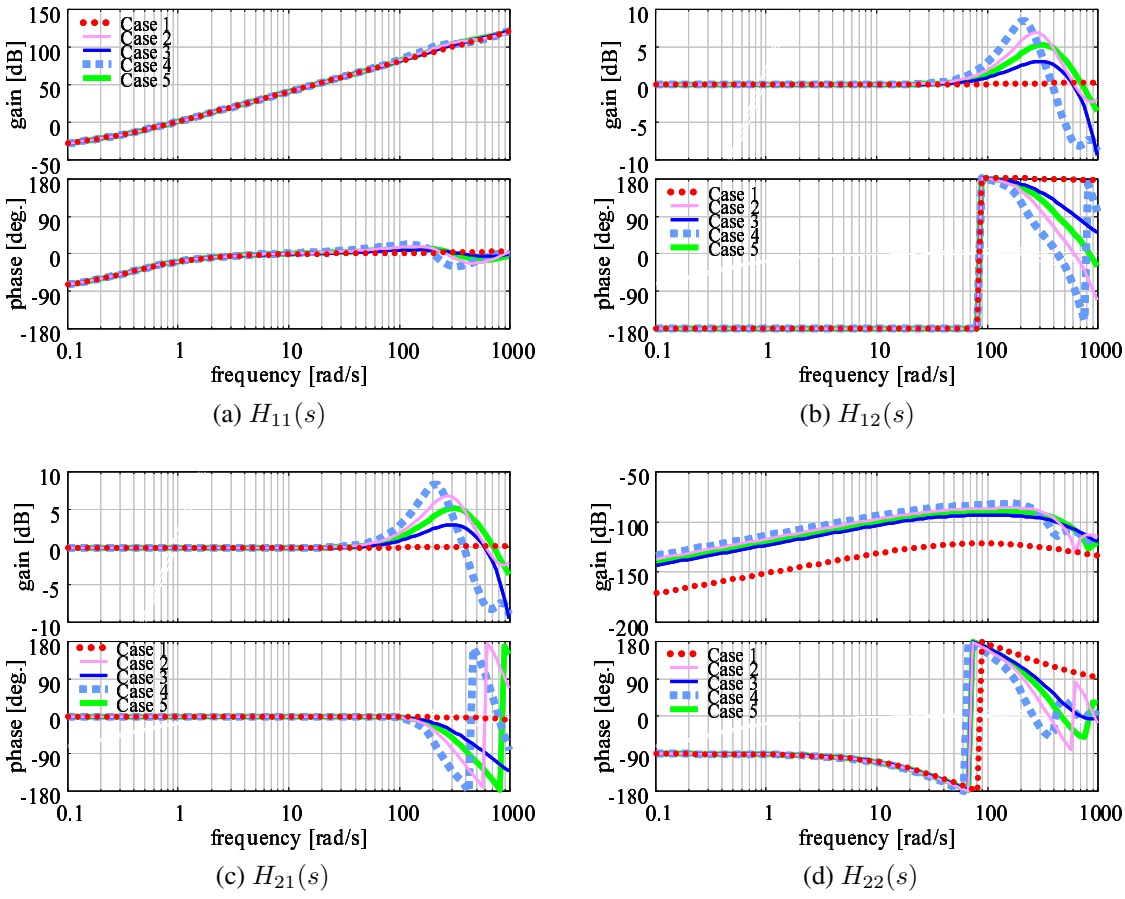

(a) $H_{11}(s)$ (b) $H_{12}(s)$

(c) $H_{21}(s)$ (d) $H_{22}(s)$

Fig. 5-27: Analysis on influence of force signal on bilateral teleoperation performance

- H_{22} satisfied the ideal condition in all situations.

The above mentioned characteristics can be utilized in needs-oriented design of a system.

Selection of data for transmission packet

The data to be filled in a transmission packet is selected according to the analysis results shown above. If delay is in priority, data at the latest sampling point is transmitted. If a time interval of data renewal is in priority, on the other hand, data at multiple sampling points is transmitted.

In terms of the position, the time interval influence the gain of H_{11} in the low frequency range and the delay influence the gain of H_{21} in the middle frequency range. The operational force will be large if the gain of H_{11} in the low frequency range is large. On the other hand, difference is not confirmed in H_{21} in the low frequency range, the most important range. In addition, the influence of the position parameters on H_{21} is much smaller than that of the force parameters. Consequently, priority is given to the time

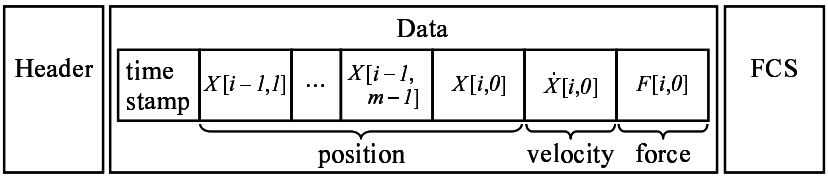

Fig. 5-28: Data packet in the proposed method

interval and thus data at multiple sampling points are filled in the transmission packet for the position signal.

Focusing on the velocity signal, the time interval and the delay influence H_{12} and the delay influence H_{21}. Since the influence of the delay is greater even for H_{12}, priority is given to the delay and thus data only at the latest sampling point is filled in a transmission packet for the velocity signal.

In the force signal, although both the time interval and the delay influence H_{12} and H_{21}, the delay gives greater impact on increase in the peak gain. Since the large peak gain may destabilize the system, priority is given to the delay and data only at the latest sampling point is thus filled in the transmission packet as the force signal. It should be noted that, however, the bandwidth of transmitted force may decrease due to a long time interval. It may decrease the bandwidth of reproduction of tactile sensation.

Consequently, the transmission packet is proposed to be filled with the following data as shown in Fig. 5-28.

- position: data at multiple sampling points
- velocity: data at the latest sampling point
- force: data at the latest sampling point

5.3.3 Performance Analysis

Conditions

Method B, Method C, and the proposed method are compared using the following five indices: reproducibility, operationality, tracking, drift, and stability. The details of indices are described in Section 2.4.3. Analyses were conducted for cases with and without a communication delay. The parameters used for analyses are shown in Table 5-9. As described in Section 5.3.2, the time interval T_d and the delay due to utilization of data in the transmission packet L_d in each method are represented as follows:

- Method B:
  $T_{dp} = T_{dv} = T_{df} = T_c$, $L_{dp} = L_{dv} = L_{df} = 0$;
- Method C:
  $T_{dp} = T_{dv} = T_{df} = T_r$, $L_{dp} = L_{dv} = L_{df} = (m-1)T_c/m$; and
- proposed method:
  $T_{dp} = T_r,\ T_{dv} = T_{df} = T_c$, $L_{dp} = (m-1)T_c/m,\ L_{dv} = L_{df} = 0$.

Results with Negligible Communication Delay

Fig. 5-29 shows the bode diagrams of indices in the cases when a communication delay is negligible. The delay is assumed to be $L_c = 0.0$ ms in the analyses.

Fig. 5-29(a) shows the bode diagram of reproducibility. The ideal condition is $|P_r| = 1$ in all frequencies. The peak value in the proposed method was almost the same as that in Method B and smaller than that in Method C. The result indicates that Method B and the proposed method are superior to Method C in terms of reproducibility.

Operationality is compared in Fig. 5-29(b). The ideal condition is $|P_o| = 0$. The response in the low frequency range is more important than that in the high frequency range since the frequency of motions of a human operator is generally low. The gain in the low frequency range was smaller in Method C and the proposed method than in Method B. A slight difference among methods was confirmed in the high frequency range. It can be mentioned from the result that Method C and the proposed method are superior to Method B in terms of operationality.

Fig. 5-29(c) shows the bode diagram of tracking. The ideal condition is $|P_t| = 0$. The magnitude of the gain was in the following order:

- Method C $<$ Method B $=$ proposed method in the low frequency range;
- Method C $<$ proposed method $<$ Method B in the middle frequency range; and
- Method C $=$ proposed method $<$ Method B in the high frequency range.

Although the responses differed depending on signal transmission methods, the gain was small enough to satisfy $|P_t| = 0$ in all cases. The result shows that difference in position tracking performance among the methods was negligible.

The performance of drift, which is position coincidence during the contact motion, is shown in Fig. 5-29(d). The ideal condition is $|P_d| = 0$. Although the difference among the cases was small and the ideal condition seemed to be satisfied in all cases, the magnitudes of gains were in the following order:

- proposed method $<$ Method C $<$ Method B in the low frequency range; and
- proposed method $=$ Method C $<$ Method B in the high frequency range.

The bode diagram of the open loop transfer function $P_s(s)$ shown in Fig. 5-29(e) indicates that higher stability was achieved with Method B or the proposed method. The stability margins were almost the same in Method B and the proposed method.

The results of analyses are summarized as follows:

- reproducibility was higher in Method B and the proposed method;
- operationality was better in Method C and the proposed method;
- tracking was the same in all methods;
- drift was the same in all methods; and
- stability was higher in Method B and the proposed method.

The above results show that the proposed method has better performance with respect to all these indices when a communication delay is negligibly small.

Results with Communication Delay

Analyses were also conducted for the cases with a communication delay to evaluate its influence on the validity of the proposed method. In Fig. 5-30, a communication delay was assumed to be $L_c = 1.0$ ms. Although the results are not shown here, cases with a larger delay were also examined to verify the performance limits of the method. Reproducibility with $L_c = 1.0$ ms had the same tendency as that in the cases without a communication delay as shown in Fig. 5-30(a). When the communication delay was larger than 5.0 ms, only a small difference existed among the methods. Fig. 5-30(b) shows that better operationality was achieved in Method C and the proposed method even with a communication delay. This tendency did not change even when a larger communication delay existed. Figs. 5-30(c) and (d) are the bode diagrams of tracking and drift, respectively, in the cases with $L_c = 1.0$ ms. Although the gain

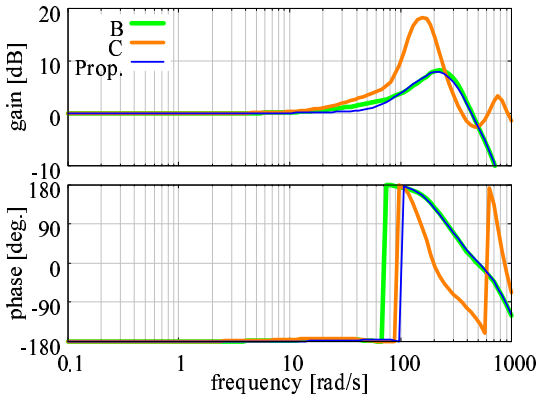

(a) reproducibility $P_r(s)$

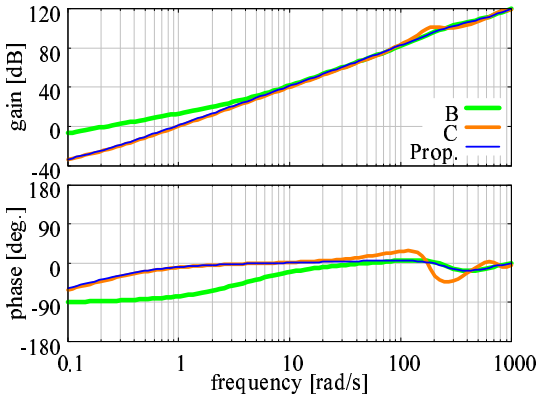

(b) operationality $P_o(s)$

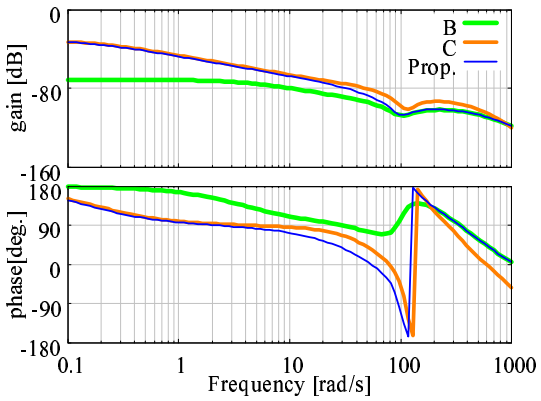

(c) tracking $P_t(s)$

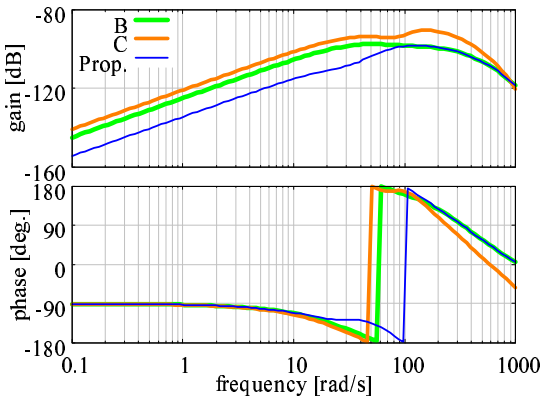

(d) drift $P_d(s)$

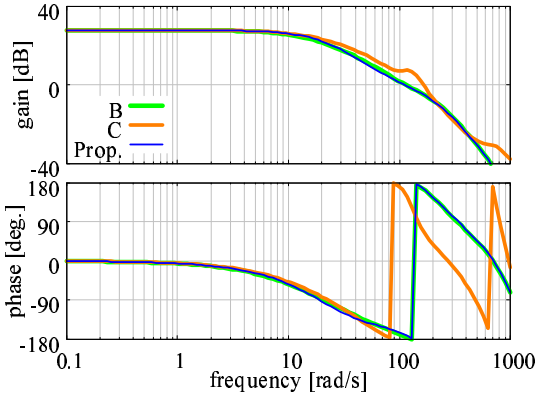

(e) stability $P_s(s)$

Fig. 5-29: Performance analysis of signal transmission method ($L_c = 0.0$ ms)

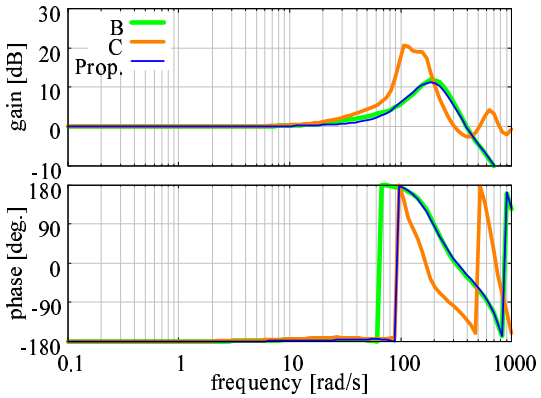

(a) reproducibility $P_r(s)$

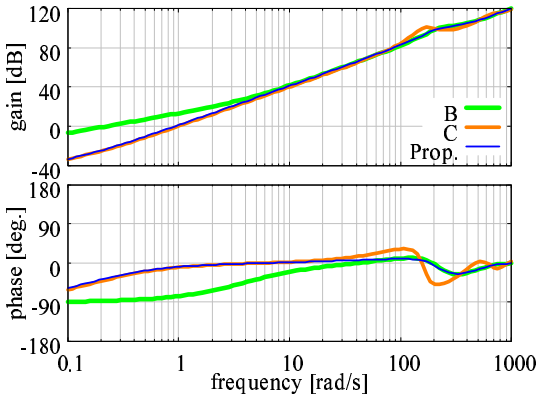

(b) operationality $P_o(s)$

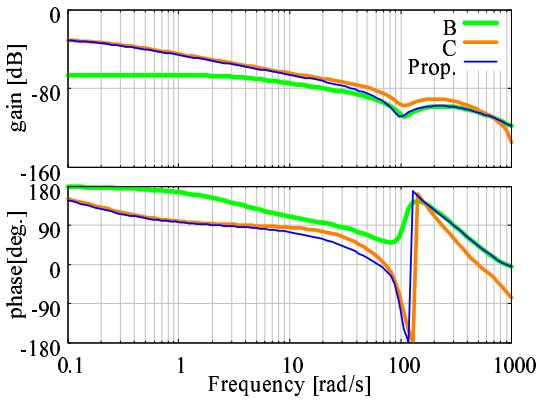

(c) tracking $P_t(s)$

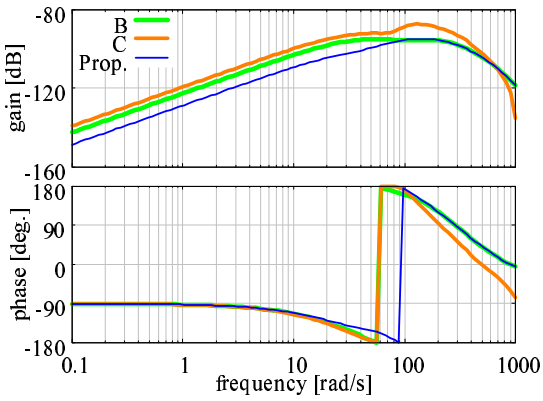

(d) drift $P_d(s)$

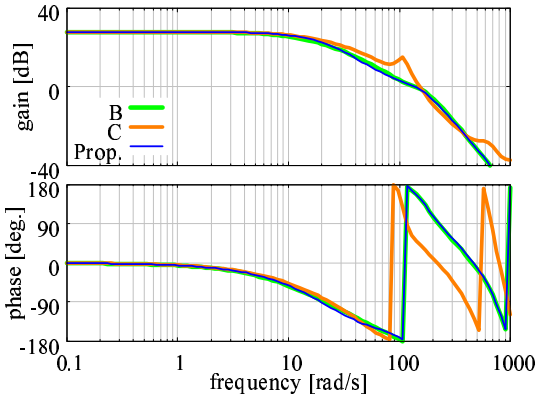

(e) stability $P_s(s)$

Fig. 5-30: Performance analysis of signal transmission method ($L_c = 1.0$ ms)

increased compared with the cases without the communication delay, they were still small enough to satisfy the ideal conditions in all methods. The gains remained small even with a larger communication delay. In terms of stability, Fig. 5-30(e) shows a similar tendency to the cases without a communication delay. The system was stable with Method B or the proposed method, while it was unstable with Method C. When a communication delay was larger, the stability of the system was deteriorated in all methods. The difference among the methods decreased with increase in a communication delay and it finally disappeared.

From the above investigation, the effectiveness of the proposed method was confirmed to be preserved even with a communication delay, when the delay was relatively small. On the other hand, differences among the methods decreased except for operationality when a communication delay was large. Even in this case, the proposed method was not worse than the other methods, better operationality and the same performance in the other indices were achieved.

5.3.4 Experiment

Experimental Setup

In this section, experiments were conducted with the system shown in Fig. 5-18. The parameters in the experiments are shown in Table 5-9. In each experiment, an operator manipulated the master robot, and the robots were operated in a non-contact motion (free motion) first, and then the slave robot was made into contact with an aluminum object (contact motion).

Experiments were conducted for the following three cases.

- Method B: transmit a packet filled with position, velocity, and force data at the latest sampling point
- Method C: transmit a packet filled with position, velocity, and force data at multiple sampling points
- proposed: transmit a packet filled with position data at multiple sampling points and velocity and force data at the latest sampling point.

Experimental Results

The experimental results are shown in Figs. 5-31 to 5-33: the results with Method B are shown in Fig. 5-31, those with Method C are shown in Fig. 5-32, and those with the proposed method are shown

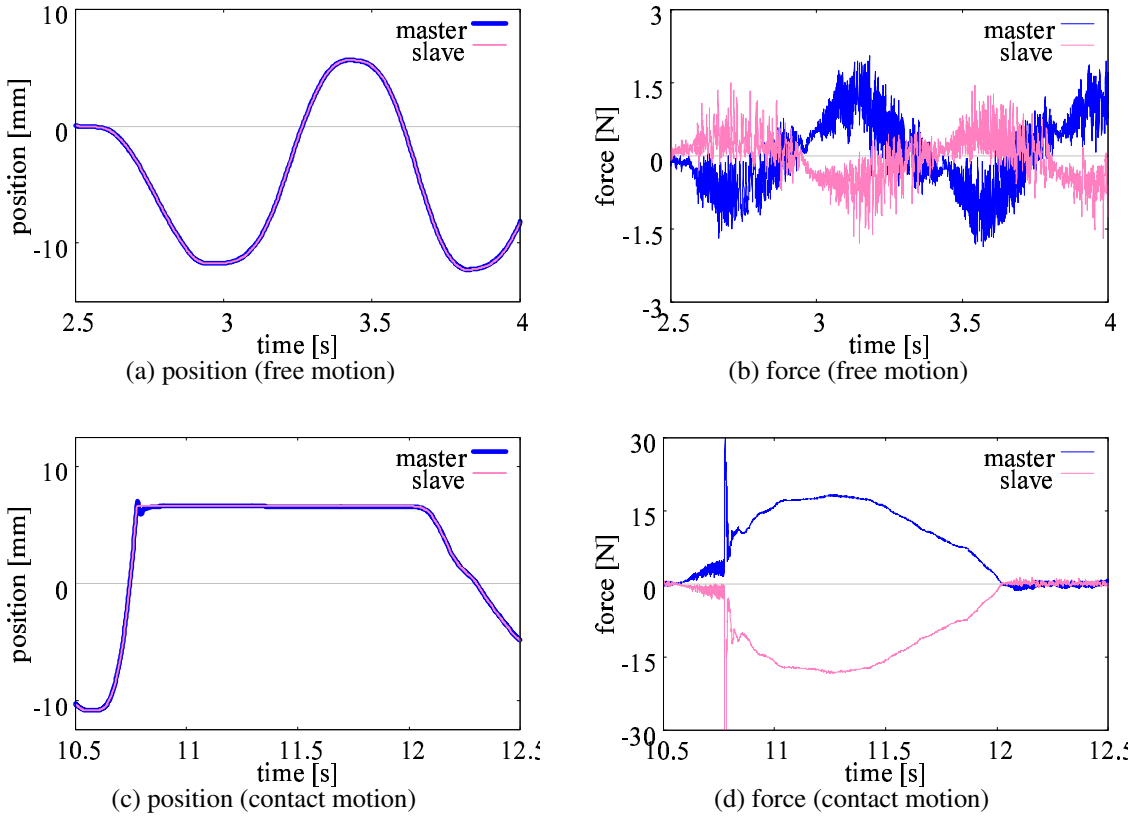

(a) position (free motion)
(b) force (free motion)
(c) position (contact motion)
(d) force (contact motion)

Fig. 5-31: Experimental results: bilateral teleoperation with Method B

in Fig. 5-33. In Method B and the proposed method, position responses of the master and slave devices well corresponded each other both in the free motion and the contact motion. Stable contact to the object was also achieved and the force responses during the contact showed the correspondence of force in the master and the slave. Focusing on the force response in the free motion, however, small oscillation was confirmed in Method B. Since the level of oscillation was larger than that in the proposed method, the oscillation was not a noise of the sensor but the real oscillation of the robot. The proposed method was therefore superior to Method B in terms of operationality. In Method C, stable contact was not achieved, although the response in the free motion was ideal, large oscillation occurred when the slave robot was made into contact with the object.

According to the above results, it was confirmed that performance of bilateral teleoperation improved with the proposed method by transmitting appropriate data considering the influence of characteristics of each signal.

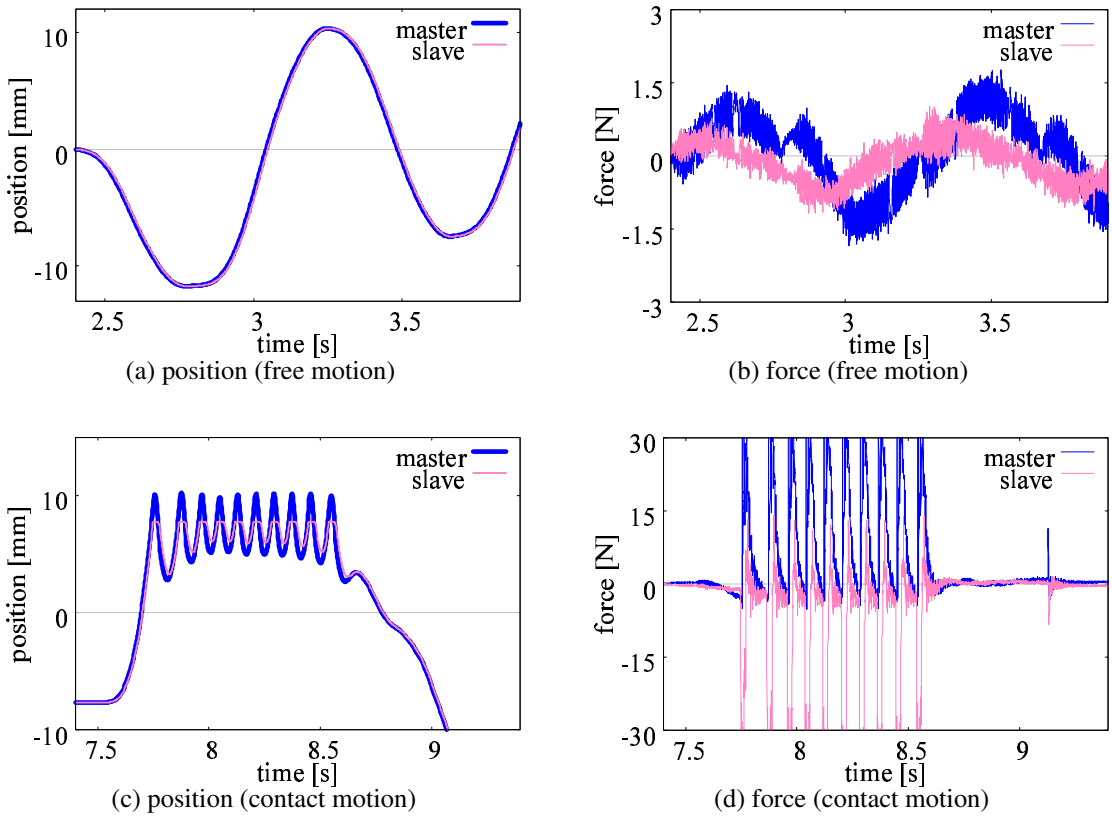

(a) position (free motion)
(b) force (free motion)
(c) position (contact motion)
(d) force (contact motion)

Fig. 5-32: Experimental results: bilateral teleoperation with Method C

5.4 Coding and Decoding Scheme for Precise Motion Control Over Network

This section tackles the problems of the limitation of the packet transmission interval from a viewpoint of processing of transmission signals. Although the signal transmission method proposed in the previous section is one of the processing schemes, this section proposes a more generally applicable coding and decoding scheme. The aims of the proposed scheme are: to overcome the trade-off between the data renewal interval or the bandwidth and the delay in the transmission signal; and to realize transmission and utilization of wide-band and small-delay signals even under severe limitation of the packet transmission interval. A method for reducing calculation cost and the transmission packet size while maintaining high control performance is also proposed.

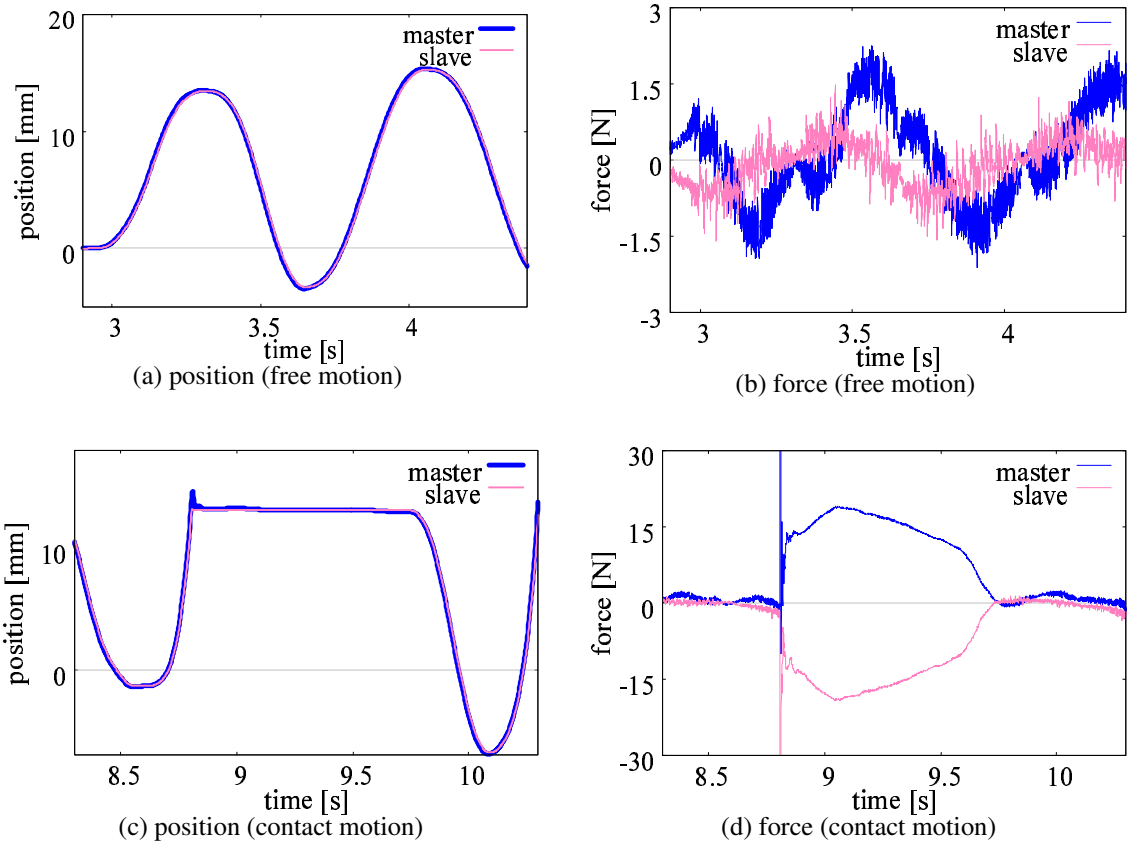

(a) position (free motion)
(b) force (free motion)
(c) position (contact motion)
(d) force (contact motion)

Fig. 5-33: Experimental results: bilateral teleoperation with proposed method

5.4.1 Signal Bandwidth Limitation due to Network

Acquisition of wide-band signals and the extremely short sampling period are required for precise motion control [118][119]. The bandwidth of the acquired signals is limited, however, when signals are transmitted through a network. When a signal is sampled, a frequency component higher than the Nyquist frequency, a half of the sampling rate, cannot be reproduced because of aliasing. This means that acquisition of a signal should be done with the sampling period short enough for the required bandwidth of the signal. On the other hand, a risk of network congestion may increase due to the performance of communication lines and communication devices when a packet transmission interval is shortened. Since network congestion causes a large communication delay and significant packet losses, a transmission interval should be set long enough to avoid network congestion. The sampling periods are therefore often set to different values for packet transmission and measurement or control as described in the previous sections.

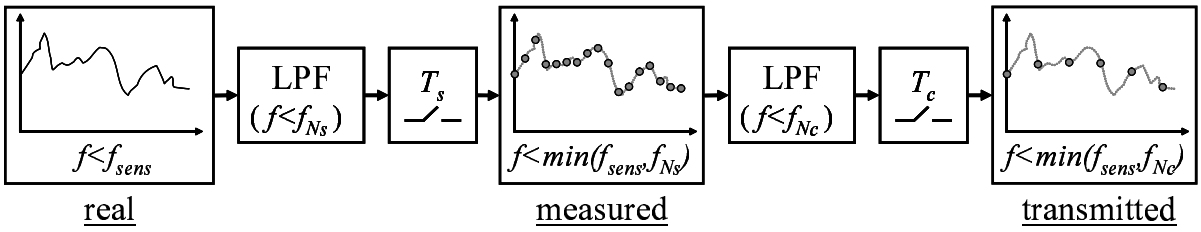

Fig. 5-34: Procedure of extraction of transmission signal

Fig. 5-34 shows the flow of extraction of transmission signals. Since the signals higher than the Nyquist frequency generate aliasing noise, it should be removed by using an LPF. The maximum frequency for the measured signals is therefore the lower of the frequency range of the sensor f_{sens} and the Nyquist frequency due to the measurement sampling period $f_{Ns}(= 1/(2T_s))$. When communication exists and the packet transmission interval T_c is set longer than the measurement sampling period, two different Nyquist frequencies exist: one is the Nyquist frequency due to measurement f_{Ns} and the other is that due to communication $f_{Nc}(= 1/(2T_c))$. When the packet transmission interval is set longer than the control sampling period, the Nyquist frequency due to communication f_{Nc} is lower than f_{Ns}. An LPF for anti-aliasing is required before extracting the transmission signals from the measured signals. The maximum frequency for the transmission signals is then limited to the lower of f_{Nc} and f_{sens}. It means that some measured components become unavailable to be transmitted due to communication if the frequency range of the sensor is higher than the Nyquist frequency due to communication. The bandwidth limitation explained above may deteriorate the performance of a system.

5.4.2 Coding and Decoding Scheme for Precise Motion Control over Network

This subsection proposed a coding and decoding scheme to transmit wide-band signals with small processing delay. The scheme uses an LPF to keep the delay due to processing small, and discrete Fourier transform (DFT) to transmit the frequency component higher than the Nyquist frequency due to communication. The proposed method is thus named as “LPF-DFT combined scheme”. The proposed method focuses on the fact that the delay due to processing is small when the data at the latest sampling period is transmitted as Method B in the previous section and the delay is generated by transmitting multiple data and using them from the oldest. In this research, the packet transmission interval is assumed to be set longer than the measurement sampling period due to limitations on the communication line and

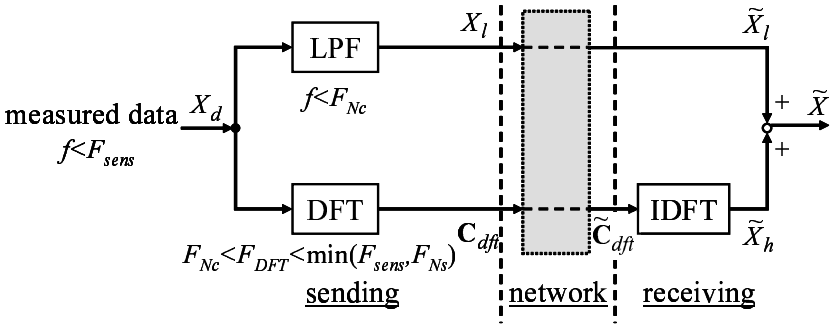

Fig. 5-35: LPF-DFT combined coding and decoding scheme

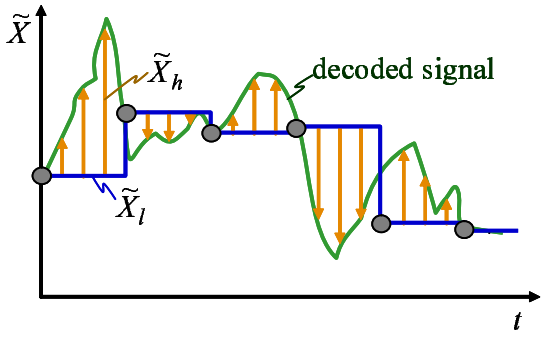

Fig. 5-36: Overview of decoding in the LPF-DFT combined scheme

devices and expressed as follows:

$$T_c = mT_s, \tag{5.18}$$

where m is an integer larger than 1. An overview of the proposed coding and decoding scheme is shown in Figs. 5-35 and 5-36. Here, X_l denotes a signal component lower than the Nyquist frequency of packet transmission, $\boldsymbol{c}_{dft}$ denotes frequency spectra, f_{DFT} denotes the frequency range for DFT calculation, and ˜ denotes a received value. The proposed method deals with low and high frequency components in different manners. In addition to transmission of the low frequency signal, the high frequency component is transmitted as frequency spectrum and added to the low frequency component on the received side to widen the bandwidth of the decoded signals. The details of the process are described below.

On the sending side, a signal lower than the Nyquist frequency of packet transmission X_l is extracted by the LPF.

$$X_l = G_l(s)X_d, \tag{5.19}$$

where $G_l(s)$ denotes an IIR type or an analog LPF with a cutoff frequency g_l lower than f_{Nc}. In addition to the extraction of X_l, DFT calculation is performed to extract the high frequency component excluded in X_l.

$$\begin{aligned} \boldsymbol{c}_{dft}[k] &= \sum_{n=0}^{N-1} X_d[n] e^{-j(2\pi kn/N)} \\ (k &= K_{MIN},\ K_{MIN}+1,\ \cdots,\ K_{MAX}) \end{aligned} \tag{5.20}$$

Here, $\boldsymbol{c}_{dft}$ denotes frequency spectra of X_d and N denotes the number of data used for the DFT calculation. Since a larger N provides a higher frequency resolution, while calculation cost increases and older data are included, N is generally set to the number of measurement sampling points in one or two packet transmission interval. K_{MIN} and K_{MAX} are set as $K_{MIN} = 0$ and $K_{MAX} = N - 1$ in general DFT. In the proposed LPF-DFT combined scheme, however, K_{MIN} is set as $K_{MIN} \approx \frac{g_l N T_s}{2\pi} (\approx f_{Nc} N T_s)$ and K_{MAX} is determined considering $min(f_{sens}, f_{Ns})$ and the bandwidth required for control. In addition to dealing the low and high frequency components in different manners, one of the characteristics of the LPF-DFT combined scheme is setting K_{MAX} at a different value to $N - 1$. The bandwidth of the signal is widened, while calculation cost and the size of a transmission packet increase with a larger K_{MAX}. Thus, K_{MAX} should be set to the bare minimum value.

In transmission of the signals, a sampled value of X_l and a frequency spectra $\boldsymbol{c}_{dft}$ are transmitted as a packet every T_c.

On the receiving side, the high frequency component $\tilde{X}_h$ is added to the low frequency component $\tilde{X}_l$ as shown in Fig. 5-36 to widen the bandwidth of the decoded signal. $\tilde{X}_l$ is renewed at every packet receiving point and it is hold at a constant value at the sampling points between two successive receiving points. $\tilde{X}_h$ is reproduced from $\boldsymbol{c}_{dft}$, which is renewed at every packet receiving point, using inverse discrete Fourier transform (IDFT).

$$\tilde{X}_l[n] = \tilde{X}_l[0] \tag{5.21}$$

$$\begin{aligned} \tilde{X}_h[n] &= \frac{1}{N} \sum_{k=K_{MIN}}^{K_{MAX}} \boldsymbol{c}_{dft}[k] e^{j(2\pi kn/N)} \\ (n &= 0, \cdots, N-1) \end{aligned} \tag{5.22}$$

Here, n is the number of sampling points from the renewal of $\boldsymbol{c}_{dft}$. The sum of $\tilde{X}_l$ and $\tilde{X}_h$ is used as a decoded signal on the receiving side.

$$\tilde{X}[n] = \tilde{X}_l[n] + \tilde{X}_h[n] \tag{5.23}$$

The LPF-DFT combined coding and decoding scheme enables the receiving side system to use signals with frequency components higher than the Nyquist frequency f_{Nc}. Wide-band signal transmission with small processing delay therefore becomes possible even under the severe limitation of the packet transmission interval.

5.4.3 Expected Advantage of LPF-DFT Combined Scheme

The advantages of the LPF-DFT combined scheme over the conventionally proposed methods are discussed in this subsection. As a method for shortening the interval of the transmission data, the upsampling technique or a method of transmitting the values at multiple control sampling points between two successive packet transmission points as a packet [114] can be applied. Those method and the LPF-DFT combined scheme are similar in the point that the value of the transmission signal is renewed more than once in one packet transmission interval. The advantage of the LPF-DFT combined scheme over the upsampling is that the bandwidth of the transmission signal can be widened only by the LPF-DFT combined scheme. The difference between these schemes is the value to be inserted between packet transmission points: upsampling inserts zero and the LPF-DFT combined scheme inserts a value derived from frequency spectrum of a high frequency component. The above-mentioned advantage comes from transmission of a high frequency component using DFT. The advantages of the LPF-DFT combined scheme over the latter method are that the delay due to processing and utilization of the data in the transmission packet is decreased and the data in the transmission packet is efficiently extracted by reflecting the bandwidth of the measured signals and importance for a control performance. The former point is achieved by separating handling of low and high frequency components. The latter point is achieved by extracting the signals as frequency spectra. Expansion to the data compression can be expected by determining the bandwidth or weighting of the frequency spectra with consideration of the difference in magnitude of the influence on control performance depending on the frequency of the signals. When considering the use of the frequency spectra for data compression, a discrete cosine transform (DCT) is widely used in the fields of audio and visual. A DCT-based method has also been proposed for application to haptic data compression for haptic communication [109]. The LPF-DFT combined scheme is similar to this method in terms of transmitting signals by using frequency spectra, but with two main differences as follows:

(i) process low and high frequency signal components in different manners: extract low frequency

signals using an LPF instead of DFT; and

(ii) perform DFT calculation only for a limited frequency range.

The first point has two aspects; one is the use of the LPF and the other is separation of the handling of the signal into two. The use of the LPF may impose both the adverse and preferable influences. A continuous or IIR type LPF gives weight to the latest data, while DFT imposes a constant delay depending on a window size. Because of the difference in delay, the decoded signal will not correspond perfectly to the original signal when an LPF is used, but the decoded signal performs as if the delay is smaller. It may impose the preferable influence on the performance of acceleration control. The separation of the handling in the LPF-DFT combined scheme enables systems to transmit low and high frequency components using different means or rates. This means that the latency, the communication path, or cost of the communication can be designed independently for the low and high frequency components when taking their influence on the performance into consideration.

The second point is important for the implementation of the method on hard real-time systems. Increase in calculation cost due to DFT is generally concerned in implementation of methods with DFT calculation. The increase is small in the LPF-DFT combined scheme, however, since the number of data processed in one calculation period is relatively small and DFT and IDFT calculations are performed only for the frequency range of $K_{MIN}/T < f_{DFT} < K_{MAX}/T$. The performance requirement for the calculation device is lower in the LPF-DFT combined scheme and it can be implemented on hard real-time systems with no adverse impacts.

5.4.4 Performance Analysis

In this subsection, frequency analyses were conducted to clarify the characteristics of the proposed LPF-DFT combined coding and decoding scheme and its influence on motion control. As mentioned in the previous subsection, the decoded signal may not correspond to the original signal perfectly with the LPF-DFT combined scheme due to the difference in phase delay characteristics between the LPF and DFT. On the other hand, the delay in the low frequency component may be smaller with the LPF-DFT combined scheme than that with the DFT-based scheme. This subsection first verifies the influence on the decoded signal. The influence of characteristics of the coding schemes on motion control performance is also verified by taking up the bilateral teleoperation system as an example of a motion control system severely influenced by the bandwidth limitation.

Modeling

The network path $N(s)$ was assumed to include not only the communication delay but also processes for signal transmission such as filtering and DFT calculation. It can therefore be regarded as a signal transmission path. The following three cases were considered as signal transmission in this section and the model of each signal transmission path is derived in this subsection.

- transmit only low frequency signals (LPF-based scheme)
- transmit frequency spectra extracted by DFT (DFT-based scheme)
- transmit LPF value and frequency spectra of high frequency component (LPF-DFT combined scheme)

In the LPF-based scheme, an LPF with cutoff frequency lower than the Nyquist frequency of packet transmission is applied and the filtered value is held for the packet transmission interval. The signal transmission path can be modeled as shown in Fig. 5-37(a) and the equation below:

$$N_{LPF}(s) = G_l(s)S_{T_c}(s)H_{T_c}(s)e^{-L_c s}, \tag{5.24}$$

where

$$G_l(s) = \frac{g_l}{s + g_l}. \tag{5.25}$$

Here, $S(s)$ denotes a sampler, $H(s)$ denotes a zero-order-holder, the subscripts of $S(s)$ and $H(s)$ denote the sampling period and holding period, respectively, and L_c denotes communication delay.

DFT and IDFT calculation conducted in the DFT-based scheme and LPF-DFT combined scheme generates constant delay depending on the window size and limits the frequency range of the signal to that of frequency spectra used for decoding. The value is renewed at every measurement sampling point. The signal transmission path using DFT for the limited frequency range can be modeled as shown in Fig. 5-37(b) and the equation below:

$$N_{DFT}(s) = G_{DFT}(s)S_{T_s}(s)H_{T_s}(s)e^{-L_c s}, \tag{5.26}$$

where

$$G_{DFT}(s) = \begin{cases} e^{-T_c s} & (f_{min} \leq f \leq f_{max}) \\ 0 & (f < f_{min} \cup f > f_{max}). \end{cases} \tag{5.27}$$

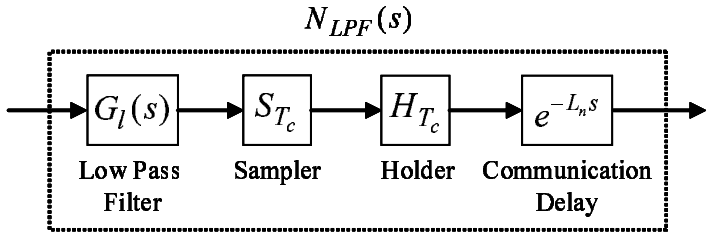

(a) LPF-based scheme

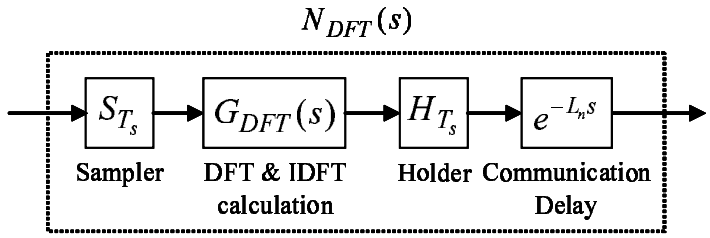

(b) DFT-based scheme

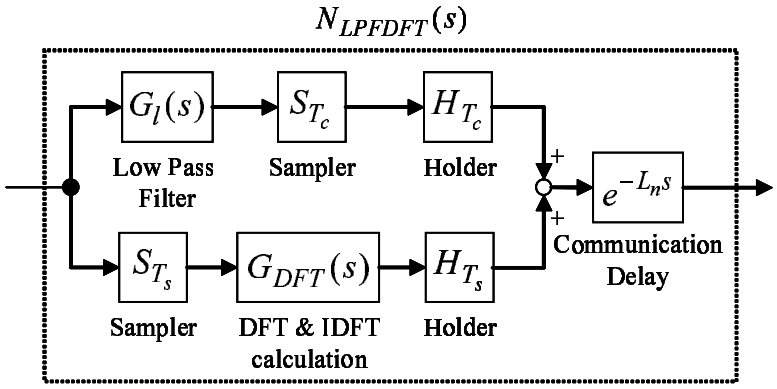

(c) LPF-DFT combined scheme

Fig. 5-37: Models of signal transmission path

f_{min} is usually set to zero in the DFT-based scheme.

The process of the LPF-DFT combined scheme contains both LPF process and DFT process. It can thus be expressed as shown in Fig. 5-37(c) and the following equation.

$$N_{LPFDFT}(s) = \{G_l(s)S_{T_c}(s)H_{T_c}(s) + G_{DFT}(s)S_{T_s}(s)H_{T_s}(s)\}e^{-L_c s} \tag{5.28}$$

Here, f_{min} is determined by K_{MIN} and f_{max} is determined by K_{MAX} in (5.20) in the LPF-DFT combined scheme.

Table 5-10: Control parameters in analysis and experiments on coding schemes

Control sampling period	T_s	0.2	ms
Signal transmission sampling period	T_c	5.0	ms
Communication delay	L_c	0.0 and 5.0	ms
Position feedback gain	K_p	3600.0	$1/\mathrm{s}^2$
Velocity feedback gain	K_v	120.0	1/s
Force feedback gain	K_f	1.0	$\mathrm{m/Ns}^2$
Analysis			
Spring coefficient of operator	K_h	400.0	N/m
Damping coefficient of operator	D_h	40.0	Ns/m
Spring coefficient of environment	K_e	10000.0	N/m
Damping coefficient of environment	D_e	10.0	Ns/m
Cutoff frequency of LPF	g_l	600	rad/s
Experiment			
Cutoff frequency of DOB	g_{dis}	1800	rad/s
Cutoff frequency of RFOB	g_{dis}	1800	rad/s
Number of data used in DFT calculation	N	25	

Analysis of signal transmission path

Firstly, the characteristics of the signal transmission path with the LPF-based scheme, the DFT-based scheme, or the LPF-DFT combined scheme themselves were analyzed and compared. The sampling periods and the cutoff frequency of the LPF were set to the values shown in Table 5-10. The communication delay was assumed to be negligible ($L_c = 0.0$ ms) in this analysis to verify only the difference due to signal transmission processes. f_{min} and f_{max} were set as $f_{min} = 0$ rad/s and $f_{max} = 5000$ rad/s in the DFT-based scheme, and set as $f_{min} = g_l$ rad/s and $f_{max} = 5000$ rad/s in the LPF-DFT combined scheme.

The bode diagrams of $N_{LPF}(s)$, $N_{DFT}(s)$, and $N_{LPFDFT}(s)$ are shown in Fig. 5-38. Comparing the LPF-based scheme and the DFT-based scheme, the gain decreased from around 100 rad/s in the LPF-based scheme, while the gain was maintained at 0 dB up to the set frequency f_{max} in the DFT-based scheme. It means that high frequency signals are eliminated in the LPF-based scheme, while wide-band signals can be transmitted with the DFT-based scheme. In terms of phase delay, the delay is larger in the DFT-based scheme compared with the LPF-based scheme. The characteristics of the LPF-DFT combined scheme were the same as those of the LPF-based scheme in the frequency range lower than g_l and the same as those of the DFT-based scheme in the frequency range higher than g_l: the gain decreased

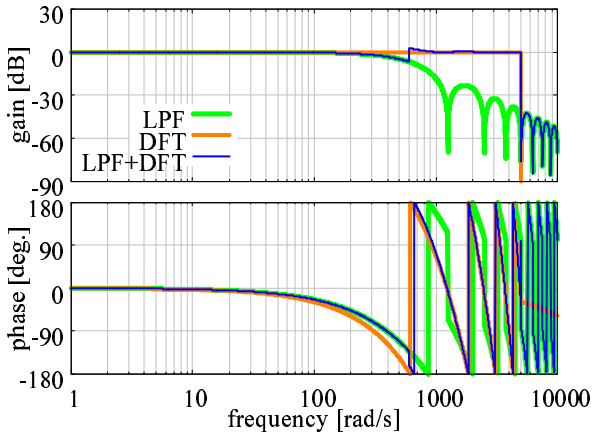

Fig. 5-38: Bode diagram of signal transmission path

at a frequency around g_l but was maintained at 0 dB up to f_{max} and the phase delay was smaller than that in the DFT-based scheme in the frequency range lower than g_l. It means that the delay is smaller in the lower frequency range and the gain is maintained up to the set frequency in the LPF-DFT combined scheme. No adverse characteristics due to the difference in phase delay between the LPF and DFT were confirmed. The results support the advantages of the LPF-DFT combined scheme mentioned in the previous subsection and confirm that the LPF-DFT combined scheme has preferable characteristics for utilization in control.

Influence on Bilateral Teleoperation Performance

The influence of characteristics of the signal transmission path mentioned above on the performance of motion control was analyzed next. This subsection takes up a bilateral teleoperation system as a motion control system that requires introduction of a network and is severely influenced by the bandwidth limitation. Reproduction of wide-band haptic sensation is important in bilateral teleoperation to help an operator to execute complicated tasks. However, it requires an extremely short sampling period and wide-band signals. When the rate of packet transmission between the master side and the slave side is limited, a switching motions or force at the contact moment may not be reproduced since the bandwidth of the transmitted position and force signals is inadequate.

The analyses were conducted for the system with the four-channel-based controller shown in Fig. 5-2. A Smith predictor-based delay compensation was applied to the controller. An operator and an environment were modeled as a spring and damper model expressed in (2.37) and (2.38). This analysis

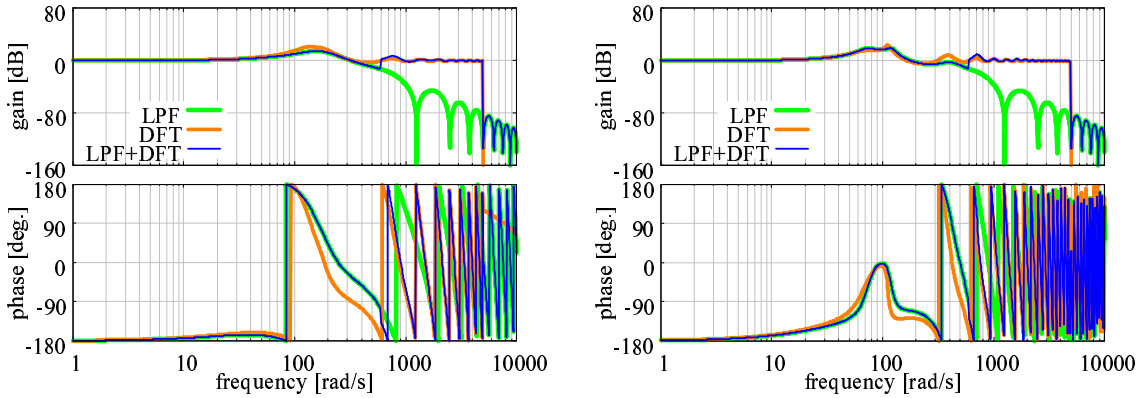

(a) $L_c = 0.0$ ms (b) $L_c = 5.0$ ms

Fig. 5-39: Analysis on influence of coding on bilateral teleoperation performance: reproducibility P_r

introduces the following four indices described in Section 2.4.3 to evaluate the performance of bilateral teleoperation: reproducibility, operationality, tracking, and drift. Analyses were conducted for the cases with a negligible communication delay ($L_c = 0.0$ ms) and those with a constant delay ($L_c = 5.0$ ms) using the parameters shown in Table 5-10.

Figs. 5-39 to 5-42 show the bode diagrams of the respective indices. Reproducibility shown in Fig. 5-39(a) dropped from around g_l in the LPF-based scheme. It shows that a contact force in a frequency higher than g_l cannot be reproduced. On the other hand, reproducibility was ideal up to f_{max} in the DFT-based scheme and the LPF-DFT combined scheme. Fig. 5-39(b) shows the same tendency in the case with a communication delay. The results show that the DFT-based scheme and the LPF-DFT combined scheme are superior to the LPF-based scheme in terms of reproducibility.

Fig. 5-40 shows the bode diagram of operationality. Although the behavior was almost the same in all schemes, the enlarged view shows that the value was about 2 dB smaller in the LPF-based scheme and the LPF-DFT combined scheme than in the DFT-based scheme. It means that a smaller operational force is required in the LPF-based scheme and the LPF-DFT combined scheme. It may be due to the smaller phase delay in the low frequency range. Fig. 5-40(b) shows that the tendency was almost the same even in the case with a communication delay, although the gain increased entirely and fluctuated at frequencies around 100 rad/s. The difference between the DFT-based scheme and the LPF-based scheme or that between the DFT-based scheme and the LPF-DFT combined scheme decreased but there was still 1.2 dB difference.

The bode diagram of tracking is shown in Fig. 5-41. Although the gain was small enough to satisfy the

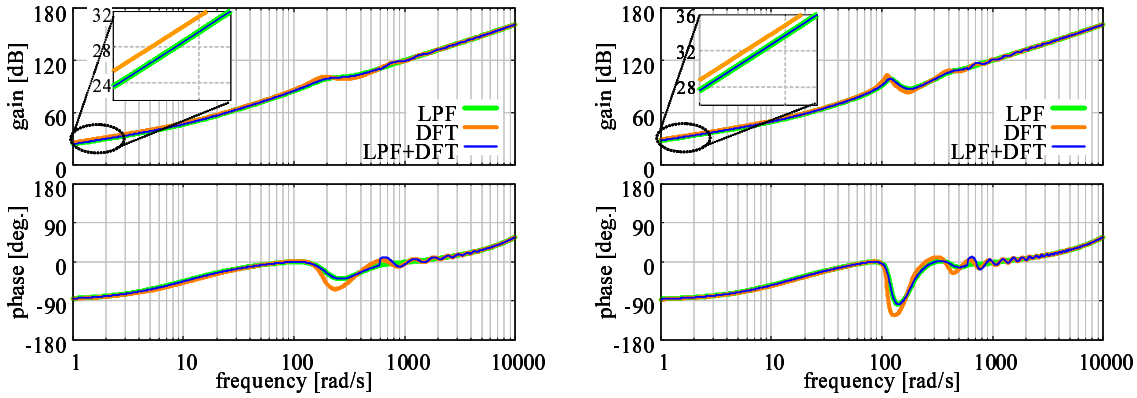

(a) $L_c = 0.0$ ms (b) $L_c = 5.0$ ms

Fig. 5-40: Analysis on influence of coding on bilateral teleoperation performance: operationality P_o

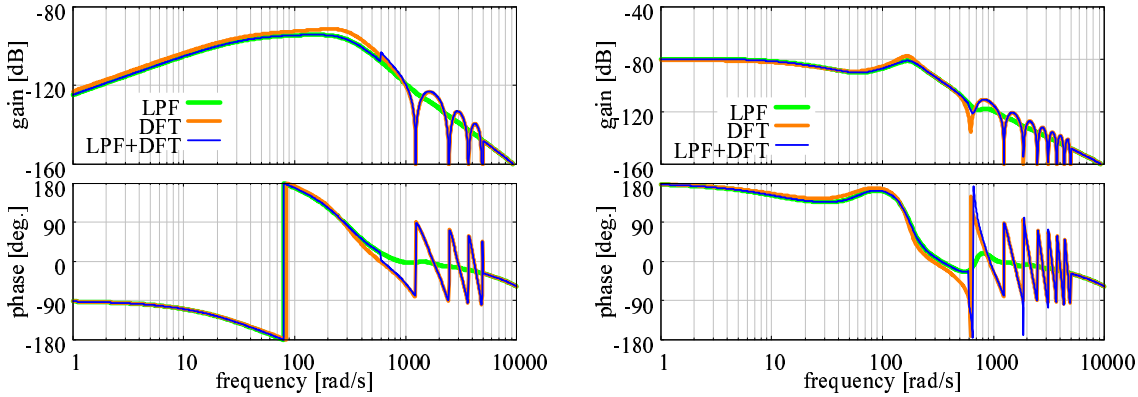

(a) $L_c = 0.0$ ms (b) $L_c = 5.0$ ms

Fig. 5-41: Analysis on influence of coding on bilateral teleoperation performance: tracking P_t

ideal condition in all cases, the gain was smaller in the LPF-based scheme and the LPF-DFT combined scheme than in the DFT-based scheme when a communication delay was negligible. In the case with a communication delay, the gain increased and gain peak appeared but the gain still kept small enough to satisfy the ideal condition in all cases. The difference among the schemes disappeared.

The bode diagrams of the drift shown in Fig. 5-42 are similar to those of tracking. Although the gain was small enough to satisfy the ideal condition in all cases, the gain in the LPF-based scheme and the LPF-DFT combined scheme was smaller than that in the DFT-based scheme when a communication delay was negligible. The difference among the schemes disappeared when $L_c = 5.0$ ms.

The above results show that the LPF-DFT combined scheme has the characteristics the same as the better of the LPF-based scheme and DFT-based schemes. No deterioration of the performance compared

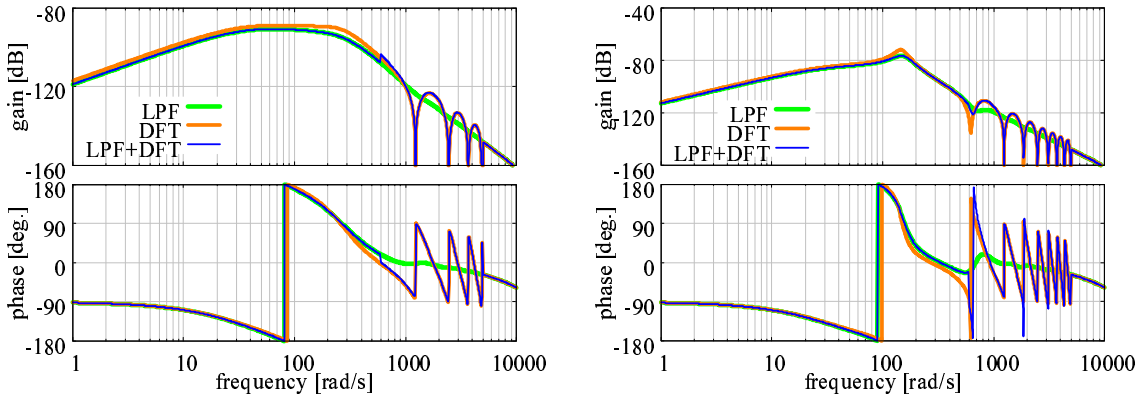

(a) $L_c = 0.0$ ms (b) $L_c = 5.0$ ms

Fig. 5-42: Analysis on influence of coding on bilateral teleoperation performance: drift P_d

with other schemes or adverse influence due to summation of values with different phase delay was confirmed.

5.4.5 Experimental Verification

Experimental Setup

Experiments were conducted using a pair of master and slave robots shown in Fig. 5-18 to verify the effectiveness of the LPF-DFT combined scheme in the real system. As in the cases of experiments in the previous sections, the force signal was estimated from the output of the encoder using the reaction force observer (RFOB) and the disturbance observer (DOB) was applied to each robot. In this experiment, the master and slave robots were controlled using the same computer and the network was virtually constructed in the computer. The parameters in the experiments are listed in Table 5-10. The same as in the analysis, experiments were conducted for the following three cases:

- LPF-based scheme: transmit only low frequency signals;
- DFT-based scheme: transmit frequency spectra extracted by DFT; and
- LPF-DFT combined scheme: transmit LPF value and frequency spectra extracted by DFT.

The settings in each case are listed in Table 5-11. Although it is possible in the LPF-DFT combined scheme to transmit low and high frequency components separately through different communication lines, these were transmitted together through the same line in this experiments. Firstly, the signal trans-

Table 5-11: Settings in experiment on coding schemes

	Cutoff frequency	Frequency spectra	
	g_l [rad/s]	K_{MIN}	K_{MAX}
LPF-based scheme	600.0	-	-
DFT-based scheme	-	0	4
LPF-DFT combined scheme	600.0	1	4

mission performance was verified by using the force signal at a contact moment. Secondly, experiments on bilateral teleoperation were executed to verify the influence on motion control performance.

Experimental Results on Signal Transmission

In order to verify the performance of signal transmission, the transmitted and decoded signals were compared with the original signal in Fig. 5-43 and Table 5-12. The same sampled force signal of 0.5 s around the contact moment was used in all the cases. The original values in the figures of the time domain response are shifted for a packet transmission interval for easier comparison.

The decoded values tend to follow the original values in all cases. On the other hand, a large impact force occurring at the contact moment was not decoded in the LPF-based scheme, while the force were sufficiently decoded in the DFT-based scheme and the LPF-DFT combined scheme. The results in the frequency domain show that contact force higher than 100 Hz was not decoded in the LPF-based scheme. In the DFT-based and LPF-DFT combined schemes, the frequency distribution of the decoded signals corresponded to that of the original almost perfectly even in the frequency range higher than 100 Hz. These results confirm the effectiveness of the transmission of the frequency spectra extracted by DFT. These results also show superiority of these schemes over the upsampling technique. Although the upsampling technique can heighten the sampling rate of the decoded signal as in the DFT-based and LPF-DFT combined schemes, it cannot widen the bandwidth of the decoded signal. In the DFT-based and LPF-DFT combined schemes, small deviation of the decoded signal was confirmed at boundaries of packets. This discontinuity is caused by the boundary condition assumed in DFT and use of coefficients of the limited frequency range in coding and decoding. DFT assumes the original signal to be repeat of the extracted signals. This assumption causes discontinuity at the boundaries and large values in high frequency coefficients. Since the LPF-DFT combined scheme performs DFT and IDFT calculation only for the limited frequency range and frequency resolution is not high enough, elimination of high frequency coefficients causes boundary artifact. This boundary noise can be reduced by using discrete

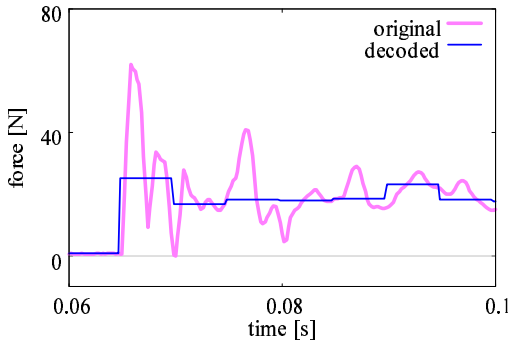

(a) time domain (LPF)

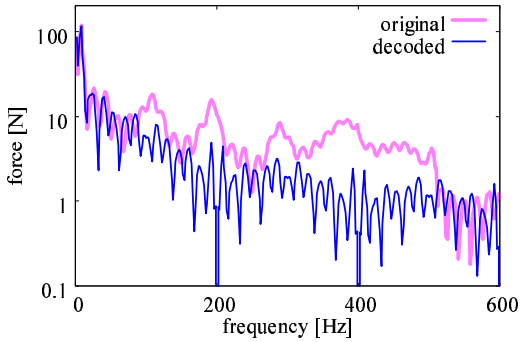

(b) frequency domain (LPF)

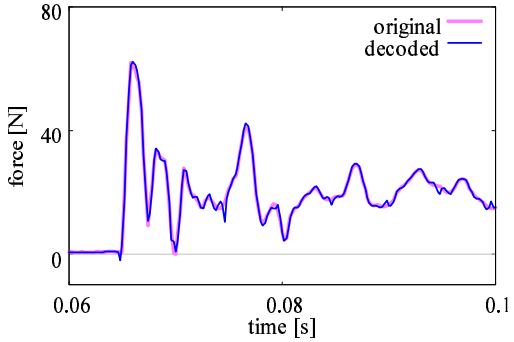

(c) time domain (DFT)

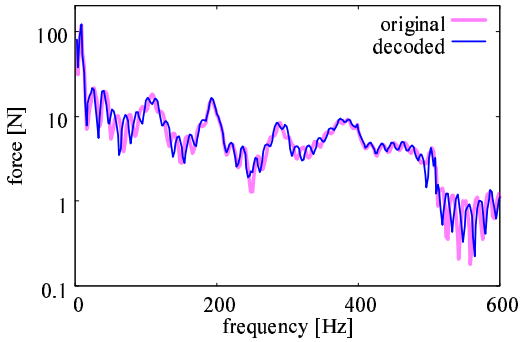

(d) frequency domain (DFT)

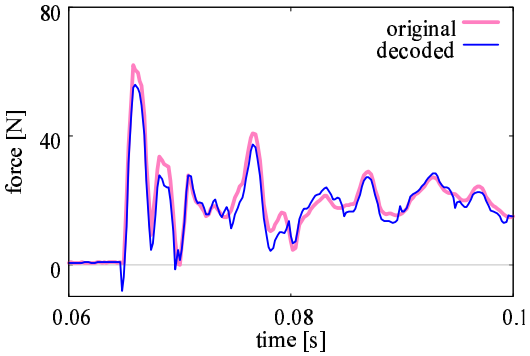

(e) time domain (LPF-DFT)

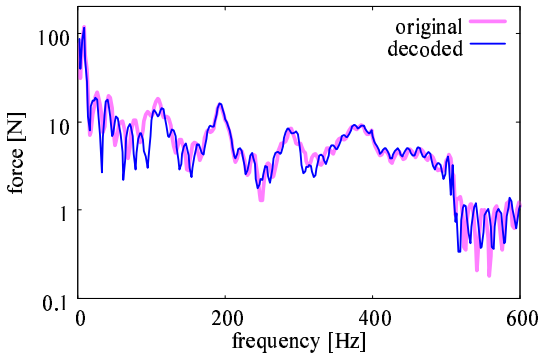

(f) frequency domain (LPF-DFT)

Fig. 5-43: Experimental results: coding and decoding of contact force

cosine transform (DCT) instead of DFT. Since DCT assumes the original signal as an even function, discontinuity at boundaries decreases and information tends to concentrate in a fewer coefficients in the low frequency range in DCT than that in DFT. Application of DCT is thus effective for further improvement of the performance of the LPF-DFT combined scheme.

When comparing the DFT-based and LPF-DFT combined schemes, the error was larger in the LPF-

Table 5-12: Experimental results: errors in transmitted contact force (Ave.±SD)

	time domain [N]	freq. domain [N]
LPF-based scheme	0.62±2.44	3.48±2.90
DFT-based scheme	0.10±0.27	1.25±1.55
LPF-DFT combined scheme	0.28±0.88	1.42±2.02

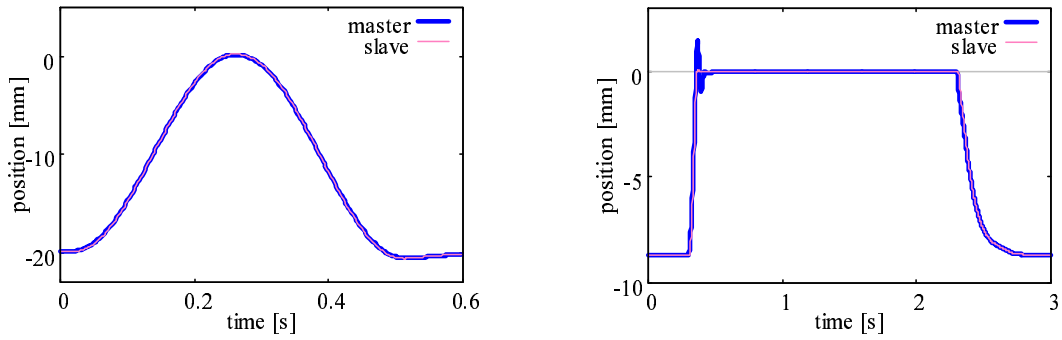

(a) free motion (b) contact motion

Fig. 5-44: Experimental results: overview of motion in bilateral teleoperation

DFT combined scheme, especially in the time domain. This is due to the use of the LPF in the LPF-DFT combined scheme and difference in phase delay characteristics between LPF and DFT. As mentioned in Section 5.4.3, the decoded value does not perfectly correspond to the original, while the influence of the signal delay due to the DFT calculation decreases when the low frequency signal is extracted by the LPF. The influence of the error on the performance of motion control is verified next.

Experimental Results on Bilateral Teleoperation

For quantitative evaluation of bilateral teleoperation performance, the master robot was moved almost the same in each case with a pseudo-operator input. An overview of each motion is shown in Fig. 5-44. The experiments were conducted for the cases with negligible communication delay and the constant communication delay: $L_c = 0.0$ and 5.0 ms. The results are shown below only for operationality and reproducibility, for which the significant influence was expected, with $L_c = 5.0$ ms. Other evaluation data are summarized in Table 5-13. Here, $\sum F_m$ is an index for operationality and represents the magnitude of a total force required for a sequence of an operation. The ratio of the maximum force generated in the master and the slave $|F_m|_{max}/|F_s|_{max}$ shows availability of reproduction of an impact force, and is ideally 1. F_{fm} and F_{fs} denote frequency domain values, PSD, of force generated in the master and the slave. The median of $|F_{fm}/F_{fs}|$ is an index of reproducibility in the frequency domain.

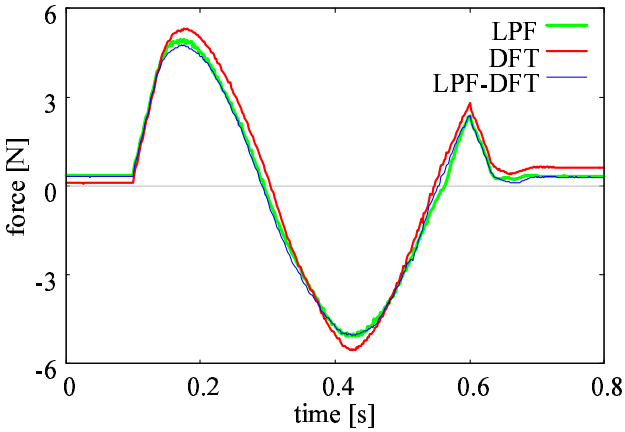

Fig. 5-45: Experimental results: operational force in non-contact motion

Fig. 5-45 shows that the operational force in the non-contact motion. It was smaller in the LPF-based scheme and the LPF-DFT combined scheme than in the DFT-based scheme by 10 %. This tendency agrees with the results of analysis. The smaller operational force was achieved in the LPF-DFT combined scheme because weight was given to the latest value due to the use of an LPF and a delay in the signals appears to be attenuated. In the non-contact motion, as shown in Table 5-13(a), position tracking errors between the master and slave devices were sufficiently small and almost the same in all the cases. Moreover, the results for the cases with $L_c = 0.0$ ms had a tendency similar to those for the cases with $L_c = 5.0$ ms as shown in Table 5-13.

In the contact motion, the slave stably came into contact with the object and the position and force corresponded well between the master and the slave in all the cases. The force responses of the master and the slave and the frequency distribution of the force are shown in Fig. 5-46. Sample data of 0.5 s around the contact moment were used for deriving the frequency distribution. Fig. 5-46 shows that the impact force reproduced in the master was much smaller in the LPF-based scheme compared with that occurring in the slave. As shown in Table 5-13(b), the ratio of the force generated in the master to the force generated in the slave is closer to the ideal value of 1 in the DFT-based or LPF-DFT combined scheme than in the LPF-based scheme. There was only a small difference between the DFT-based scheme and the LPF-DFT combined scheme in force error in terms of reproduction, although the error in terms of signal transmission was larger in the LPF-DFT combined scheme. In the frequency distribution, frequency components higher than 100 Hz were not reproduced in the master in the LPF-based scheme. On the other hand, they were reproduced properly in the DFT-based or LPF-DFT combined scheme.

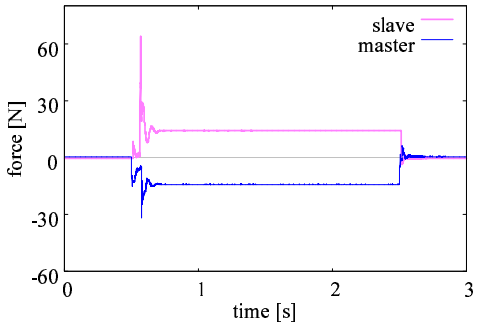

(a) time domain (LPF)

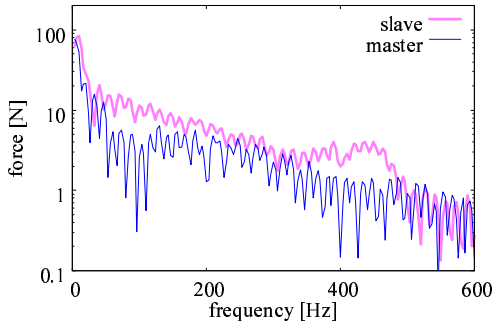

(b) frequency domain (LPF)

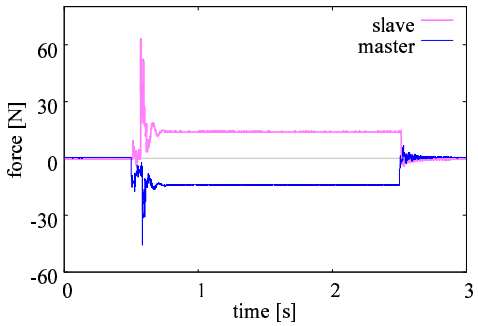

(c) time domain (DFT)

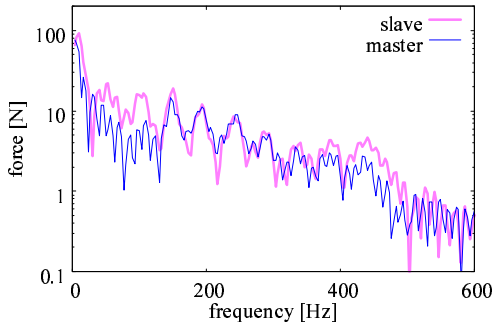

(d) frequency domain (DFT)

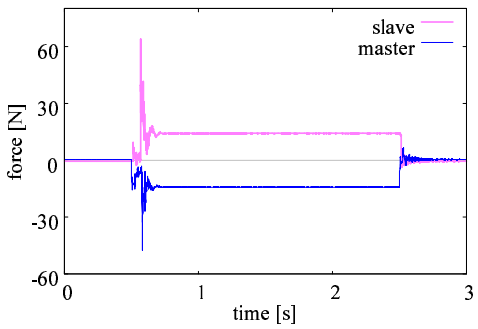

(e) time domain (LPF-DFT)

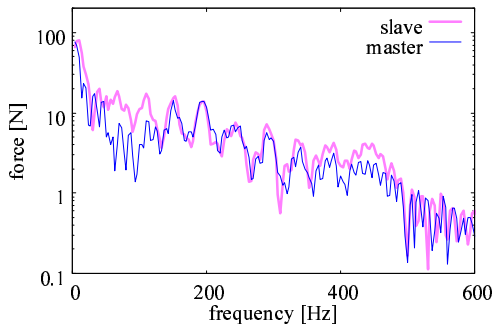

(f) frequency domain (LPF-DFT)

Fig. 5-46: Experimental results: force response in contact motion

This result proves that the bandwidth of the force reproduction was increased by the transmission of the force spectra extracted by DFT. As shown in Table 5-13(b), a position error in the contact motion was the almost the same in all the cases. As in the case of the non-contact motion, a tendency of difference among the schemes was almost the same in the case with $L_c = 0.0$ ms.

The above results show that the LPF-DFT combined scheme can improve reproducibility, especially the bandwidth of transmission of haptic sensation, while keeping the operational force small. Improve-

Table 5-13: Experimental results: comparison of coding scheme on bilateral teleoperation performance

(a) non-contact motion

	position error AVE±SD [mm]	operational force $\sum F_m$ [N·s]
$L_c = 0.0$ ms		
LPF-based scheme	0.039±0.021	1.73
DFT-based scheme	0.045±0.025	1.93
LPF-DFT combined scheme	0.042±0.027	1.72
$L_c = 5.0$ ms		
LPF-based scheme	0.092±0.056	2.61
DFT-based scheme	0.113±0.065	2.89
LPF-DFT combined scheme	0.094±0.057	2.62

(b) contact motion

	position error	reproducibility	
	AVE±SD [mm]	$\lvert F_m\rvert_{max}/\lvert F_s\rvert_{max}$	$median(\lvert F_{fm}/F_{fs}\rvert)$
$L_c = 0.0$ ms			
LPF-based scheme	0.022±0.104	0.476	0.497
DFT-based scheme	0.027±0.128	0.726	0.743
LPF-DFT combined scheme	0.028±0.110	0.769	0.797
$L_c = 5.0$ ms			
LPF-based scheme	0.051±0.225	0.497	0.483
DFT-based scheme	0.059±0.232	0.725	0.759
LPF-DFT combined scheme	0.060±0.240	0.740	0.743

ment of performance is expected also in other motion control and thus high performance motion control is expected to be achieved even under the limitation of the packet transmission interval. It was also confirmed that the scheme is applicable to the hard real time system.

5.5 Optimization of Transmission Data for Bilateral Teleoperation Based on LPF-DFT Combined Scheme

5.5.1 Problems in Application of LPF-DFT Combined Scheme to Bilateral Teleoperation

In order to transmit vivid haptic sensation in bilateral teleoperation and to execute advanced tasks properly, it is important to acquire wide-band signals and transmit them without delay. As described

in the previous section, introduction of the LPF-DFT combined scheme to signal transmission between the master device and the slave device in bilateral teleoperation enables the system to transmit wide-band signals with small delay even under severe limitation of the packet transmission interval. The performances such as the bandwidth of force transmission are thus improved. The calculation cost and the transmission packet size increase in this scheme, however, in comparison with the case in which only the low frequency component is transmitted. Considering the application to a multi-degree-of-freedom system and concurrent control of multiple systems, it is essential to reduce the calculation cost and the transmission packet size. Those in the LPF-DFT combined scheme are determined by K_{MAX} in (5.20). A smaller K_{MAX} decreases the calculation cost and the packet size, while control performance deteriorates if K_{MAX} is too small. There is thus a trade-off between quality of a transmission signal or control performance and the calculation cost or the packet size. The following subsection is devoted to propose a method for reducing the calculation cost and the packet size while maintaining high control performance.

5.5.2 Optimization of Transmission Signal

The signals transmitted in the four-channel-based controller shown in Fig. 5-2 are position, velocity, and force signals. As mentioned in Section 5.3, the influence of the time interval of data renewal and that of the delay on bilateral teleoperation performance differ depending on the types of signals. Similar to that, the required bandwidth may differ depending on the types of signals. This section proposes a method for optimizing the transmission signal by designing the bandwidth of the transmission signal independently for each signal, with consideration of the magnitude of the influence of the bandwidth limitation of the respective signals on control performance. Optimization in this section means reductions in calculation cost and the packet size without deterioration of performance.

Analysis of Influence of Bandwidth Limitation

Performance analyses were conducted to clarify the influence of bandwidth limitation of each signal on the bilateral teleoperation performance. Reductions in calculation cost and the packet size are realized without deterioration of performance by deciding the bandwidth of the transmission signal of each signal based on the analysis results.

As a means to express bandwidth limitation, an LPF is widely used. The ideal DFT model expressed in (5.27) is used in this section instead of an LPF, however. When an LPF is used, not only the bandwidth

but also the phase characteristics of the LPF impose the influence on the analysis result. On the other hand, what should be clarified in the analysis is the influence of bandwidth limitation due to K_{MAX} in the LPF-DFT combined scheme. The phase characteristics of the signal do not change according to K_{MAX}. The ideal DFT model is therefore used to avoid the influence of the phase characteristics. Equation (5.27) indicates that the gain is maintained completely, while constant delay exists in the frequencies lower than f_{limit} and signals higher than f_{limit} are completely eliminated. The operator model and the contact environment model expressed in (2.37) and (2.13) are utilized as the inputs to the master and the slave, respectively.

The analyses were conducted for the following four cases:

- set bandwidth limitation of all signals high ($f_p = f_v = f_f = f_h$)
- set bandwidth limitation of position signal low and that of the other signals high ($f_p = f_l,\ f_v = f_f = f_h$)
- set bandwidth limitation of velocity signal low and that of the other signals high ($f_v = f_l,\ f_p = f_f = f_h$)
- set bandwidth limitation of force signal low and that of the other signals high ($f_f = f_l,\ f_p = f_v = f_h$)

Here, f_p, f_v, and f_f are the bandwidth limitations of position, velocity, and force signals, respectively. The higher value for bandwidth limitation f_h was set to 2500.0 rad/s and the lower value f_l was set to 380.0 rad/s. Here, f_l was determined with consideration of the packet transmission interval T_c, and f_h was determined with consideration of the bandwidth of tactile sensation of human (0 - 400 Hz). The parameters used in the analysis are shown in Table 5-14.

Analyses were conducted using the following four indices: reproducibility, operationality, tracking, and drift. Fig. 5-47 shows the bode diagram of each performance index. As shown in Fig. 5-47(a), reproducibility was greatly influenced by the bandwidth limitation of the force signal. When the bandwidth of the force signal was limited to f_l, the gain plunged at the frequency and haptic sensation higher than the frequency thus could not be reproduced. Although the influence of bandwidth limitation of the velocity signal was also confirmed in Fig. 5-47(a), the magnitude was much smaller than that for the force signal. No influence of the limitation of the position signal was confirmed. The above result shows that there is a difference in the magnitude of the influence depending on types of signals. Fig. 5-47(b) shows that

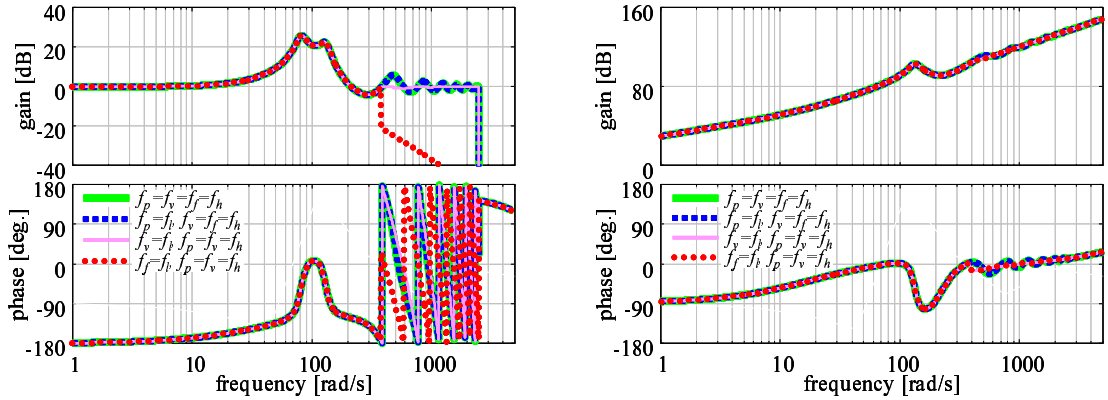

(a) reproducibility P_r

(b) operationality P_o

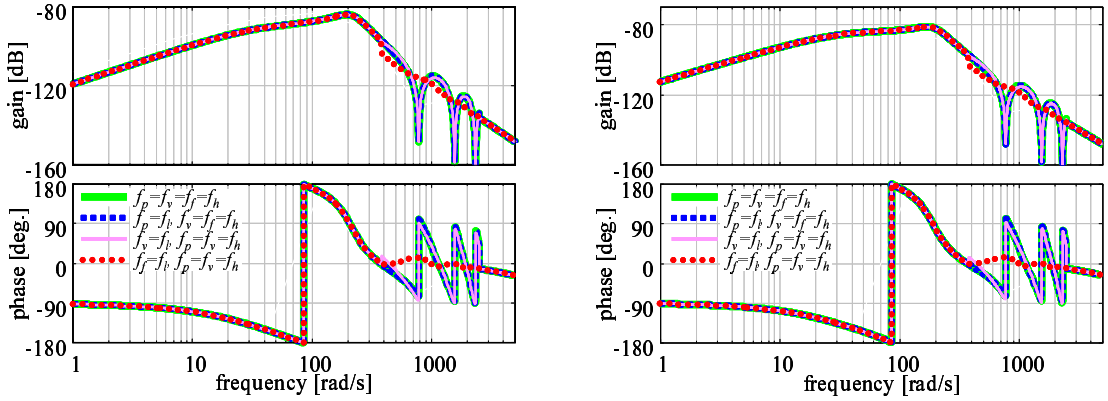

(c) tracking P_t

(d) drift P_d

Fig. 5-47: Analysis on influence of frequency limitation of each signal

operationality was almost the same in all cases. The influence of bandwidth limitation of any signal was confirmed to be negligible. Figs. 5-47(c) and (d) show the results of tracking and drift, respectively. The gain of tracking or drift was sufficiently small in all cases to consider that the ideal condition was satisfied. However, a deviation of the gain was confirmed in the high frequency range in the case with the limitation of the force signal. The influence of the limitation of the force signal was the greatest, as in the case of reproduction, when the magnitude of the influence of the bandwidth limitation of each signal was compared. The influence was much smaller in the case of the velocity signal and was not confirmed in the case of the position signal.

Table 5-14: Control parameters in analysis and experiments on optimization of transmission signal

Control sampling period	T_r	0.2	ms
Signal transmission sampling period	T_c	8.0	ms
Communication delay	L_c	1.0	ms
Position feedback gain	K_p	3600.0	$1/s^2$
Velocity feedback gain	K_v	120.0	1/s
Force feedback gain	K_f	1.0	m/Ns^2
Simulation			
Spring coefficient of operator	K_h	400.0	N/m
Damping coefficient of operator	D_h	40.0	Ns/m
Spring coefficient of environment	K_e	10000.0	N/m
Damping coefficient of environment	D_e	10.0	Ns/m
Experiment			
Cutoff frequency of DOB	g_{dis}	1800	rad/s
Cutoff frequency of RFOB	g_e	1800	rad/s
Number of data used in DFT calculation	N	40	

Design of Bandwidth of Transmission Signal

The analysis results show that the influence of the bandwidth limitation of bilateral teleoperation performance is mainly due to the limitation of the force signal. The influence of the limitation of the velocity is smaller than that on the force and the influence of the limitation of the position is considered to be extremely small. Consequently, the most important thing to attain high performance bilateral teleoperation is transmitting a wide-band force signal. The packet size can be reduced effectively by determining the bandwidth of a transmission signal independently for each signal on the basis of the degree of the influence.

The amount of the transmission data is therefore expected to be reduced without deterioration of control performance by giving priority to extraction and transmission of wide-band components of the force signal and extracting and transmitting only the low frequency component of the position signal. For the velocity signal, since its influence is small, the high frequency component is transmitted only when there is room in calculation and transmission. The force signal usually includes noise and the measurable bandwidth of the force is limited due to the performance of the sensor. The bandwidth of DFT calculation and that of the transmission signal for each signal are proposed to be designed as follows:

- position: no DFT calculation performed (transmit only X_l);

- velocity: depending on the allowance of calculation and communication; and
- force: equivalent to or higher than the bandwidth of sensing.

5.5.3 Experiments

Experiments were conducted with the experimental system shown in Fig. 5-18. For the simplicity reason, the communication between the master and slave devices was virtually constructed in a computer. Although various data compression schemes can be applied to the coefficients of DFT in the LPF-DFT combined scheme, the LPF value and coefficients of DFT were transmitted directly without compression in the experiments. The parameters the same as those in the analysis as shown in Table 5-14 were used. Experiments were executed for the following four cases and performance was compared with a focus on tracking performance between the master and slave, an operational force, and reproducibility of a contact force.

- Case 1: transmit only low frequency signals (LPF-based scheme)
- Case 2: use same and wide bandwidth for all signals (LPF-DFT combined scheme without optimization)
- Case 3: set bandwidth independently for each signal using proposed method (proposed: LPF-DFT combined scheme with optimization)
- Case 4: use same bandwidth for all signals and same packet size to Case 3 (LPF-DFT combined scheme without optimization)

K_{MIN}, K_{MAX}, and the number of data in one transmission packet S_p in each case are shown in Table 5-15. The sum of the numbers of position, velocity, and force data in one packet was 3 in Case 1, 15 in Case 2, and 9 in Case 3 and Case 4. It means that the packet size was reduced by 40 % in the proposed method (Case 3) compared with Case 2. Although it is general in bilateral teleoperation that an operator manipulates the master robot, a pseudo operator input was given to the master in the experiments to attain similar motion in all cases and to compare the performance in each condition. Both a free motion and a contact motion to an aluminum object were executed under each condition. The outline of each motion is shown in Fig. 5-48.

Fig. 5-49 shows the force inputted to execute the free motion shown in Fig. 5-48(a). The position tracking error and the magnitude of the operational force are summarized in Table 5-16. The results

Table 5-15: Settings in experiments on optimization of transmission signal

	S_p	g_l [rad/s]	K_{MIN}	K_{MAX} position	K_{MAX} velocity	K_{MAX} force
Case 1	3	380.0	-	-	-	-
Case 2	15	380.0	1	3	3	3
Case 3 (proposed)	9	380.0	1	-	2	3
Case 4	9	380.0	1	2	2	2

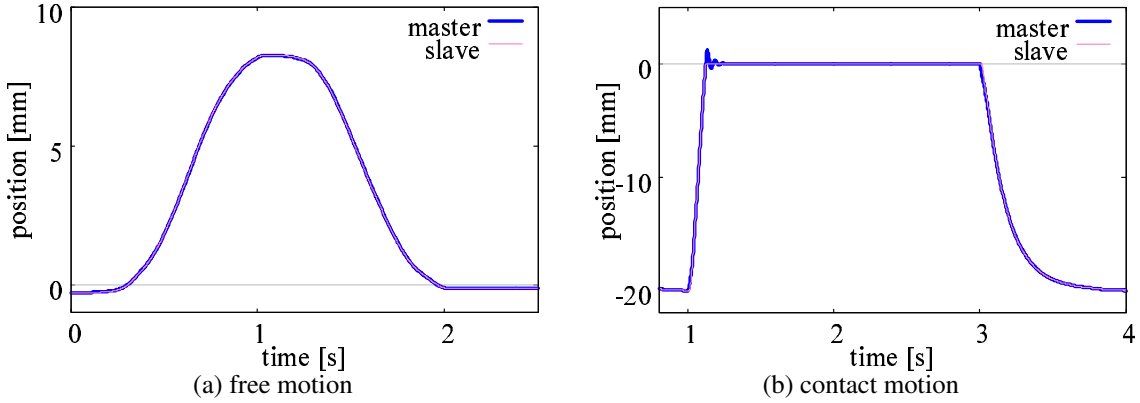

(a) free motion (b) contact motion

Fig. 5-48: Experimental motion: bilateral teleoperation

Table 5-16: Experimental results: performance comparison in free motion

	position error (AVE±SD [mm])	operational force ($\sum F_m$ [N·s])
Case 1	$6.30e^{-3}$±$5.29e^{-3}$	1.73
Case 2	$5.54e^{-3}$±$4.85e^{-3}$	1.63
Case 3	$6.14e^{-3}$±$4.34e^{-3}$	1.56
Case 4	$4.43e^{-3}$±$4.16e^{-3}$	1.60

show that the operational force was almost the same and the position tracking error was very small in all cases. It was confirmed from the results that implementation of the proposed optimization method did not deteriorate position tracking performance or operationality. The results also show that the operational force was also the same even when only low frequency signals were transmitted in Case 1. This result agrees with the analysis results.

The drift and reproducibility of a contact force were evaluated in the contact motion. Fig. 5-50 shows force responses in the contact motion and frequency distributions of the forces occurring in the master and the slave at the contact moment. The frequency distribution was derived from sampled data of 0.5 s around the contact moment. The average position error, the ratio of the magnitudes of the force generated

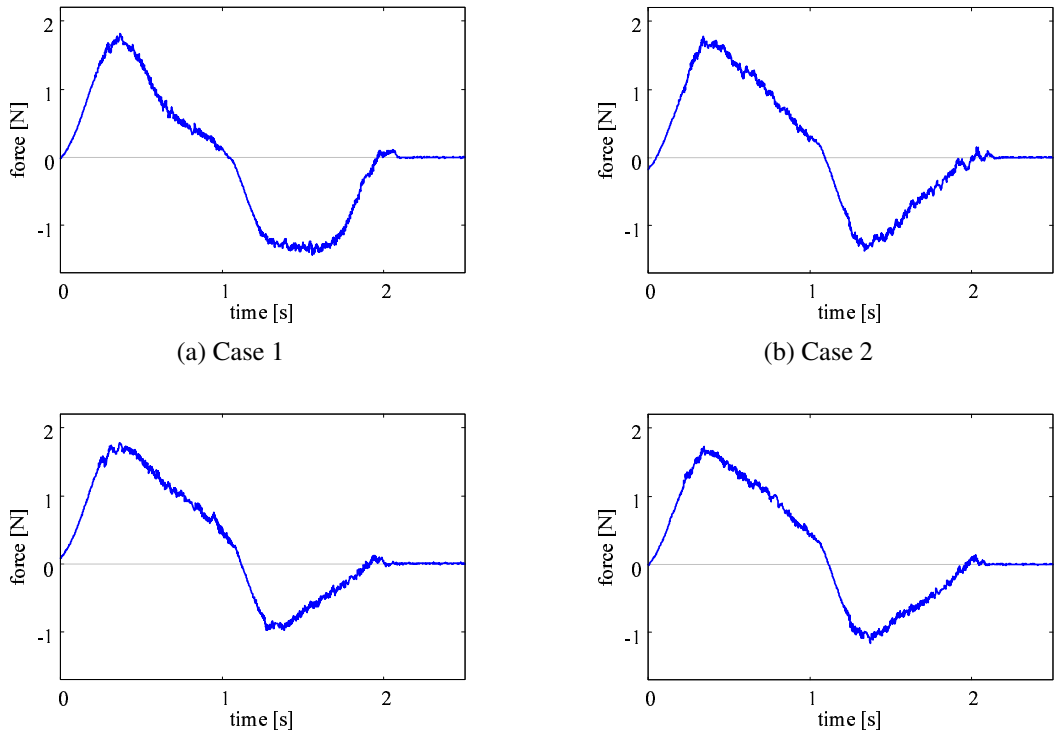

(a) Case 1 (b) Case 2

(c) Case 3 (d) Case 4

Fig. 5-49: Experimental results: inputted operational force (F_m) in free motion

at the contact moment, and the median of the ratio of the magnitudes of forces in each frequency are summarized in Table 5-17. Stable contact was achieved in all cases as shown in the force responses in Fig. 5-50. The position and force agreed well between the master device and the slave device. Especially in the position error, no prominent difference among the cases was confirmed as shown in Table 5-17. On the other hand, in the case of the magnitude of the force generated in the master at the moment of contact, the value was markedly small in Case 1. This is considered to be the result of the bandwidth limitation of the transmission signal in Case 1. The value of the large impact force generated in the slave at the moment of contact could not be transmitted to the master side due to the bandwidth limitation. The frequency distribution shows that a difference between the master and slave devices was large in all frequency ranges when only low frequency signals were transmitted in Case 1. It means that a considerable portion of elements was not reproduced in the master device. On the other hand, the frequency distribution in the master was similar to that of the slave in a wide bandwidth when the LPF-DFT combined scheme was applied in Case 2. The result almost the same as Case 2 was achieved in Case 3 although the packet size was reduced. In Case 4, the value of the master deviated from that of the slave in the frequency range

Table 5-17: Experimental results: performance comparison in contact motion

	position error	reproducibility	
	AVE±SD [mm]	$\|F_m\|_{max}/\|F_s\|_{max}$	$median(\|F_{fm}/F_{fs}\|)$
Case 1	0.024±0.107	0.35	0.38
Case 2	0.028±0.112	0.79	0.96
Case 3	0.029±0.123	0.81	0.97
Case 4	0.036±0.152	0.52	0.57

higher than 1800 rad/s. The evaluation values for reproducibility shown in Table 5-17 also show that the performance the same as Case 2 and better than Case 4 was achieved in Case 3.

It was confirmed from the results that the proposed optimization method for the transmission signal could reduce the packet size effectively without deterioration of the performance. The performance the same as the case with a large transmission packet could be achieved with a small transmission packet. When there was a limitation of the transmission packet size, reproducibility improved with the proposed method compared with the case using the same K_{MAX} for all signals.

5.6 Summary

This chapter aims at improvement of performance of motion control systems connected or controlled through a network. The limitation of the packet transmission interval was mainly focused on and the problems due to the limitation were tackled from viewpoints of sampling periods and handling of transmission signals. As a network motion control system that especially requires high precision motion control and is greatly affected by performance of a network, a bilateral teleoperation system was selected as a main target in this chapter.

This chapter firstly proposed the design guideline for sampling periods of a networked motion control system with reference to the previous researches. Although better performance can generally be achieved with short sampling periods, there are limitations on each sampling period. The basic idea of the guideline is that the best performance under limitations on the system can be acquired by designing sampling periods independently with consideration only of limitations on the corresponding sampling period. Performance analyses, simulations, and experiments were conducted to verify the influence of changing input, output, and control sampling periods under the severe limitation of the packet transmission interval concretely. The performance was confirmed to be improved by shortening the sampling

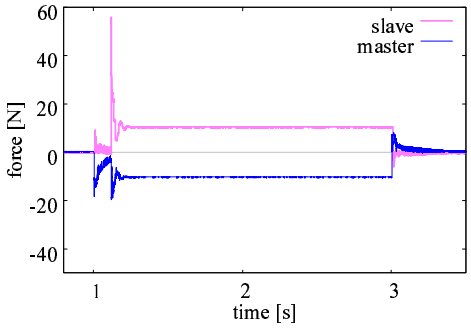

(a) time domain (Case 1)

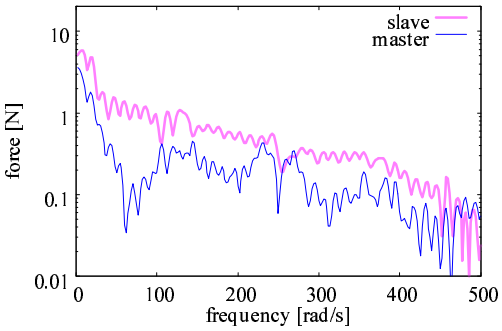

(b) frequency domain (Case 1)

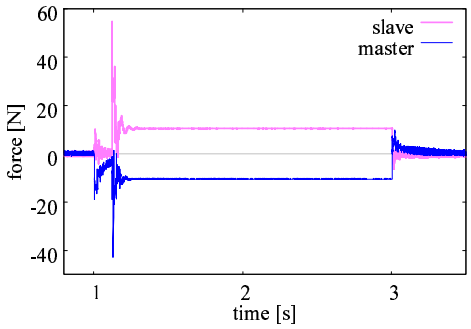

(c) time domain (Case 2)

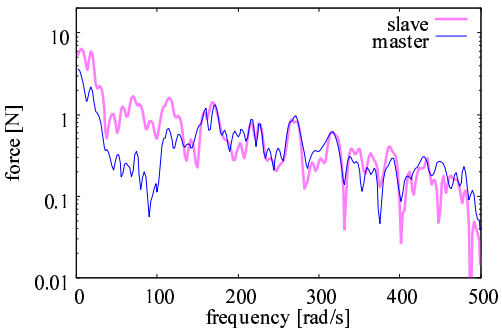

(d) frequency domain (Case 2)

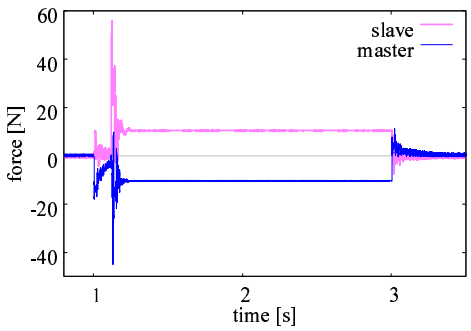

(e) time domain (Case 3)

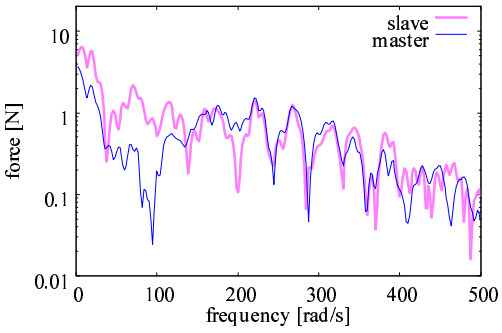

(f) frequency domain (Case 3)

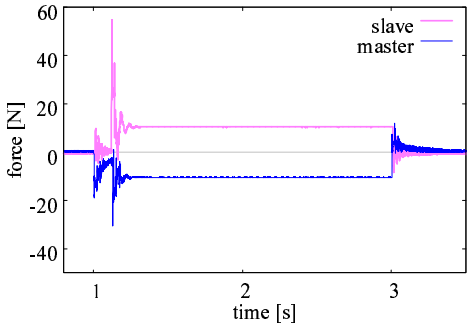

(g) time domain (Case 4)

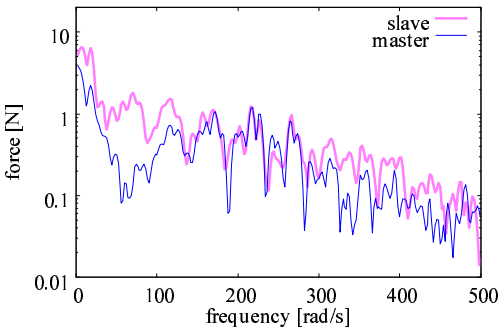

(h) frequency domain (Case 4)

Fig. 5-50: Experimental results: force response in contact motion

periods, even if the packet transmission interval was kept long and the cutoff frequency of the disturbance observer was kept low. Moreover, the cutoff frequency can be heightened by shortening the output and control sampling periods. The performance was improved further by heightening the cutoff frequency according to shortening of the sampling periods, even though the performance did not catch up with the cases with a short packet transmission interval.

Secondly, the signal transmission method for bilateral teleoperation over a network was proposed with a focus on the quality of signals transmitted between the master device and the slave device. Although the performance improves by shortening the control sampling period even if the transmission signal is not renewed in every sampling point, the performance can be improved if the time interval of renewal of the transmission signal can be shortened. On the other hand, the delay in the transmission signal increases due to the process of utilization of the transmission signal when the time interval of the renewal is tried to be shortened. The proposed method focused on the fact that the influence of signal quality on control performance differs depending on the types of signals. The author proposed to determine which data should be filled in a transmission packet for the respective signals depending on their characteristics. The proposed method transmits position data at multiple sampling points, velocity data at the latest sampling point, and force data at the latest sampling point as a packet at every n control sampling points. The proposed method was confirmed to be superior in terms of stability, reproducibility, and operationality when a communication delay was relatively small. Performance of tracking and drift were the same as those in the conventional methods. Even in the case with a large communication delay, the method has higher operationality, although differences in the other indices among the methods decrease. The validity of the proposed method was also verified by the experimental results. Although the proposed method is designed for a bilateral teleoperation system in this thesis, the idea of the proposed method can also be applied to other networked motion control systems.

Thirdly, a coding and decoding scheme was proposed to transmit wide-band small-delay signals even under severe limitation of the packet transmission interval. The bandwidth of a signal transmitted through a network is generally limited to the Nyquist frequency determined by the packet transmission interval. Moreover, the delay due to signal transmission methods generally occurs if the bandwidth of the signal is tried to be widened. The proposed method named “LPF-DFT combined scheme” solves those problems by separating handling of low and high frequency components. The method uses both a low-pass filter and discrete Fourier transform for coding and inverse discrete Fourier transform for decoding. It is shown from the analysis results that the LPF-DFT combined scheme has characteristics the same as those of the

better of the LPF-based scheme and the DFT-based scheme and no adverse influence of summation of components with different phase delay exists. Improvement in the bandwidth of transmission signals and the reproduction of the force while keeping an operational force small were confirmed from the results of the analyses and experiments conducted on bilateral teleoperation. In order to improve the performance further, discrete cosine transform (DCT) can be effectively applied to the LPF-DFT combined scheme as an alternative of DFT. In selection of signal processing technique, correlation of the parameters in the technique and the frequency is important. In addition to that point, DCT has preferable characteristics for the LPF-DFT combined scheme that information tends to concentrate in fewer coefficients at the low frequency range. The discontinuity of the decoded signal at boundary due to utilization of coefficients of the limited frequency range, which was confirmed in the LPF-DFT combined scheme, can thus be reduced by using DCT instead of DFT. Although low and high frequency components were transmitted through the same communication line in verification in this chapter, transmitting them separately using different communication lines may be required in some applications. In this case, time stamp in each transmission packet is strongly recommended to be included in a transmission packet. Moreover, development of a method for handling the difference in a delay, a jitter, and an incidence of packet losses between low and high frequency components is required in order to maintain high quality of the decoded signal even in the presence of large difference in characteristics of communication lines. The proposed LPF-DFT combined scheme can also be applied to signal transmission in systems other than bilateral teleoperation. In terms of signal transmission in bilateral teleoperation, a method for reducing calculation cost and a transmission packet size while keeping performance high was also proposed, since the calculation cost and transmission packet size increase in the LPF-DFT combined scheme as compared with the LPF-based scheme. In this method, the bandwidth of the transmission signal is determined independently for each signal based on the magnitude of the influence of the bandwidth limitation of the respective signals on bilateral teleoperation performance. Priority is given to set the bandwidth for transmission of a force signal equivalent to that of measurement, and only a low-frequency signal is transmitted for a position signal. The bandwidth for transmission of a velocity signal is then determined depending on allowance of calculation and communication. The experimental results show that the proposed method reduced the transmission packet size by 40 % and realized performance the same as that for the case with a large size packet.

The constraints on the packet transmission, especially the influence of limitation of a packet transmission interval, can be solved and the performance of the networked motion control can thus be improved

by designing the sampling periods using the proposed design guideline and applying the proposed signal transmission method or the proposed coding scheme for packet transmission. Improvement of the performance with the proposed methods is expected to promote introduction of a network to motion control systems and expand the application fields of motion control. For further improvement, a combination of the proposed methods with the upsampling technique or other mode-based interpolation techniques may also be effective in some application. It is important to select a method suitable for each system with careful consideration on characteristics and requirements of the system.

Chapter 6

Contact Detection for Environment-Adaptive Motion Control

6.1 Introduction

In recent years, an increasing number of robots have been operated in unstructured environments. The robots often come into contact with objects both intentionally and unintentionally. Unintentional destruction of objects or destabilization of control systems should be avoided upon contact. Stable contact is also necessary in order to execute tasks that require interaction with objects.

As mentioned above, "contact" is an important subject and thus has been studied in various manners. For example, modeling of the characteristics of a contact object and that of the contact motion or states have been conducted [120]. Contact force estimation based on the disturbance observer structure had been proposed as a reaction force observer [35]. As a method for extracting the characteristics of an object, identification of impedance is widely performed. The recursive least square method is the most popular scheme for identifying the impedance during operations [121]. Introduction of frequency analysis techniques such as wavelet transform has also been proposed to abstract and classify the characteristics of contact objects [122][123].

Even with various researches, stable contact operation is still a challenging issue in control. Difficulties in contact motion mainly come from limitations on acquirable information about the contact and sudden and discontinuous change in situations. As a solution for the difficulties, this research deals with contact state detection. If the contact state can be detected at the moment of a contact event, it can be used as a trigger for automation control and for changing gains and control schemes to achieve stable ma-

nipulation. Notification of contact is important especially in teleoperation because safety and efficiency of the operation improve if an operator can know whether or not the remote robot has come into contact with objects. Further, a risk in remote operations can be reduced by detecting contact and making an initial response upon contact automatically on the slave side when communication delay exists.

Focusing on a method for detecting contact states, there are many researches on contact or collision detection for computer graphics [124][125]. "Contact" in this thesis, however, represents the state in which the body or tip of a robot physically comes into contact with real objects, especially unstructured objects. For this term, the most popular way is setting a threshold to a force value and use a force signal for judgment. The threshold is usually set to a non-zero value due to the presence of an error and noise in the measured force signal. This means that contact cannot be detected when a robot comes into contact with an object gently or with a small force. As an alternative, an estimated impedance value can be used for contact detection. The estimated impedance is small or ideally zero in a non-contact state and a non-zero value differs depending on the material property of a contact object in a contact state. The contact state can thus be detected by the change in the impedance theoretically. A similar idea was used for rupture detection [126]. It is difficult to detect a contact event directly from a change in the estimated impedance, however. A change in the impedance is slow and small if contact is made slowly or gently, and it is also difficult to estimate the impedance accurately at the moment of transition from a non-contact state to a contact state since the applied force is small and difficult to be distinguished from noise. In that sense, it seems to be difficult to detect a contact event directly from a change in the estimated impedance. Another method using a sequential hypothesis testing method has also been proposed [127]. This method is superior in the point that it can recognize changes in the characteristics of an object surface. However, it requires complicated hypothesis models, and detection performance deteriorates when a robot is moved not manually but automatically and small vibration occurs. Although each method has each advantage, it is difficult to detect contact at the moment of a contact event due to sensing noise and error especially when contact is made gently or with a small force.

In this chapter, a novel real-time contact detection method is proposed to improve the accuracy of contact detection, especially during operations in force sensorless motion control in unstructured environments. The proposed method is based on the idea of active sensing and applies a dither signal to an input in addition to an ordinary control input. The dither is an intentionally applied small noise or vibration. This method is based on the phenomenon that the dither influence on the output of the system attenuates when contact occurs. This chapter also tackles technical issues on application of the method

on motion control systems. Experiments on contact detection are carried out to verify the validity of the proposed method.

6.2 Problems of Contact Detection

In this section, problems in measurement of a contact force and difficulties in contact detection are explained through introducing conventional approaches. The contact state in this chapter is defined as a state in which the body or tip of a robot physically comes into contact with real objects and a reaction force larger than zero occurs. On the other hand, the non-contact state means a state in which a reaction force does not occur.

As a method for detecting a contact state, the most popular and easiest way is to set a threshold for the force and judge the state as a contact state when the force is larger than the threshold. There are mainly two means to acquire a contact force: implementation of force sensors and estimation from other signals. Although implementing force sensors is the simplest way and provides accurate values, it is sometimes difficult to implement the sensor in appropriate places due to limitations of the size, shape, and material of the tip of a robot. Moreover, the bandwidth of a measured force is limited due to the structure of the sensor and the noise. As an alternative to force sensors, the reaction force observer [35] has been proposed as described in Section 2.3.2. It estimates a contact force by using a velocity signal and a current input reference. The bandwidth of measurement is determined by the cutoff frequency of the observer. Although the reaction force observer is a very convenient way to acquire a force value without a force sensor, it requires setting nominal values of the motor coefficient and the mass for the reaction force estimation to the actual values in the real system. It also requires to identify the amounts of forces other than the external force, such as F_{int}, F_g, F, and $D(\dot{x})$. Since it is usually difficult to set the above-mentioned parameters exactly to the real values, a force estimation error exists as shown in Fig. 6-1. A non-zero value is outputted even in a non-contact state, and the error fluctuates with movement. In order to reduce the estimation error, a constant velocity test and a step velocity test are often executed to identify a friction model and a mass or inertia [36]. It is impossible, however, to eliminate the influence of model uncertainty perfectly even with the above-mentioned tests, and a certain amount of the estimation error may remain. This estimation error or noise inhibits accurate contact detection using the force threshold. Since noise exists in a measured contact force and a non-zero value is outputted even in non-contact motions, the threshold should be decided by taking these values into consideration. If the threshold is set

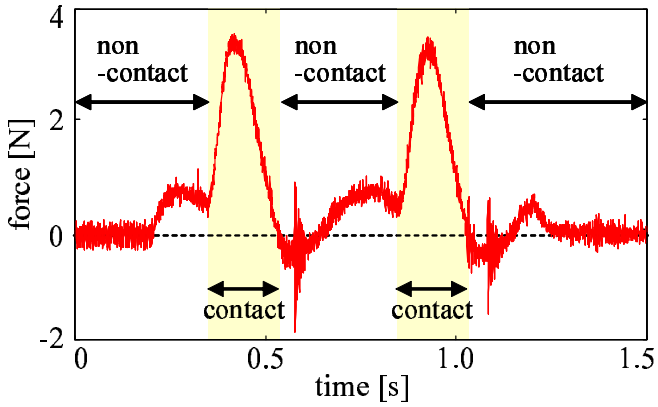

Fig. 6-1: Contact force estimated by reaction force observer

larger, erroneous detection during non-contact motions decreases. On the other hand, a contact state with a small contact force cannot be judged as contact and a risk of detection failure increases. The detection performance is therefore limited by the performance of contact force measurement.

As an alternative of using the force threshold, an estimated impedance value can be used for contact detection. Another method using a sequential hypothesis testing method had also been proposed [127]. Although each method has each advantage, it is difficult to detect contact at the moment of a contact event due to the sensing noise and error especially when contact is made gently or with a small force.

6.3 Application of Dither for Contact Detection

A real-time force sensorless contact detection method is proposed in order to achieve higher contact detection performance. The difficulty in accurate contact detection at the moment of a contact event in the conventional methods is mainly due to lack of information in a non-contact state and small difference in measured values in non-contact and gentle contact states. Since a force signal is small both in a non-contact state and a gentle contact state, it is difficult to distinguish the characteristics and detect transition from non-contact to contact states. The proposed method solves this problem with the idea of active sensing and application of a dither signal.

The dither signal is an intentionally applied small noise or vibration [128]. It is widely used to randomize and reduce quantization errors in A/D converters [129]. Adding a dither signal to an input is also effective for linearizing and suppressing friction [130]. In the field of a tactile sensor, the vibration of a resonator is used to detect the characteristics of an object [131]. The tactile sensor is operated in a longi-

tudinal mode and detects the softness and hardness of an object as changes in the resonance frequency. The use of vibration is extended to contact detection in the proposed method.

When a dither signal is inputted in addition to a control input, the influence of the dither appears in the output of the system depending on the frequency and the magnitude of the dither signal. However, this influence may be absorbed when the system comes into contact with an object. It is therefore possible to detect contact by monitoring the alteration of the dither influence. The proposed method detects contact by the following steps:

(1) adding a dither signal to the input of the system;

(2) monitoring the frequency component of the output in the dither frequency by using time-frequency analysis; and

(3) judging the state as a contact state when the magnitude of the frequency component is lower than the threshold.

The details of the contact detection processes are described below.

In selection of the dither wave form, priority is given to the correlation between the frequency and parameters of the dither wave form since the proposed method monitors the frequency component only in a predetermined frequency. A sinusoidal wave is thus selected as the dither wave form. A dither current input I_a^{dither} and a total input current I_a are derived as follows:

$$I_a^{dither} = A_{I^d} \sin(\omega_d t) \tag{6.1}$$

$$I_a = I_a^{ref} + I_a^{dither}. \tag{6.2}$$

Here, I_a^{dither} denotes a dither current input, A_{I^d} denotes an amplitude of the dither, ω_d denotes a frequency of the dither, and I_a^{ref} denotes a control input. Since the dither influences a motion or a task if the amplitude of the dither is large, it is important to select the dither frequency and the signal for monitoring so that the influence of the dither can easily be observed even with a small dither input.

In selection of a signal to be monitored, it is important that the influence of the dither can be distinguished from the output due to the motion. For these points, it is preferable to select the signal that rarely has a non-zero value in a steady state. With consideration of the above points, an acceleration signal is selected to be used for contact detection.

In order to abstract frequency components of the output, a time-frequency analysis technique such as short-time Fourier transform (STFT) [132] is used. In STFT, a Fourier transform is executed in sections

by using a time-shifted and fixed-size window function. It is thus possible to acquire both time and frequency information. STFT for a sampled signal is expressed as follows:

$$X_S[m,\omega] = \sum_{n=-\infty}^{\infty} x[m+n]w[n]e^{-j\omega n}, \tag{6.3}$$

where $x[n]$ denotes a discrete signal, $w[n]$ denotes a window function, m denotes the number of samples shifted, ω denotes a frequency, and $X_S[m,\omega]$ denotes a frequency component of the frequency ω at sample m. The size of the window function is determined with consideration of the frequency of the dither. Since $X_S[m,\omega]$ is a complex number, the power spectral density (PSD) is derived as the gain and argument is derived as the phase for contact detection. Time and frequency resolutions in STFT are determined by the size of the window function, and these resolutions are in trade-off relation. Although a wavelet transform [133] is better in terms of flexibility in the relation between time and frequency resolutions, STFT is sufficient for the proposed contact detection method, since transform only in the dither frequency needs to be focused on and correlation between the parameters of the transform and the frequency is important. In terms of calculation cost, the increase is kept small since the calculation of (6.3) needs to be performed only for one prescribed ω that corresponds to the dither frequency.

Contact judgment is performed using the result of time-frequency analysis as follows:

$$flag_{contact} = \begin{cases} 1 & (X^{acc}_{PSD}[m,\omega_d] < X^{acc}_{thres}) \\ 0 & (else), \end{cases} \tag{6.4}$$

where X^{acc}_{PSD} denotes PSD of acceleration and X^{acc}_{thres} denotes a threshold for judgment.

6.4 Mechanism of Dither-based Contact Detection

The mechanism of contact detection using the dither is described by modeling a contact object as a spring and damper model. Determination of the frequency of the dither is also discussed. Systems in non-contact and contact states can be modeled as the systems shown in Fig. 6-2. A transfer function from the dither input force to the acceleration output in a non-contact state $G^a_{nc}(s)$ and that in a contact state $G^a_c(s)$ are given as follows:

$$G^a_{nc}(s) = \frac{1}{M} \tag{6.5}$$

$$G^a_c(s) = \frac{s^2}{Ms^2 + D_e s + K_e s}. \tag{6.6}$$

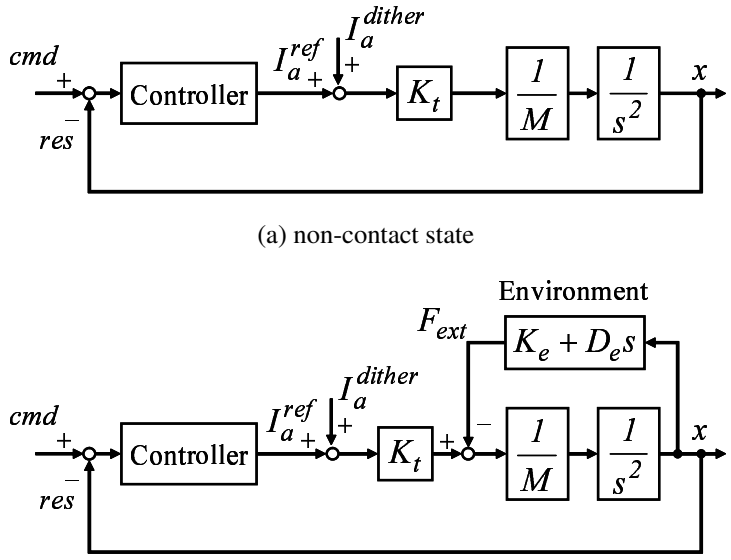

(a) non-contact state

(b) contact state

Fig. 6-2: Model of systems in contact state and non-contact state

In order to verify the influence of the dither, bode diagrams of the transfer functions from the dither to the acceleration, from the dither to the position, and from the dither to the force in the following conditions are shown in Fig. 6-3.

- non-contact state
- contact with hard object ($K_e = 10000.0$ N/m, $D_e = 10.0$ Ns/m)
- contact with soft object ($K_e = 2500.0$ N/m, $D_e = 100.0$ Ns/m)

A difference between a non-contact state and a contact state was confirmed in the low frequency range: the gain of acceleration decreased in a contact state compared with that in a non-contact state. The maximum frequency in which the difference exists depends on the characteristics of a contact object. This result shows that contact can be detected based on attenuation of the frequency component by setting a frequency of the dither low enough to allow observation of the difference in any anticipated environment and monitoring the frequency component of acceleration. As shown in Fig. 6-3(a), however, the influence of the dither easily appears in the position response when the frequency of the dither is low. A lower frequency dither also deteriorates the time resolution of abstraction of the frequency component using the time-frequency analysis. The frequency of the dither should therefore be set as high as possible

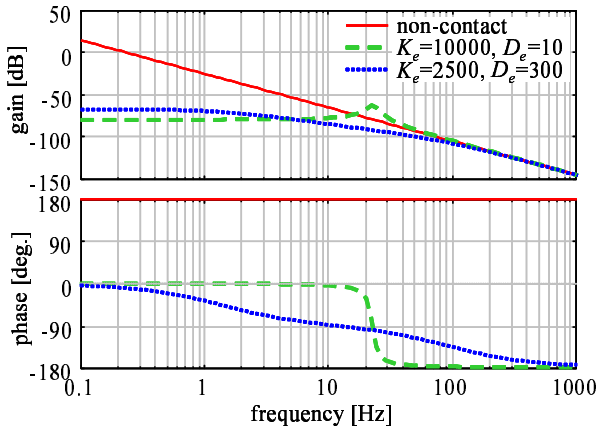

(a) from dither to position

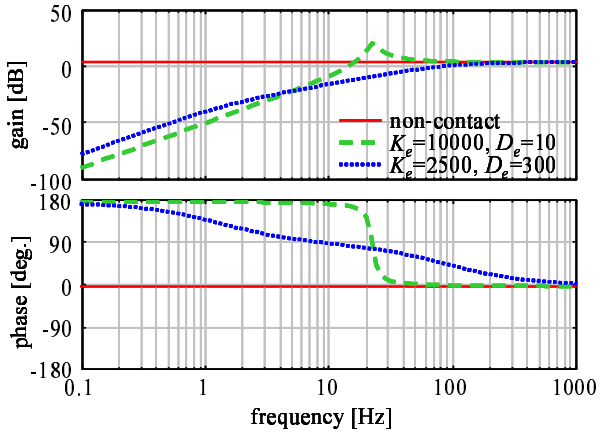

(b) from dither to acceleration

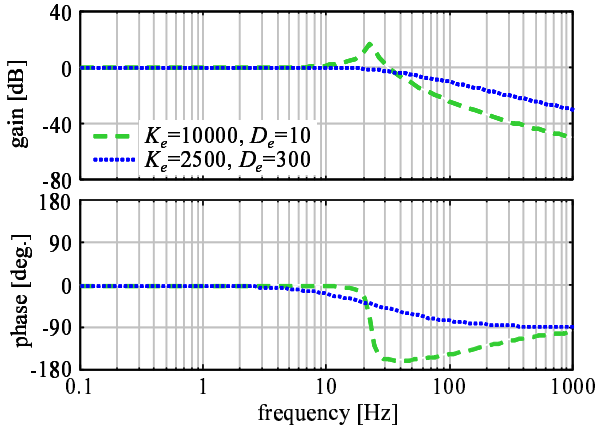

(c) from dither to force

Fig. 6-3: Analysis on influence of dither input

while satisfying the limit for observation of difference between a non-contact state and a contact state. Although the proposed method focuses mainly on the gain, a difference due to a contact state appears not only in the gain but also in the phase as shown in Fig. 6-3. The phase information can therefore be used in addition to the gain to improve contact detection performance when the limitation of the dither frequency is severe.

6.5 Reduction in Dither Influence on Motion

6.5.1 Influence of Dither on Motion

The contact detection method using a dither is expected to have higher detection performance compared with conventional methods. The influence of the dither on the motion is small, but exists in this method, however, since the dither signal is added to an ordinary control input. The influence of the dither appears especially in the force in a contact state. As shown in Fig. 6-3(a), the influence of the dither on the position response can be kept small by selecting the frequency of the dither appropriately. On the other hand, the influence of the dither necessarily appears in the force in a contact state when the dither is selected to allow observation of a difference in the acceleration between non-contact and contact states. Since the sum of the command value and the dither is applied to the object, the measured force includes the force due to the dither. Use of the value to control may amplify the dither influence or affect the control performance. In the case of teleoperation, force sensation including the influence of the dither is transmitted to an operator and the operator feels small vibration. It may deteriorate operationality of teleoperation. It is therefore desirable to eliminate the influence of the dither on the force value in a contact state. Here, the influence of the dither appears on the force value only in a contact state, and it is negligible in a non-contact state even when the reaction force observer is used to acquire a force value, since small acceleration instead of force proportional to the dither input occurs in a non-contact state. The problem to be solved in this section is thus limited to reduction of the dither influence in a force value in a contact state.

This section considers the following two cases and proposes a countermeasure for each case.

- elimination of the dither element in a control signal is desired although application of the dither to an object is acceptable
- application of the dither on an object itself is ideally avoided

The situations can be classified into the cases by considering required tasks of a subject system. As an advantage of application of the dither to an object, it is possible to acquire characteristics of an object. Since a response to the dither differs depending on the characteristics of an object as shown in Fig. 6-3, the contact object can be discriminated by the difference in the response. Even if the dither is very small, application of the dither to an object is not preferable in some cases, however, such as in the cases when the object is extremely fragile or characteristics of the object change by application of force.

The former case requires separation of the dither element from the measured force while applying the force including the dither to an object. A method for eliminating the dither element by using a high-order observer had been proposed for a system using the dither for friction suppression [134]. This method eliminates the dither element in the measured force by modeling the influence of the dither as a second order system. Although the method successfully eliminates the dither element, extremely high-precision measurement is indispensable and an applicable system or bandwidth is limited since it requires a second order derivative of the force signal for calculation. This section proposes a method using the ratio of an ordinary control input and a dither input, which is simpler and can easily be adapted to any system.

The latter case requires stopping application of the dither in a contact state. It means that a method different from the former case needs to be implemented. This section proposes a method in which the dither is applied in limited situations and application of the dither is avoided in a contact state while keeping high detection performance. The details of the respective methods are described in the following subsections.

6.5.2 Elimination of Dither Element from Measured Contact Force

Firstly, a method for separation and elimination of the dither element from a measured force is proposed in this subsection for the cases in which application of the force including the dither on an object is acceptable. The method is based on the fact that both the control input and the dither input are calculated in a controller and known values. When the dither is applied for contact detection, an input to an actuator is represented as (6.2). The force commensurate with the total input current is applied to an object in a contact state. Assuming that the system is an ideal system without friction and non-linear elements and the frequency of the control input and that of the dither inputs are relatively low compared with the resonant frequency, the contact force can be considered as the sum of the force due to the control input and the force due to the dither input. Thus in theory, the dither element in the measured force can be

separated using the ratio between the total input and the dither input.

$$F_c = \frac{I_a^{ref}}{I_a}\hat{F}_{ext} \tag{6.7}$$

$$F_d = \frac{I_a^{dither}}{I_a}\hat{F}_{ext} \tag{6.8}$$

Here, F_c denotes force due to the control input and F_d denotes force due to the dither input. Then F_c instead of $\hat{F}_{ext}$ is used for control. Although this is very simple, the value tends to diverge due to non-ideal elements in real systems when I_a is small. On the other hand, the influence of the dither appears on a force value only in a contact state as mentioned above. I_a has a certain amount in this situation. The above calculation should therefore be performed only when I_a is larger than the predetermined threshold. F_c is derived as follow:

$$F_c = \begin{cases} \frac{I_a^{ref}}{I_a}\hat{F}^{ext} & (|I_a| > I_{athres}^{calc}) \\ \hat{F}^{ext} & (|I_a| \leq I_{athres}^{calc}), \end{cases} \tag{6.9}$$

where I_{athres}^{calc} denotes a threshold for calculation of the ratio between the total input and the dither input.

6.5.3 Stop Application of Dither in Contact State

In this subsection, a method in which application of the dither is stopped in a contact state while keeping high detection performance is proposed. The purpose of application of the dither is detection of contact at the moment of a contact event. Since it is difficult to observe transition from a non-contact state to a contact state in the conventional methods, the dither is applied to acquire adequate information for detection even in a non-contact state. The contact event can be detected if the dither is applied in the non-contact state. In other words, it is possible to detect a contact state by applying the dither only in the non-contact state and not applying it in a contact state if transition from a contact state to a non-contact state can be detected without using the dither. The author therefore proposes to detect a contact event by the following steps: apply the dither in a non-contact state; stop applying the dither and continue monitoring of a sign of transition to a non-contact state with another method after the contact event is detected; and then resume application of the dither when the sign of end of the contact is detected. A contact state has already started just at the time when the force changes from zero, but the force decreases from a certain value before a state changes from a contact state to a non-contact state and finally becomes zero when a non-contact state is obtained as shown in Fig. 6-4.

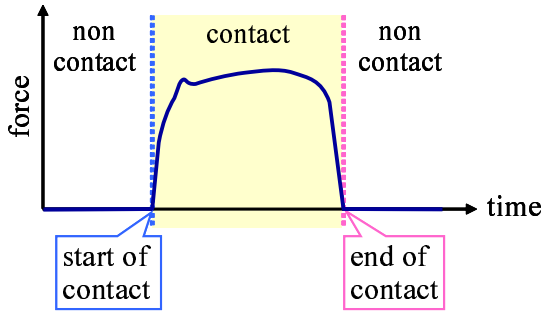

Fig. 6-4: Change of contact force in transition of contact state

A sign of transition to a non-contact state can be detected using the following two criteria.

$$\hat{F}^{ext}[n] < F_{thres}^{onoff} \tag{6.10}$$

$$\hat{F}^{ext}[n] < \hat{F}^{ext}[n-1], \tag{6.11}$$

where $\hat{F}^{ext}[n]$ denotes a measured force at $t = nT_s$ and F_{thres}^{onoff} denotes a threshold for detection of the transition. F_{thres}^{onoff} is set to the lower of the predetermined value F_{thres}^{onoffb} and a force value just after contact is detected. When F_{thres}^{onoffb} is set large, the sign of the transition tends to be detected even during continuous contact, and a risk of resuming application of the dither in a contact state increases. On the other hand, a risk of deterioration in contact detection performance increases when F_{thres}^{onoffb} is set small since mis-detection of the transition occurs due to the measurement error or friction. The dither is not resumed properly in this case. Although the threshold should be designed considering the magnitude of negative effects of applying the dither to the object, it is generally set by giving priority to resume the dither properly and maintaining high detection performance. In addition, an average value is used for judgment when a large noise exists in the measured force. Satisfaction of both criteria is used as a sign of transition to a non-contact state. The procedures of determination of ON or OFF of the dither are summarized in Fig. 6-5. The detection of the sign of transition to a non-contact state mentioned above is utilized only to judge whether or not the dither should be applied and not used for contact detection. The final judgment of a contact state is executed based on (6.4) by using the frequency component of the acceleration in the dither frequency.

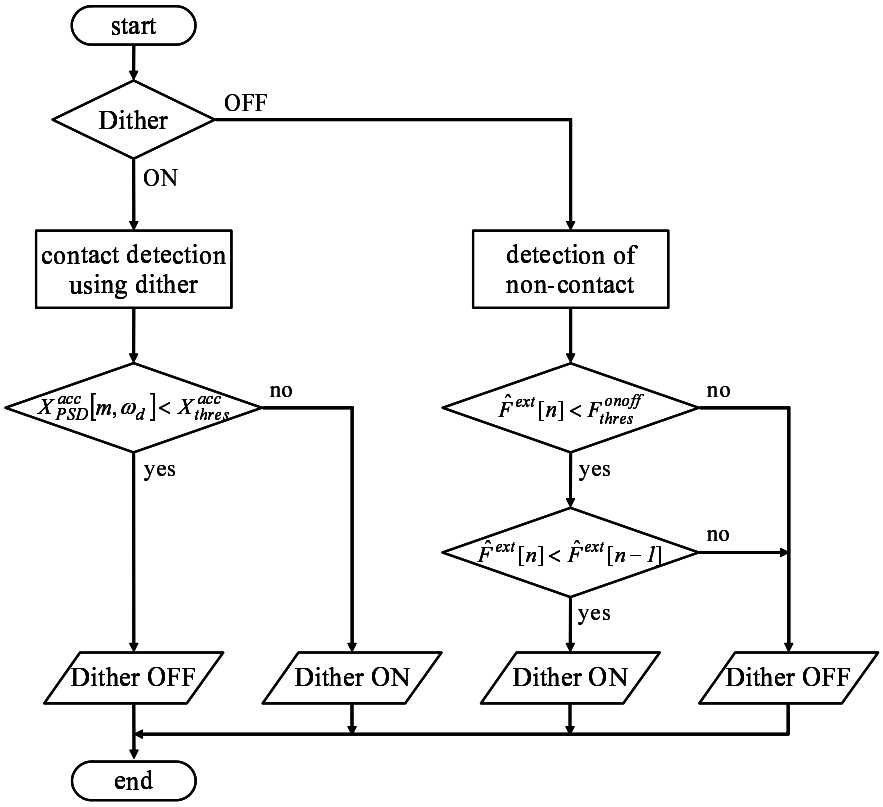

Fig. 6-5: Procedure to determine application of dither

6.6 Experiments

6.6.1 Experimental Setup

Experiments on contact detection were conducted to verify the validity and applicability of the proposed method. The master-slave teleoperation system shown in Fig. 5-18 was used. A four-channel-based controller with the disturbance observer shown in Fig. 2-12 was implemented on the system. A pseudo operator input was given to the master robot to execute non-contact and contact motions. The dither was applied only to the slave robot since contact occurs on the slave side. Two types of objects, metal and rubber, were used in experiments. The frequency of the dither was determined according to Section 6.3 and a preliminary experiment. The threshold of PSD of the acceleration for contact detection was determined from the value observed when the robots were not moved in a preliminary experiment. In order to verify accuracy of contact detection, the object was placed at $X = 0.0$ mm. Firstly, contact detection performance of the proposed dither-base contact detection method was verified and compared

Table 6-1: Parameters in analysis and experiments on contact detection

Control sampling period	T_r	0.2	ms
Position feedback gain	K_p	1600.0	$1/\mathrm{s}^2$
Velocity feedback gain	K_v	80.0	1/s
Force feedback gain	K_f	1.0	$\mathrm{m/Ns}^2$
Cutoff frequency of DOB	g_{dis}	2000.0	rad/s
Cutoff frequency of RFOB	g_e	2000.0	rad/s
Frequency of dither	f_d	10.0	Hz
Amplitude of dither	A_{Id}	1	mA
Window size of STFT	N	1000	
STFT calculation interval	T_{STFT}	5.0	ms
Force threshold (low)	F_{thres}^{low}	0.8	N
Force threshold (high)	F_{thres}^{high}	2.5	N
Threshold of PSD of acceleration	X_{thres}^{acc}	$1.0e^{-6}$	

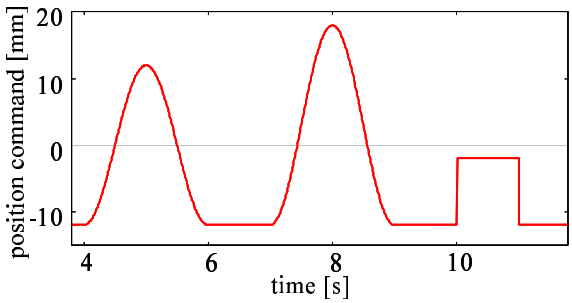

Fig. 6-6: Pseudo-operational command in experiments

with the force threshold-based method. Secondly, the influence of the dither on the motion was verified to confirm the effectiveness of the methods proposed in Section 6.5. Table 6-1 shows the parameters used in the experiments.

6.6.2 Experiment on Contact Detection Performance

First, contact detection performance of the proposed dither-base contact detection method was verified. In addition to the proposed method, contact detection using the threshold of the force value was also executed as a comparative method. Two types of threshold, relatively high and relatively low, were used in the method. The contact detection performance of the proposed method was compared with the force threshold based method in this subsection. The pseudo-operational input in the experiment is shown in Fig. 6-6.

The experimental results with a metal object and a rubber object are shown in Figs. 6-7 and 6-8, respectively. Each figure shows the position responses of the master and slave robots, the reaction force in the slave measured using the reaction force observer, the PSD of the acceleration in the dither frequency, and the results of contact detection. The threshold for each signal is also shown in the figure. The slave was in a contact state when its position exceeded $X = 0.0$ mm.

As shown in Fig. 6-7(c), the PSD of the frequency component of the acceleration in the dither frequency decreased when the slave was in a contact state. As a result, contact could be detected accurately by monitoring the PSD, as shown in Fig. 6-7(d), even when a contact force was small. Focusing on the conventional method, the method with the higher force threshold could not detect contact around $t = 4$ to 6 s. Even though the slave did not contact with the object around $t = 10$ s, misdetection due to the force at start-up occurred in the method with the lower force threshold. These detection errors were not confirmed in the proposed method. As a problem in the proposed method, contact states could not be detected at the start and end of contact. This phenomenon is due to the window size required for adequate resolution of STFT to abstract the frequency component in the dither frequency. The timing of detection was almost the same, however, as in the cases with the high force threshold. The influence of the window size may also be reduced by using phase information for judgment or adopting a more advanced time-frequency analysis technique. Fig. 6-8 shows the results with the rubber object. Although the decrease in the PSD was smaller in Fig. 6-8(c) compared with that in Fig. 6-7(c), similar detection performance was achieved even with the rubber object, which is softer than the metal. The results also show that erroneous detection in a non-contact state often occurred due to deviation in the measured force when the force threshold was set low. The erroneous detection was prevented in the proposed method. The above results show that higher contact detection performance can be achieved with no significant adverse influence in the proposed method.

6.6.3 Experiments on Dither Influence Reduction

In this subsection, the influence of the dither on a motion is verified. Then, effectiveness of the methods for reduction of the dither influence is verified by comparing magnitudes of the influence of the dither and detection performance. Experiments were conducted for the following three cases:

- Case 1: dither-based contact detection only;
- Case 2: dither-based contact detection with elimination of the dither influence on measured force

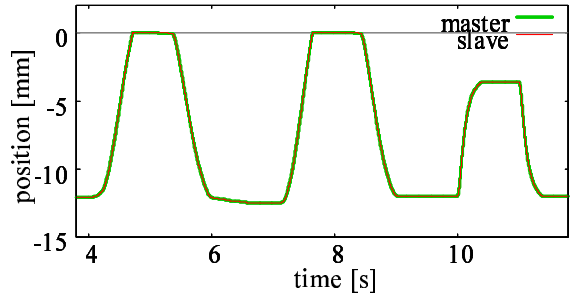

(a) position

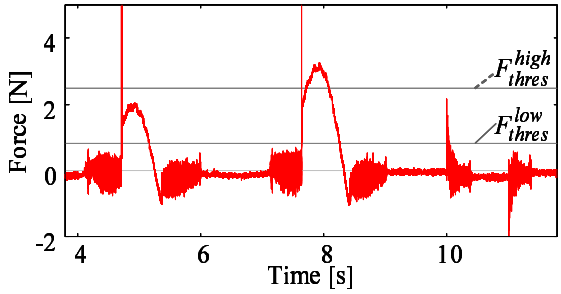

(b) force

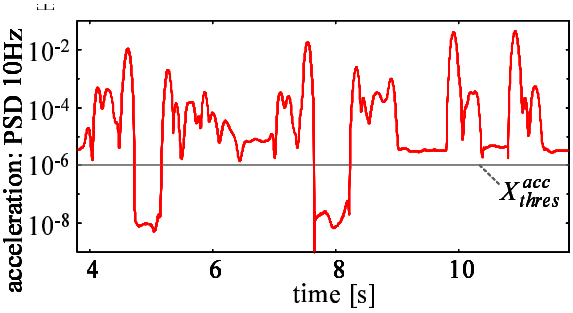

(c) PSD of acceleration at dither frequency

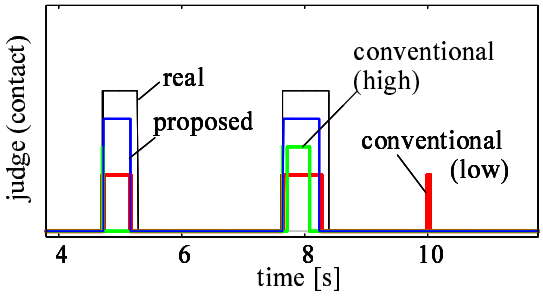

(d) contact detection

Fig. 6-7: Experimental results: contact detection with metal object

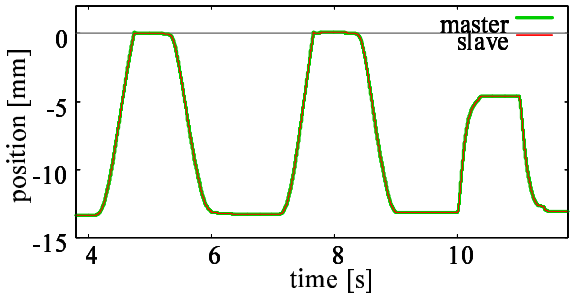

(a) position

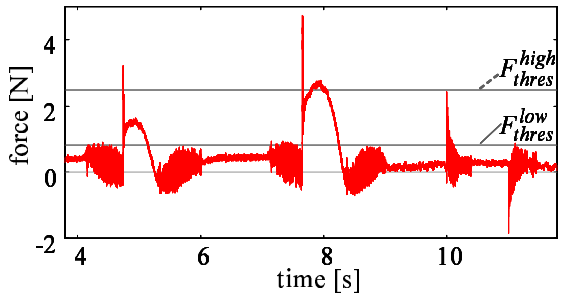

(b) force

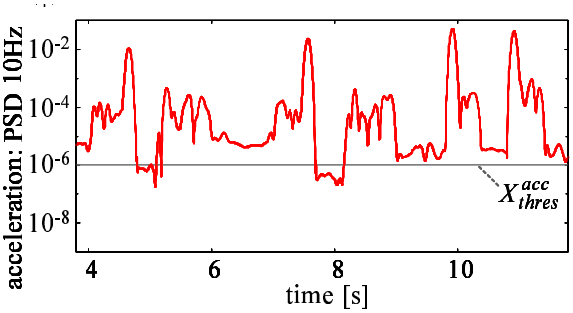

(c) PSD of acceleration at dither frequency

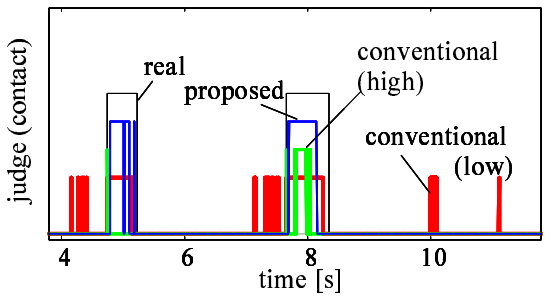

(d) contact detection

Fig. 6-8: Experimental results: contact detection with rubber object

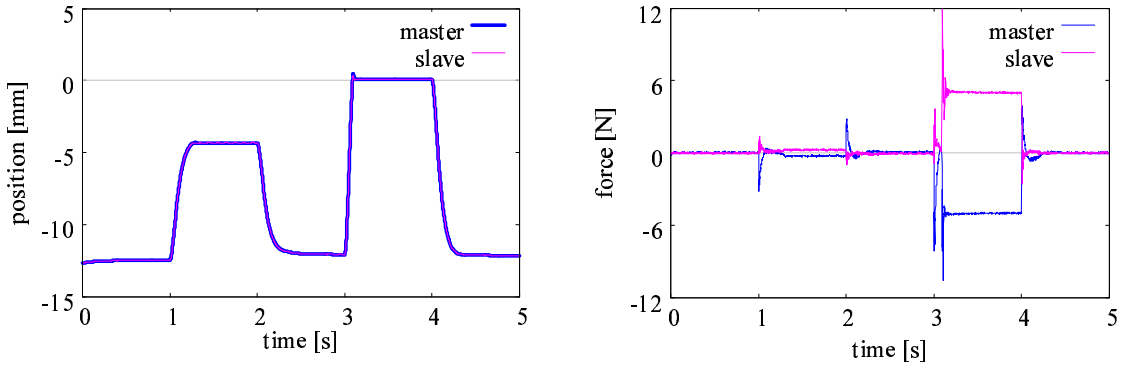

(a) position (b) force

Fig. 6-9: Overview of experimental results

(Section 6.5.2); and

- Case 3: dither-based contact detection with application of the dither in limited situation (Section 6.5.3).

Case 2 is for the cases in which application of the dither to an object is acceptable but elimination of the dither elements in a control signal is desired. Case 3 is for the cases in which application of the dither on an object itself is preferable to be avoided.

An overview of the position and force responses of the master and slave robots are shown in Fig. 6-9. The tracking between the master and slave robots was confirmed and the influence of the dither on position was smaller than 5 μm in all cases. Fig. 6-10 compares the force reproduced in the master robot when the slave robot came into contact with the rubber object. It shows that the influence of the dither existed in Case 1. It may disturb the operator to execute tasks and deteriorate operationality. The magnitude of the dither element appearing in Case 1 was about 0.1 N although the magnitude of the dither was 0.03 N. It shows a negative effect on the control that the dither was amplified in the control loop. The element was successfully eliminated with each of the proposed method in Case 2 and Case 3. The difference between Case 2 and Case 3 was the timing of application of the dither. As shown in Fig. 6-11, the dither was always applied in Case 2, while application of the dither was properly stopped when the slave came into contact with the object and properly resumed when the slave went away from the object in Case 3.

Contact detection performance is verified in Figs. 6-12 and 6-13. Contact was detected accurately in all cases both with the metal object and the rubber object. The detection errors at the start and the end of

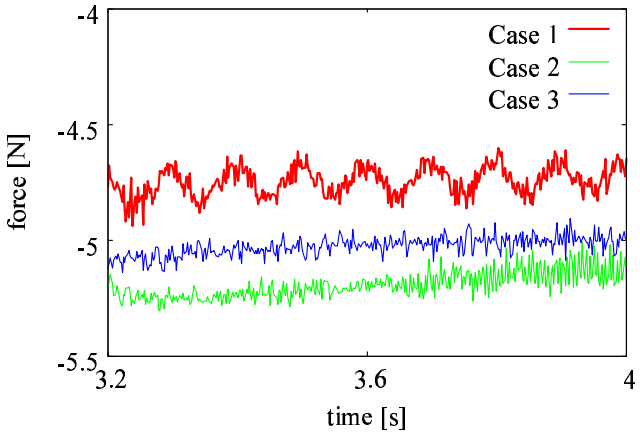

Fig. 6-10: Experimental results: influence of dither on transmitted force

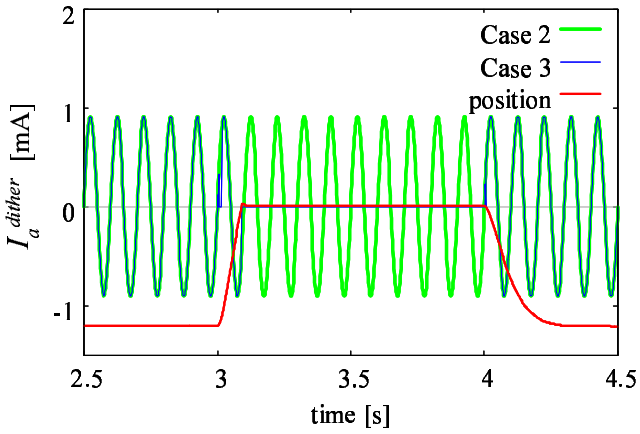

Fig. 6-11: Experimental results: application dither during operation

contact were due to the window size of STFT as mentioned in the previous subsection. Deterioration of the performance was not confirmed with the proposed methods for reduction of the dither influence. The above results show that the methods can eliminate the dither influence on the motion properly without deterioration of contact detection performance.

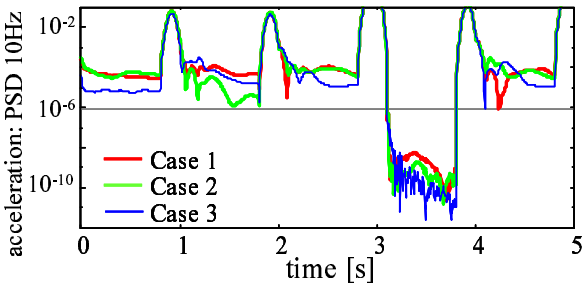

(a) PSD of acceleration at dither frequency

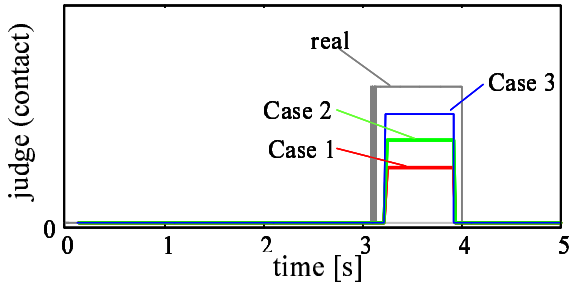

(b) contact detection

Fig. 6-12: Experimental results: contact detection with metal object with dither influence reduction

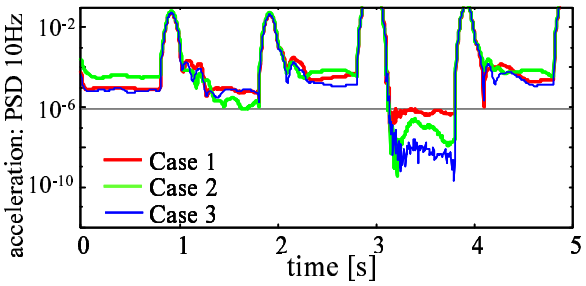

(a) PSD of acceleration at dither frequency

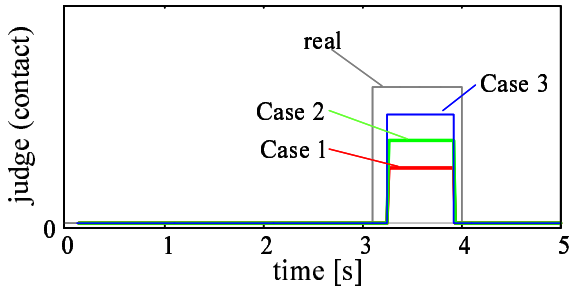

(b) contact detection

Fig. 6-13: Experimental results: contact detection with rubber object with dither influence reduction

6.7 Summary

This chapter aims at improvement of adaptability of robots to unstructured environments. Since recognition of the state is the fundamental issue for stable operation, a method for detecting contact during operations in unstructured environments was proposed based on the idea of active sensing. The proposed method realizes force sensorless detection by applying a dither and monitoring the decrease in the frequency component of the acceleration in the dither frequency by using STFT. The experimental results show that contact detection performance was improved with the proposed method compared with the cases using the force threshold. This chapter also tackled the technical issues of application of the dither-based contact detection method. Since the dither signal is added to an ordinary control input, the influence of the dither on the motion is small but exists in the method. This chapter considered the following two cases and proposed a method for reducing the influence of the dither on the control performance or the motion for each case: application of the dither on the object is acceptable; and it is preferable to be avoided. A method for separating the dither element from a measured force using the ratio of inputs while applying the force including the dither to an object was proposed for the former case. A method of applying the dither in the limited situation and avoiding application of the dither in a contact state was proposed for the latter case. Reduction of the dither influence on the motion without deterioration of detection performance was confirmed with the proposed methods in the experiments. Improvement in accuracy of force estimation using the reaction force observer and that in the performance of motion control are also expected with the method.

Chapter 7

Conclusions

The primary objective of this thesis is promotion of utilization of robots for aiding human beings in a true sense in a wider variety of fields. By setting improvements in accuracy and applicability of robust motion control based on acceleration control as a technical goal, this thesis developed sensing and control technologies to achieve this goal. There are various constrains in implementation of motion control. This thesis mainly focused on the factors limiting the performance of robust motion control and proposed the methods for achieving higher performance even under the constraints. The issues to be dealt with in this thesis were classified into the following two main parts.

- development of fundamental technologies for improvement of robust motion control performance
- development of applied and advanced technologies for expanding application of robotic technology to more complicated and sophisticated tasks

The existing motion control techniques were explained in Chapter 2 as the basis of the topics in this research. Robust acceleration control is a key control technique for motion control since position and force can be dealt with in a unified manner using acceleration and higher robustness can be attained regardless of a desired motion by acceleration control. The disturbance observer is an effective tool to realize acceleration control. In the development of fundamental technologies, the performance limit of the disturbance observer was focused on. The author took up the sampling period and noise in sensing as main factors limiting the performance and proposed the following methods:

(a) multirate sampling method for acceleration control (Chapter 3); and

(b) velocity measurement method for acceleration control and its combined use with the multirate sampling method (Chapter 4).

Then in the development of applied and advanced technologies, issues in the system connected and controlled through a network and those in mechanical contact with environments were focused on. The following methods were then proposed for each topic:

(c) design guideline of sampling periods and processing methods of transmission signals to overcome the limitation of the packet transmission interval (Chapter 5); and

(d) dither-based contact detection method for force sensorless motion control (Chapter 6).

In development of method (a) described in Chapter 3, higher significance of the output sampling period than the input sampling period was shown by focusing on the relationship between the sampling periods and the performance of acceleration control. From this viewpoint, a novel multirate sampling method with a shorter output sampling was proposed for wide-band acceleration control-based on the idea completely different from conventional methods. The disturbance observer was redesigned for the system with a new definition of the disturbance torque. The proposed multirate sampling method shortens the delay in acceleration information and widens the bandwidth of acceleration control. Improvements in stability and control performance were confirmed in the stability analysis, simulations, and experiments. The performance close to that with the short sampling period for the input and output was achieved by applying the proposed multirate sampling method with the proposed disturbance observer.

In development of method (b) described in Chapter 4, the synchronous-measurement method (S method) was focused on as a velocity measurement method effective for acceleration control. An instantaneous speed observer for the method was proposed to further improve performance of S method. A method for combined use of the measurement method and the multirate sampling method was also provided. The proposed observer solves the problems of destabilization and performance limit due to the existence of sampling points without measurement in S method. Thus utilization of the proposed observer greatly widened the bandwidth of acceleration control and dramatically improved the performance compared with that obtained by applying only S method. Since the velocity measurement resolution is high even with the short sampling period in the proposed velocity measurement method, which is a combination of S method and the proposed instantaneous observer, the performance improved further by using the measurement method together with the multirate sampling method proposed in Chapter 3 (method (a)).

It was confirmed from the experimental results that robust motion control with higher performance could be attained by the combined use of the methods.

The target of method (c) described in Chapter 5 was motion control systems connected and controlled through a network. The limitation of the packet transmission interval was mainly focused on as a factor limiting the performance of the networked motion control system. The problems of the limitation of the interval was regarded as the problem relating to the sampling period and that relating to the transmission signal. The methods for attaining higher performance even under the limitation were proposed from the both viewpoints. From a viewpoint of the sampling period, a design guideline of sampling periods in a networked control system was proposed. The basic idea in the guideline is that the best performance under limitations on a system can be achieved by designing the sampling periods independently with consideration only of limitations on the respective sampling periods. Performance improvement with the proposed guideline was confirmed even in the case where the packet transmission interval could not be shortened and the cutoff frequency of the disturbance observer was kept low. Moreover, the cutoff frequency could be heightened by shortening the output and control sampling periods with the proposed guideline. The bandwidth of robust motion control was thus heightened and the performance was further improved. From a viewpoint of the transmission signal, a signal transmission method for bilateral teleoperation and a coding scheme for transmission signals were proposed. The former method, the signal transmission method, focused on the fact that the influence of signal quality on control performance differs depending on kinds of the signal. The proposed signal transmission method determines data to be filled in the transmission packet independently for each signal with consideration of the influence of signal quality of the respective signals on control performance. The performance improvement in terms of stability, reproducibility, and operationality was confirmed by the performance analysis and experiment. The latter method, a coding scheme named LPF-DFT combined scheme, is a more common method, which is applicable not only to bilateral teleoperation. The proposed LPF-DFT combined scheme realizes wide-band signal transmission with a small processing delay by dealing with the low frequency component and the high frequency component in different manners: use a low-pass filter for the low frequency component and use discrete Fourier transform for the high frequency component. The above-mentioned characteristics were confirmed in the analysis and experiments. Improvement in reproduction of the force while keeping an operational force small was confirmed from the results of the analysis and experiments conducted on bilateral teleoperation.

The method (d) described in Chapter 6 focused on difficulty in mechanical contact with environments. Interaction with environments is indispensable in advanced motion control. In order to provide additional information to promote stable application, a contact detection method was proposed especially for force sensorless motion control in unstructured environments. Based on the idea of active sensing, the proposed method applies a dither signal, an intentionally applied small noise or vibration, to an input and detects contact by monitoring the decrease in the frequency component of the acceleration in the dither frequency. Methods of reducing the influence of the dither on the motion were also proposed. Improvement in contact detection performance compared with the force threshold-based method was confirmed in the experiments. The influence of the dither on the motion was confirmed to be negligibly small. Improvement in the accuracy of force estimation in the reaction force observer and improvement in the performance of motion control can be expected with the method.

The possibility and future perspective of the research are discussed below. Improvement in computing power is significant in recent years thanks to development of devices such as FPGA, DSP, and computers. The time period required for acquisition of an encoder signal or for calculation in the control seems to become shorter and shorter. It may thus become possible to set the output and control sampling periods extremely short in the near future. On the other hand, it is difficult to shorten the input sampling period according to shortening of the output and control sampling periods since the input sampling period highly depends on the frequency of PWM or the performance of components of an analog circuit in a motor driver. In the single-rate control, it should be selected whether setting all sampling periods long according to the limitation of the input sampling period or setting the sampling periods short with understanding that the input such as current cannot catch up with. But it is not an effective usage of resources. The proposed multirate sampling period can promote an effective use and maximize the advantages of shortening the output and control sampling periods. The proposed method is thus expected to play a larger role in future applications. Moreover, it is important to select an appropriate velocity measurement method carefully especially when the output sampling period is set extremely short. It is difficult in a fixed-time method (M method) to make the best use of the short sampling period due to noise, since the velocity resolution deteriorates by shortening the sampling period. The fixed-position method (T method), M/T method, and the synchronous measurement method (S method) are good candidates in this case. Considering the use of a high resolution encoder, S method is especially preferable in terms of the measurable speed range and the velocity resolution. The combined use of the multirate sampling method and velocity measurement based on S method can be treated as a basic and standard design. The design

of sampling periods and reduction in sensing noise described above are the issues most systems have in common. Thus these are important for raising the level of basic performance of any motion control. Furthermore, the interesting aspect of the multirate sampling method is that it may expand the capability of controllers with its time-variant characteristics. Most of the controllers used for motion control are linear time-invariant. The multirate sampling method enables the system to be periodic time-variant and thus expands the possible characteristics of controllers. Since the proposed multirate sampling method is based on a viewpoint different from conventional multirate sampling methods with a focus on a different requirement or limitation, combined use of the conventional and the proposed multirate sampling methods is also expected to be effective in a complex and large scale system with various components and limitations. One of examples of the system is networked control systems. In networked control systems, a time interval of acquisition of remote signals is generally strictly limited. The characteristics of a networked control system is similar to those of the target systems in the conventional multirate sampling method, in which the output signal cannot be acquired in the short sampling period. Although various attempts have been made in designing appropriate sampling periods and extracting and processing transmission signals to solve this problem in this thesis, combined use of a multirate sampling method with interpolation seems to be an effective candidate in some applications. It is important to select a method suitable for the system considering the limitations and requirements in the respective systems. In future applications, fusion or collaboration with visual information or audio information may be required. The ideas of the methods proposed for networked control systems in this thesis are expected to be effective in transmission of and collaboration with these information. Especially, the coding scheme may be applicable to transmission of other information although the approach is different from general approaches in these fields. Focusing on the contact motion, high contact detection performance in the proposed method enables the system to provide additional information to a controller or an operator for using as a trigger to switch the tasks, for promoting efficient and safe operation, or for helping automatic adaptation with various environments. It must be an effective tool to execute more complicated tasks more reliably.

Even with the proposals made in this thesis, there are still a lot of issues to be solved for expanding application of robotic technology. For example, this thesis does not show how to assure the safety not to harm human beings or other surrounding objects, or the ways for upper level decision making. Even just in motor control, this thesis dealt with only a part of limitations and further development and improvement are required. The achievement of this research may thus be just a small step to make robotic technology truly effective to support human lives but the author believes that it is an indispensable step

for further development.

References

[1] M. Peckham, "Google's driverless cars now officially licensed in Nevada," TIME, 2012.

[2] "iRobot: Robots for Defense and Security," iRobot Corporation. [Online]. Available: http://www.irobot.com/en/us/learn/defense.aspx

[3] "Intuitive Surgical, Inc." [Online]. Available: http://www.intuitivesurgical.com

[4] J. Jones, "Robots at the tipping point: the road to irobot roomba," *IEEE Robotics and Automation Magazine*, vol. 13, no. 1, pp. 76–78, 2006.

[5] K. Čapek and D. Wyllie, *R.U.R (Rossum's Universal Robots)*. Echo Library, 2010.

[6] Hesiodus, S. Lombardo, and R. Lamberton, *Works and Days: And Theogony*, ser. Classics Series. Hackett Publishing Company Incorporated, 1993.

[7] B. Brodsky, *The Golem: a Jewish legend*. Lippincott, 1976.

[8] M. Shelley, *Frankenstein: Or the Modern Prometheus*. Floating Press, 2008.

[9] F. Moon, *The Machines of Leonardo Da Vinci and Franz Reuleaux: Kinematics of Machines from the Renaissance to the 20th Century*, ser. History of mechanism and machine science. Springer London, Limited, 2007.

[10] H. H. Yorinao and K. Murakami, *Japanese automata : Karakuri zui : an eighteenth century Japanese manual of automatic mechanical devices*. Murakami Kazuo, 2012.

[11] N. Tesla, "Method of and apparatus for controlling mechanism of moving vessels or vehicles," U.S. Patent 613 809.

[12] S. Behnke, “Humanoid Robots - From Fiction to Reality?” *Künstliche Intelligenz*, vol. 22, pp. 5–9, 2008.

[13] R. C. Goertz, “Mechanical master-slave manipulator,” *Nucleonics*, vol. 12, pp. 45–46, 1954.

[14] G. C. Devol, “Programmed article transfer,” U.S. Patent 2 988 237.

[15] S. Nof, *Handbook of Industrial Robotics*, ser. Electrical and electronic engineering. Wiley, 1999, no. 1.

[16] F. Operto, “Ethics in advanced robotics,” *IEEE Robotics and Automation Magazine*, vol. 18, no. 1, pp. 72–78, 2011.

[17] R. Sparrow, ““Just Say No” to drones,” *IEEE Technology and Society Magazine*, vol. 31, no. 1, pp. 56–63, 2012.

[18] R. Arkin, P. Ulam, and A. Wagner, “Moral decision making in autonomous systems: Enforcement, moral emotions, dignity, trust, and deception,” *Proc. of the IEEE*, vol. 100, no. 3, pp. 571–589, 2012.

[19] I. Asimov, *I, Robot*. Gnome Press, 1950.

[20] A. Sabanovic and K. Ohnishi, *Motion Control Systems*. Wiley, 2011.

[21] K. Ohnishi, M. Shibata, and T. Murakami, “Motion control for advanced mechatronics,” *IEEE/ASME Trans. on Mechatronics*, vol. 1, no. 1, pp. 56–97, 1996.

[22] M. C. Berg, A. N, and J. D. Powell, “Multirate digital control system design,” *IEEE Trans. on Automatic Control*, vol. AC-33, pp. 1139–1150, 1988.

[23] M. Ferre, M. Buss, R. Aracil, C. Melchiorri, and C. Balaguer, *Advances in Telerobotics*, 1st ed., ser. Springer Tracts in Advanced Robotics. Springer-Verlag Berlin Heidelberg, 2007.

[24] J. P. Hespanha, P. Naghshtabrizi, and Y. Xu, “A survey of recent results in networked control systems,” *Proc. of the IEEE*, vol. 95, no. 1, pp. 138–162, 2007.

[25] J. Baillieul and P. J. Antsaklis, “Control and communication challenges in networked real-time systems,” *Proc. of the IEEE*, vol. 95, no. 1, pp. 9–28, 2007.

[26] T. Tsuji, T. Hashimoto, H. Kobayashi, M. Mizuochi, and K. Ohnishi, "A wide-range velocity measurement method for motion control," *IEEE Trans. on Industrial Electronics*, vol. 56, no. 2, pp. 510–519, 2009.

[27] Y. Hori, T. Umeno, T. Uchida, and Y. Konno, "An instantaneous speed observer for high performance control of DC servomotor using DSP and low precision shaft encoder," in *Proc. of Int. Power Electronics and Motion Control Conf.*, 1991, pp. 647–652.

[28] M. Iwasaki, K. Seki, and Y. Maeda, "High-precision motion control techniques: A promising approach to improving motion performance," *IEEE Industrial Electronics Mag.*, vol. 6, no. 1, pp. 32–40, 2012.

[29] T. Yoshikawa, "Dynamic hybrid position/force control of robot manipulators–description of hand constraints and calculation of joint driving force," *IEEE J. of Robotics and Automation*, vol. 3, no. 5, pp. 386–392, 1987.

[30] I. Godler, H. Honda, and K. Ohnishi, "Design guidelines for disturbance observer's filter in discrete time," in *Proc. of IEEE Int. Workshop on Advanced Motion Control*, 2002, pp. 390–395.

[31] K. Yang, Y. Choi, and W. K. Chung, "Performance analysis of discrete-time disturbance observer for second-order systems," in *Proc. of IEEE Conf. on Decision and Control*, 2003, pp. 4877–4882.

[32] R. Roberts, R. Paul, and B. Hillberry, "The effect of wrist force sensor stiffness on the control of robot manipulators," in *Proc. of IEEE Int. Conf. on Robotics and Automation*, vol. 2, 1985, pp. 269–274.

[33] Y. Li and X. Chen, "On the dynamic behavior of a force/torque sensor for robots," *IEEE Trans. on Instrumentation and Measurement*, vol. 47, no. 1, pp. 304–308, 1998.

[34] Y. F. Li and X. B. Chen, "On the dynamic behavior of a force/torque sensor for robots," *IEEE Trans. on Instrumentation and Measurement*, vol. 47, no. 1, pp. 304–308, 1998.

[35] T. Murakami, F. Yu, and K. Ohnishi, "Torque sensorless control in multidegree-of-freedom manipulator," *IEEE Trans. on Industrial Electronics*, vol. 40, no. 2, pp. 259–265, 1993.

[36] K. Ohnishi, N. Matsui, and Y. Hori, "Estimation, identification, and sensorless control in motion control system," *Proc. of the IEEE*, vol. 82, no. 8, pp. 1253–1265, 1994.

[37] S. Katsura, Y. Matsumoto, and K. Ohnishi, "Analysis and experimental validation of force bandwidth for force control," *IEEE Trans. on Industrial Electronics*, vol. 53, no. 3, pp. 922–928, 2006.

[38] R. Volpe and P. Khosla, "A theoretical and experimental investigation of explicit force control strategies for manipulators," *IEEE Trans. on Automatic Control*, vol. 38, no. 11, pp. 1634–1650, 1993.

[39] G. Zeng and A. Hemami, "An overview of robot force control," *Robotica*, vol. 15.

[40] P. F. Hokayem and M. W. Spong, "Bilateral teleoperation: An historical survey," *Automatica*, vol. 42, pp. 2035–2057, 2006.

[41] S. Tachi and T. Sasaki, "Impedance controlled master slave manipulation system part i: Basic concept and application to the system with time delay," *J. of the Robotics Society of Japan*, vol. 8, no. 3, pp. 241–252, 1990.

[42] T. Sakaki and S. Tachi, "Impedance controlled master and slave manipulation system part ii: Modification of force sensation and extension of operation capability," *J. of the Robotic Society of Japan*, vol. 8, no. 3, pp. 253–264, 1990.

[43] B. Hannaford, "A design framework for teleoperators with kinesthetic feedback," *IEEE Trans. on Robotics and Automation*, vol. 5, no. 4, pp. 426–434, 1989.

[44] D. A. Lawrence, "Stability and transparency in bilateral teleoperation," *IEEE Trans. on Robotics and Automation*, vol. 9, no. 5, pp. 624–637, 1993.

[45] K.Hashtrudi-Zaad and S. E. Salcudean, "On the use of local force feedback for transparent teleoperation," in *Proc. of IEEE Int. Conf. on Robotics and Automation*, 1999, pp. 1863–1869.

[46] T. B. Sheridan, "Space teleoperation through time delay: Review and prognosis," *IEEE Trans. on Robotics and Automation*, 1993.

[47] J. Funda and R. P. Paul, "A symbolic teleoperator interface for time-delayed underwater robot manipulation," in *Proc. of Ocean Technologies and Opportunities in the Pacific for the 90's*, 1991, pp. 1526–1533.

[48] A. Kron and G. Schmidt, "Haptic telepresent control technology applied to disposal of explosive ordnances: Princples and experimental results," in *Proc. of IEEE Int. Symp. on Industrial Electtronics*, 2005, pp. 1505–1510.

[49] T. Hirabayashi, J. Akazono, T. Yamamoto, H. Sakai, and H. Yano, "Teleoperation of construction machines with haptic information for underwater applications," *Automation in Construction*, vol. 15, no. 5, pp. 563–570, 2005.

[50] S. E. Butner and M. Ghodoussi, "Transforming a surgical robot for human telesurgery," *IEEE Trans. on Robotics and Automation*, vol. 19, no. 5, pp. 818–824, 2003.

[51] R. H. Taylor and D. Stoianovici, "Medical robotics in computer-integrated surgery," *IEEE Trans. on Robotics and Automation*, vol. 19, no. 5, pp. 765–781, 2003.

[52] G. H. Ballantyne, "Robotic surgery, telerobotic surgery, telepresence, and telementoring - review of early clinical results," *Surgical Endoscopy And Other Interventional Techniques*, vol. 16, no. 10, pp. 1389–1402, 2002.

[53] E. P. W. van der Putten, R. H. M. Goossens, J. J. Jakimowicz, and J. Dankelman, "Haptics in minimally invasive surgery – a review," *Minimally Invasive Therapy & Allied Technology*, vol. 17, no. 1, pp. 3–16, 2008.

[54] A. M. Okamura, "Methods for haptic feedback in teleoperated robot-assisted surgery," *Industrial Robot*, vol. 31, no. 6, pp. 499–508, 2004.

[55] Y. Yokokohji and T. Yoshikawa, "Bilateral control of master-slave manipulators for ideal kinesthetic coupling – formulation and experiment," *IEEE Trans. on Robotics and Automation*, vol. 10, no. 5, pp. 605–620, 1994.

[56] W. Iida and K. Ohnishi, "Reproducibility and operationality in bilateral teleoperation," in *Proc. of Int. Workshop on Advanced Motion Control*, 2004, pp. 217–222.

[57] T. Tsuji, K. Natori, H. Nishi, and K. Ohnishi, "A controller design method of bilateral control system," *European Power Electronics and Drives Journal*, vol. 16, no. 2, pp. 22–28, 2006.

[58] K. Hashtrudi-Zaad and S. E. Salcudean, "Bilateral parallel force/position teleoperation control," *J. of Robotic Systems*, vol. 19, no. 4, pp. 155–167, 2002.

[59] K. Hashtrudi-Zaad and S. E. Salcudean, "Analysis and evaluation of stability and performance robustness for teleoperation control architectures," in *Proc. of IEEE Int. Conf. on Robotics and Automation*, 2000, pp. 3107–3113.

[60] I. Aliaga, Á. Rubio, and E. Sánchez, "Experimental quantitative comparison of different control architectures for master-slave teleoperation," *IEEE Trans. on Control Systems Technology*, vol. 12, no. 1, pp. 2–11, 2004.

[61] A. Peer and M. Buss, "Stability analysis of a bilateral teleoperation system using the parameter space approach," in *Proc. of the IEEE/RSJ Int. Conf. on Intelligent Robots and Systems*, 2008, pp. 2350–2356.

[62] P. Arcara and C. Melchiorri, "Control schemes for teleoperation with time delay: A comparative study," *Robotics and Autonomous Systems*, vol. 38, no. 1, pp. 49–64, 2002.

[63] B. Hannaford, "Stability and performance tradeoffs in bi-lateral telemanipulation," in *Proc. of IEEE Intl. Conf. on Robotics and Automation*, vol. 3, pp. 1764–1767.

[64] S. Sakaino, T. Sato, and K. Ohnishi, "Modal transformation for bilateral control and co-operational robot motion – kinematics and dynamics –," in *Proc. of the IEEE Int. Conf. on Industrial Electronics*, 2009, pp. 1–6.

[65] K. Hashtrudi-Zaad and S. E. Salcudean, "Transparency in time-delayed systems and the effect of local fotce feedback for transparent teleoperation," *IEEE Trans. on Robotics and Automation*, vol. 18, no. 1, pp. 108–114, 2002.

[66] I. Godler, K. Hashimoto, and T. Ninomiya, "Stability, gain and sampling time of discrete time acceleration control loop," in *Proc. of IEEE Int. Symp. on Industrial Electronics*, 2001, pp. 1305–1308.

[67] P. Antsaklis and J. Baillieul, "Special issue on technology of networked control systems," *Proc. of the IEEE*, vol. 95, no. 1, pp. 5–8, 2007.

[68] V. Jacobson, "Congestion avoidance and control," *ACM SIGCOMM Computer Communication Review*, vol. 18, no. 4, pp. 314–329, 1988.

[69] K. J. Åström, P. Hangander, and J. Sternby, "Zeros of sampled system," *Automatica*, vol. 20, no. 1, pp. 31–38, 1984.

[70] M. Tomizuka, "Zero phase error tracking algorithm for digital control," *ASME J. Dynamic Systems, Measurement, and Control*, vol. 109, no. 1, pp. 65–68, 1987.

[71] K. Ogata, *Discrete-Time Control Systems*, ser. Prentice Hall International editions. Prentice-Hall International, 1995.

[72] T. Hara and M. Tomizuka, "Performance enhancement of multi-rate controller for hard disk drives," *IEEE Trans. on Magnetics*, vol. 35, no. 2, pp. 898–903, 1999.

[73] H. Fujimoto and Y. Hori, "Visual servoing based on intersample disturbance rejection by multirate sampling control," in *Proc. of IEEE Conf. on Decision and Control*, 2001, pp. 334–339.

[74] H. Fujimoto, Y. Hori, and A. Kawamura, "Perfect tracking control based on multirate feedforward control with generalized sampling periods," *IEEE Trans. on Industrial Electronics*, vol. 48, no. 3, pp. 636–644, 2001.

[75] M. Tomizuka, "Multi-rate control for motion control application," in *Proc. of IEEE Int. Workshop on Advanced Motion Control*, 2004, pp. 21–29.

[76] O. Khatib, "A unified approach for motion and force control of robot manipulators: The operational space formulation," *IEEE J. of Robotics and Automation*, vol. 3, no. 1, pp. 43–53, 1987.

[77] P. Grant, "Multirate signal processing," *Electronics Communication Engineering Journal*, vol. 8, no. 1, pp. 4–12, 1996.

[78] J. Franca, A. Petraglia, and S. Mitra, "Multirate analog-digital systems for signal processing and conversion," *Proc. of the IEEE*, vol. 85, no. 2, pp. 242–262, 1997.

[79] T. Ohmae, T. Matsuda, K. Kamiyama, and M. Tachikawa, "A microprocessor-controlled high-accuracy wide-range speed regulator for motor drives," *IEEE Trans. on Industrial Electronics*, vol. 29, no. 3, pp. 207–211, 1982.

[80] E. Shimada, K. Aoki, T. Komiyama, and T. Yokoyama, "Implementation of deadbeat control for single phase utility interactive inverter using FPGA," in *Proc. of Int. Power Electronics Conf.*, 2005, pp. 401–404.

[81] A. Azarian and M. Ahmadi, "Reconfigurable computing architecture survey and introduction," in *Proc. of IEEE Int. Conf. on Computer Science and Information Technology*, 2009, pp. 269–274.

[82] B. Carvalho, A. J. N. Batista, F. Patrício, M. Correia, H. Fernandes, J. Sousa, and C. A. F. Varandas, "Multi-rate DSP/FPGA-based real-time acquisition and control on the ISTTOK Tokamak," *IEEE Trans. on Nuclear Science*, vol. 55, no. 1, pp. 54–58, 2008.

[83] H. Fujimoto, A. Kawamura, and M. Tomizuka, "Generalized digital redisign method for linear feedback system based on N-delay control," *IEEE/ASME Trans. on Mechatronics*, vol. 4, no. 2, pp. 101–109, 1999.

[84] B. Gopinath, "On the control of linear multiple input-output systems," *Bell System Tech. J.*, vol. 50, no. 3, pp. 1063–1081, 1971.

[85] M. Araki and K. Yamamoto, "Multivariable mulirate sampled-data systems: State-space description, transfer characteristics, and nyquist criterion," *IEEE Trans. on Automatic Control*, vol. 31, no. 2, pp. 145–154, 1986.

[86] B. Bose, *Power Electronics and Variable Frequency Drives: Technology and Application*. IEEE. Press, 1997.

[87] D. R.W., L. Garces, F. Profumo, R. D. Lorenz, T. Nondahl, and V. Stefanovic, *Microprocessor control of motor drive and power converters*. IEEE Tutorial Course Note Book from 1991, '92 & '93, IEEE, IAS Annual Meetings, IEEE Publishing Services #THO587-6.

[88] M. Prokin, "Double buffered wide-range frequency measurement method for digital tachometers," *IEEE Trans. on Instrumentation and Measurement*, vol. 40, no. 3, pp. 606–610, 1991.

[89] Z. Zhou, T. Li, T. Takahashi, and E. Ho, "FPGA realization of a high-performance servo controller for PMSM," in *Proc. of IEEE Applied Power Electronics Conf. and Expo.*, vol. 3, 2004, pp. 1604–1609.

[90] R. C. Kavanagh, "Improved digital tachometer with reduced sensitivity to sensor nonideality," *IEEE Trans. on Industrial Electronics*, vol. 47, no. 4, pp. 890–897, 2000.

[91] P. R. Belanger, "Estimation of angular velocity and acceleration from shaft encoder measurements," in *Proc. of IEEE Conf. on Robotics and Automation*, 1992, pp. 585–592.

[92] S. Sakai and Y. Hori, "Ultra-low speed control of servomotor using low resolution rotary encoder," in *Proc. of IEEE Conf. of Industrial Electronics Society*, 1995, pp. 615–620.

[93] "What is periomatic^{TM}." [Online]. Available: http://www.cocores.co.jp/english/tech.html

[94] R. Bonert, "Design of a high performance digital tachometer with a microcontroller," *IEEE Trans. on Instrumentation and Measurement*, vol. 38, no. 5, pp. 1104–1108, 1989.

[95] T. Tsuji, M. Mizuochi, and K. Ohnishi, "Modification of measurement time for digital tachometers," in *Proc. of Japan Industry Application Society Conf.*, 2005, pp. 233–238.

[96] T. Tsuji, M. Mizuochi, and K. Ohnishi, "Technical issues on velocity measurement for motion control," in *Proc. of Int. Power Electronics and Motion Control Conf.*, 2006, pp. 326–331.

[97] L. Kovudhikulrungsri, "Discrete-time observer with dual sampling rates and its applications to drive control with wide speed range," Dr. Thesis, The University of Tokyo, 2003.

[98] J. Marescaux, J. Leroy, M. Gagner, F. Rubino, D. Mutter, M. Vix, S. E. Butner, and M. K. Smith, "Transatlantic robot-assisted telesurgery," *Nature*, vol. 413, pp. 379–380, 2001.

[99] Y. Li, L. Yang, and G. Yang, "Network-based coordinated motion control of large-scale transportation vehicles," *IEEE/ASME Trans. on Mechatronics*, vol. 12, no. 2, pp. 208–215, 2007.

[100] S. Tatikonda and S. Mitter, "Control under communication constraints," *IEEE Trans. on Automatic Control*, vol. 49, no. 7, pp. 1056–1068, 2004.

[101] F.-L. Lian, J. R. Moyne, and D. Tilbury, "Performance evaluation of control networks: Ethernet, controlnet, and devicenet," *IEEE Control Systems Magazine*, vol. 21, no. 1, pp. 66–83, 2001.

[102] R. Liu, A. Monti, F. Ponci, and A. Smith, "A design approach for digital controllers using reconfigurable network-based measurements," *IEEE Trans. on Instrumentation and Measurement*, vol. 59, no. 5, pp. 1073–1081, 2010.

[103] W. P. M. H. Heemels, A. R. Teel, N. van de Wouw, and D. Nešić, "Networked control systems with communication constraints: Tradeoffs between transmission intervals, delays and performance," *IEEE Trans. on Automatic Control*, 2010.

[104] O. J. Smith, "A controller to overcome dead time," *ISA J.*, vol. 6, no. 2, pp. 28–33, 1959.

[105] K. Natori, T. Tsuji, K. Ohnishi, A. Hace, and K. Jazernik, "Time-delay compensation by communication disturbance observer for bilateral teleoperation under time-varying delay," *IEEE Trans. on Industrial Electronics*, vol. 57, no. 3, pp. 1050–1062, 2010.

[106] E. Fridman and U. Shaked, "A descriptor system approach to h_∞ control of linear time-delay systems," *IEEE Trans. on Automatic Control*, vol. 47, no. 2, pp. 253–270, 2002.

[107] S. Azuma and T. Sugie, "Synthesis of optimal dynamic quantizers for discrete-valued input control," *IEEE Trans. on Automatic Control*, vol. 53, no. 9, pp. 2064–2075, 2008.

[108] T. Sikora, "Trends and perspectives in image and video coding," *Proc. of the IEEE*, vol. 93, no. 1, pp. 6–17, 2005.

[109] H. Tanaka and K. Ohnishi, "Lossy data compression using FDCT for haptic communication," in *Proc. of IEEE Int. Workshop on Advanced Motion Control*, pp. 756–761.

[110] G. N. Nair, F. Fagnani, S. Zampieri, and R. J. Evans, "Feedback control under data rate constraints: An overview," *Proc. of the IEEE*, vol. 95, no. 1, pp. 108–137, 2007.

[111] R. Anderson and M. Spong, "Bilateral control of teleoperators with time delay," *IEEE Trans. on Automatic Control*, vol. 34, no. 5, pp. 494–501, 1989.

[112] G. Niemeyer and J.-J. Slotine, "Stable adaptive teleoperation," *IEEE J. of Oceanic Engineering*, vol. 16, no. 1, pp. 152–162, 1991.

[113] D. Yashiro and K. Ohnishi, "Multirate sampling method for bilateral control with communication bandwidth constraint," in *Proc. of IEEE Int. Conf. on Industrial Technology*, 2009.

[114] H. Mitome, D. Yashiro, and K. Ohnishi, "Data communication taking latency between position controller and plant into account," in *Proc. of Annu. Conf. of IEEJ Industry Application Society*, 2010, (in Japanese).

[115] D. Yashiro and K.Ohnishi, "Performance analysis of bilateral control system with communication bandwidth constraint," *IEEE Trans. on Industrial Electronics*, 2011.

[116] C. L. Philips and H. T. Nagle, *Digital control system analysis and design*, third edition ed. Prentice Hall, 1995.

[117] M. Mizuochi and K. Ohnishi, “Investigation on influence of signal data quality on control performance,” in *Papers of the IEEJ Technical Meeting on Industrial Instrumentation and Control*, 2011, (in Japanese).

[118] I. Godler, H. Honda, and K. Ohnishi, “Design guidelines for disturbance observer’s filter in discrete time,” in *Proc. of IEEE Int. Workshop on Advanced Motion Control*, 2002, pp. 390–395.

[119] M. Mizuochi, T. Tsuji, and K. Ohnishi, “Multirate sampling method for acceleration control system,” *IEEE Trans. on Industrial Electronics*, vol. 54, no. 3, pp. 1462–1471, 2007.

[120] C. M. N. Diolaiti, “Contact impedance estimantion in robotic system,” *IEEE Trans. on Robotics*, vol. 2, no. 4, pp. 768–771, 2005.

[121] M. Shibata, T. Murakami, and K. Ohnishi, “A unified approach to position and force control by fuzzy logic,” *IEEE Trans. on Industrial Electronics*, vol. 43, no. 1, pp. 81–87, 1996.

[122] B. E. Miller and J. E. Colgate, “Using a wavelet network to characterize real environments for haptic display,” in *Proc. of ASME Int. Mechanical Engineering Cong. and Expo.*, 1998, pp. 257–264.

[123] S. Katsura, K. Irie, and K. Ohishi, “Visualization of environmental information by haptograph based on wideband force control,” in *Proc. of Annu. Conf. of the IEEE Industrial Electronics Society*, 2008, pp. 368–373.

[124] A. Maciel, R. Boulic, and D. Thalmann, “Efficient collision detection within deforming spherical sliging contact,” *IEEE Trans. on Visualization and Computer Graphics*, vol. 13, no. 3, pp. 518–529, 2007.

[125] W. Chou and J. Xiao, “Real-time and accurate multiple contact detection between general curved objects,” in *Proc. of Int. Conf. on Intelligent Robots and Systems*, 2006, pp. 556–561.

[126] Y. Kasahara, K. Kitamura, K. Ohnishi, Y. Morikawa, and N. Shimojima, “Rupture detection for exenteration of tissues using two-dof haptic surgical forceps robot,” in *Proc. of IEEE Int. Workshop on Advanced Motion Control*, 2010, pp. 284–289.

[127] B. Eberman and J. Salisbury, “Application of change detection to dynamic contact sensing,” *Int. J. of Robotics Research*, vol. 12, no. 5, pp. 369–394, 1994.

[128] M. McDonnell, “Is electrical noise useful? [point of view],” *Proc. of the IEEE*, 2011.

[129] L. Schuchman, “Dither signals and their effect on quantization noise,” *IEEE Trans. on Communication Technology*, vol. 12, no. 4, pp. 162–165, 1964.

[130] A. A. Pervozvanski and C. Canudas, “Asymptotic analysis of the dither effect in systems with friction,” *Automatica*, vol. 28, no. 1, pp. 105–113, 2002.

[131] S. Kudo, “The study of sensitivity on piezoelectric vibratory tactile sensor using a longitudinal bar resonator,” in *Proc. of Int. Cong. on Acoustics*, 2010, pp. 1–6.

[132] M. Portnoff, “Time-frequency representation of digital signals and systems based on short-time fourier analysis,” *IEEE Trans. on Acoustics, Speech, and Signal Processing*, vol. 28, no. 1, pp. 55–69, 1980.

[133] O. Rioul and P. Duhamel, “Fast algorithms for discrete and continuous wavelet transform,” *IEEE Trans. on Information Theory*, vol. 38, no. 2, pp. 569–586, 1992.

[134] T. T. Phuong, R. Furusawa, M. Nandayapa, C. Mitsantisuk, and K. Ohishi, “FPGA-based wide-band force control system with friction-free and noise-free force observation,” *IEEJ J. of Industry Applications*, vol. 1, no. 3, pp. 178–190, 2012.

Acknowledgments

This dissertation is the summary of my researches from April 2004 to March 2006 and from April 2010 to September 2013 as a member of Ohnishi laboratory in Keio University. I first joined Professor Dr. Ohnishi's research group when I was in my master program. Although I started my career in Mechanical Engineering Laboratory of Hitachi, Ltd. after receiving the M.E. degree in 2006, I decided to join Professor Dr. Ohnishi's group again as a doctoral student in 2010 while continuing my career as a full-time researcher in Hitachi, Ltd. I would like to express my gratitude to all people who gave me the opportunities, supported me, or gave me meaningful advices.

First of all, I would like to express my deep and sincere gratitude to my supervisor Professor Dr. Kouhei Ohnishi. He kindly took me in his laboratory when I entered master program and when I decided to rejoin as a doctoral student. He gave me a lot of essential comments and advices, which are greatly helpful for me to carry out researches. He also provided me a lot of opportunity to attend conferences and discuss with other researchers. I appreciate for his kindness and patience throughout my days in the laboratory.

I am deeply appreciate to the members of my Ph. D. Dissertation Committee, Professor Dr. Toshiyuki Murakami, Associate Professor Dr. Hiroaki Nishi, and Associate Professor Dr. Toru Namerikawa, for giving me a number of advices and helping me to improve this thesis. It was a great opportunity for me to review my research and consider it more deeply.

I greatly appreciate my bosses and colleagues in Hitachi, Ltd. and Hitachi Construction Machinery Co., Ltd. Special thanks go to Department Manager Mr. Kazuhiro Umekita at Hitachi Ltd., Senior Researcher Unit Leader Dr. Saku Egawa at Hitachi, Ltd., and Senior Researcher Mr. Akinori Ishii at Hitachi Construction Machinery Co., Ltd., who are my supervisors in company. I also appreciate Chief Manager Dr. Toshimichi Minowa at Hitachi Construction Machinery Co., Ltd., who was my Department Manager when I started doctoral research. My bosses gave me a chance to engage in the doctoral

program. They and my colleagues understood my situation and always supported me and inspired me. Even though the researches were not directly relating to my research in company, they gave me a lot of advices. Without their understandings and supports, I could not complete this work with continuing my career in the company.

I also would like to express my sincere gratitude to Professor emeritus Dr. Koichiro Sawa at Keio University, Associate Professor Dr. Takahiro Yakoh at Keio University, Associate Professor Dr. Seiichiro Katsura at Keio University, Associated Professor Dr. Toshiaki Tsuji at Saitama University, Lecturer Dr. Kenji Natori at Chiba University, Associate Professor Dr. Tomoyuki Shimono at Yokohama National University, Dr. Hiroyuki Tanaka at General Electric, Ms. Ena Ishii at Toshiba Corp., Lecturer Dr. Daisuke Yashiro at Mie University, Mr. Takahiro Nozaki, Mr. Takahiro Mizoguchi, and the all of current and past SUM members. The comments from them and discussion with them helped me promoting my researches and also motivated me a lot. Although my situation may be strange for current students, they kindly took me in and helped me a lot. I enjoyed discussing and spending time with them. Associated Professor Dr. Toshiaki Tsuji was my tutor when I was in my master and he guided me and supported me throughout my days in the group from various standpoints.

I am also deeply grateful to Professor emeritus Dr. Kiyotaka Shimizu at Keio University. I was in his Laboratory when I was an undergraduate student. My research life started there. He told me what the research is, and the importance of thinking deeply and paying attention even to detail.

Many professors and researchers outside Keio University also helped me. Especially, Professor Dr. Yoichi Hori at University of Tokyo, Professor Dr. Kiyoshi Ohishi at Nagaoka University of Technology, Professor Dr. Hiroshi Fujimoto at University of Tokyo, Professor Dr. Yutaka Uchimura at Shibaura Institute of Technology, gave me opportunities of discussion and fruitful advices through conferences or meetings. Discussion with them always inspired me.

I would like to thank friends and medical staffs. Actually, my days during the doctoral program were not very easy. I thank my friends for understanding my situation and supporting me. Medical doctors and staffs , especially in Orthopedics of Teikyo University School of Medicine University Hospital Mizunokuchi, Pain Clinic of NTT Medical Center Tokyo, and Katsuta Orthopedics, always encouraged and provided me appropriate supports and treatments for continuing my career.

I am grateful to my parents for bringing me up and supporting me. They are my great supporters. My father, who passed away when I was an undergraduate student, was a researcher and Professor in biochemistry. Even though the field is different, my passion to research may be inherited from him. He

cared about my learning environment and showed me attitude toward research throughout his life. My mother always supported me and encouraged me. She provided me environment to concentrate on my research and my job in company. Although I might make her worry a lot, she always stayed with me with her great love. I cannot imagine my research life without them.

There are a lot of people who helped me although I could not mention here. I would like to express my sincere gratitude again to all people who have supported me.

August 2013

Mariko Mizuochi

List of Achievements

Journals (as First Author)

[1] Mariko Mizuochi, Toshiaki Tsuji, Hiroaki Nishi, and Kouhei Ohnishi, "Realization of Acceleration Control Using Multirate Sampling Method," *IEEJ Transaction on Industry Applications*, vol. 126, no. 3, pp. 261–268, 2006 (in Japanese).

[2] Mariko Mizuochi, Toshiaki Tsuji, and Kouhei Ohnishi,"Multirate Sampling Method for Acceleration Control System," *IEEE Transaction on Industrial Electronics*, vol. 54, no. 3, pp. 1462–1471, 2007.

[3] Mariko Mizuochi and Kouhei Ohnishi,"Coding and Decoding Scheme for Wide-band Haptic Transmission," *Journal of Japan Society of Computer Aided Surgery*, vol. 13, no. 3, pp. 348–349, 2011 (in Japanese).

[4] Mariko Mizuochi and Kouhei Ohnishi, "Optimization of Transmission Data in Bilateral Teleoperation," *IEEJ Transaction on Industry Applications*, vol. 133, no. 3, pp. 314–319, 2013 (in Japanese).

Journals (as Co-author)

[1] Toshiaki Tsuji, Takuya HASHIMOTO, Hiroshi Kobayashi, Mariko Mizuochi, and Kouhei Ohnishi,"A Wide-Range Velocity Measurement Method for Motion Control," *IEEE Transaction on Industrial Electronics*, vol. 56, no. 2, pp. 510–519, 2009.

International Conference (as First Author)

[1] Mariko Mizuochi, Toshiaki Tsuji, and Kouhei Ohnishi, "Multirate Sampling Method for Acceleration Control System," *IEEE International Symposium on Industrial Electronics, ISIE '05*, Dubrovnik,

Croatia, vol. 4, pp. 1629–1634, June 20–23, 2005.

[2] Mariko Mizuochi, Toshiaki Tsuji, and Kouhei Ohnishi, "Force Sensing and Force Control Using Multirate Sampling Method," *The 31st Annual Conference of the IEEE Industrial Electronics Society, IECON '05*, Raleigh, U.S.A., pp. 1919–1924, November 2–6, 2005.

[3] Mariko Mizuochi, Toshiaki Tsuji, and Kouhei Ohnishi, "Improvement of Disturbance Suppression based on Disturbance Observer," *The 9th IEEE International Workshop on Advanced Motion Control, AMC '06*, Istanbul, Turkey, pp. 229–234, March 27–29, 2006.

[4] Mariko Mizuochi and Kouhei Ohnishi, "Coding and Decoding Scheme for Wide-band Bilateral Teleoperation," *The 12th IEEE International Workshop on Advanced Motion Control, AMC '12*, Sarajevo, Bosnia and Herzegovina, March 25–27, 2012.

[5] Mariko Mizuochi and Kouhei Ohnishi, "Contact Detection using Dither in Force Sensorless Motion Control," *IEEE International Conference on Mechatronics, ICM '13*, Vicenza, Italy, pp. 254–259, February 27–March 1, 2013.

[6] Mariko Mizuochi and Kouhei Ohnishi, "Low-impact Dither-based Contact Detection in Motion Control," *The 39th Annual Conference of the IEEE Industrial Electronics Society, IECON '13*, Vienna, Austria, November 10–13, 2013. (to be presented)

International Conference (as Co-author)

[1] Toshiaki Tsuji, Mariko Mizuochi, Hiroaki Nishi, and Kouhei Ohnishi, "A Velocity Measurement Method for Acceleraion Control," *The 31st Annual Conference of the IEEE Industrial Electronics Society, IECON '05*, Raleigh, U.S.A., pp. 1943–1948, November 2–6, 2005.

[2] Toshiaki Tsuji, Mariko Mizuochi, and Kouhei Ohnishi, "Technical Issues on Velocity Measurement for Motion Control," *The 12th International Power Electronics and Motion Control Conference, EPE-PEMC '06*, Portoroz, Slovenia, pp. 326–331, August 30–September 1, 2006.

Domestic Conference (as First Author)

[1] Mariko Mizuochi, Toshiaki Tsuji, Hiroaki Nishi, and Kouhei Ohnishi, "Realization of Acceleration Control Using Multirate Sampling Method," *IEEJ Technical Meeting on Industrial Instru-*

mentation and Control, IIC '05, Nagoya, IIC-05-9, vol. 1-15, pp. 49–54, March 9–10, 2005 (in Japanese).

[2] Mariko Mizuochi, Toshiaki Tsuji, Hiroaki Nishi, and Kouhei Ohnishi, "High-accuracy Motion Control based on Accurate Velocity Measurement," *IEEJ Technical Meeting on Industrial Instrumentation and Control, IIC '06*, IIC-06-11, Hamamatsu, pp. 59–64, March 8–9, 2006 (in Japanese).

[3] Mariko Mizuochi, Akinori Ishii, and Jinichi Yamaguchi, "Development of Dynamic Stability Measurement System for Construction Machinery," *The Robotics and Mechatronics Conference of the Japan Society of Mechanical Engineers, ROBOMEC '10*, Asahikawa, pp. 1A1-B15(1)–1A1-B15(2), June 13–16, 2010 (in Japanese).

[4] Mariko Mizuochi and Kouhei Ohnishi, "Investigation on Influence of Signal Data Quality on Control Performance," *IEEJ Technical Meeting on Industrial Instrumentation and Control, IIC '11*, IIC-11-30, Chiba, pp. 23–28, March 8–9, 2011 (in Japanese).

[5] Mariko Mizuochi and Kouhei Ohnishi, "Signal Transmission Method for Bilateral Teleoperation over Network," *Annual Conference of the IEEJ Industry Application Society, JIASC '11*, Okinawa, no. 2-44, pp. II-549–II-554, September 6–8, 2011 (in Japanese).

[6] Mariko Mizuochi and Kouhei Ohnishi, "Coding and Decoding Scheme for Wide-band Haptic Transmission," *The 20th Annual Congress of Japan Society of Computer Aided Surgery, JSCAS '11*, Yokohama, pp. 348–349, November 22–24, 2011 (in Japanese).

[7] Mariko Mizuochi and Kouhei Ohnishi, "Bilateral Control over Network using Coding based on Frequency Analysis Technique," *IEEJ Technical Meeting on Industrial Instrumentation and Control, IIC '12*, IIC-12-135, Yokohama, pp. 13–18, March 6–7, 2012 (in Japanese).

Domestic Conference (as Co-author)

[1] Toshiaki Tsuji, Mariko Mizuochi, and Kouhei Ohnishi, "Modification of Measurement Time for Digital Tachometers," *Annual Conference of the IEEJ Industry Application Society, JIASC '05*, Fukui, vol. 2, pp. 233–238, August 29–31, 2005.

[2] Toshiaki Tsuji, Hiroshi Kobayashi, Mariko Mizuochi, and Kouhei Ohnishi, "Multirate Sampling Control for Reducing Time/Space Quantization Error," *IEEJ Technical Meeting on Industrial Instrumentation and Control, IIC '07*, IIC-07-91, Nagaoka, pp. 38–42, March 6–7, 2007 (in Japanese).

Awards

[1] FANUC FA & Robot Foundation Original Paper Award, March, 2008

Career

[1] April 2006 – present
Researcher
Hitachi, Ltd.
Mechanical Engineering Research Laboratory (April 2006 – March 2011)
Hitachi Research Laboratory (April 2011 – present)